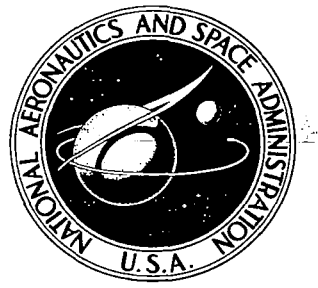

NASA CONTRACTOR REPORT

NASA CR-1712

STUDY AND DEVELOPMENT OF TURBOFAN NACELLE MODIFICATIONS TO MINIMIZE FAN-COMPRESSOR NOISE RADIATION

Volume II - Acoustic Lining Development

Prepared by
THE BOEING COMPANY
Seattle, Wash. 98124
for Langley Research Center

NATIONAL AERONAUTICS AND SPACE ADMINISTRATION • WASHINGTON, D. C. • JANUARY 1971

1. Report No.	2. Government Accession No.	3. Recipient's Catalog No.
NASA CR-1712		

4. Title and Subtitle	5. Report Date
STUDY AND DEVELOPMENT OF TURBOFAN NACELLE MODIFICATIONS TO MINIMIZE FAN–COMPRESSOR NOISE RADIATION. VOLUME II – ACOUSTIC LINING DEVELOPMENT.	January 1971
	6. Performing Organization Code
7. Author(s)	8. Performing Organization Report No.
	10. Work Unit No.
9. Performing Organization Name and Address The Boeing Company Seattle, Wash. 98124	11. Contract or Grant No. NAS 1-7129
12. Sponsoring Agency Name and Address National Aeronautics and Space Administration Washington, D.C. 20546	13. Type of Report and Period Covered Contractor Report May 1, 1967 to Nov. 1, 1969
	14. Sponsoring Agency Code

15. Supplementary Notes

16. Abstract An acoustic lining development program is described, which covers selection of facing materials and lining concepts suitable for attenuating turbofan engine noise generated by a fan compressor and development of acoustic lining design technology. A theoretical method for predicting lining attenuation in a duct without airflow is presented and is combined with an empirical prediction method developed from parametric results of the flow-duct tests to establish a lining design procedure. Concurrent and interrelated investigations, which comprised the acoustic lining development program, are described as is the facilities equipment used. Evaluation of more than 40 types of acoustic facing materials resulted in the selection of woven metallic fiber, metallic felt, reinforced metallic felt, and resin impregnated fiberglass laminate facing materials as most suitable for acoustic linings in a turbofan nacelle environment. A study of lining concepts resulted in selecting a broadband resistive-resonator type lining as best suiting engine-fan-duct and inlet-installation requirements. Results are presented of analytical and experimental investigations undertaken to develop an acoustic lining design procedure and to select suitable lining concepts and materials for reducing fan-compressor-generated noise in turbofan engines. A comprehensive acoustic-lining flow-duct test program established the parameters controlling the amount and peak frequency of attenuation provided by a lining. Test results also showed metallic and nonmetallic linings, having the same flow resistance and geometry, provide similar attenuation characteristics. Good correlation was obtained between the results of the flow-duct and full-scale-engine tests. Evaluation of acoustic and mechanical properties of polyimide-fiberglass sandwich panels as acoustic linings resulted in the selection of this material for follow-on boilerplate fan-duct development.

17. Key Words (Suggested by Author(s))	18. Distribution Statement
Noise, aircraft Material, acoustic Acoustically absorptive duct linings	Unclassified - Unlimited

19. Security Classif. (of this report)	20. Security Classif. (of this page)	21. No. of Pages	22. Price*
Unclassified	Unclassified	184	$3.00

*For sale by the National Technical Information Service, Springfield, Virginia 22151

STUDY AND DEVELOPMENT OF TURBOFAN NACELLE MODIFICATIONS TO MINIMIZE FAN-COMPRESSOR NOISE RADIATION

OVERALL REPORT ORGANIZATION

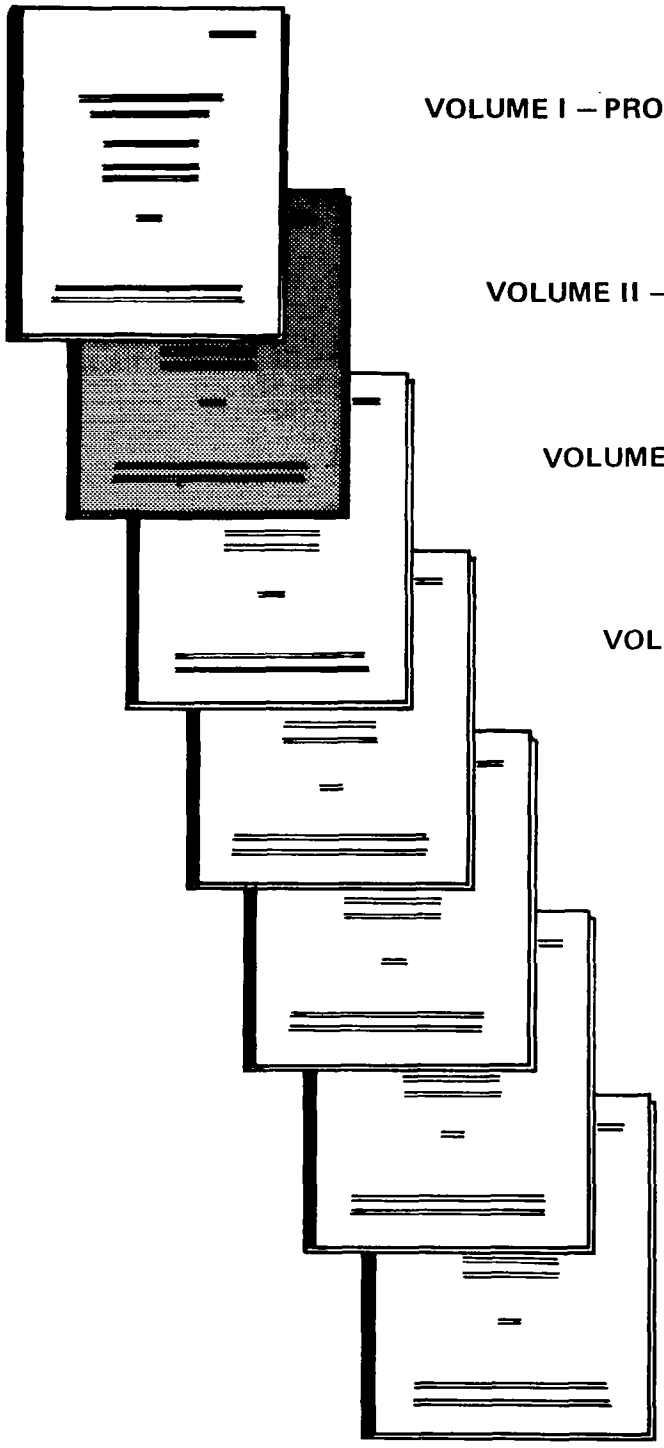

VOLUME I – PROGRAM SUMMARY

VOLUME II – ACOUSTIC LINING DEVELOPMENT

VOLUME III – CONCEPT STUDIES AND GROUND TESTS

VOLUME IV – FLIGHTWORTHY NACELLE DEVELOPMENT

VOLUME V – SONIC INLET DEVELOPMENT

VOLUME VI – ECONOMIC STUDIES

VOLUME VII – SUBJECTIVE EVALUATION TESTS

CONTENTS

CONTENTS—Concluded

TABLES

FIGURES

FIGURES—Continued

FIGURES—Continued

FIGURES—Concluded

STUDY AND DEVELOPMENT OF TURBOFAN NACELLE MODIFICATIONS TO MINIMIZE FAN-COMPRESSOR NOISE RADIATION

VOLUME II

ACOUSTIC LINING DEVELOPMENT

The Boeing Company
Seattle, Washington

SUMMARY

An acoustic lining development program was conducted (1) to determine acoustic lining concepts and acoustic lining facing materials suitable for application in a turbofan engine nacelle when noise generated by the fan compressor must be suppressed and (2) to expand the technology for designing acoustic linings.

From results of a lining concept study, a broadband resistive-resonator-type lining was determined to best suit engine fan duct and inlet installation requirements. Evaluations of more than 40 types of acoustic facing materials resulted in the selection of woven metallic fiber, metallic felt, reinforced metallic felt, and polyimide resin-impregnated fiberglass laminated materials, henceforth referred to as polyimide-fiberglass, as most suitable for acoustic linings in a turbofan nacelle environment.

A comprehensive acoustic-lining flow duct test program established lining separation distance, lining cavity depth, lining length, acoustic impedance, lining flow resistance, wall particle velocity, wall sound pressure level (SPL), and duct airflow Mach number as the most important design parameters that control the magnitude and the peak frequency of attenuation provided by a lining. Results of these tests also showed that metallic and nonmetallic linings having the same flow resistance and geometry will provide similar attenuation characteristics. Good correlation was obtained between the results of flow duct and full-scale engine tests.

Evaluations of various acoustic linings resulted in the selection of polyimide-fiberglass sandwich panels for use in the boilerplate fan duct development. Desired acoustic properties are provided by the close control of lining flow resistance that can be achieved with the material. Results of mechanical properties tests, environmental tests, and simulated operational tests indicated that the polyimide-fiberglass linings would be suitable as the basic structure in the turbofan nacelle environment.

A theoretical method for predicting lining attenuation in a duct without airflow was developed, which provided good agreement with experimental results. The theoretical

method was combined with an empirical prediction method, developed from parametric results of the flow duct tests, to establish a lining design procedure.

INTRODUCTION

Prior to this program, theoretical and experimental work had been initiated to acquire additional technology for predicting acoustic lining attenuation characteristics and for selecting suitable facing materials (refs. 1 and 2). A survey of available acoustic facing materials was in progress, and equipment for evaluating the acoustic materials and lining concepts had been partially developed. This prior work was used in establishing an evaluation criteria and provided a base for the more comprehensive materials development program described in this report.

The concurrent and interrelated investigations, which made up the materials development program, are described as is the facilities equipment used. One initial effort involved procurement of potential lining materials and the evaluation of their suitability for use in engine nacelle environments. Evaluations are presented, and materials selected as suitable are identified.

In addition to the description and results of a lining concept study, this volume presents the results of flow duct tests with a series of acoustic lining panels. Critical duct and lining parameters and their influence on the attenuation characteristics of the linings are identified.

The development of both a theoretical and an empirical method for predicting lining performance is described. Resulting design equations are presented, and their limitations are identified. A design procedure utilizing both the theoretical and empirical prediction methods is discussed.

Development of polyimide-fiberglass laminates for use in fabricating acoustic linings is described, and results of material properties tests are presented. The techniques used in fabricating the laminates (porous and nonporous) and in assembling the acoustic lining panels are outlined.

Finally, investigation results of the influence of turbine-generated noise on perceived noise levels of a turbofan engine are presented, together with a discussion of possible methods for attenuating this noise component.

SYMBOLS

a	boundary value of x coordinate, centimeters
A_N	attenuation, decibels
A*	normalized attenuation
b	boundary value of y coordinate, centimeters
B_T	number of turbine blades in 2nd, 3rd, and 4th stages
c	speed of sound, centimeters/second or feet/second
C_x,C_y	constants (wave equation solution)
c_z	phase velocity in z direction, centimeters/second
d	lining depth, inches
d_c	lining cavity depth, inches
dB	decibel
EPNL	effective perceived noise level, EPNdB
f	frequency, hertz
f_{bc}	band center frequency, hertz
f_n	center frequency of band number n, hertz
f_o	frequency at which $X_s = R_s$, hertz
f_p	frequency of peak attenuation, hertz
$*f_p$	frequency of peak attenuation at M = 0.28, hertz
g	gravitational constant
h	lining separation, inches
Hz	hertz (cycles/second)

j	imaginary operator, $\sqrt{-1}$
k	acoustic wave number, $\frac{2\pi}{\lambda}$
k_x, k_y, k_z	components of complex wave number in x, y, z coordinates
L	length, inches
m, n	duct mode harmonic orders
M	Mach number
N	number of components
N_1	low-pressure compressor rotor speed, rpm
p	rms acoustic pressure, dynes/centimeter^2
p(z)	rms acoustic pressure at duct station z, dynes/centimeter^2
PNdB	unit of PNL
PNL	perceived noise level, PNdB
R	flow resistance, universal gas constant, acoustic room constant
R_s	resistive component of acoustic impedance, rayls (cgs)
rayl (cgs)	unit of acoustic resistance, centimeter-gram-second
R_E	effective flow resistance at velocity u, rayls (cgs)
R_N	nominal flow resistance at velocity u = 25 centimeters/second (0.84 feet/second), rayls (cgs)
t	time, seconds
T	absolute temperature, °R
u	rms particle velocity, centimeters/second
u_s	velocity through a porous media, centimeters/second
U	velocity, feet/second

x,y,z	rectangular coordinates
X,Y,Z,T	variable functions of p (x,y,z,t)
X_S	reactive component of acoustic impedance, rayls (cgs)
Y_A	acoustic admittance, 1/rayls (cgs)
Z_S	acoustic impedance (specific), rayls (cgs)
α	wave number phase constant
α_N	normal incidence acoustic absorption coefficient
β	wave number propagation constant
γ	ratio of specific heats
η	normalized acoustic admittance = $Y_A \rho c$
κ	constant
ν	constant
τ	constant
ϕ	angle between direction of propagation and refraction, degrees
λ	acoustic wavelength, centimeters
μbar	microbar
ρ	density of air, slugs/foot^3
ω	angular frequency, radians/second

Subscripts

i	integer
∞	freestream

BASIC CONCEPTS FOR ATTENUATING SOUND IN DUCTS

One method of reducing radiation of fan-compressor-generated noise from a turbofan engine consists of introducing acoustical linings in the fan inlet and exhaust ducts. The attenuation of sound propagation in ducts with acoustically absorbing walls is influenced by characteristics of the lining concept used and of the porous facing material that forms part of the lining. A synopsis follows of the lining concepts and porous facing materials studied and of the procedure adopted to develop suitable linings.

Lining Concepts

Three basic concepts of resonator, resistive, and resistive-resonator linings (fig. 1) were considered potentially suitable for engine duct linings. The two resonator concepts shown in figures 1a and 1c consist of a thin sheet of perforated plate or porous material as a facing for the duct interior. Facing materials are spaced away from the duct walls to form a cavity, which provides the resonant property of the lining. The cavity is divided into compartments by an open cellular structure, such as honeycomb cells, to form a locally reacting impedance. Figure 1b shows a homogeneous resistive absorber consisting of a continuous-layer absorptive material.

Typical attenuation characteristics of the three concepts studied are shown in figure 1. The perforated plate and honeycomb combination is similar to an array of Helmholtz resonators. As indicated by the solid curve in figure 1a, the attenuation spectrum of this lining is that of a sharply tuned resonator, effective over a narrow frequency range when used in an environment with low airflow velocity or low SPL. This concept can provide a broader bandwidth of attenuation as shown by the dashed curve in figure 1a in a very high noise level environment where the particle velocity through the perforations is high.

The homogeneous layer absorber in figure 1b is effective over a wide frequency range, but the materials currently available were found unsuitable for use in an engine environment.

The broadband resistive-resonator concept shown in figure 1c was selected as the basic model from which to develop duct linings because it can provide substantial acoustic attenuation over a wide frequency range and was judged the most suitable concept for use in an engine environment.

Facing Materials

The basic acoustical characteristics of a facing material are its acoustic impedance and a related quantity known as flow resistance of the porous material. The influence of these two characteristics on the acoustic efficiency of duct linings was investigated in the study described in the following section. The study was initiated by surveying available porous materials potentially suitable for use as part of engine duct linings.

Development Procedures

Acoustic lining technology, as applied to the attenuation of turbofan engine-generated noise, was limited at the time this program was initiated. To extend the necessary technology, a materials development program was undertaken. The program was comprised of the following major areas of investigation conducted concurrently:

- Materials search
- Acoustic lining development
- Lining theory development

The materials search first required the selection of suitable porous materials for absorbing acoustic energy, available either commercially or by development for this particular purpose. Candidate materials obtained were evaluated against established criteria, initially through visual inspection of physical characteristics, and then by tests using a flow-resistance apparatus and an acoustic-impedance tube to determine the acoustic properties. The more promising materials were used in the fabrication of acoustic lining panels of a standardized configuration, which were tested in a flow duct facility. The flow duct facility, which simulates the environment of an engine fan duct, permits evaluating the influence of acoustic properties of the materials on the magnitude and spectrum of the attenuation achieved.

After selecting the most promising facing and honeycomb materials, the flow duct study investigated acoustic efficiency of various linings adaptable for duct linings. The study also acquired sufficient data to develop a parametric analysis of the major geometric and acoustic characteristics influencing the attenuation and attenuation spectrum of duct linings.

Concurrently, a theoretical study was initiated to develop an understanding of the basic physics of sound propagation and attenuation in lined ducts. The theoretical study was used to guide experimental work and was the basis for development of a method for predicting the attenuation of duct linings.

The most successful lining concepts from the flow duct study were incorporated in a full-scale engine experimental duct and tested. Results then were correlated with flow duct data.

The results from the parametric analysis of lining data, the full-scale engine tests, and the theoretical analysis were used to develop a lining design procedure. This procedure was used to select a fan duct lining configuration for further evaluation in a full-scale engine boilerplate fan duct. Figure 2 shows the interrelationship of the major phases of the materials and acoustic lining development program and the associated analyses and test activities.

ACOUSTIC EVALUATION METHODS

An evaluation of potential metallic and nonmetallic facings materials was made to define their important acoustic properties. The properties evaluated included flow resistance, acoustic impedance, absorption coefficient, and acoustic attenuation. Discussion of the properties evaluated and the apparatus used is presented in this section.

Flow Resistance

The specific flow resistance of a porous material is defined as the resistance per unit area to steady airflow through it. It is expressed by the ratio of the pressure differential ΔP across the material to the airflow velocity u_s through the material and is generally abbreviated "flow resistance."

$$R = \frac{\Delta P}{u_s} = \frac{\text{dynes/cm}^2}{\text{cm/sec}} \quad \text{[rayls (cgs)]} \tag{1}$$

This quantity is defined here as nominal flow resistance R_N when the velocity through the material is 25 cm/sec and as effective flow resistance R_E when the velocity has other values.

The flow resistance R measured in a flow-resistance tube with a steady airflow velocity u_s is approximately equivalent to the resistive component R_s of the impedance Z_s of a material subjected to acoustic waves having the same root mean square (rms) acoustic particle velocity u. A method for calculating the latter velocity from the acoustic pressure at the surface of a porous lining is given in equation (2).

$$u = \sqrt{\sum_{n=1}^{N} \left| \frac{p\,(f_n)}{R_s\,(f_n) + j\,X_s\,(f_n)} \right|^2} \qquad (2)$$

where:

u = rms particle velocity in the lining material

p = rms sound pressure at the lining surface

$R_s(f_n)$ = resistive impedance

$X_s(f_n)$ = reactive impedance

f_n = center frequency of band number n

N = total number of bands

$[R_s(f_n) + j\,X_s(f_n)]$ = acoustic impedance = Z_s

j = imaginary operator = $\sqrt{-1}$

The flow resistance of porous materials is measured with the apparatus shown in figures 3 and 4.

A test sample is secured in the test section by an annular clamp, and the steady flow resistance R is determined by measuring the airflow velocity through the sample with a metering flow tube. The pressure drop across the sample is obtained by a manometer measuring the pressure differential between the inside of the tube and the ambient atmosphere. Two test section tube sizes are used (3.8 cm and 10 cm) to provide measurement of flow resistance over a steady flow velocity at the face of the sample between values of 3 and 900 cm/sec.

Acoustic Impedance

Impedance tube.—A standard Bruel and Kjaer impedance tube was used to make measurements for computing the acoustic impedance of the porous materials and specimen sections of acoustic lining panels. Figures 5 and 6 show the tube and auxiliary equipment. The impedance of facing materials alone was obtained with a sample of the facing backed by an air cavity. The impedance of lining configurations was obtained with honeycomb spacer in the cavity. Specific acoustic impedance of the samples was derived from the measured acoustic standing wave ratio from which the complex ratio of the sound pressure to the normal particle velocity is computed at the surface of the test sample.

Acoustic energy dissipation.—The effectiveness of an acoustic lining in dissipating acoustic energy in a duct is dependent upon the resistive component R_S of its specific acoustic impedance Z_S. This quantity is defined as the impedance of a porous material to the oscillatory particle motion imposed by an oscillatory acoustic pressure. The specific acoustic impedance Z_S, generally abbreviated "acoustic impedance," has two components; namely, a resistive $R_S(f)$ and a reactive $X_S(f)$ component that are frequency f dependent. Acoustic impedance is expressed in the complex form $Z_S = R_S(f) + j\, X_S(f)$. The reactive component $X_S(f)$ is due to the inertia of the air in the facing of the lining and the stiffness or inertia of the air in the cavity behind the lining.

Absorption Coefficient

The normal incidence absorption coefficient of the porous materials and acoustic lining panels was derived from the measurements made in an acoustic impedance tube. The coefficient α_N is the ratio of the acoustic energy absorbed by the sample in the tube to the acoustic energy impinging on it.

Acoustic Attenuation

Three types of tests were conducted to determine acoustic attenuation properties of the facing materials and lining concepts. First, tests were conducted using the flow duct facility to determine the attenuation properties of various facing materials. Second, using the same flow duct facility, acoustic lining concepts were evaluated by means of acoustic lining panels. Third, the most promising lining concepts and facing materials were tested in the fan exhaust duct of a full-scale engine.

Flow duct tests.—Tests were conducted in the flow duct facility to measure the acoustic attenuation or power insertion loss of various panels faced with a number of selected facing materials. Power insertion loss is equal to the difference in the power spectra measured with a lined duct and an unlined baseline duct with the same noise and airflow input conditions. Since the sound power level in a reverberant chamber is equal to the logarithmic sum of the sound pressure level and a constant (characteristic of the chamber), the difference between sound power spectra is equal to the difference between corresponding sound pressure level spectra. In all the following work, therefore, the terms "attenuation" and "power insertion loss" are interchangeable.

To reduce the number of tests made with a given lining configuration, advantage was taken of the fact that the attenuation achieved in a duct 6 in. wide and lined on one wall was equal to that provided in a duct 12 in. wide and lined on two facing walls, thus reducing these tests by half. The facility used is described in the following section. The results obtained permitted parametric evaluation of geometric and acoustic characteristics of the linings.

Flow duct facility.—The flow duct facility was developed for evaluating acoustic characteristics of duct lining panels and facing materials. Test provisions included a range of high-velocity airflow through the duct test section with airflow and noise propagating in the same direction to simulate the fan exhaust ducts of a turbofan engine. A schematic diagram of the facility is shown in figure 7. A reverberant chamber provided a diffuse acoustic source for the test duct and also acted as a plenum chamber to ensure uniform airflow into the duct test section. The plenum chamber volume was approximately 45 ft^3. The large diffuser in the air supply line reduced the entry air velocity into the plenum chamber and hence improved the flow duct inlet aerodynamics. A bellmouth at the duct inlet ensured minimum aerodynamic distortion in the test section and minimized the generation of aerodynamic noise.

Three noise sources were available in the reverberation/plenum chamber.

- Aerodynamic noise generated by the air turbulence in the supply line
- A jet noise source to augment the above aerodynamic noise source
- An air-driven siren generating discrete tones over the frequency range from 2000 to 8000 Hz with a fundamental peak amplitude of 150 dB in a 1/10-octave bandwidth measured in the reverberation/plenum chamber

The test duct was connected to a calibrated semireverberant receiving chamber in which the total acoustic power transmitted through the duct was measured. The chamber volume was approximately 1750 ft^3 and was vented by an acoustically lined exhaust stack.

Three sizes of test section—6 by 10 in., 4 by 10 in., and 6 by 7 in. in cross section—were used in the test program. Wall positioning was adjustable to maintain constant working section dimensions for various thicknesses of lining treatments. The length of the lining test

panels could be varied from 0 to 44 in., the latter being the full length of one test section element. Longer ducts could be tested by bolting two or more test sections together. An S-bend duct, 24 in. long with a 6-in. offset, also was used for one test series. Lining panel test specimens could be mounted on any one of the four walls in the test section. Figure 8 shows the range of test section configurations used in the study. The maximum airflow velocity through the test section was Mach 0.45 in the 6- by 10-in. duct and Mach 0.65 in the 6- by 7-in. duct.

The majority of lining panel tests was conducted in the Boeing-Seattle flow duct facility; however, some tests in which the duct airflow direction was reversed were conducted in the Boeing-Wichita flow duct facility. The latter facility can be operated with air flowing the same direction as the sound propagation to simulate an engine fan duct as well as with air flowing in the opposite direction to simulate an engine inlet. The two facilities have the same basic acoustic and flow characteristics.

Test procedure: The acoustic evaluation of an acoustic lining panel configuration was obtained by the measurement of acoustic power in the receiving chamber with and without test panels installed in the flow duct.

Noise generated by the fan and compressor of a jet engine has both broadband and discrete frequency characteristics. Early tests, therefore, were conducted to determine whether linings responded differently to the two types of noise. Results showed no measurable difference in attenuation at siren frequencies of 1800 and 2700 Hz. It was concluded that duct linings absorbed equal amounts of acoustic energy for either broadband or discrete frequency noise in a given bandwidth. All subsequent tests were conducted using broadband noise inputs only.

Flow duct experiments were conducted at ambient laboratory temperature and pressure conditions; hence, for engine operating environments of other ambient levels, the design calculations must take into account changes in temperature and density, which are reflected in the effective flow resistance of the linings.

Duct wall pressure: Theoretical work indicated that the effective flow resistance of a lining increases with the magnitude of the rms particle velocity normal to the panel surface. The magnitude of this velocity is dependent upon both the acoustic pressure and the airflow turbulence pressure occurring at the lining surface. Wall pressure measurements were made to compute the rms particle velocity so that effective flow resistance (equivalently the resistive impedance) of the linings tested could be determined at the various test airflow Mach numbers. To measure the aeroacoustic spectra at the surface of porous laminates, microphones were wall-mounted close to each end of the test panels (40-in. separation). The microphone diaphragms were mounted flush with the laminate surface and without a diaphragm protective grid.

Aerodynamic measurements: To measure the horizontal and vertical velocity profiles in the duct test section, a traversing pitot tube apparatus was installed close to each end of

the test panels with a 40-in. separation along the duct. Tests to calibrate the facility showed low turbulence in the test section because of care taken with the aerodynamic design of the bellmouth inlet into the test section. Vertical- and horizontal-velocity profiles in the test section were uniform with a normal boundary layer growth along the test section walls producing a downstream boundary layer thickness of approximately 0.5 to 1 in. in the 6-in. duct. Turbulence and boundary layer effects on the acoustic attenuation in ducts were not studied separately.

Full-scale engine evaluation of acoustic linings.—Subsequent to the development of duct-acoustic-lining concepts using the flow duct facility, a number of duct-lining configurations were evaluated in a full-scale engine fan duct. This study provided data for selecting the most promising configuration for evaluation in a boilerplate version of the final flight nacelle. The study was conducted using the engine test facility described below. The acoustic attenuation properties of fan duct linings evolved from the earlier flow duct tests were determined.

Test configurations: Acoustic linings to be evaluated were installed in the constant-area section of an extended three-quarter-long fan duct. A constant treatment length of 50 in. was used for all configurations except two, which were 25 in. long and were tested to investigate the influence of lining length. The surfaces treated, in various combinations, were:

- Outer wall
- Inner wall
- Radial splitters
- Circumferential splitter (with a porous septum)

Nonporous blanking panels were fitted in the test ducts to maintain a constant flow area when some of the acoustically treated panels were not used (fig. 9). Two views of the fan discharge duct linings are shown in figures 10 and 11.

Full-scale engine facility: Tests to investigate the acoustic performance of duct linings installed in a full-scale engine fan duct were conducted using a Pratt & Whitney JT3D-3B turbofan engine. The basic engine with an existing short fan duct (fig. 12) was used as an acoustics baseline. The lining studies were conducted with an experimental three-quarter-long fan duct installation (fig. 13). Tests were conducted with a bellmouth inlet and also with an existing large blow-in door inlet.

Test site: A plan view of the test site (fig. 14) indicates the area was cleared of trees to ensure a good acoustic test environment. Figure 15 shows a general aerial view of the test site with the test engine and inlet noise directionalizer installed. The vertical array of microphones at a 75-ft radius was supported over the engine by the boom and a supporting

cable network. The horizontal array of microphones was located at a 200-ft radius (fig. 16).

Engine noise directionalizers: To isolate the aft-radiated noise, an inlet noise directionalizer was used to direct fan noise radiated from the inlet away from the aft microphone positions. Figure 17 shows a general view of the test installation with the inlet directionalizer in position. The acoustic treatment on the interior surfaces consisted of a 4-in.-thick fiberglass layer secured with a fine wire mesh screen. The directionalizer inlet had adjustable louvers for additional redirection of inlet noise and noise attenuation.

A jet exhaust directionalizer also was used in some tests to direct jet noise away from the aft-located microphone position. This facility consisted of a 37-in.-diameter circular duct fitting over the primary exhaust pipe nozzle and extending 40 ft aft of the exit nozzle plane. The section was terminated by a 20-ft length of duct inclined away from the microphone array at a 45° angle.

MATERIALS SEARCH

The materials search had as its end objective the selection of potentially suitable acoustic materials for use in turbofan nacelles. This activity was an extension of work initiated prior to the program which is reported in references 1 and 2. A survey of manufacturer/vendor sources of acoustic materials was completed. Material selection criteria and evaluation techniques were further developed and were used in determining the potential of material samples received. Development of a nonmetallic lining was undertaken as a supplement to the search for commercially available materials.

Manufacturer/Vendor Survey

Approximately 40 companies were contacted in the search for potentially suitable acoustic lining materials. Several hundred individual samples of metallic and nonmetallic materials were received for evaluation. A search also was made for suitable acoustic panel core materials and for bonding materials to be used in assembling the acoustic panels.

Evaluation Criteria

Acoustic material samples were compared to the following criteria as an initial step in selecting a suitable material.

- Structural integrity by visual inspection, bearing in mind the following operational environments: maximum flow velocity over the materials surface equivalent to a 0.8 Mach number; air temperatures from -50° to 450° F; and maximum spectral

SPL (1/24-octave bandwidth) of 160 dB. In general, continuous fiber construction was considered preferable to materials that are likely to disintegrate under high-speed airflow scrubbing, turbulent pressures, and vibration.

- Surface smoothness by visual inspection. A maximum surface smoothness was desirable to minimize drag effects.

- Nominal flow resistance within a range from 1 to 100 rayls (cgs).

- Absorption coefficient at normal incidence α_N with typical lining back space greater than 0.7 in the frequency range of interest, i.e., 2 to 8 kHz.

Materials meeting the specified criteria were further evaluated by measuring flow resistance over a range of airflow velocities, acoustic impedance, and duct lining attenuation characteristics.

Pratt & Whitney Evaluations

To supplement the standard impedance tube tests in which there is no airflow over the surface of the sample, a study was conducted to measure acoustic impedance of materials with one surface of the sample exposed to a flow of air to simulate the environment in an engine duct.

A subcontract for this work was given to Pratt & Whitney Aircraft Division of United Aircraft Corporation. A description of the work is given in reference 3.

Polyimide-Fiberglass Laminate Development

Concurrent with the search for suitable materials from external suppliers, an acoustic material study was initiated to develop a promising concept of a nonmetallic structural load-bearing material for manufacturing duct acoustical linings. The material developed was polyimide resin-impregnated fiberglass fabric (polyimide-fiberglass). The material was manufactured in multiple-ply laminates and could be made with nominal acoustic flow-resistance values in the range desired for acoustic lining purposes, namely from 1 to 100 rayls (cgs).

Suitable honeycomb core spacers also were developed in conjunction with manufacturers and were made from fiberglass fabric impregnated with polyimide resin. The laminates were bonded to the honeycomb spacers using the same resin. Details of the material manufacturing process and the laminate bonding to the honeycomb is described later in this report and in reference 4.

Results

Materials survey.—Of the materials obtained for evaluation, many were unsuitable as lining materials because of their brittleness, weakness, loose weave, and similar characteristics that rendered a material unsuitable for use in an engine nacelle environment. Other materials were judged unsuitable because of their poor capability to absorb sound.

Among the materials that were potentially suitable, the following four materials were considered most promising and were selected for the more comprehensive studies.

- Polyimide-fiberglass laminate
- Woven metallic fiber sheet
- Metallic felt sheet
- Metallic fiber and felt sheet

A summary of the most important materials tested and found suitable for duct linings is given in table I. This table also includes a materials description code. Typical results of materials judged unsuitable are given in table II. A summary of the desired characteristics of porous sheet materials resulting from this study are presented in table III. For convenience, table IV lists the porous materials evaluated in the study and the acoustical evaluation methods used. Survey results are summarized in references 1, 4, and 5, and detailed test data are given in reference 6.

Flow resistance.—For all the materials selected for testing, at least one measurement of flow resistance was made at the nominal flow-resistance (25 cm/sec) velocity. Representative samples of materials tested were then subjected to further testing of the variation of airflow resistance over the surface of the sample and variation of the flow resistance as a function of airflow through the samples.

Figures 18 and 19 show typical results of the flow resistance of metallic and nonmetallic materials found to be potentially suitable for acoustic linings. The change of flow resistance with particle velocity (above the nominal value measured at 25 cm/sec) varied greatly between materials; the reason for this effect is discussed below.

Acoustic impedance.—The acoustic impedance was measured for all samples of material selected for further study. Figure 20 is a representative example of the type of impedance data measured. Materials tested were broadly divided into two categories; namely, those with a generally high- and those with a generally low-reactive impedance component. The resistive impedance component of most materials was similar, and the value at very low frequencies was close to their flow-resistance value.

Tests of a variety of porous materials revealed that the increase in flow resistance with velocity through the material is strongly dependent upon the acoustic reactive impedance of the material. For example, woven metallic or wire screen materials have, in general, a low-reactive impedance and exhibit correspondingly small changes of flow resistance with increasing particle velocity through them. The nonmetallic resin-impregnated materials, however, such as polyimide-fiberglass fabric, have a comparatively high-reactive impedance and exhibit a larger change in flow resistance with an increase in particle velocity. Properties of perforated plates were studied in the Pratt & Whitney subcontract; it was found that the reactive impedance of porous plates was even greater than the nonmetallic materials tested.

Absorption coefficient.—The acoustic absorption coefficients of material specimens were calculated from impedance-tube data for typical lining cavity backing distances. The absorption coefficients of samples of the same material but with different nominal flow-resistance values were compared. In both the cases of metallic materials with a low-reactive impedance and nonmetallic materials with a high-reactive impedance, the absorption coefficient varied predominantly as a function of the nominal flow resistance alone. For a standard impedance tube SPL of 120 dB, low values of flow resistance [e.g., 4 rayls (cgs)] yielded low peak absorption coefficients (e.g., 0.4), whereas higher values of nominal flow resistance [e.g., 40 rayls (cgs)] yielded high peak absorption coefficients approaching a value of unity at the optimum frequency. Typical results are shown in figures 21 and 22. Testing of a 30-rayl (cgs) sample with SPL's up to 140 dB confirmed this observation (fig. 23).

Pratt & Whitney test.—The results of tests with more than 50 specimens of perforated plates, resistive materials (metallic and nonmetallic), and perforated plates backed with resistive material showed that the resistive component of the impedance and the flow resistance of the specimens both increased with increasing airflow velocity in the duct. These results confirm the trends observed with a flow-resistance tube at Boeing.

Details of the test procedure and full results of the subcontracted work are given in reference 3.

Conclusions

Flow duct data evaluation led to the conclusion that for a given set of duct environmental conditions the same acoustic attenuation could be achieved with any of the successful materials examined, provided that both the flow resistance and the acoustic impedance of the linings were identical at the particular environmental conditions and that the material sample panels were constructed with the same geometric dimensions. This result means that each type of thin porous surface material considered (i.e., resin-impregnated glass fiber fabrics, fiber-metal laminates, perforated plates, and woven wire screens) can work successfully. The selection of material for use as an acoustic duct lining, therefore, is more dependent upon its weight, cost, strength, and the manufacturing requirements. Each type of material, however, requires certain adjustments to the acoustic and geometric variables of the material and its support structure to achieve equal levels of noise reduction and compliance with

mechanical and economic constraints. Both the resin-coated glass cloth and the fiber-metal materials need about the same adjustment to meet flow-resistance requirements for a particular duct environment.

A comparison of the Pratt & Whitney results showed that perforated-plate material requires the greatest amount of adjustment and full-scale development testing to realize the full potential of its mechanical and economic features. This is because the increased rate of flow resistance for perforated plate is more nonlinear as a function of the particle velocity through it than that of other materials. Fine-pore perforated plate, not yet evaluated, may have more linear flow-resistance characteristics.

ACOUSTIC LINING EVALUATION

Flow Duct

Test configurations.—For the parametric study, panels were manufactured primarily from polyimide resin-impregnated glass fabric. Flow resistance and other parameters could be varied from panel to panel more readily than with metallic materials since the material was manufactured within the company. However, extensive investigations were conducted using metallic panel linings, and the results obtained with the two kinds of materials were correlated. More than 60 combinations of panel geometry and facing material were evaluated in over 300 tests. Single-layer lining panels were used for the main parametric study; however, other general panel concepts were also fabricated and tested.

The test program included variations of lining length and width, honeycomb cell size and depth, and the wall spacing in the flow duct test section. Overall panel dimensions were maintained constant within the following increments: 11, 22, and 44 in., respectively, in length and 7 or 10 in. in width. Panel cavity depths were varied from 1/4 to 1 in., and the honeycomb core cell size was varied from 1/8 to 1 in. Dimensions were selected to produce a peak attenuation spectrum in the 2000- to 2500-Hz range that simulated the peak fan noise measured in the JT3D engine fan duct. In addition to the variation of panel geometry, the lining-facing flow resistance was varied between a nominal flow resistance of 3 through 100 rayls (cgs). The tests were conducted at airflow velocities of M = 0.12, 0.19, 0.28, and 0.37.

Lining concepts evaluated included:

- Single-layer linings with a porous laminate separated by a honeycomb core with an impervious backing plate. A variety of geometric dimensions was tested.

- Double-layer linings with two porous laminates separated by a honeycomb core and the inner laminate spaced with honeycomb core from the impervious backing plate. Total core thicknesses up to 2 in. were tested.

- Slanted-core linings of both the single- and double-layer configurations
- Multiple wall treatments in which from one to four walls of the flow duct were treated with linings of equal length
- Mixed-depth, single-layer linings in which the duct was lined with single-layer lining panels having different depths on opposite walls
- Porous splitters to add acoustic absorption without appreciably changing the duct geometry
- S-bend curved-lined ducts

It was expected that double-layer linings would provide higher attenuation levels over broader bandwidths than obtained from single-layer linings. Early tests showed that the acoustic advantages were not so great as expected. Double-layer linings were heavier and more complex to manufacture, and this part of the test program was, therefore, less extensive than for single-layer linings. Most double-layer linings tested were of equal core depths with the outer laminate having a smaller flow resistance than the inner one [e.g., 10 and 40 rayls (cgs)].

The reactive impedance influence on acoustic performance of linings was studied by comparing attenuation spectra of geometrically identical panels with different magnitudes of reactive impedance.

Test results.—The flow duct test results are summarized here for single-layer linings and other lining concepts. Detailed test results are given in references 5 and 6, and the more important results in Appendix A of this report. In the tests, the influence of the various lining and duct parameters on the acoustic attenuation and its frequency spectrum were determined by varying a single parameter at a time. The parametric effects for single-layer linings were examined first.

Single-layer linings: Typical results of single-lining panel tests are given in figure 24, showing a comparison of attenuation spectra obtained with identical lining geometries but with different facing materials. The influence of duct and lining parameters were first examined for their effect on the attenuation frequency and then on the magnitude of the attenuation of duct linings.

Peak attenuation frequency was influenced by several parameters; the duct size or, equivalently, the lining separation had a major influence (fig. 25). As indicated, peak attenuation frequency is reduced from about 3 to about 2 kHz when the lining separation distance is increased from 4 to 12 in. The lining cavity depth also influences peak frequency, as shown in figure 25; increasing the depth from 0.25 to 0.75 in. decreases peak frequency from about 3 to 2 kHz in a 6-in. duct.

Honeycomb-core dimensions in the direction of airflow along the duct had only a small effect on peak frequency in the range of core dimensions tested (i.e., 1/4 through 1 in.).

Duct airflow velocity also influenced the frequency of peak attenuation, increasing it when the sound and airflow were in the same direction and decreasing it when in opposite directions. The general trend of frequency change with Mach number and airflow direction is summarized in figure 26. The magnitude of the reactive impedance of a lining changes the peak frequency with a large reactive impedance decreasing the frequency. The relationship between the peak frequency and the lining reactance is shown in figure 27 from which it is concluded that the nonmetallic linings evaluated in the program peak typically at a frequency 10 percent lower than the metallic linings, which have a lower reactive impedance.

The flow duct tests showed that the attenuation provided by a lining was influenced predominately by the following characteristics: lining length L, lining separation h, cavity depth d, flow resistance R, and airflow Mach number M. Honeycomb cell size and the reactive impedance X_s (f) had only a slight effect on attenuation.

A typical family of attenuation spectra obtained with various lining lengths is shown in figure 28. The attenuation spectra were examined for both peak frequency and 1-octave bandwidth attenuation. Care had to be exercised in the analysis of peak data because with the long lining lengths tested in the small ducts, the peak values often were distorted by the noise floor. The octave bandwidth attenuation for this study was defined by the maximum height of a rectangle, 1 octave wide, that could be fitted within the attenuation curve (fig. 28).

The influence of lining length on peak and 1-octave bandwidth attenuation is shown in figure 29. The data indicate that approximately the first 10 in. of a lining are the most effective in providing both peak and 1-octave bandwidth attenuation. Beyond this point, the rate of increase in attenuation with lining length is essentially linear. This effect is substantiated theoretically in references 7 and 8 in which it is concluded that the more oblique sound waves are rapidly attenuated in the initial portion of the lined duct, leaving grazing waves that attenuate at a slower rate in the remainder of the lined duct.

The influence of lining location in the duct was investigated by positioning a 22-in. length of lining on two walls at the upstream and downstream ends of the 44-in. test section. Varying lining position showed no difference in acoustic performance.

Lining separation was one important parameter influencing attenuation (fig. 30). Attenuation varied inversely with lining separation, and it was evident that large lined ducts are poor sound attenuators compared to small ducts.

The influence of the lining depth on attenuation is shown in figure 31. The data indicate that there is an optimum lining depth for maximum attenuation. This influence, in the limited range of sizes tested (1/4 to 1 in.), was greater on the peak attenuation than on a 1-octave bandwidth attenuation; namely, 5 dB over the range tested. An optimum cavity depth of 1/2 in. was found for the lining separation tested. Cavity depths smaller or greater than the above yielded less peak attenuation (fig. 31).

Various cell core shapes and materials were tested and found to have little or no influence on attenuation so long as the cell had a distinct cavity shape.

Airflow velocity in the duct was found to influence lining attenuation differently with respect to the inlet and exhaust modes. The effect of airflow velocity on the peak and octave-bandwidth frequency attenuation is summarized in figure 32. The data show that an increasing Mach number in the exhaust mode decreases the attenuation in both bandwidths, but decreases the peak and increases the 1-octave bandwidth attenuations in the inlet mode.

The influence of lining flow resistance on lining attenuation was demonstrated from the test results in two ways. First, variation of the nominal flow resistance (of an otherwise constant geometry lining) tested at a constant airflow Mach number showed that there was an optimum flow resistance for a given lining and duct geometry (fig. 33). Second, for a panel with a fixed geometry and fixed nominal flow resistance, the optimum effective flow resistance varied with the airflow Mach number and lining depth (fig. 34). Results also showed that the optimum value of flow resistance is dependent upon the frequency bandwidth of the attenuation (figs. 33 and 35).

It was found that for each duct environment, lining characteristics, duct dimensions, and rms particle velocity, an optimum flow resistance exists that produces maximum attenuation of sound for a given length of treatment. Optimum effective flow resistances for a combination of lining depths and lining separations are shown in figure 36.

The influence of the reactive impedance of a lining was twofold: first, for a given lining depth, an increase in reactive impedance decreases the frequency of peak attenuation; and second, for a given length of lining, an increase in reactive impedance tends to decrease the attenuation bandwidth (fig. 24).

The resistive component of the impedance R_s is closely approximated by the flow resistance R of the lining and both quantities are essentially independent of frequency. The reactive component $X_s(f)$ has an influence on the flow resistance of a lining by influencing the rms particle velocity.

From wall pressure measurements (fig. 37) made with linings of varying flow resistances and impedance characteristics, the corresponding rms particle velocities were computed using equation (2).

Wall pressure measurements at the lining surface contain combined effects of sound pressure variation and airflow Mach number variation. Figure 38 illustrates the corresponding particle velocities, computed by equation (2), for the range of Mach numbers tested.

Typical results of the calculations, showing the relationship between flow resistance and particle velocity for high- and low-impedance lining, also are included in figure 38.

Other lining concepts: Test results of other lining concepts are summarized as follows.

- Double-layer linings produced a characteristic attenuation spectrum with two attenuation peaks (fig. 39) where the level of the first peak is greater than the second and is associated in frequency with the total lining depth. The second peak could not be identified in a simple way with any combination of the depth dimensions of the double-layer panel. The increased attenuation resulting from double-layer as compared to single-layer linings of equal total depth appears in figure 40 and shows an increase in high-frequency attenuation. The additional attenuation increases with increasing total depth.

- Test results of slanted-core linings compared with normal upright-core linings showed that the peak attenuation frequency of slanted-core linings was determined by a factor intermediate to the normal and slanted depths. Upright-core linings provided more attenuation over a wider frequency range than the slanted-core linings.

- Attenuation of a fixed length of lined duct increased with the number of walls treated (fig. 41). It was evident that treating a second and opposite wall produced a substantial increase in attenuation (walls A + B in fig. 41), but treating the shorter sides, which had a greater lining separation than the first pair of linings, produced smaller increments of attenuation.

- Tests of single-layer linings with different depths on opposite walls showed a broader bandwidth of attenuation than linings with equal depths but with a lower peak value. Three examples (fig. 42) indicate the trend observed. In subsequent tests, it was found that two succeeding sections of lining with equal depths on opposite walls, but with different depths in each section, produced a broader attenuation bandwidth (15 percent wider at 6 dB down from the peak) and a higher peak attenuation (31 dB in lieu of 28 dB) than the examples shown in figure 42.

- The results of treated-splitter tests confirmed the prediction that a splitter without an impervious septum in the center would not effectively increase the attenuation of a treated duct. The treated splitters containing an impervious septum effectively reduced the duct width by half and provided an increase in attenuation.

- The few tests conducted with curved-lined ducts showed that this subject requires further study to produce valid results. Limited results obtained in the study were inconclusive.

- The NASA-Langley duct linings tested had acoustic characteristics similar to other linings tested that had the same total lining depth and flow resistance.

Full-Scale Engine

Test program.—Acoustics tests conducted during the program are described in table V. Test conditions were controlled to corrected low compressor rotor speeds. Five test conditions fell within the following ranges: low compressor speed N_1 of 3800 to 6650 rpm and static gross thrust between 4000 and 17 500 lb.

In tests where acoustic or blanking panels were added to the radial splitters, the reduced duct flow area affected the engine aerodynamic match at thrusts over 12 000 lb.

At each test condition, acoustic data were recorded after 3 min of engine stabilization time. Engine performance data were monitored for 5 min. Performance parameters recorded were N_1, N_2, P_{amb}, $P_{T_{2.5}}$, P_{T_7}, T_{T_7}, thrust, ambient temperature, humidity, and wind.

Each test condition was repeated at least three times. Baseline tests were conducted periodically throughout the program to ensure that the test vehicle, test site, and acoustic instrumentation were producing consistent data. They were conducted with the existing short fan duct configuration. A full description of data recorded during the tests is included in reference 1.

Details of the linings tested are given in table VI. Each outer wall, when treated, consisted of a double-layer lining treatment. Configurations 1 through 13 (fig. 9) were tested with acoustical linings manufactured from metallic felt (material D). In addition, configuration 1 was also tested with linings made from polyimide-fiberglass (material A). All honeycomb cells were constructed from resin-impregnated paper.

The metallic felt had the following characteristics: 0.040-in.-thick fiber, 50 rayls (cgs) for single linings and the interior linings in double-layer configurations, and 10 rayls (cgs) for external linings in double-layer configurations.

The polyimide resin-impregnated fiberglass cloth linings consisted of three-ply laminates having a flow resistance of 25 rayls (cgs) for single linings, 40 rayls (cgs) for inner double-layer linings, and 8 rayls (cgs) for outer double-wall linings.

Test results.—Following is a summary of acoustic data obtained from full-scale engine tests.

- Table VII shows typical octave-bandwidth data and perceived noise level (PNL) obtained for the baseline untreated engine nacelle measured at 200-ft horizontal radius and 75-ft vertical radius. The latter data are extrapolated to a radius of 200 ft by correcting for spherical divergence and atmospheric acoustic absorption effects in accordance with reference 9. The data are for the three engine conditions of 3800, 5000, and 6100 N_1.

- Typical 1/24-octave bandwidth spectra are shown in figures 43 and 44 for engine N_1 of 5000 and 5700, respectively. These data were measured with the unsuppressed baseline engine, with treatment configuration 7, and without the jet exhaust elbow directionalizer. These spectra have been selected as an example of data because they show the maximum attenuation of fan noise achieved in the test program, using configuration 7 (fig. 9). The potential limitation to noise reduction due to turbine-generated noise also is indicated in figure 43 and is discussed in further detail in Appendix C. Figures 43 and 44 show the combined primary and secondary jet noise spectra that were predicted using the method described in reference 10.

Analysis of results: The octave bandwidth SPL having the largest influence on PNL is that containing the high-SPL fan-generated discrete-frequency components (ref. 11). In the case of the JT3D engine, the fan discrete frequencies were in the 7th-octave bandwidth (2400 to 4800 Hz). Therefore, data were analyzed in terms of this octave SPL and in terms of the corresponding PNL for the engine noise spectrum. This form of analysis permits selection of the most efficient lining configuration for further testing in the boilerplate fan duct.

The attenuation measured in the 7th octave for each lining configuration was plotted for the azimuth of peak fan noise radiation (100° to 140°), and the corresponding PNL was computed. Typical data are shown for the mean approach power conditions (N_1 = 5000 rpm) in figure 45. The most efficient lining treatment results are summarized in figure 46. Data show the relative 7th-octave SPL and PNL at two approach power conditions and the relative acoustic-attenuation merits of the best lining configurations evaluated. From these data, the following comments on the relative merits of lining location are drawn:

- Inner wall—Configurations 1 (outer wall) versus 2 (outer and inner walls) did not show an appreciable increase in the attenuation due to the inner-wall treatment, but configurations 7 (outer and inner walls and splitters) versus 10 (outer wall and splitter) showed an increase of 3 dB due to the inner-wall treatment.

- Radial splitters—Configurations 1 (outer wall) versus 10 (outer wall and splitters) and 2 (outer and inner walls) versus 7 (outer and inner walls and splitters) show an improvement of 3 dB due to treatment of the radial splitters.

- Circumferential splitters—Configurations 7 (outer and inner walls and splitters) versus 9 (outer and inner walls, splitters, and circumferential splitters) show a small gain in attenuation of 1dB, but it should be noted that these splitters did not contain an impervious septum.

The influence of lining treatment length on attenuation is shown in figure 47. Configurations with two walls treated and with four walls treated show that a doubling of the treatment length from 25 to 50 in. increased attenuation in the 7th-octave bandwidth by approximately 6 dB and decreased the PNL by approximately 3 PNdB. Also, in both cases, the initial portion of the treatment provides the greatest noise attenuation contribution.

Finally, the acoustical attenuation provided by metallic felt (material D) and nonmetallic polyimide-fiberglass (material A) linings is compared in figure 48. The analysis in terms of 7th-octave ΔdB and ΔPNdB showed that the polyimide-fiberglass lining chosen for these tests provided more attenuation than the metallic felt linings.

The full-scale tests showed that a reduction of 12 PNdB of aft-radiated fan noise was achieved with a lining treatment 50 in. long and with all sides of each duct channel treated. This configuration was selected, therefore, for further development and testing in the full-scale engine boilerplate fan duct.

Turbine-generated noise: During the acoustic study of noise radiated from a JT3D turbofan engine, turbine-generated noise was detected (figs. 43 and 44). A detailed investigation of turbine noise was conducted to identify the source more precisely and to establish its effect as a potential noise floor in the study of the reduction of aft fan noise. A summary of a separate investigation on the effect of this noise on the reduction of perceived noise is given in Appendix C.

DEVELOPMENT OF LINING TECHNOLOGY

Results of the lining development study were used in conjunction with a theoretical analysis to develop a method for determining the sound-attenuation characteristics of duct linings. Lining design curves were developed from a correlation of full-scale engine and flow duct test results.

Development of Lining Theory

Concurrent with experimental work, a theoretical study was conducted to develop methods for predicting sound attenuation by duct linings. As various theoretical concepts

and models were evolved during the program, they were verified with experimental tests in the flow duct facility. Conversely, some of the experimental results were interpreted using the theoretical work developed.

The theoretical method (refs. 1 and 7) for attenuation without airflow was solved by means of a computer program. The solutions are for acoustically lined straight ducts having various cross sections ranging from rectangular to concentric segments, with particular application to turbofan engines.

The theory is based on the linear wave equation and was solved by separating the variables so that the attenuation of each acoustic mode propagated in a duct is computed. The total attenuation in the duct was obtained by summing all the modes and dividing the pressure wave into the sum as follows:

$$p = \sum_{i=1}^{\infty} a_i X_i Y_i Z_i T_i \tag{3}$$

where X, Y, Z, and T are functions of the coordinates x and y across the duct, z along the duct, and time t alone, respectively, and the values of the constant a_i are chosen to describe the sound waves at the duct entrance. Considering for example the fundamental blade passage frequency of a fan, the solution is related to a single frequency component, and the Z-dependent part of the solution represents a wave moving down the duct (shown in App. B, fig. B-1) as:

$$Z(z) = \exp(-jk_z Z) \tag{4}$$

where $k_z = \alpha + j\beta$.

The solution of the theory is in the form of sound attenuation along the duct between stations z_1 and z_2 expressed in decibels as:

$$A_N(z_2 - z_1) = -8.68(z_2 - z_1) \tag{5}$$

Appendix B summarizes the development of theoretical work and the basic assumptions.

A theoretical study to predict attenuation of sound propagation in a lined duct without airflow also was conducted by Pratt & Whitney under subcontract. Results of this study were compared with experimental results from flow duct lining tests; there was limited agreement between predicted and measured attenuation outside the range of the peak attenuation frequency, but little agreement in the peak frequency region. Modifying the

theoretical predictions by means of an empirical formula improved the agreement with experimental results. However, further work is required to refine the prediction method and to include the effects of airflow velocity. A full description of this work is given in reference 3.

Parametric Analysis of Lining Data

The parameters showing the greatest influence on attenuation and frequency of peak attenuation were further analyzed to develop a basic lining technology for designing engine duct linings.

Parameters of greatest influence were:

- Lining cavity depth d
- Separation between lined surfaces h
- Lining length L
- Duct airflow Mach number M
- Sound pressure p
- Particle velocity at walls u
- Specific flow resistance R_s
- Specific acoustic impedance Z_s

The relationship between the first group of four parameters d, h, L, and M have been combined into two empirical equations, which permits predicting a lining attenuation spectrum from a given duct geometry, or, conversely, the geometry required to yield a desired attenuation spectrum. The empirical prediction method is described in the following section and is based upon reference 6.

The relationship between the next four parameters p, u, R_s, and Z_s is discussed in the subsequent section.

Empirical prediction method.—The parametric results involving d, h, L, and M have been summarized in an empirical form suitable for preliminary design calculations. Subsequent refinement and optimization of lining design can be accomplished by model tests or more complex theoretical analysis. A principal difficulty encountered to date with theoretical models has been an inability to account for the influence of airflow effects. Also, analytical methods are so complex at present that their solution requires the aid of computers

and some of the results require verification by experiment. The following empirical prediction method, developed from the flow duct results, is valid over the range of duct sizes from 4- to 12-in. lining separation, lining cavity depths from 1/4 to 1 in., and flow Mach numbers from -0.4 to 0.4 that are representative values of the parameters for low-bypass-ratio turbofan engines. A positive Mach number refers to air flowing in the same direction as the sound propagation, and a negative Mach number to air flowing against the direction of sound propagation.

Influence on frequency: The influence of the parameters on the attenuation spectrum was derived as follows. First, the combined influence of the lining depth d and the duct size h (lining separation distance) were evaluated for a typical flow Mach number M (fig. 25). A parabolic function for the variation of peak attenuation frequency f_p with h and d was derived. To improve the fit of the function, a linear variation of the vertex h_{min} of the parabolas with lining depth d was introduced in the form:

$$h_{min} = -5.3d + 19.3 \tag{6}$$

From the data in figure 25, it was found that h_{min} varied with lining depth as

$$f_{p_{min}} = 1530\,(d - 1.2)^2 + 1200 \tag{7}$$

Similarily, the peak frequency $^*f_p$ was a function of the duct size in the form

$$^*f_p = \kappa\,(h - h_{min})^2 + f_{p_{min}} \tag{8}$$

where:

$^*f_p$ = f_p at M = 0.28

κ = a constant

A linear variation between Mach number and f_p was introduced, representing an average value for the range of duct sizes and lining depths:

$$f_p = 800\,M + (f_p \text{ at } M = 0) \tag{9}$$

$$\text{i.e., } f_p = {}^*f_p + 800\,(M - 0.28) \tag{10}$$

Substituting equations (6), (7), and (8) into (10) and evaluating κ from experimental results (i.e., $\kappa = 4.86$), the final expression for peak attenuation frequency was obtained:

$$f_p = [4.86\,(h + 5.3d - 19.3)^2 + 1530\,(d - 1.2)^2 + 800\,M + 980],\ \text{Hz} \tag{11}$$

$$\text{for } 0.25 \leqslant d \leqslant 1.0 \text{ in.},\ 4 \leqslant h \leqslant 12 \text{ in.},\ -0.4 \leqslant M \leqslant 0.4$$

When the above quadratic equation is solved for either h or d, the smaller value is the correct answer. Equation (11) fits well with experimental results.

Duct linings in turbofan engines usually are required to provide broadband coverage because of the unsteady characteristics of engine noise as well as the variation of engine speed in operation. The relation of bandwidth center frequency f_{bc} to peak attenuation frequency f_p was found to vary with attenuation bandwidth as shown in figure 49. This relationship may be used to modify the results obtained from equation (11) to cover a range of attenuation bandwidths.

Although equation (11) was derived for linings of high-reactive impedance, it also is applicable to low-reactive impedance linings provided a correction accounting for the change of reactance is made. Some information on the effect of reactive impedance was obtained by comparison of experimentally measured and theoretically predicted attenuation spectra at low Mach numbers. The analysis showed that the peak frequency for low-reactance linings was increased by the amounts shown in figure 50. Results for linings 0.5 to 1.0 in. deep collapsed on a single curve and correlated well with the experiment.

Influence on attenuation: Parametric results also were summarized in a similar manner to obtain an estimation of lining attenuation. The basic equations were developed for units of length in inches and for 1-octave bandwidth. A supplemental method is used to account for other bandwidths and effects of airflow velocity and direction of flow. It was assumed that lining width did not influence attenuation in rectangular ducts provided the width was approximately twice the lining separation distance or greater.

A composite summary plot of attenuation for varying lining length and duct size was made, which showed that for lining lengths greater than 10 in. a linear variation of attenuation was observed with different slopes for each duct size converging to a 4.5-dB value on the ordinate. Hence, it was assumed that attenuation A_N varied as

$$A_N = \frac{dA_N}{dh} L + 4.5 \text{ dB} \tag{12}$$

where dA_N/dh is the rate of attenuation change and varies with lining separation distance h. A curve of the form shown in equation (13) fitted the experimental data:

$$\frac{dA_N}{dh} = \nu 10^{\tau h} \tag{13}$$

The two constants ν and τ were found to be $\nu = 1.26$, $\tau = -0.09$. Hence,

$$\frac{dA_N}{dh} = 1.26 (10^{-0.09h}) \tag{14}$$

By substituting equation (9) into (7)

$$A_N = 1.26\,(10^{-0.09h}) + 4.5 \text{ dB} \tag{15}$$

for $L \geqslant 10$ in.

Variation in attenuation with lining depth was adjusted by means of the normalized curve of experimentally measured data where

$$A^* = \frac{\text{attenuation for depth d}}{\text{attenuation for d = 0.5 in.}}$$

The parabolic function

$$A^* = 1.06 - 0.96\,(d - 0.75)^2 \tag{16}$$

was developed from experimental data to correct for depth effect of lining depths between 0.25 and 1.0 in.

Multiplying equations (15) and (16)

$$A_N = [1.26\,(10^{-0.09h}) + 4.5] \times [1.06 - 0.96\,(d - 0.75)^2], \text{ dB}$$
$$\text{for } L \geqslant 10 \text{ in.}, \; 0.25 \leqslant d \leqslant 1.0 \text{ in.}, \; 4 \leqslant h \leqslant 12 \text{ in.}, \; 0 \leqslant M \leqslant 0.4 \tag{17}$$

where A_N = attenuation for 1-octave bandwidth.

Results from equation (17) checked well with experimental data.

The usefulness of equation (17) was expanded to cover the full range of inlet and exhaust Mach numbers as well as attenuation bandwidths by using the information in figures 51 and 52 where attenuation normalized with respect to equation (17) is shown as a function of Mach number and bandwidth.

Impedance and flow resistance.—The influence of the second group of parameters (p, u, R_S, and Z_S) on the attenuation spectrum is discussed in terms of the effects on frequency and attenuation, respectively.

Influence on frequency: The acoustic impedance of a lining, represented by $Z_S = R_S(f) + j\,X_S(f)$, has an influence on the peak attenuation frequency as follows. The resistive component of the impedance R_S is almost frequency-independent with the exception of its effect on lining depth and lining separations. The reactive component $X_S(f)$, however, is strongly dependent upon frequency and a variation of this quantity has a substantial effect on the peak frequency of attenuation. Results from identical linings tests with different reactive impedances disclosed a change in peak attenuation frequency as shown in figure 24.

The attenuation of metallic linings with a low-reactive impedance peaked at a higher frequency than nonmetallic linings or perforated plate with a high-reactive impedance. Influence of the reactive impedance on the frequency is shown in figure 27.

The flow resistance R of a lining is a close approximation to the previous resistive impedance R_S, and its effect on the frequency of peak attenuation has been small enough to be disregarded in predictions of the attenuation spectrum of linings.

Influence on attenuation: The magnitude of the reactive impedance of a lining affects the attenuation indirectly through its influence on the peak frequency. Because the attenuation of low-reactance linings peaks at a higher frequency than high-reactance linings, it is necessary to retune the latter by changing the cavity depth to obtain the same peak attenuation frequency. Because an optimum attenuation occurs at a given lining cavity depth, an adjustment of the high-reactance lining to a shallower depth to achieve the same peak frequency results in a decrease in attenuation. This means that a fixed length of low-reactance lining is 10 to 15 percent more effective than a high-reactance lining, but high-reactance linings have the advantage of a smaller cavity depth to attenuate a given frequency. Hence, they hold this dimension to a minimum. The latter feature makes a high-reactance material more desirable for such applications as lined splitters in ducts and lined inlet guide vanes or rings.

Flow duct tests revealed that the attenuation of a given fixed configuration varies substantially with linings having different flow resistances (fig. 33). Upon further investigation, it was found that the effective flow resistance R_E (or resistive impedance) of a porous-wall lining varies with the magnitude of the particle velocity u normal to it. This velocity is determined by the sum of the acoustic pressure p of the sound pressure impinging on the lining and the aerodynamic pressure fluctuations generated by the turbulence in the air flowing along the duct, which, in turn, is proportional to the airflow velocity along the duct. Furthermore, this resistance is dependent upon the reactive component of the acoustic impedance (fig. 38).

Flow Duct–Engine Data Correlation

Lining configurations.–An analysis was made to correlate the acoustic attenuation obtained with an identical duct lining configuration tested in the flow duct facility and in the full-scale engine fan duct. Figure 53 shows principal duct configuration dimensions tested. One wall was lined with a double-layer treatment (outer fan duct wall), and the remaining three walls with single-layer treatments. The configuration corresponds to configuration 7 (fig. 9) tested in the full-scale engine experimental fan duct.

Test conditions.–The test conditions in the two duct environments were as follows. The airflow Mach number was 0.28 in both cases, corresponding to an approach power

condition for the engine. The SPL in the 3rd-octave bandwidth, containing the fundamental fan blade passing frequency, was 142 and 138 dB, respectively, in the engine fan duct and the flow duct.

Correlation of results.—The engine duct data were corrected for wall SPL and duct cross-sectional area, and the flow duct data were corrected for treatment length. Relative attenuations measured in the two facilities, when corrected, were in good agreement (fig. 54). It should be noted that only one lining configuration was evaluated in this manner at a single engine power condition. The results are fully described in references 1 and 2.

Design Technology

A technology for designing duct acoustical linings was developed from theoretical and experimental data discussed earlier in this section. The basic information required for designing a duct lining is:

- Frequency spectrum to be attenuated
- Required magnitude of attenuation
- Duct airflow Mach number
- Duct wall rms pressure or SPL

The length of duct lining and the separation between lined surfaces, needed to achieve the noise attenuation objective, are dependent upon the duct geometry needed to meet aerodynamic requirements of the engine. Application of the design procedure is summarized as follows.

First approximation.—As a first step, the relationship between duct geometry (selected for aerodynamic reasons) and the acoustic attenuation is determined using the computerized theoretical method. The program can rapidly produce a large number of order-of-magnitude attenuations of the input noise spectra for a range of duct cross-sectional dimensions, lining depths, and lining lengths, assuming there is no airflow in the duct.

From computer study results, a duct geometry and acoustic lining design can be selected that will satisfy both the aerodynamic and acoustic requirements.

Second approximation.—Having established a duct geometry, a more realistic estimate of the attenuation spectrum is obtained. The empirical prediction method is used to estimate the attenuation of a selected duct geometry, which also includes the influence of the duct airflow Mach number and the particular characteristics of the linings tested in the flow duct.

Lining area.—The final lining configuration (number of walls treated and lining length) is selected from duct-attenuation design curves, which were developed from flow duct data combined with full-scale engine test data. This process corrects flow duct data for the following engine environmental effects: airflow-velocity profile distortion, engine duct-lining manufacturing variations and discontinuities, thermal gradients, and duct curvature. Two sets of design curves were developed for two-wall and four-wall lining configurations for a range of airflow Mach numbers. The data shown in figures 55 and 56 are for the case of M = 0.3.

Lining depth.—Linings depths are selected by an iteration process based upon the depth obtained from the empirical prediction method and the selection of combinations of lining depths for the various duct walls required to achieve maximum attenuation for a minimum lining length.

Flow resistance.—A general optimum value of flow resistance for all linings cannot be specified since the optimum value has been shown to depend upon several pertinent variable parameters for a particular application. To determine a particular optimum flow resistance, a knowledge of the rms particle velocity at the lining surface was required. This velocity is computed either from wall transducer measurements, made in an experimental engine duct, or from predicted values derived from estimates of the acoustic spectrum and the aerodynamic turbulence spectrum in the engine ducts. The optimum flow resistance then is obtained from data similar to figure 38. Alternatively, the optimum flow resistance can be obtained from parametric data (figs. 35 and 36), which requires a knowledge of duct and lining dimensions as well as the pressure spectrum at the duct wall.

Flow duct evaluation.—The final duct-lining configurations evolved from the previously described lining-design method were evaluated in the flow duct facility prior to the manufacture of full-scale boilerplate-treated ducts for evaluation on a full-scale engine test rig.

POLYIMIDE-FIBERGLASS SANDWICH MATERIAL PROPERTIES AND FABRICATION TECHNIQUES

Polyimide resin-impregnated fiberglass fabric laminate face skins and honeycomb core were selected for the acoustic sandwich material for the boilerplate fan duct and the flight-worthy treated nacelles (fig. 57). Prime reasons for this selection were the following.

- As a noise attenuation material, its capabilities were as good as any material evaluated. In addition, it has the advantages of close-tolerance control of acoustic skin porosity and easy variation in porosity with length of treatment, which optimizes attenuation.

- Polyimide-fiberglass sandwich material offered good structural properties, thus obviating the need for separate structural support. Also, it possessed good strength retention when exposed to the high temperatures of engine environment.

- It had good resistance to sonic and structural fatigue.

- It had good resistance to contaminants in the engine environment.

- The sandwich panels could be readily fabricated into complex curved surfaces.

- Polyimide-fiberglass appeared to have good life potential.

Material properties data and fabrication technology for polyimide materials were developed to provide the necessary level of confidence in the selection. These are presented in the sections that follow.

Material Properties

Polyimide resins are thermosetting, organic polymers with excellent elevated temperature properties that are synthesized from dianhydride and a diamine. Their thermal stability is attributed to the aromatic components in their structure. When glass fabric is impregnated with polyimide resin, the resulting material is called "prepreg" and can be procured in a variety of cloth styles. The prepregs procured were in a partially cured stage, which creates a relatively stable, if transitory, condition of the impregnating resin. A partially cured prepreg has reasonably tolerant handling requirements and relatively good shelf life when stored at temperatures below 40° F. Subsequent heating of the resulting laminate during the fabrication process results in cross-linking of the polyimide structure and excellent adhesion between the various glass fabric layers of the laminate.

Structural polyimide sheet and solid members are formed by laminating prepreg glass fabric. A typical five-ply acoustic laminate, sectioned to show the laminate construction, is shown in figure 58. Typical prepreg layers are laminated to the desired thickness on a tooling surface with the required geometry. No adhesive, other than that contained in the prepreg, is required. This assembly is cured at 350° F in a vacuum environment to ensure removal of volatiles, which is essential to achieving the required physical properties. Postcuring at 500° F in an air-circulating oven achieves the desired elevated temperature properties of the laminate.

The desired laminate strength, acoustic porosity, and surface roughness limitations influence the choice of prepreg cloth style for each of several plies and their arrangement within the finished laminate. Figure 59 indicates the general tensile strength ranges that have been achieved for porous laminates of three to six plies and their acoustic flow-resistance ranges in rayls (cgs). For use on the treated nacelle, rayl (cgs) values from 9 to 34 were of

primary interest. It can be noted that the greater the number of plies of prepreg, the higher the strength and rayl (cgs) value. The range of strength and flow resistance possible within a given number of plies is directly due to (1) the choice of prepreg cloth weave and yarn and (2) relative angular orientation of the warp direction of each ply. Figure 58 shows the variation in cloth styles and their angular orientation for a typical porous laminate. The angle of warp orientation for any single ply may range from 0° to 45° relative to that of the first ply; thus, within the limits of work to date, design of a laminate to specific porosity and strength requirements is largely an empirical process. By careful control during the manufacturing process, it has been possible to hold porosity to within ± 3 rayls (cgs) of the nominal for laminate areas up to 50 ft^2. To satisfy aerodynamic requirements for surface smoothness, a relatively fine cloth weave prepreg is normally selected for the outer ply, which is located adjacent to the airflow. Tooling is designed to have this outer ply in contact with the tool surface in the laminate layup process. Nonporous laminates are of simpler construction. Strength being of primary concern, a single, tightly woven prepreg is laid up at constant fabric warp angle to the desired thickness and strength.

Figure 60 shows the variation of tensile strength of polyimide-impregnated glass fabric laminate with respect to temperature for several porous and nonporous laminates. The superior strength retention at elevated temperatures of polyimide laminates as compared to epoxy laminates is clearly indicated. Figures 61 through 63 show, respectively, the variation of compression strength, tension modulus, and interlaminar shear with temperature of several porous and nonporous polyimide resin laminates. Figure 64 shows the tensile fatigue properties for both porous and nonporous laminates at room temperature and at 500° F.

Unlike polyimide prepreg, honeycomb-core materials formed of polyimide-impregnated glass fabric are supplied in the final cured state. The core is formed of prepreg sheets that are joined at the node bond lines at each cell with a polyimide adhesive. Additional polyimide resin is added by dip coating for increased strength. Core is presently available in nominal densities of from 2 to 7 lb/ft^3 and 3/16- to 1/2-in. hexagonal cell sizes. Design requirements for the treated nacelle are met by 7 lb/ft^3 and 3/8-in. cell size core. Figure 65 shows the variation of core inplane shear strength as a function of temperature. Bias weave arrangement of the glass fabric provides for maximum strength. Figure 65 also shows shear strength variation with temperature of the polyimide adhesive for adhesive bonds between the laminate and the core. Comparison of adhesive shear strength to that of the core shows that sandwich-panel strength is currently limited by adhesive strength and the need to restrict the amount of adhesive used to minimize the loss of porosity. It may be inferred from figure 65 that selection of a slightly lighter core density for the treated nacelle could result in a weight reduction while meeting structural design requirements. This consideration would be significant in a possible production airplane application. Liquid adhesive is used to join both porous and nonporous laminate skins to core surfaces and solid laminate members and is used more extensively than the other types. It is applied by roller coating core surfaces to achieve an adhesive fillet of approximately 1/16-in. width. This limitation is a compromise between strength requirements and maintaining adequate porosity of acoustic laminates. Film adhesive may be used in place of liquid adhesive to join nonporous laminate

skins and solid members to core. Since it can be placed in the joint as a sheet, it is easier to apply and provides uniformity in bonding. It is not acceptable for use in the bonding of porous laminate due to the effect on porosity. Both tape and pourable foam adhesives are available and are used for potting honeycomb core, joining of solid members to core, and core splicing.

Influence of Environment on Material Properties

The effect of environmental exposure on mechanical properties of typical porous and nonporous laminates and sandwich panels was determined from tests in which both laminates were subjected to skydrol and humidity environments and produced negligible changes in material strength properties.

Sandwich panels were subjected to test environments where the exposure was typical of flight environment. Typical panels, assembled in the manner of the treated nacelle fan ducts, were subjected to a severe sonic fatigue environment for a 25-hr period. Figure 66 shows the test specimen configuration. The acoustic input was essentially a flat sound spectra from 60 to 850 Hz at an average level in excess of 160 dB. Panel resonances were not sharply defined, and the maximum wall deflections were less than 0.01 in. There was no evidence of fatigue failure, and sandwich test specimens prepared from test panels revealed no degradation of material properties when compared to control specimens.

Typical panels also were subjected to approximately 1000 cycles of a test environment simulating conditions that would be encountered in flights between Seattle, Hawaii, Fairbanks, and return to Seattle. The test facility is shown schematically in figure 67. The test was designed to provide panel exposure to the extremes that could be encountered during 4000 hr of flight time. Test parameters, which were simultaneously controlled, include temperature and pressure in accordance with the figure 68 schedule, moisture content, airflow across the surface, and noise within the duct. The test specimens were monitored for change in deflection under load, weight, and visible deterioration. The results of structural tests on specimens made from the test panels indicate no change in weight or material properties.

In addition, typical sandwich-panel specimens were completely filled with water and then frozen, and it was determined that sandwich panels could be damaged in this manner. As anticipated, the bond between the porous laminate and the core was broken. However, in order to achieve failure, the core had to be completely filled with water. Partially filled specimens did not fail in the test. Moreover, the only way in which the sandwich could be completely filled required complete submersion of the specimen in a vacuum chamber. Efforts that failed to fill the cells included pressurized spray for 1 hr followed by ultrasonic vibration while submerged in water for 1/2 hr. Although it was concluded that the possibility of sandwich failure due to freezing of an undrained panel was extremely remote,

all inlet sandwich panels incorporate water-drainage provisions. The drainage path is provided by cross-linking the core cells with notches located adjacent to the laminate. Some minor acoustic performance deterioration results from installation of these water-drainage provisions.

A typical glass fabric polyimide sandwich panel was further tested to determine its characteristics when exposed to fire. The nonporous laminate side of the sandwich panel was exposed to a 6-in.-diameter flame at 2000° F for 30 min. The panel was not under load during test. Cracks began forming in the laminate after 3 min of exposure. Local distortion and cracks continued to propagate slowly with time. Figure 69 shows the panel after a 30-min test. The panel was in remarkable condition with no evidence of delamination or penetration through the second laminate face.

A test of a typical polyimide glass sandwich panel equal in thickness to the inner fan duct wall was conducted to determine thermal conductivity in the expected operating temperature range. The results (fig. 70) were utilized in nacelle cooling system design.

Panel Fabrication

Two types of sandwich-panel construction are used in the treated nacelle fabrication: single- and double-ply sandwich construction (fig. 71). Single-ply sandwich is the construction used for panels that are exposed to acoustic environment on one face only, such as external duct walls. They consist of a porous laminate skin, the core, a nonporous laminate skin, and their adhesive bonds. Double-ply sandwich consists of an impervious center septum laminate, honeycomb core, and a porous laminate skin on each face. Double-ply sandwich construction is used where the sandwich panel is located between two adjacent acoustic flow channels such as the circumferential splitters in the engine inlet. While detail differences in procedures are required to meet special requirements, the following description of single-ply sandwich construction is typical of procedures used for all sandwich constructions.

Fabrication of the polyimide sandwich is a multistage process in which a single tool conforming to a flow channel surface contour is utilized in separate operations for acoustic laminate fabrication, core subassembly fabrication, and panel assembly and bonding. Product quality is ensured through quality control checks of each fabrication step. For example, laminates for tensile test specimen are prepared concurrently with, and in the same sequence as, the layup of acoustic laminate. Compliance with acoustic flow-resistance [rayl (cgs)] tolerances and test specimen minimum tensile requirements is a prerequisite to panel fabrication. During each sandwich subassembly bonding operation, preparation of a flatwise tension test assembly for each skin-to-core bond and a double-lap bond shear test assembly for each oven load containing a laminate-to-laminate bond is required. Acceptance of the sandwich panel is contingent upon compliance of the test samples with specified minimum values.

A typical prepreg laminate layup ready for oven curing is represented in figure 72. The two bleeder cloth layers and the vacuum bag ensure removal of volatiles and excess resin during the curing cycle. Variations in the bleeder cloth provide fine adjustment in the flow-resistance [rayl (cgs)] values obtained for porous laminate layup. The laminate buildup is oven cured at 365° F for 2 hr under a vacuum of 24 in. of mercury, minimum. Postcure at 550° F for 2 hr does not require vacuum or bleeders.

Core material of the required thickness is heated by infrared lamps to 650° ± 50° F and is formed in a press using simply constructed form tools. Where large areas are involved, the core is spliced as required by joining core segments with tape foam adhesive (fig. 73). Adhesive is limited to filling one cell width on each side of the splice line to limit loss of acoustic surface area. Solid laminate members, which will frame the core at all panel edges, and others, which may be inserts within the core area, are laid up on the same tool used to lay up the porous skin (fig. 74). The core is trimmed to match the resulting pattern, placed on the tool, and bonded to the solid laminate by means of tape foam adhesive. This subassembly is sealed in a nylon or mylar bag with a vacuum bleeder system attached and is cured at 350° F. After cure, the subassembly is removed from the tool; liquid adhesive is applied to both faces of the core/laminate subassembly and is followed by oven drying for 30 min at 260° F.

The tool is used next as a bonding and assembly fixture in sandwich-panel fabrication. Figure 74, which shows the inner wall of the wrap cowl or constant-area section of the fan exhaust duct wrap cowl, illustrates this manufacturing procedure. The porous skin is placed on the tool; a second coat of liquid adhesive is applied to the interfacing core subassembly, and within 4 hr the subassembly is positioned on the porous skin. Again, the vacuum bleeder bag system is applied and the adhesive cured at 350° F.

After cure, film adhesive is applied to the remaining face of the core/solid laminate subassembly, and the nonporous laminate skin is laid up to the required thickness. The bleeder bag is added for the final cure, which is followed by postcure to final strength in an air-circulating oven at 500° F. Final trim completes the panel.

Fastener inserts intended for use in environments below 250° F may be potted in place in prepared cavities in the core using epoxy foam adhesives after postcure. Fastener inserts intended for use above 250° F are potted in place prior to postcure using polyimide tape foam. Vacuum bleeder bagging around the potted area and cure is required.

CONCLUDING REMARKS

Salient results of the program to develop an acoustically and structurally suitable lining material and the associated lining technology for use in attenuating turbofan engine-generated noise follow.

- A broadband resistive-resonator concept was selected as most suitable for lining engine fan ducts and inlets since it would provide the desired attenuation characteristics.

- Polyimide resin-impregnated fiberglass was selected for attenuating material because: (1) it is acoustically as good as any material tested and is capable of close-tolerance control of and variation in porosity to optimize attenuation; (2) it has good structural capability, obviating the need for separate support structure; (3) it has good resistance when exposed to engine environmental temperatures, contaminates, and sonic fatigue; (4) it can be readily fabricated into complex curved shapes; and (5) it appears to possess good life potential. Material properties tests and manufacturing techniques were successfully developed. The required material strength was verified at each successive fabrication step. The very satisfactory performance of polyimide-fiberglass materials in environmental exposure tests was further substantiated by results of flight and ground tests reported in volumes III and IV.

- Separation between lined surfaces, lining cavity depth, lining length, flow resistance, acoustic impedance, wall SPL, wall-particle velocity, and duct airflow Mach number are the controlling parameters in determining lining attenuation characteristics.

- A lining design technology was evolved from theoretical and parametric studies and was used in selecting the linings for the boilerplate/prototype fan duct development (for a frequency spectrum of 1000 through 10 000 Hz).

- An empirical method for predicting the principal duct and lining dimensions required to achieve a desired attenuation was developed from a parametric study of flow duct test results. The method also may be used to predict attenuation that will be provided by a known duct and lining configuration.

- Metallic and nonmetallic linings having the same geometry and effective flow resistance will provide essentially identical attenuation characteristics. Reinforced metallic felt, metallic felt, woven metallic fiber, and resin-impregnated glass fabric materials were selected as the most suitable for acoustic linings from more than 40 types of materials evaluated.

- Single-layer linings, in which the cavity depth is varied either on opposing walls or along the length of the linings, will provide broadband noise attenuations equivalent to combined double- and single-layer linings.

- A theoretical method for predicting lining attenuation was developed, which provides good agreement with experimental results at low duct airflow velocities ($M \leqslant 0.1$). Further development of the method is required to correct for the effects of higher flow velocities.

- Turbine-generated noise, isolated during full-scale engine tests, has little influence on the PNL of the JT3D engine. However, turbine noise could be a factor in limiting noise reduction for engines with lower jet noise levels and/or increased turbine noise due to changes in design or operating characteristics.

The Boeing Company
Commercial Airplane Group
Seattle, Washington, September 1969

APPENDIX A

FLOW DUCT RESULTS

Flow duct test data representing the more important parametric studies in this program are shown in figures A-1 through A-54. The results for each test configuration are presented in the form of power insertion loss (attenuation) spectra for four duct airflow Mach numbers. All of these tests were conducted using a broadband noise source and simulated the fan exhaust mode with the noise and airflow propagating in the same direction. The data were reduced using a 1/10-octave bandwidth, continuously sweeping wave analyzer.

APPENDIX B

LINING THEORY

Development of Lining Theory

The transmission and attenuation of sound through lined ducts have been treated by many investigators. The problem and its solution as described in this appendix closely follow that of reference 12 but add a broadening of concepts and applications. The theoretical analysis was made to develop a method for predicting sound attenuation in ducts with particular application to turbofan engines. The theory (refs. 1 and 8) is for straight ducts with various cross sections, ranging from rectangular to concentric cylindrical segments. It is assumed that airflow velocity along the duct is zero. The method developed also includes duct-lining optimization on the basis of maximum reduction in perceived-flyover-noise level depending on the shape of the input spectrum. A brief outline of the analysis is presented to indicate principal assumptions made in the prediction method.

Wave equation.—The sound pressure p in the duct is assumed to be low enough for the linear wave equation to be valid; thus,

$$\frac{1}{c^2}\frac{\partial^2 p}{\partial t^2} - \nabla^2 p = 0 \tag{B1}$$

By separating the variables to obtain a solution in terms of the normal modes of the duct, the following equation is obtained:

$$p(x,y,z,t) = X(x)Y(y)Z(z)T(t) \tag{B2}$$

where:

x,y,z = rectangular coordinates of the duct as shown in figure B-1

X,Y,Z,T = functions of x, y, z, t alone

t = time

p = acoustic pressure

c = speed of sound

If harmonic waves are assumed to be traveling in the positive z direction along the duct, equation (B2) can have a solution of the form

$$X(x) = C_x \cos k_x x + S_x \sin k_x x \tag{B3}$$

$$Y(y) = C_y \cos k_y y + S_y \sin k_y y \tag{B4}$$

$$Z(z) = \exp(-jk_z z) \tag{B5}$$

$$T(t) = \exp(j\omega t) \tag{B6}$$

where:

S_x, S_y = constants

C_x, C_y = constants

k_x = wave number in x coordinate

k_y = wave number in y coordinate

k_z = wave number in z coordinate

ω = angular frequency

j = imaginary operator

A general solution as a superposition of these solutions is

$$p = \sum_{i=1}^{\infty} a_i X_i Y_i Z_i T_i \tag{B7}$$

where values of the constants a_i are chosen in such a way that any particular sound pressure distribution at the sound-source end of the duct can be accurately described with the functions X_i, Y_i, Z_i, T_i.

Expanding equation (B1) gives

$$\frac{1}{c^2}\frac{\partial^2 p}{\partial t^2} - \frac{\partial^2 p}{\partial x^2} - \frac{\partial^2 p}{\partial y^2} - \frac{\partial^2 p}{\partial z^2} = 0 \tag{B8}$$

Also, however, $\partial^2 p/\partial x^2 = \partial^2 X/\partial x^2\, YZT$, and similarly for the other variables. Denoting $\partial^2 X/\partial x^2 = X''$, etc., and dividing by XYZT gives

$$\frac{1}{c^2}\frac{T''}{T} - \frac{X''}{X} - \frac{Y''}{Y} - \frac{Z''}{Z} = 0 \tag{B9}$$

Since each of the terms in equation (B9) depends only on one variable, by means of separation constants, equation (B9) is written thus:

$$\frac{T''}{T} = -\omega^2 \tag{B10}$$

$$\frac{X''}{X} = -k_x^2 \tag{B11}$$

$$\frac{Y''}{Y} = -k_y^2 \tag{B12}$$

$$\frac{Z''}{Z} = -k_z^2 \tag{B13}$$

The separation constants $-k_x^2$, $-k_y^2$, $-k_z^2$ correspond to wave numbers, and $-\omega^2$ to angular frequency.

The relation between the separation constants introduced in equations (B10) through (B13) is

$$\frac{\omega 2}{c^2} - k_x^2 - k_y^2 - k_z^2 = 0$$

and defining, for convenience, $k = \frac{\omega}{c}$ gives

$$k^2 = k_x^2 + k_y^2 + k_z^2 \tag{B14}$$

The partial differential equation thus has been transformed into a number of ordinary differential equations that are easy to solve.

Solution.—A solution is required that represents a wave propagating in the positive z direction (fig. B-2). Considering, for example, the fundamental (blade passage) frequency of a fan, the solution can be related to a single frequency component ω. The z-dependent and the t-dependent parts of the solution then must have the form

$$Z(z)\,T(t) = e^{j(\omega t - k_z z)} \tag{B15}$$

where ω is the angular frequency and k_z the axial wave number. For the x- and y-dependent parts, the solutions to equations (B3) and (B4) are used.

Boundary equations are obtained as follows (fig. B-1). At the walls, x = 0, x = a and y = 0, y = b where a and b are the cross-sectional duct dimensions.

For a hard-walled duct, the particle velocity perpendicular to the wall must be zero; hence, the pressure gradients must be zero; i.e.,

$$\frac{\partial p}{\partial x} = 0 \tag{B16}$$

$$\frac{\partial p}{\partial y} = 0 \tag{B17}$$

and for the acceleration a_x in the x direction

$$a_x = \frac{\partial u}{\partial t} \quad \text{and} \quad \rho a' = -\frac{\partial p}{\partial x}$$

where ρ = air density.

Performing the differentiation on equation (B2) using equations (B16) and (B17) gives for

$$x = 0, \; S_x = 0$$

$$y = 0, \; S_y = 0$$

$$x = a, \; \sin k_x a = 0$$

$$y = b, \; \sin k_y b = 0$$

where:

$$k_x = \frac{m\pi}{a}, \; (m = 0, 1, 2, \ldots.)$$

$$k_y = \frac{n\pi}{b}, \; (n = 0, 1, 2, \ldots.)$$

These solutions can be interpreted physically by drawing the x-dependent part of the pressure for different values of m as shown in figure B-2. Each solution thus corresponds to a mode of propagation. To solve a particular problem, a combination of duct modes with different m and n, taken with different amplitude and phase, must be made to match the sound pressure distribution at the source end of the duct. As can be seen from equation (B14), the speed of propagation

$$c_z = \frac{\omega}{k_z} \tag{B18}$$

is different for the different modes.

The solution is applied to the calculation of sound attenuation in a duct with absorptive-resonant linings by introduction of boundary conditions representing the acoustic admittance $Y_A(x,y)$, etc., of the linings as follows:

$$Y_A(x,y), = \frac{u_n}{p}$$

where p is the acoustic pressure and u_n is the perpendicular particle velocity into the lining surface.

Using the standard relationship

$$u = \frac{1}{j\omega\rho} \nabla\rho$$

particle velocity u_n perpendicular to the lining surface thus is determined by:

$$u_y = \pm u_n = \frac{1}{j\omega\rho}\left[\frac{\partial p}{\partial y}\right]\Bigg|_{y = y_o} \tag{B19}$$

for surface $y_o = 0$, $y_o = b$ with + at $y = 0$ and - at $y = b$

and

$$u_x = \pm u_n = \frac{1}{j\omega\rho}\left[\frac{\partial p}{\partial y}\right]\Bigg|_{x = x_o} \tag{B20}$$

for surface $x_o = 0$, $x_o = a$ with + at $x = 0$ and - at $x = a$.

Differentiation of equation (B2) and equations (B3) to (B6) yields the admittances $Y_A(\ )$,

$$Y_A(x, 0) = \frac{1}{j\omega\rho} \frac{k_y S_y}{C_y} \tag{B21}$$

$$Y_A(x, b) = \frac{1}{j\omega\rho} \frac{k_y \left(-C_y \sin k_y b + S_y \cos k_y b\right)}{\left(C_y \cos k_y b + S_y \sin k_y b\right)} \tag{B22}$$

$$Y_A(0, y) = \frac{1}{j\omega\rho} \frac{k_x S_x}{C_x} \tag{B23}$$

$$Y_A(a, y) = \frac{1}{j\omega\rho} \frac{k_x \left(-C_x \sin k_x a + S_x \cos k_x a\right)}{\left(C_x \cos k_x a + S_x \sin k_x a\right)} \tag{B24}$$

putting $\eta = \rho c$ Y_A as the normalized admittance yields

$$-jk\eta(x, b) \doteq k\left[\frac{jk_y \sin k_y b + k\eta(x, 0) \cos k_y b}{-jk_y \cos k_y b + k\eta(x, 0) \sin k_y b}\right] \tag{B25}$$

$$-jk\eta(a, y) = k\left[\frac{jk_x \sin k_x a + k\eta(0, y) \cos k_x a}{-jk_x \cos k_x a + k\eta(0, y) \sin k_x a}\right] \tag{B26}$$

The separation constants in equation (B14) are given by the acoustic admittances $Y_A(a, 0)$ and $Y_A(0, b)$ of linings in a duct of width a and height b. Attenuation of sound per unit length of duct in the positive Z direction can be determined from equation (B15) for the pressure by introducing $k_z = \alpha + j\beta$ where α = the phase constant and β = the attenuation constant ($\beta \leqslant 0$).

Thus,

$$Z(z) = \exp(-j\alpha z) \exp(\beta z) \tag{B27}$$

The attenuation along the duct between stations z_1 and z_2, expressed in decibels, is then

$$A_N(z_2 - z_1) = 20 \log_{10} \frac{p(z_1)}{p(z_2)} = -8.68\beta(z_2 - z_1) \tag{B28}$$

Thus, the attenuation A_N per unit length is

$$A_N = 8.68 \, |\beta| \, , \text{dB} \tag{B29}$$

The constant β is solved from the wave number k_z, using equations (B25) and (B26); thus,

$$k_z = (k^2 - k_x^2 - k_y^2)^{1/2} \tag{B30}$$

The most important problem was to solve the equations for k_z. This was done by solving the equations for k_x and k_y in equation (B3) from the duct boundary conditions as functions of the lining admittance and by means of a numerical solution based on Newton's tangent method. A solution for an unlimited number of modes was found (ref. 8). Because the number of lining parameters that can be varied is extremely large, a computer method was developed together with an attenuation optimization process (also described in ref. 8).

Typical results.—The theory was used to compute predicted attenuation of a duct lining configuration tested in the flow duct program. Figures B-3 and B-4 show a comparison of experimental data and the theoretically predicted attenuation. Good agreement was achieved for the Mach number case M = 0, but a discrepancy occurs in the case of the higher airflow (M = 0.37). In the data compared, the higher rate of airflow has two effects: namely, to increase the frequency at which peak attenuation occurs and to reduce the peak attenuation. These effects have been consistently observed in the flow duct program. It should be noted, however, that in the case of an inlet mode, where the airflow occurs in the direction opposite to the sound propagation, the measured peak frequency occurs at a lower value than the predicted frequency, but the peak attenuation is not necessarily less than the predicted value.

APPENDIX C

TURBINE NOISE

During the acoustic study of the noise radiated from a JT3D turbofan engine, turbine-generated noise was detected. A detailed investigation followed to identify the noise source and to establish its effect as a potential noise floor in the study of aft fan noise reduction.

This appendix abstracts the main portion of the report written upon conclusion of the turbine noise study.

Experimental Program

Initial test data.—Tests were conducted at Tulalip Test Site, using a JT3D-3B engine fitted with an acoustically lined housing over the engine inlet (fig. 17) and an experimental acoustically treated fan discharge duct (fig. 13). The purpose of the inlet housing was to minimize the radiation of fan inlet noise into the aft-quadrant measuring positions in order to isolate the aft-radiated fan discharge noise as much as possible.

During the test series, five fan duct acoustic-lining configurations were tested, each with an increased quantity of treatment. These tests led to the unmasking of a high-frequency noise source in the 5000- to 10 000-Hz region, which was identified as originating from the turbine stages. Data were recorded during 15 runs at engine N_1 speed settings of 3800, 5000, and 5700 rpm, respectively. Microphones were located on a horizontal arc of 200-ft radius at increments of 10° azimuth from 80° to 140° measured from the inlet forward axis and on a vertical arc of 75-ft radius from 100° to 140° also in increments of 10°.

Additional tests.—Nine additional test runs were conducted with a 90°-elbow jet deflector installed over the primary exhaust nozzle. The installation served to deflect the discrete frequency turbine noise upward and away from the microphones located in the horizontal plane, yielding measurements of fan duct exit noise isolated from fan inlet noise, jet noise, and turbine noise. Only the microphones in the horizontal plane were operating while the jet deflector was installed.

Definition of turbine noise.—Narrowband analyses of the initial test data revealed dominant discrete frequency components in the fan noise suppressed spectra that had not been detected previously. The dominant discrete components were removed by the installation of the primary jet deflector; this led to a premise that the discrete components were turbine noise spikes (line spectra). The premise was confirmed through a comparison of frequencies with the number of blades in the turbine stages and N_1 rotor speeds. The frequencies of the spikes attributed to the turbine stages were accurately determined by means

of a narrowband wave analyzer with 5-Hz bandwidth filters in conjunction with a pure sine wave beat frequency oscillator, the frequencies of which were determined with accurate electronic counters.

The frequencies measured were found to agree identically with

$$\frac{\text{turbine rpm}}{60} \times B_T \qquad \text{(C1)}$$

where B_T = number of turbine blades in the fourth, third, second, and first turbine stages (80, 108, 114, and 130 blades, respectively).

At angles of maximum turbine noise levels, 1/24-octave bandwidth spectral plots were averaged over all the test runs; results are shown in figure C-1.

At the N_1 speed of 3800 rpm, spikes from the last three turbine stages (second, third, and fourth) can clearly be distinguished. The first-stage component, corresponding to 130 blades in equation (C1), however, could only be detected by search, using the 5-Hz bandwidth filter. At an N_1 of 5700 rpm, components from the second and third stages could no longer be distinguished. The frequencies of these components are above 10 kHz, which is beyond the limits of the measuring system used. In the spectra in figure C-1, the frequency bandwidth between 4800 and 9600 Hz is totally dominated by turbine noise. This predominant influence applies for spectra measured between the angles of 80° to 140°.

Directivity plots of 8th-octave bandwidth sound levels are presented in figure C-2. In the left-hand column, levels are presented with and without turbine components with and without the jet deflector installed. From these relative levels plus studies of narrowband analyses, overall turbine noise levels (8th-octave bandwidth) were calculated and plotted on the right side of figure C-2. These data represent accurate turbine noise directivity curves for one test configuration.

Directivity plots of 8th-octave bandwidth levels of five test configurations were superimposed, and most of the data fell within a 3-dB data scatter from which it was concluded that turbine noise levels were highly repeatable. The data show that directivity patterns are symmetrical in the vertical and horizontal planes.

Variations of peak turbine noise levels with engine N_1 rpm are summarized in figure C-3. This figure shows the octave bandwidth level of turbine noise increases slightly with N_1; the levels of the combined discrete frequencies decreases with N_1 for the second, third,

and fourth stages, but the levels of the discrete frequency component of the 80-blade fourth stage increases significantly with N_1. Noise components 10 kHz and above have little contribution to aircraft noise due to the extremely high atmospheric absorption at these frequencies.

Theoretical Analysis

The propagation phenomena of high-frequency sound waves in a nonhomogeneous environment, such as a jet exhaust duct, was theoretically examined. Results of the study showed that four mechanisms can have a substantial influence on propagation; namely:

- Thermal gradients
- Flow velocity gradients
- Flow turbulence
- Acoustic beaming

Influence of a thermal gradient.—When sound waves propagate through a medium having a thermal gradient, the direction of propagation of the wave fronts changes in accordance with the temperature change the wave encounters. This phenomenon is due to the refractive effect caused by a change in the acoustics phase velocity; thus,

$$c = (\gamma g R)^{1/2} T^{1/2}$$

where:

c = speed of sound

γ = ratio of specific heats

g = gravitational constant

R = gas constant

T = absolute temperature

When sound waves propagate from a hot region to a colder region (center of the duct toward the outer cowl), the angle of incidence to the wall is increased; conversely, when propagation is from a cold region to a hotter region, the sound wave is refracted away from the opposite wall and toward the center of the duct (fig. C-4). As illustrated in figure C-5, the refraction is not a reciprocal effect.

In conclusion, the influence of a thermal gradient is dependent upon the location of a sound source in a duct. If the source is close to a wall, the sound radiated will tend to focus along the center of the duct, but if it is near the center of the duct, it will tend to be refracted to the walls.

Influence of velocity gradient.—A flow velocity gradient in a medium being transported in a duct will have a similar effect on the propagation of sound as that of a thermal gradient. However, in this case, the refraction is caused by the sound waves being transmitted through regions of the medium with different velocities as a result of the motion of the medium.

The effects of velocity gradients on sound propagation are illustrated in figures C-4, C-5, and C-6. Again, it will be seen that the influence of a flow velocity gradient on the propagation of sound is highly dependent upon the location of a sound source in a duct. Complete reflection of sound waves also can occur at abrupt changes in velocity gradient (ref. 8).

It is concluded, therefore, that turbine noise generated along the wall of a duct will tend to concentrate along the center of the duct.

Effects of turbulence.—When sound waves propagate through a turbulent fluid, scattering of the waves can occur. The magnitude of the scatter depends upon the size of the turbulent eddies and the wavelength of the sound propagated. Scattering is comparatively large when the acoustic wave number k is of the same order of magnitude as the wave number of the main energy-bearing eddies (ref. 8). When the wavelength of sound λ is larger than the size of the eddies L, there will be little scattering. When $\lambda \simeq L$, the scattering will be distributed in all directions with a minimum in the forward direction. However, when $\lambda < L$, the scattering will be concentrated in the forward direction close to $\phi \simeq 0^\circ$ where ϕ is the angle between the direction of propagation and direction of scattered intensity.

In the case of high-frequency turbine noise propagating downstream in a jet-exhaust duct, the wavelength probably will be of the same order of magnitude as the main energy-bearing eddies. In consequence, a focusing effect of the sound along the longitudinal axis of the exhaust duct may occur.

Formation of acoustic beams.—When the wavelength of sound propagating in a duct is much smaller than the duct cross-sectional dimensions, the phenomenon of "acoustic beaming" occurs; namely, the sound propagates along the duct as though it were in a free medium. Reference 8 shows that as a result of this effect, high-frequency sound waves are attenuated much less than waves with larger wavelengths, even though the walls of the duct are adequately treated with absorbing linings designed for these high frequencies.

Impact of Turbine Noise on Perceived Noise for the JT3D Engine

Influence of turbine noise on PNL.—Throughout ground tests in the thrust range equivalent to landing approach, it was found that peak turbine noise levels measured at a radius of 200 ft were approximately 90 dB. If these levels are converted to an equivalent flyby at

400-ft altitude, by assuming four engines and the corresponding atmospheric absorption (calculated in accordance with reference 9), then the levels would be about 87 dB. This level corresponds to a Noy value of 45 (calculated in accordance with reference 10), which is equivalent to 95 PNdB. The net contribution of turbine noise to the PNL as a function of the PNL of four JT3D engines at a 400-ft altitude is shown in figure C-7. The abscissa of these curves represents PNL's during landing approach that may be varied by noise suppression. The turbine-noise component is shown to be constant, i.e., not affected by the suppression; hence, the influence of turbine noise on the total PNL can be seen. The curve representing the PNL for only turbine noise was calculated assuming the 8th-octave bandwidth was dominated by the turbine components. This assumption does not hold at low noise suppression levels or at higher PNL's.

Limit of PNL reduction.—It may be concluded from figure C-7 that if turbine noise levels determined from ground tests also apply in flight conditions at a 400-ft altitude, then 95 PNdB is the lowest PNL that can be practically attained without attenuating turbine noise. The range of PNL's for a 707-320B/C in landing approaches is between 120 and 123 PNdB; hence, noise reductions will be "turbine noise limited" below a corresponding range of 25- to 28-PNdB attenuation.

Impact of Turbine Noise on Other Engines

The existence of turbine noise in the suppressed JT3D-3B engine does not have a serious impact on perceived noise partially because the noise occurrs in the 8th-octave bandwidth, which has a lower Noy value compared with the 6th- and 7th-octave bandwidths in which the fan blade passage frequency occurs. It should be noted, however, that turbine noise is not heavily masked by broadband noise in the JT3D-series engine at lower power settings, and it may not be heavily masked in other series of turbofan engines. In engines with lower rotor speeds and fewer turbine blades, the blade turbine passage frequencies might be in the 6th and 7th octaves, which are the most sensitive in establishing PNL's. Therefore, as fan noise is suppressed, the turbine could contribute heavily to the remaining total engine noise level.

Conclusions and Recommendations for Further Study

Current JT3D engine applications.—It has been shown that the PNL's during approach conditions for an aircraft powered with JT3D engines would only be turbine noise limited after an attenuation of the fan exit noise by about 20 to 25 PNdB. Also, for takeoff conditions, jet and fan noise dominates the perceived noise, and considerable attenuation of these sources is required before turbine noise contributes significantly to the total noise level.

Future development of technology.—For future generations of high bypass engines, in which turbine noise may be a problem, it would be of value to acquire a better understanding of turbine noise fields inside a jet exhaust duct for the purpose of developing suitable suppression devices. The following investigations are proposed.

- A definition of the aeroacoustic fields inside a jet exhaust duct should be obtained to provide information on the most suitable location of acoustic treatment. Transducers installed in the wall of a primary exhaust duct could be used to measure wall pressure spectra and obtain pressure profile measurements across the duct. These measurements should be made both upstream and close to the exit nozzle.

- Some acoustic-lining suppressor tests should be made to investigate performance of this type of sound attenuation device when used in a high-temperature and high-flow velocity environment. Acoustical evaluation of lined cylinders, possibly including treated rings, could be obtained with an experimental duct extension from the exhaust nozzle of a JT3D engine.

REFERENCES

1. Andersson, A. O.; Bohn, A. J.; and Mangiarotty, R. A.: The Reduction of Fan Noise in Turbo-Fan Engines by Use of Acoustical Linings. Vol. I, Summary of Theoretical and Experimental Data. The Boeing Company, D6-17100, 1967.

2. Andersson, A. O.; Bohn, A. J.; and Mangiarotty, R. A.: The Reduction of Fan Noise in Turbo-Fan Engines by Use of Acoustical Linings. Vol. II, Detailed Theoretical and Experimental Data. The Boeing Company, D6-17100, 1967.

3. Feder, E., and Dean, L. W., III: Analytical and Experimental Studies for Predicting Noise Attenuation in Acoustically Treated Ducts for Turbofan Engines. NASA CR-1373, Sept. 1969.

4. Walton, R. H.; and Mangiarotty, R. A.: Acoustic Properties of Materials for Use in Turbofan Engine Linings. The Boeing Company, D6-22746TN, 1968.

5. Mangiarotty, R. A.: Acoustic Lining Concepts and Materials for Engine Ducts. Invited paper B2, Aircraft-Noise Session, 77th meeting, Acoustical Soc. of Am., Philadelphia, Apr. 8-11, 1969.

6. Atvars, J.; and Mangiarotty, R. A.: Duct Acoustic Lining Technology Applications to Turbofan Engines. Invited paper B3, Aircraft-Noise Session, 77th meeting, Acoustical Soc. of Am., Philadelphia, Apr. 8-11, 1969.

7. Fischer, F. W.; and Andersson, A. O.: The Optimization of Duct Linings for Sound Attenuation. The Boeing Company, D6-29356TN, 1968.

8. Morse, P. M.; and Ingard, K. U.: Theoretical Acoustics (Chapter 11, Acoustics in Moving Media). McGraw-Hill, New York, 1968.

9. Standard Values of Atmospheric Absorption as a Function of Temperature and Humidity for Use in Evaluating Aircraft Flyover Noise. Society of Automotive Engineers, ARP 866, 1964.

10. Jet Noise Prediction, SAE AIR 876, 1965.

11. Definition and Procedure for Computing the Perceived Noise Level of Aircraft Noise. Society of Automotive Engineers, ARP 865, 1964.

12. Cremer, L.: Theorie der Luftschall-Daempfung im Rechteckkanal mit Schluckender Wand und das sich dabei ergebende hoechste Daempfungsmass. Acustica, 3, Beih, 2, 249, 1953.

TABLE I.–MATERIALS EVALUATION, SUITABLE MATERIALS

Material (a)	Description
Nonmetallic	
Polyimide fiberglass laminate (Material A)	A material developed by Boeing and having acoustical absorption properties comparable to the best metal fiber liners at reduced cost and weight. Flow resistance versus particle velocity characteristics are non-linear; i.e., the laminate has a high reactive impedance compared with metallic felt and woven wire materials, but this characteristic can be controlled with fabrication ply orientation techniques and the thickness of the glass fabric or cloth. Pre-impregnated multiple-ply laminates have been developed with a flow-resistance range from 2 to 90 rayls (cgs). Laminates have been fabricated with controlled graduated flow resistance for use where sound pressure levels vary substantially along a duct. Variation of ply orientation produces more control in the magnitude of the flow resistance.
Carborazole fiberglass laminate (Material B)	A material developed by Boeing from carborazole, a high-temperature polymer used for glass fabric impregnation to produce a flexible porous laminate. Its acoustic properties are similar to polyimide-fiberglass fabric laminates.
Nonmetallic porous sheet (Material G)	A material resistant to soiling, inert to hydrocarbons and acid, having good cleaning qualities, and a working temperature range from -100° to 300° F. Twenty-three samples have been tested for flow resistance; they varied from 5 to 300 rayls (cgs).
Metallic	
Woven metallic fiber sheet (Material C)	A woven metallic material with acoustic properties similar to material D.
Metallic felt sheet (Material D)	A continuous weave metallic felt combined with a fibrous structure. Samples have been tested with nominal flow-resistance values from 10 through 80 rayls (cgs).
Metallic fiber and felt sheet (Material E)	A continuous weave metallic felt having acoustic characteristics similar to material D.
Steel wire fabric (Material F)	A range of metal screens woven from unsintered stainless steel. Weaves range from 70 x 225 to 90 x 500 strands/in^2. Samples tested with flow resistances from 20 to 100 rayls (cgs). Structurally flexible material, non-self-supporting. Has acoustic properties similar to materials D and E.
Steel wire fabric (Material N)	Similar to material F but sintered. Similar acoustic properties to material F but more rigid.

TABLE I.—MATERIALS EVALUATION, SUITABLE MATERIALS- Continued

Material (a)	Description
Metallic	
NASA dimpled metal mesh	Material developed by NASA-Langley Research Center, consisting of layers of fine mesh screen dimpled to form spacing. Acoustic flow resistance and other characteristics are similar to those of materials above, but the laminate is much thicker than the above materials.
Honeycomb core	
Metallic cell core (Material P)	Seamwelded metallic honeycomb.
Phenolic resin paper (Material Q)	Fabricated from pressed paper and phenolic resin. Several types of this hexagonal honeycomb core spacer were used in conjunction with porous materials to form lining panels.
Slant core (Material Q)	Epoxy resin-impregnated paper core, hexagonal section. Material supplied in a form permitting the cutting of slant-core up to 60° slant.
Polyimide fiberglass (Material R)	Flexible core hexagonal honeycomb. Fiberglass impregnated with polyimide resin.
Adhesives	
Epoxy resins (Materials T and U)	Epoxy resins tested had good structural strength to a temperature of 300° F. Epoxy resins discontinued due to temperature limitation.
Phenolic resin (Material V)	Has similar properties to material T but upper temperature limitation of 450° F.
Polyimide resin (Material W)	Polyimide resins tested had good structural strength to a temperature of 550° F when postcured to 600° F.

TABLE I.– MATERIALS EVALUATION, SUITABLE MATERIALS–Concluded

Code	Description	Process
Material		
A	Polyimide-fiberglass laminate	Bonded
B	Carborazole-fiberglass laminate	Bonded
C	Woven metallic fiber sheet	Sintered
D	Metallic felt sheet	Sintered
E	Reinforced metallic fiber and felt sheet	Sintered
F	Steel wire fabric	Sintered
G	Nonmetallic porous sheet	Plastic
H	Metallic foam sheet	Foamed
I	Metallic foam	Foamed
J	Ceramic foam	Slab
K	Plastic foam sheet	Rolled
L	Fiberglass woven mat	Woven
M	Reinforced ceramic foam	Foamed
N	Steel wire fabric	Rolled
O	Porous metallic powder sheet	Sintered
Core		
P	Metallic cell core	Seam welded
Q	Phenolic resin paper core	Bonded
R	Phenolic resin fiberglass core	Bonded
S	Metallic grid core	Spot welded
Resin		
T	Epoxy resin 1	
U	Epoxy resin 2	
V	Phenolic resin	
W	Polyimide resin	

TABLE II.–MATERIALS EVALUATION, TYPICAL UNSUITABLE MATERIALS

Materials (a)	Description
Facings, honeycombs, and adhesives	
Metallic foam and sheet (Materials H and I)	Nickel and copper foam metal. Brittle, tends to spall.
Ceramic foam (Material J)	Ceramic honeycomb slab material. Low structural strength, brittle; tends to spall.
Plastic foam sheet (Material K)	Nonmetallic foam material. Combustible above 175° F; highly absorbent and nonresistant to hydrocarbon derivatives.
Fiberglass woven mat (Material L)	Glass fiber mats. Low tear resistance, low structural stiffness. Negligible flow resistance.
Ceramic foam (Material M)	Similar to material J.
Porous metallic powder sheet (Material O)	Material available only in small size discs. High flow resistance, 300 rayls (cgs). Loose cellular structure.
Honeycomb core	
Metallic cell core (Material S)	Aluminum core. Cells interconnected; not as effective acoustically as sealed cells.

[a]See table I for Materials Description Code.

TABLE III.—DESIRED CHARACTERISTICS OF POROUS SHEET MATERIALS

- Acoustic flow resistance
  - Producible with mean values between 1 and 100 rayls (cgs)
  - Uniform over sheet or controlled gradation
  - Nonlinear increase in flow resistance with increasing airflow velocity should be small
- Weight
  - Not more than approximately 0.4 lb/ft^2
- Thickness
  - Between approximately 0.02 and 0.06 in.
- Strength
  - Effective ultimate tensile strength not less than 10 000 lb/in^2
  - Effective yield tensile strength not less than 4000 lb/in^2
  - Breaking strength no less than 200 lb/in.
- Environmental factors
  - High airflow velocity (up to M=0.6)
  - High sound pressure levels (up to 170 dB)
  - Subject to contamination, dust and oils
  - May need use of cleaning solvents
  - Anti-icing considerations
  - Exposed to rain, wetting, freezing, erosion, and corrosion
  - Exposed to sunshine and heat from engine
  - Should be able to withstand environment for rest of design life of airplane
- Manufacture
  - Formable into compound curved shapes
  - Should be available in large sheets, nontoxic and nonflammable
- Cost of raw material
  - Approximately \$15/ft^2 or less in 1000-ft^2 production lots

TABLE IV.—CANDIDATE MATERIALS AND ACOUSTICAL EVALUATION METHODS

- Porous surface materials
  - Metallic
    - Felted wire fibers, sintered
    - Layers of woven, wire screen, sintered
    - Sintered powders
    - Perforated plate
    - NASAMET
  - Nonmetallic
    - Layers of woven fiberglass cloth, resin or rubber impregnated
- Honeycomb-support structures
  - Metallic
    - Stainless steel or aluminum, welded or brazed
  - Nonmetallic
    - Heat-resistant phenolic-resin-impregnated fiberglass cloth (bonded)
    - Phenolic-resin-impregnated nylon-coated paper
    - Polyimide-resin-impregnated fiberglass cloth (bonded)
- Acoustical evaluations
  - Laboratory tests
    - Flow resistance
    - Acoustic impedance with and without airflow
  - Duct-model tests
  - Full-scale-engine tests

TABLE V.– DETAILS OF ENGINE TEST PROGRAM

Test identification			Duct wall configuration					
Test date, 1967	Test number, staff	Config no.	Test run no.	Outer wall	Inner wall	Radial splitter	Circum splitter	Remarks
5/9	1	1	1-6	Treated	Blanked	Normal	None	V[a] with directionalizer
5/10	1	1	10-14	↑	↑	↑	↑	H[b] without directionalizer
5/10	1	1	15-17	↕	↕	↕	↕	H with directionalizer
5/10	1	1	18-20	↕	Blanked	↕	↕	H with directionalizer and elbow
5/17	2	2	25-27	↕	Treated	↕	↕	H with directionalizer
5/17	2	2	21-24	↕	Treated	↕	↕	H with directionalizer and elbow
5/17	2	2	28-33	Treated	Treated	Normal	None	V
5/24	SD-1	–	34-36	–	–	–	–	Baseline, short duct
5/26	09A	9	40-42	Treated	Treated	Treated	Treated	Shakedown run; defective acoustical instrumentation
6/13	12	12	43-46	Blanked	Blanked	Blanked	None	H & V with directionalizer
6/14	10	10	47-49	Treated	Blanked	Treated	None	↕
6/15	6	6	50-52	Treated	Treated	Blanked	None	↕
6/19	11	11	53-55	Blanked	Blanked	Blanked	Blanked	↕
6/20	4	4	56-58	Treated	Treated	Blanked	Blanked	↕
6/22	7	7	59-61	Treated	Treated	Treated	None	↕
6/23	13	13	62-64	Blanked	Blanked	Blanked	Treated	H & V with directionalizer
6/27	SD-2	–	65-70	–	–	–	–	Baseline, short duct
7/26	SD-3	–	–	–	–	–	–	Baseline, short duct H & V without directionalizer
7/27	SD-4	–	71-73	–	–	–	–	H & V directionalizer without baffles, baseline, short duct
8/9	SD5A	–	75-77	–	–	–	–	H & V with baffled directionalizer, short duct
8/10	07B	7	78-80	Treated	Treated	Treated	None	H & V
8/10	07C	7	81-83	↕	↕	↕	None	H only with jet elbow and baffled directionalizer
8/11	09B	9	84-86	↕	↕	↕	Treated	H only with jet elbow and baffled directionalizer
8/14	09C	9	87-89	↕	↕	↕	↕	H & V without jet elbow with baffled directionalizer
8/14	09D	9	90-92	↕	↕	↕	↕	H only with jet elbow and baffled directionalizer (Side vents plugged)
			93-94	↕	↕	Treated	↕	Fiberglass removed from directionalizer vents
8/15	05A		95-97	↕	↕	Blanked	↕	H only with jet elbow and baffled directionalizer
8/15	05B	5	98-100	↕	Treated	↕	Treated	H & V with directionalizer only
8/22	01B	01B	101-103	↕	Blanked	↕	None	H only; polyimide with jet elbow
8/25	17	6	104-106	↕	Treated	↕	↕	Treatment failed, H only; H only with baffled directionalizer and jet elbow
9/1	17	6	107-109	↕	Treated	Blanked	↕	Rerun 1/2 length inside and outside; H only with baffled directionalizer and jet elbow
9/6	19	7	110-112	Treated	Treated	Treated	None	1/2 length 4 walls treated; H only with baffled directionalizer and jet elbow

[a]V = Vertical survey
[b]H = Horizontal survey

TABLE VI.—LINING DETAILS[a]

Component	Lining cavity depth, in. (b)	Cell size, in.	Cell type	Nominal flow resistance, rayls (cgs) (c)	
				Material D	Material A
Outer wall	h_o = 1/2 h_i = 7/8	2-1/2	Hexagon Material K	Outer=10 Inner =50	8 40
Inner wall	h = 1/2	1		30	25
Radial splitter[d]	h = 1/2	1		30	25
Circumferential splitter[e]	1	1		30	25

[a]Table I gives Materials Description Code and figure 9 shows configuration.

[b]Blanking plates have the same exterior dimensions as the linings they replace.

[c]Nominal flow resistance measured at a flow velocity u of 25 cm/sec.

[d]Linings 1/2 in. deep on each side of radial splitter.

[e]Total depth of circumferential splitter.

TABLE VII.—PEAK BASELINE NOISE (AVERAGE OF SIX RUNS)

Engine condition		6 th octave (1200-2400 Hz)	7th octave (2400-4800 Hz)	8th octave (4800-9600 Hz)	PNdB (37.5-9600 Hz)
Vertical					
N_1 rpm condition	3800 5000 6100	96 92 97	94 106 107	95 102 104	113 123 125
Horizontal					
N_1 rpm condition	3800 5000 6300	94 94 96	97 105 110	94 100 103	115 122 127

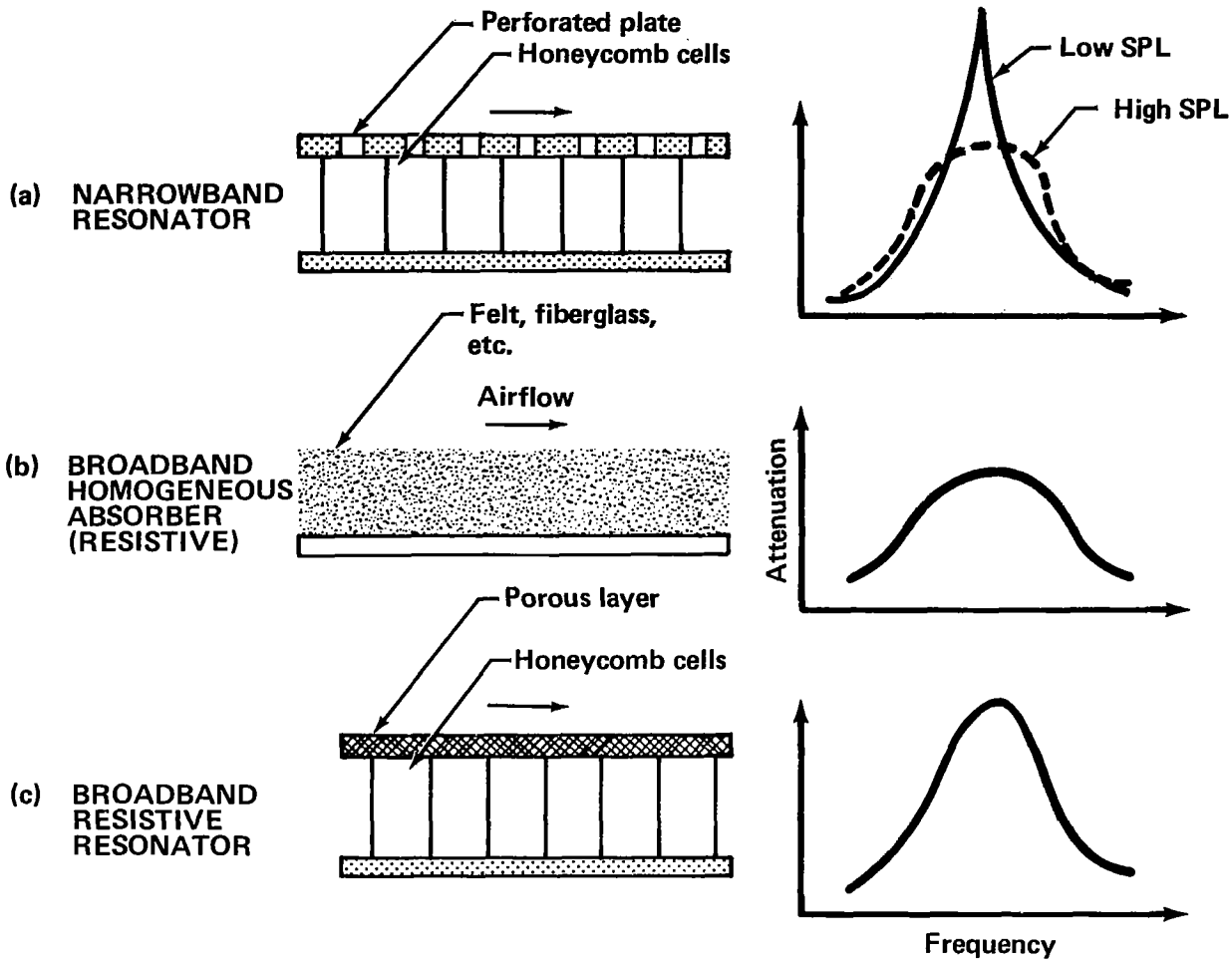

FIGURE 1.—ACOUSTIC LINING CONCEPTS

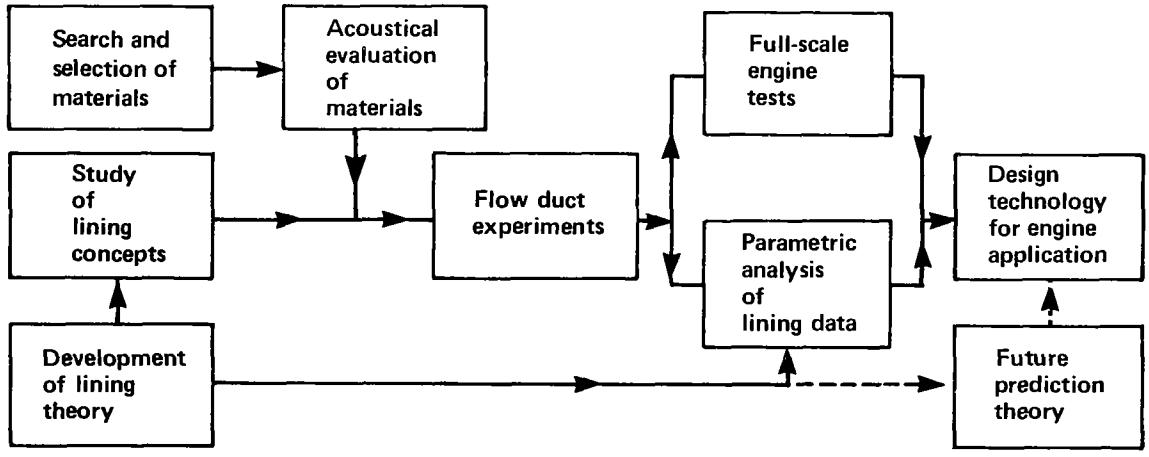

FIGURE 2.— MATERIALS AND LINING STUDY

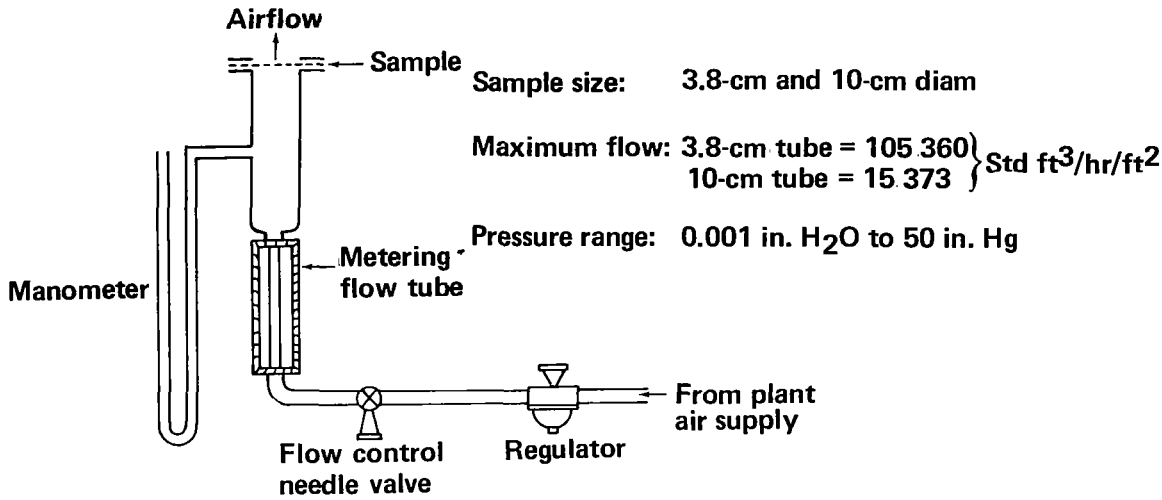

FIGURE 3.—FLOW-RESISTANCE APPARATUS

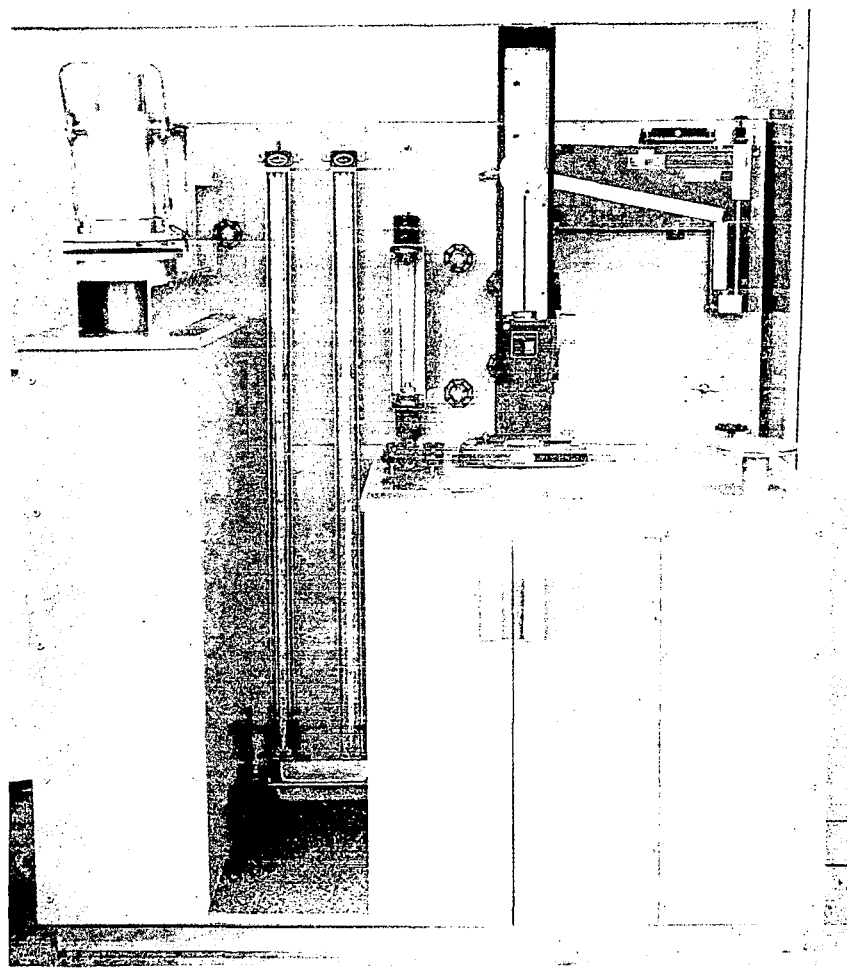

FIGURE 4.—FLOW-RESISTANCE APPARATUS

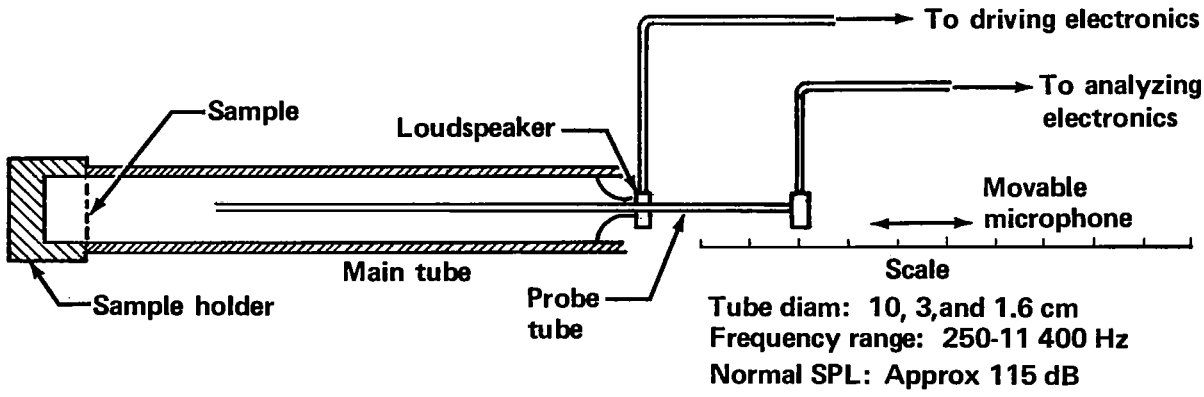

FIGURE 5.– STANDARD IMPEDANCE TUBE

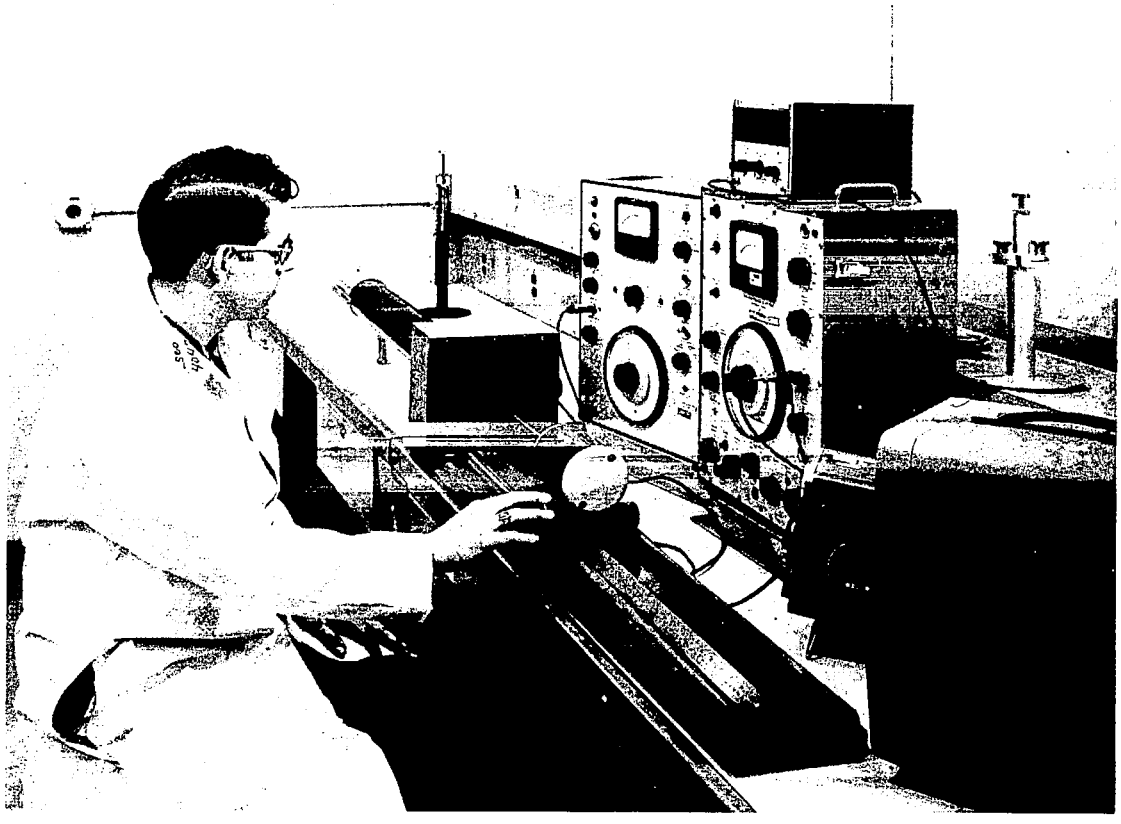

FIGURE 6.– IMPEDANCE TUBE APPARATUS

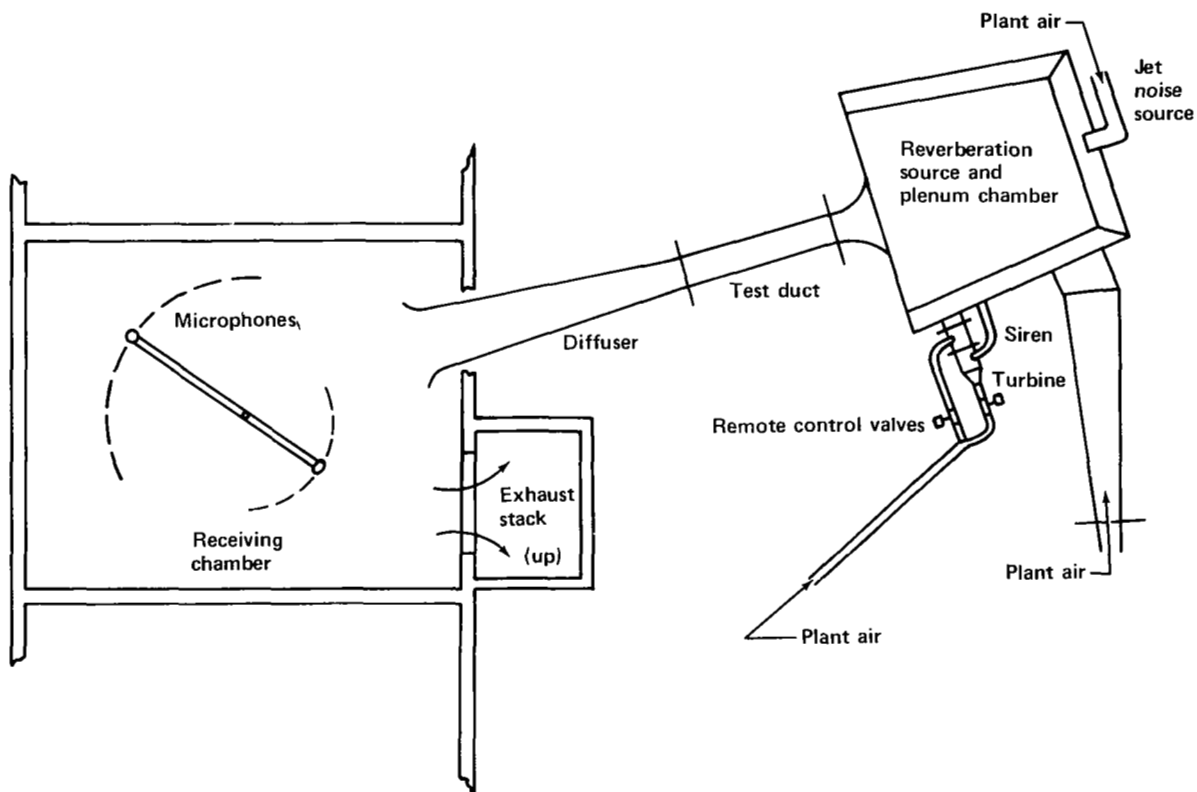

FIGURE 7.– BOEING FLOW DUCT FACILITY

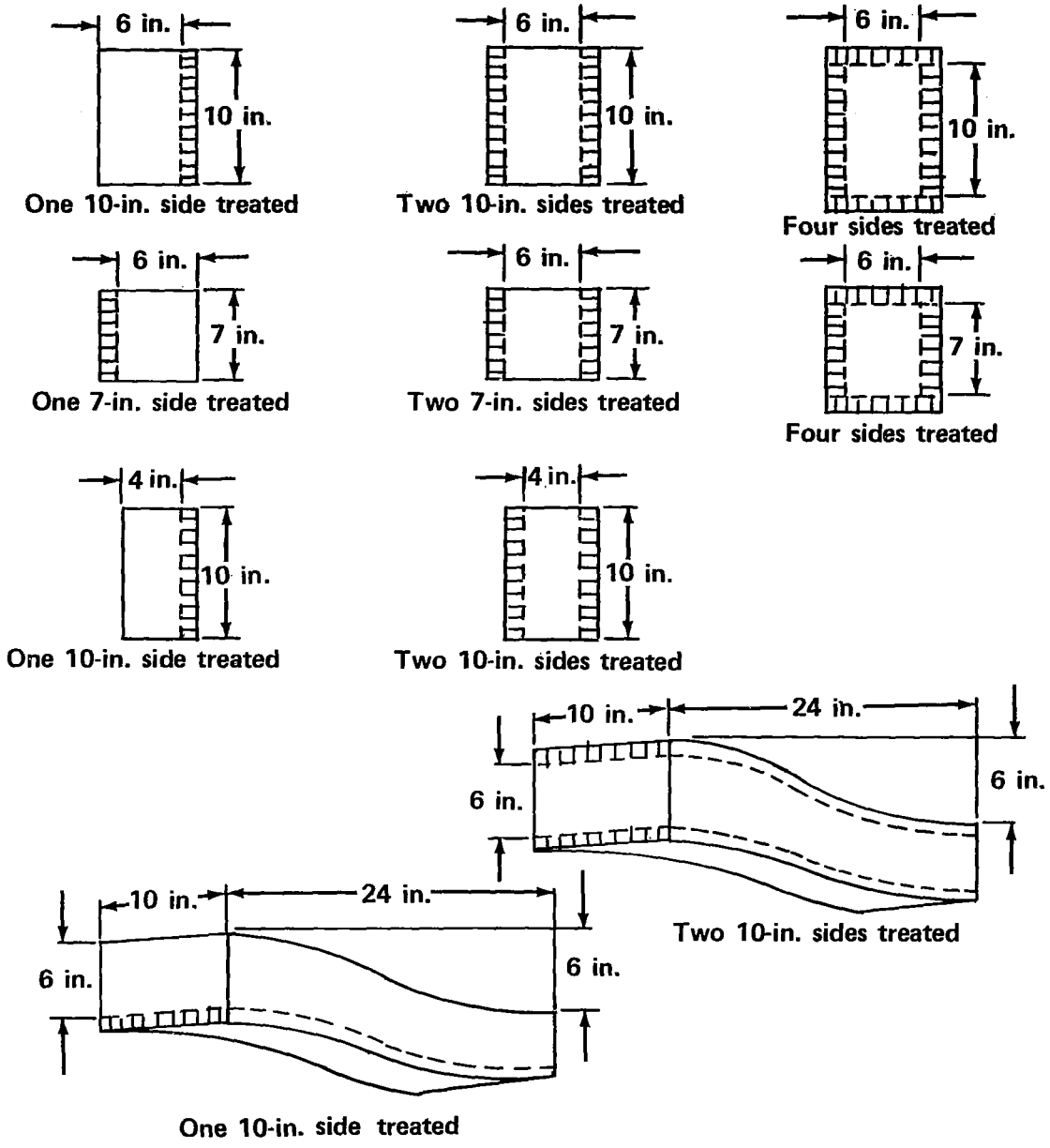

FIGURE 8.—FLOW DUCT TEST CONFIGURATIONS

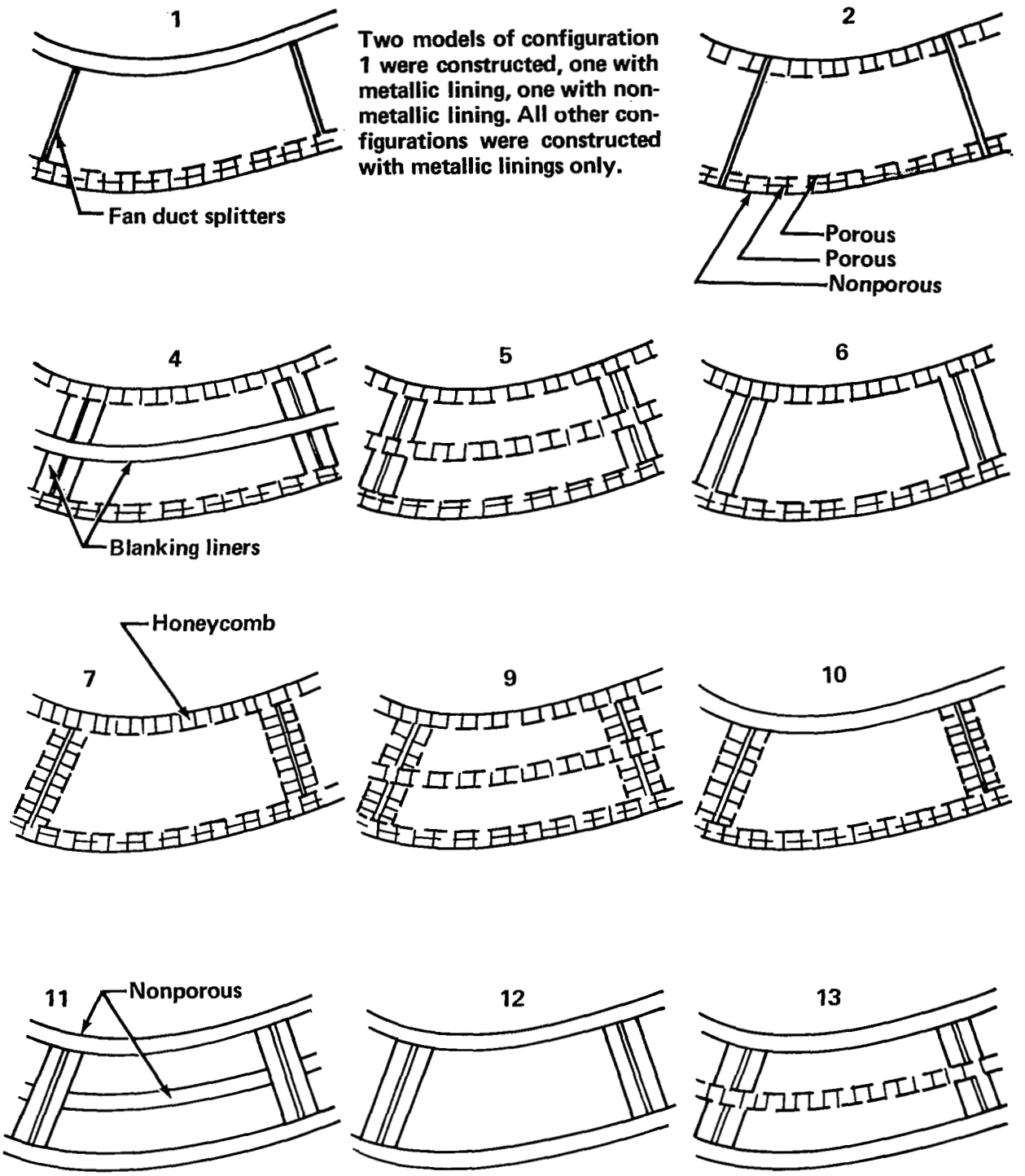

FIGURE 9.—ENGINE DUCT LINING CONFIGURATION

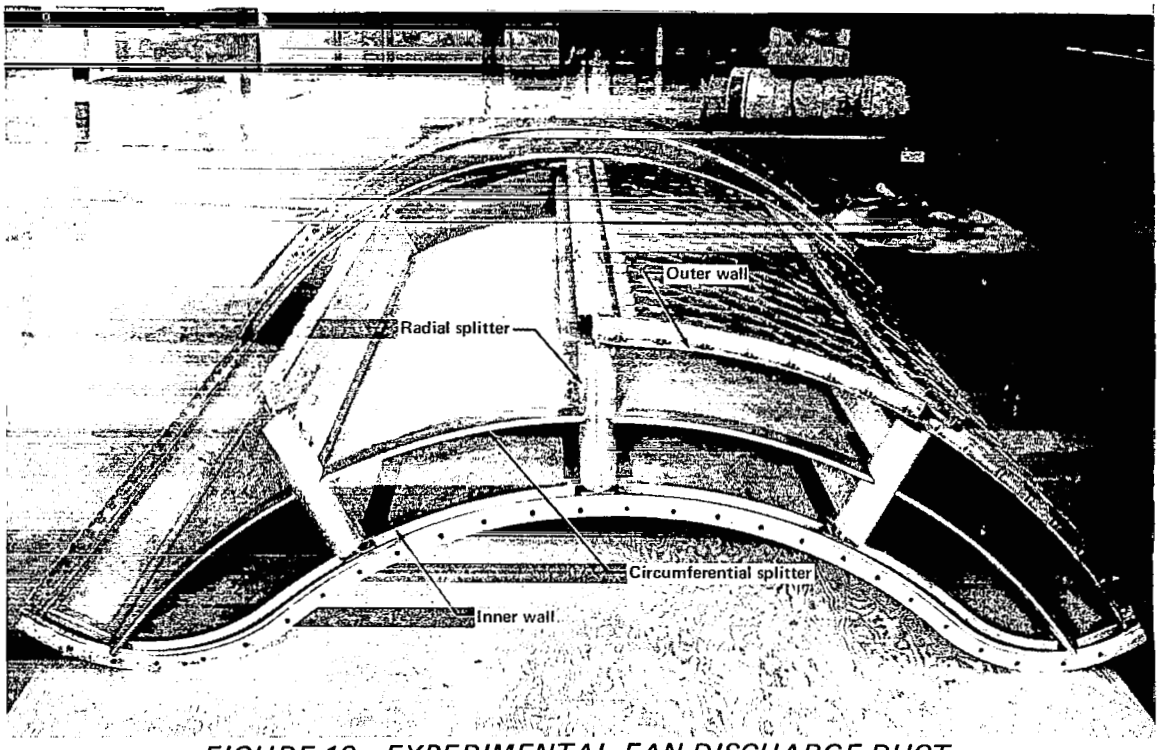

FIGURE 10.—EXPERIMENTAL FAN DISCHARGE DUCT WITH TREATMENT INSTALLED

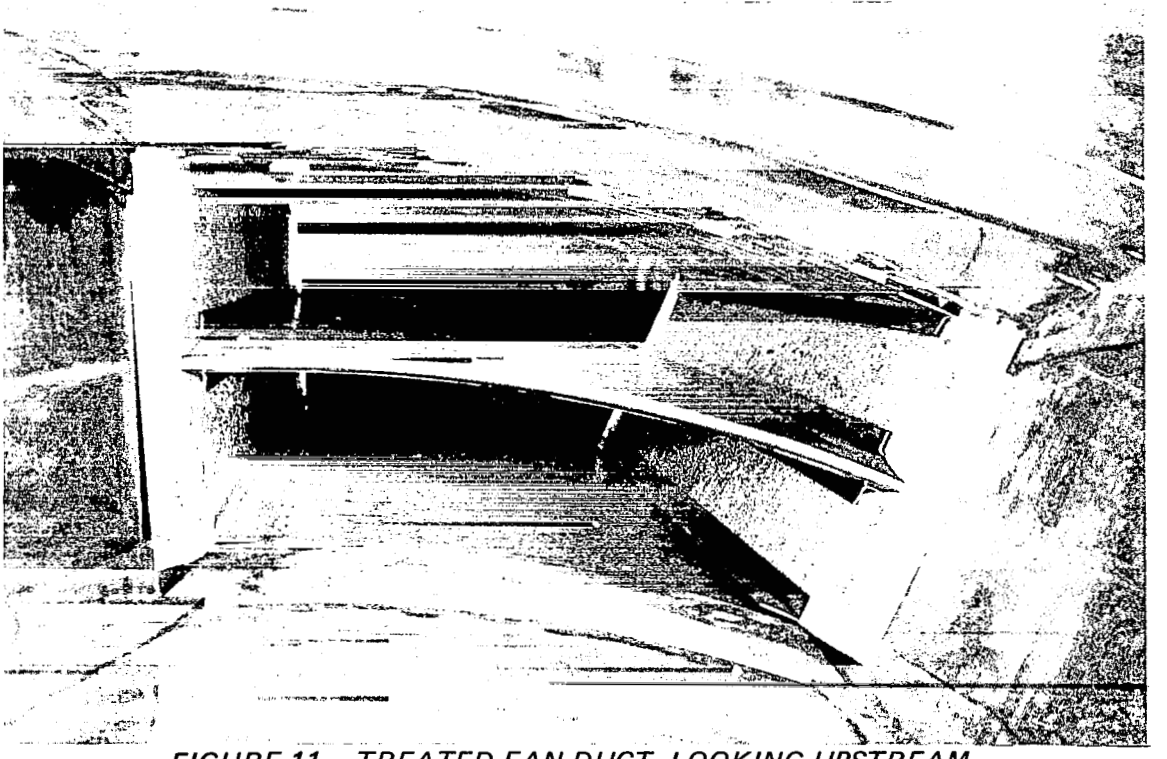

FIGURE 11.— TREATED FAN DUCT, LOOKING UPSTREAM, WITH SPLITTER CENTER PANEL

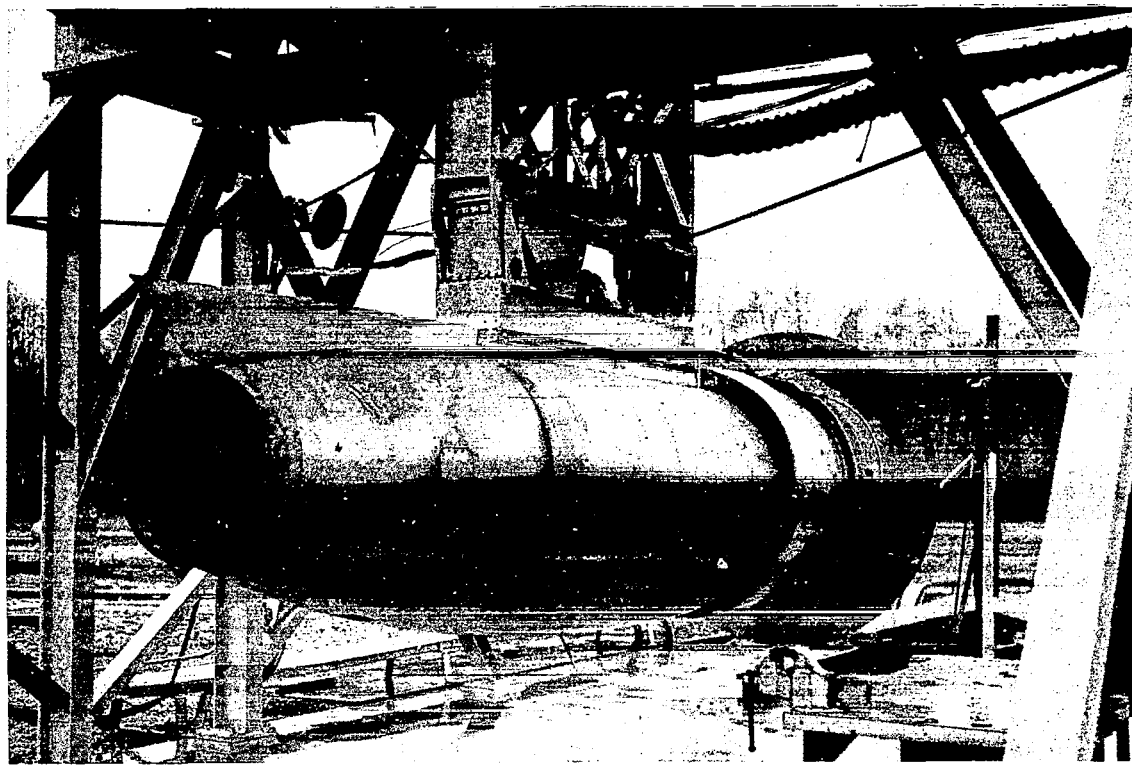

FIGURE 12.—BASELINE TEST ENGINE WITH PRODUCTION SHORT DUCTS

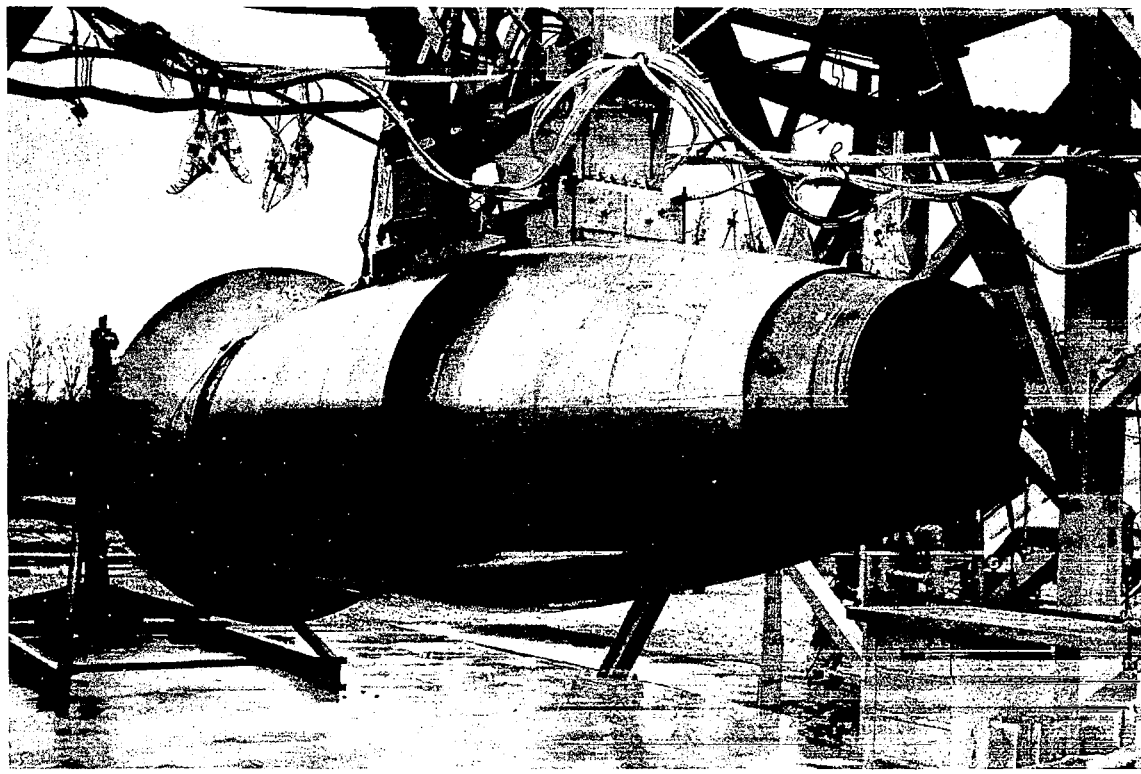

FIGURE 13.—TEST ENGINE WITH MODIFIED THREE-QUARTER-LENGTH FAN DUCTS

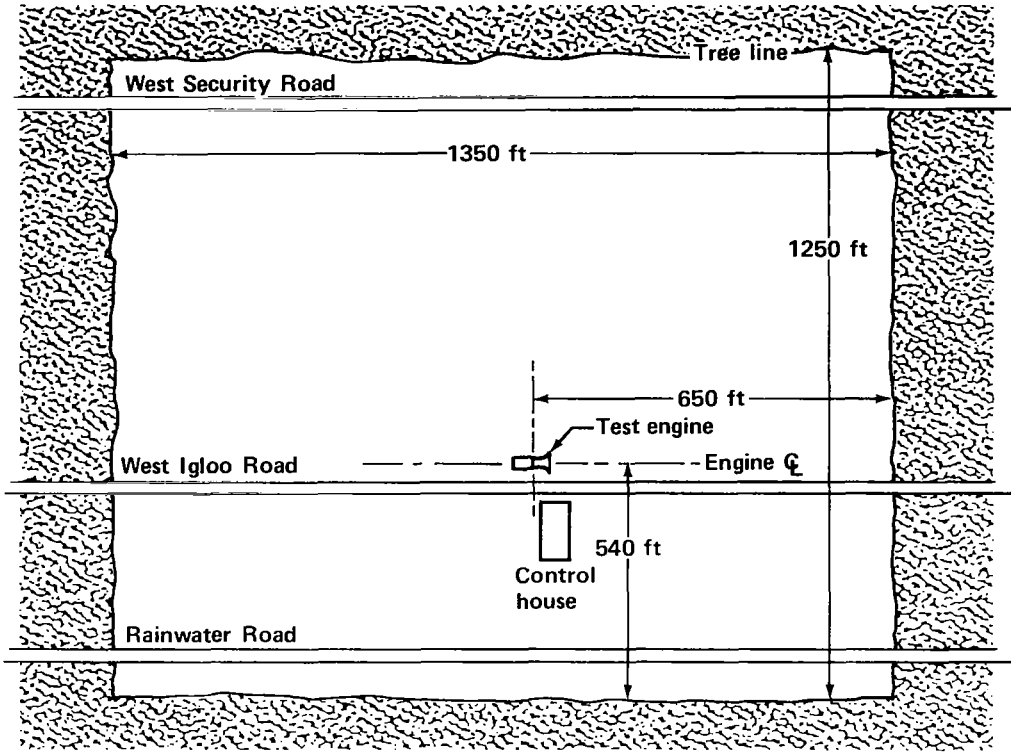

FIGURE 14.—TULALIP TEST SITE

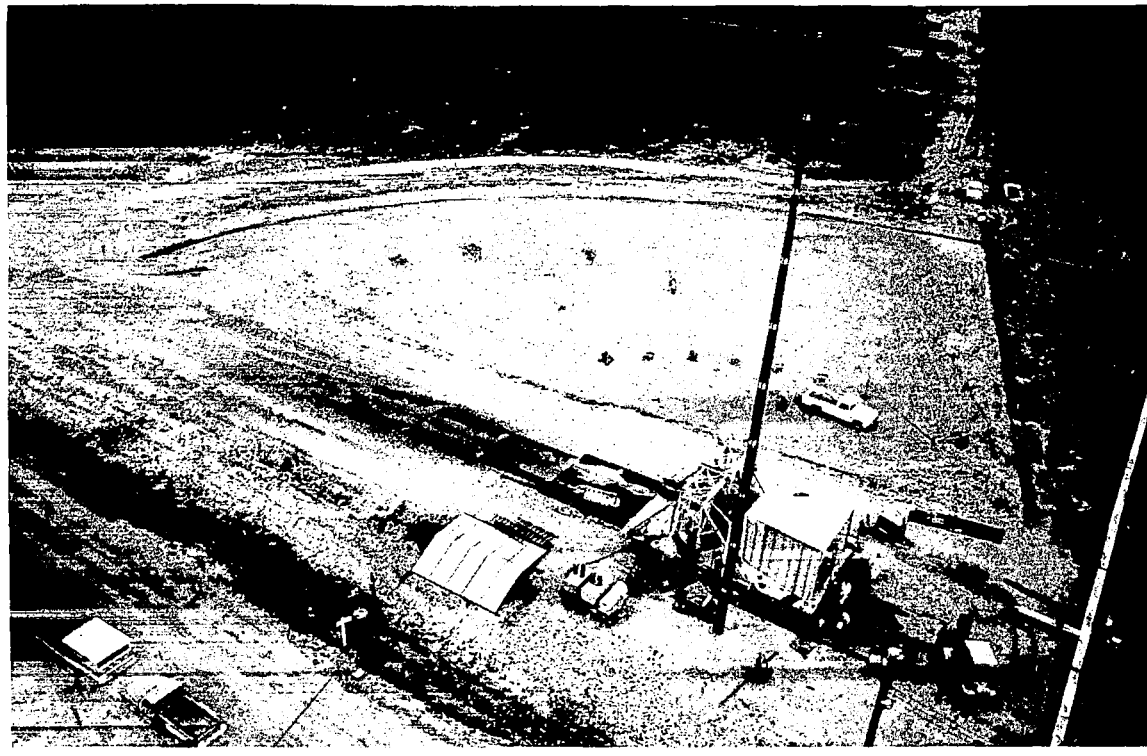

FIGURE 15.- TEST SITE AND INLET NOISE DIRECTIONALIZER

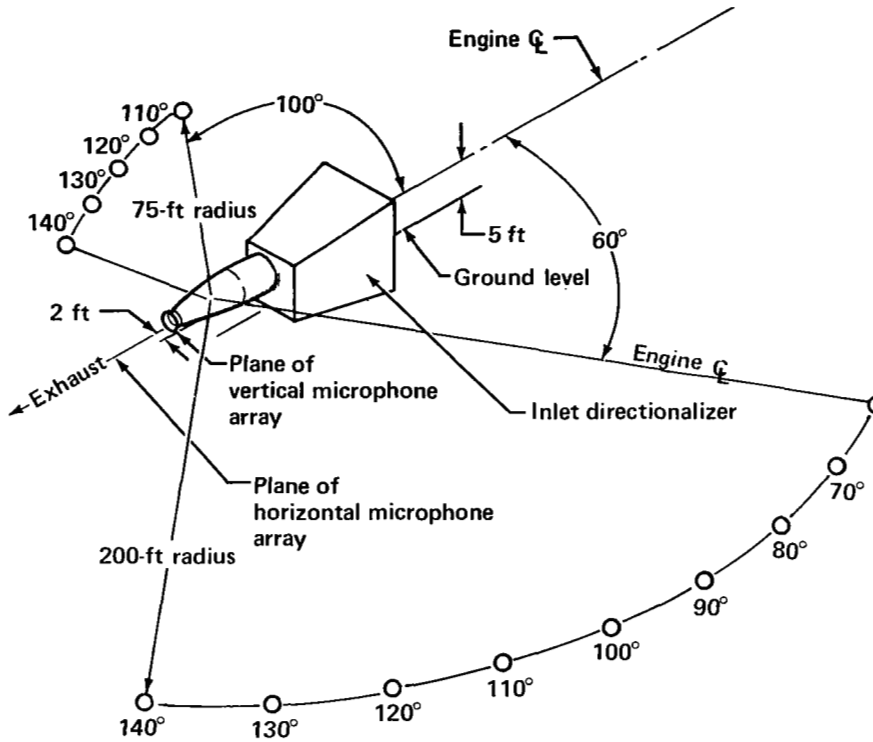

FIGURE 16.–LAYOUT OF HORIZONTAL AND VERTICAL MICROPHONE ARRAYS

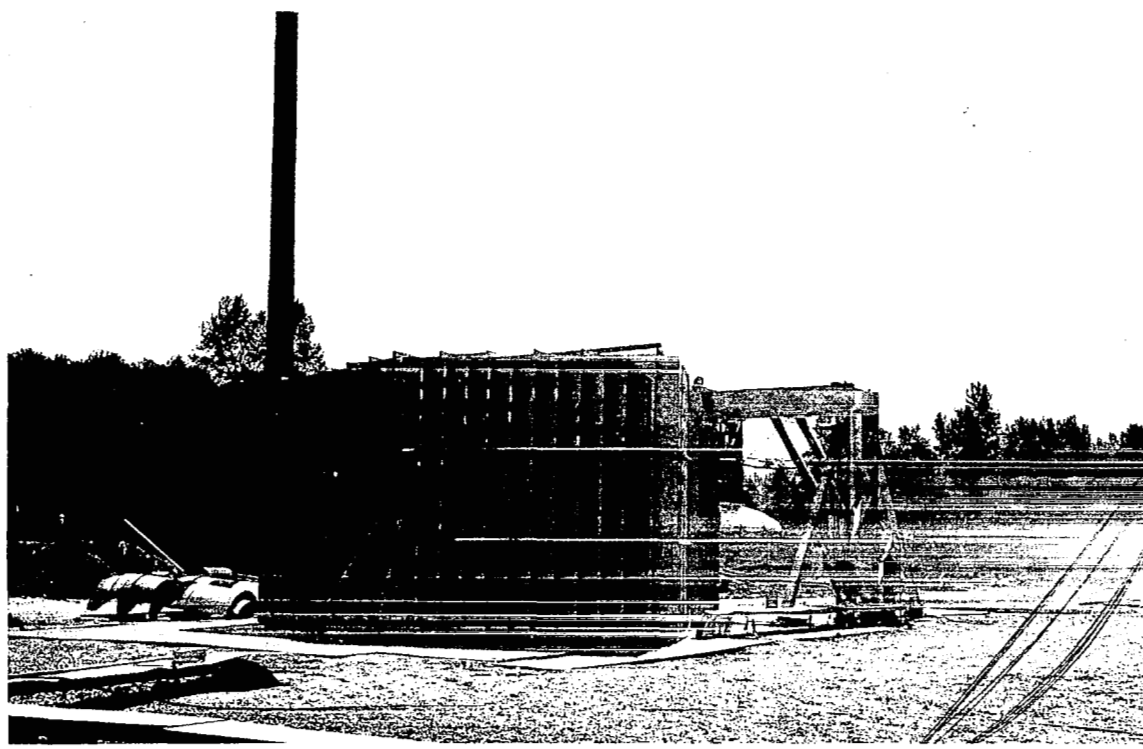

FIGURE 17.–DIRECTIONALIZER LOUVERS, EXTERIOR VIEW

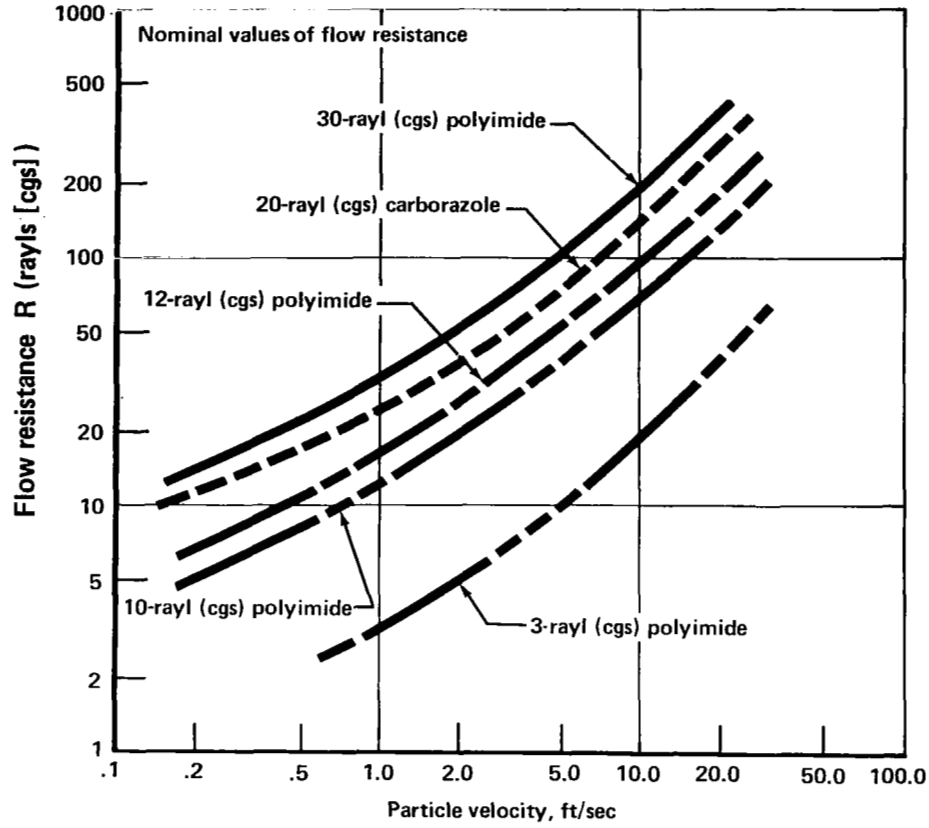

FIGURE 18.–FLOW-RESISTANCE EVALUATION OF POLYIMIDE-FIBERGLASS AND CARBORAZOLE-FIBERGLASS POROUS LAMINATES

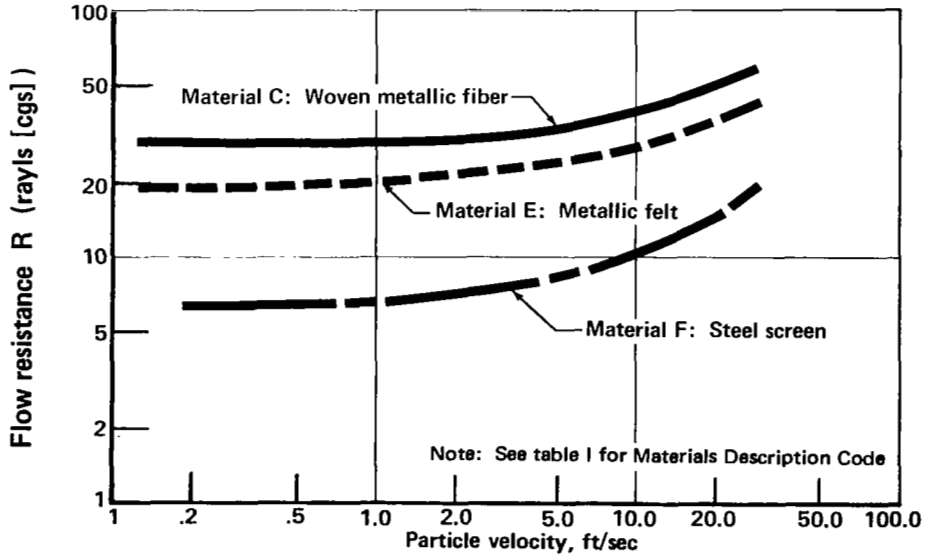

FIGURE 19.–FLOW-RESISTANCE CHARACTERISTICS OF VARIOUS METALLIC MATERIALS

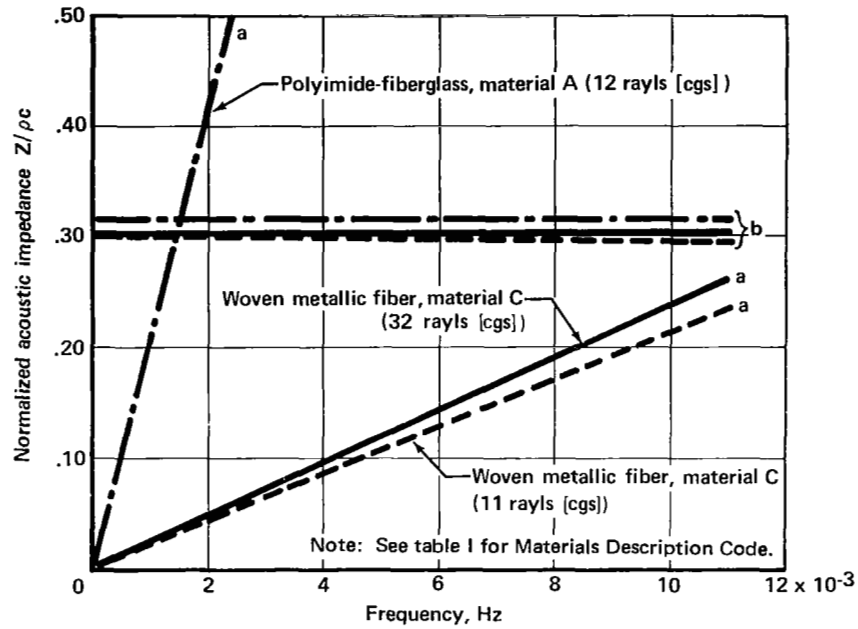

a Reactive impedance

b Resistive impedance

FIGURE 20.–IMPEDANCE CHARACTERISTICS OF METALLIC AND NONMETALLIC POROUS LAMINATES

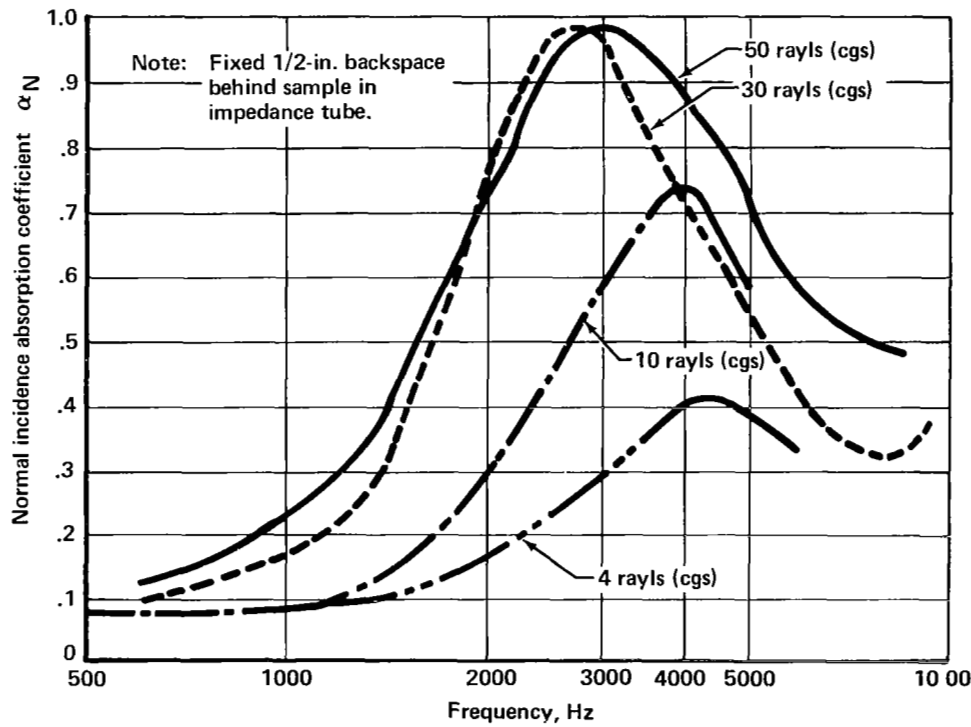

FIGURE 21.–POLYIMIDE-FIBERGLASS, MATERIAL A, VARIATION OF ABSORPTION COEFFICIENT WITH LAMINATE FLOW RESISTANCE

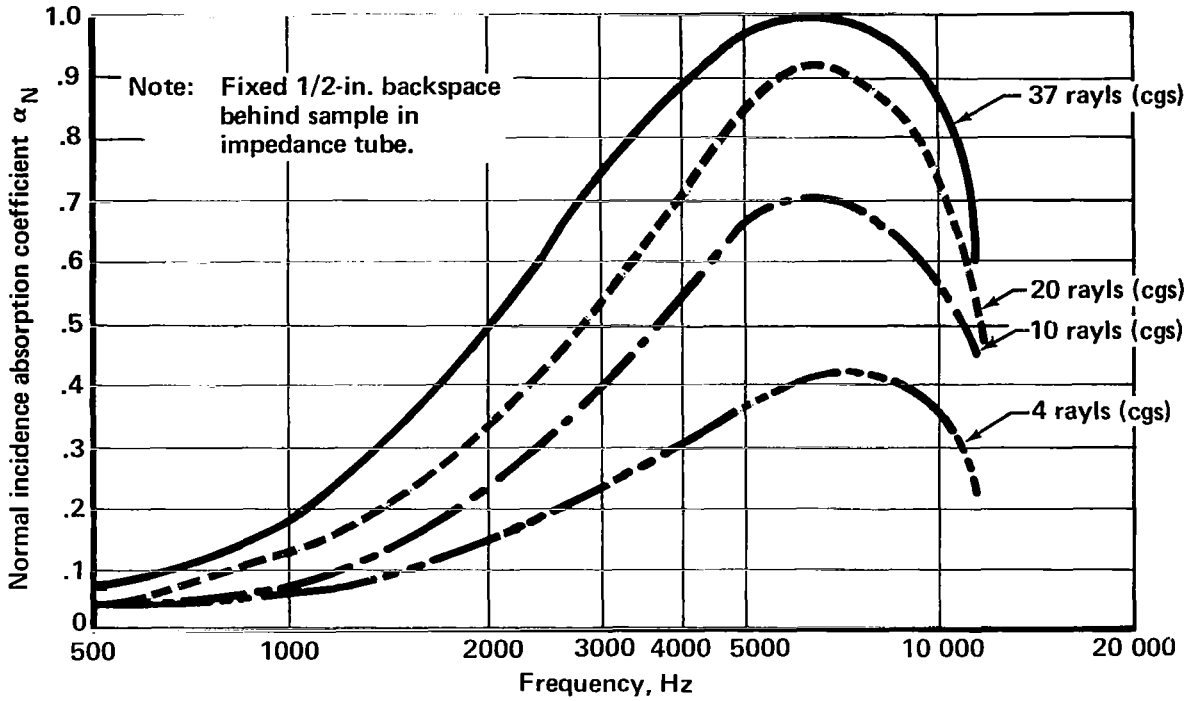

FIGURE 22.–WOVEN METALLIC FIBER, MATERIAL C, VARIATION OF ABSORPTION COEFFICIENT WITH LAMINATE FLOW RESISTANCE

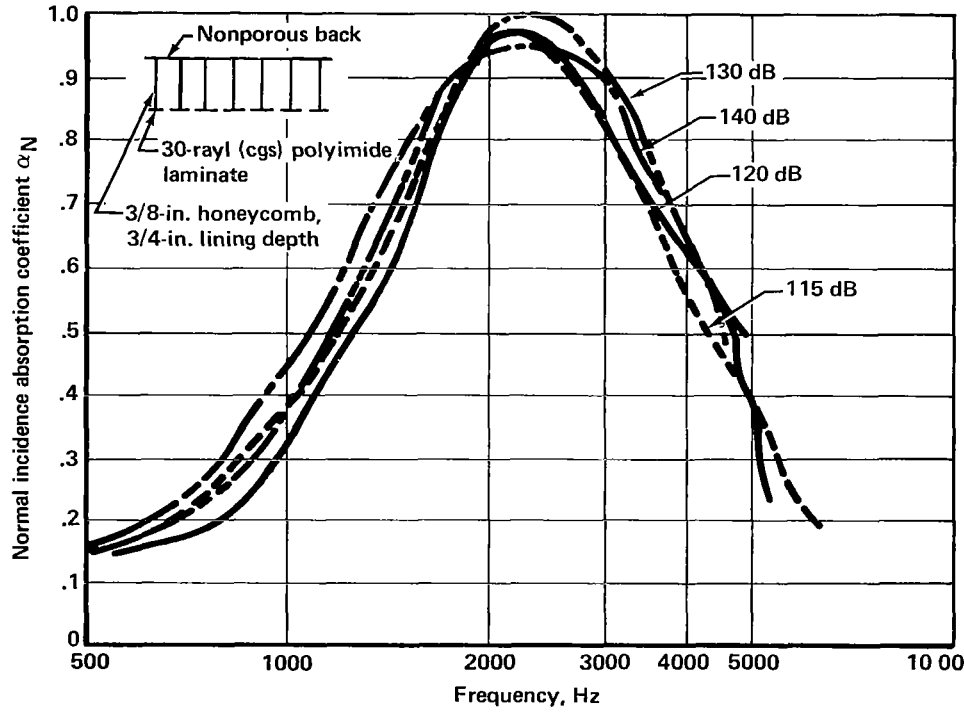

FIGURE 23.–VARIATION OF ABSORPTION COEFFICIENT WITH SOUND PRESSURE LEVEL

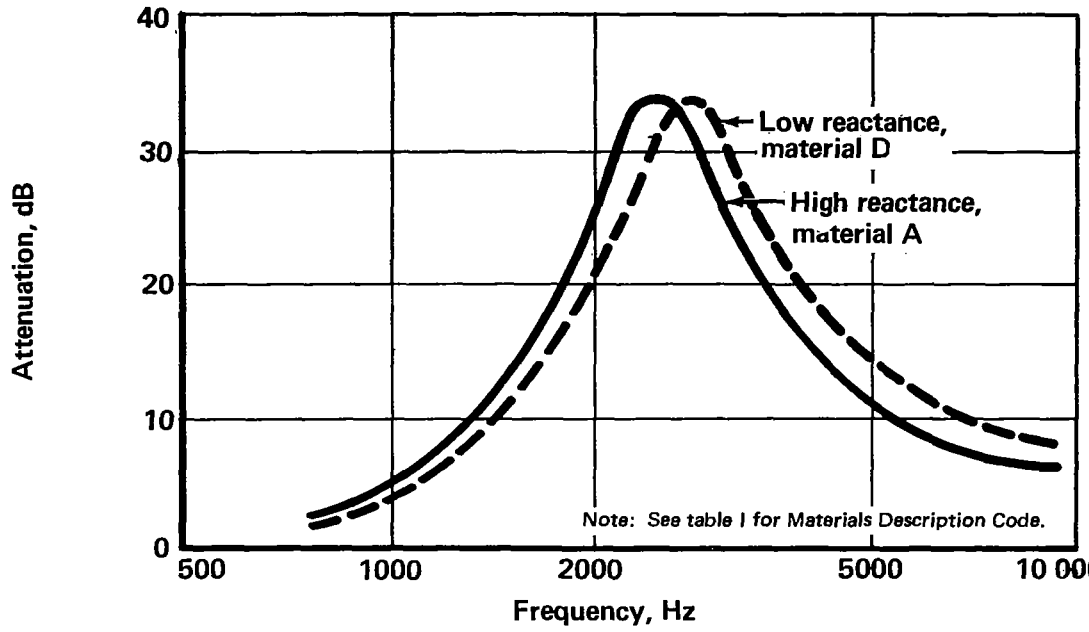

Note: Geometric dimensions and laminate flow resistance are identical for both treatments.
Lining depth: 1/2 in.
Lining separation: 6 in.
Lining length: 44 in.

FIGURE 24.–TYPICAL ATTENUATION OF DUCT LINING (BROADBAND NOISE SOURCE)

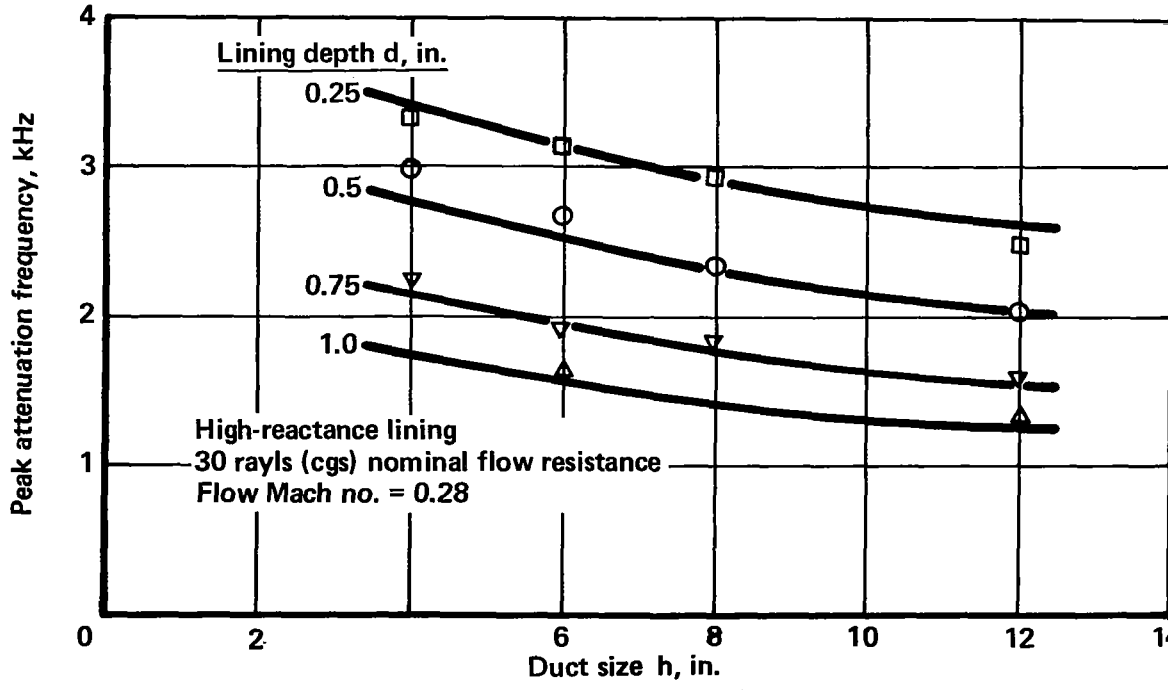

FIGURE 25.–VARIATION OF PEAK FREQUENCY WITH DUCT SIZE AND LINING DEPTH

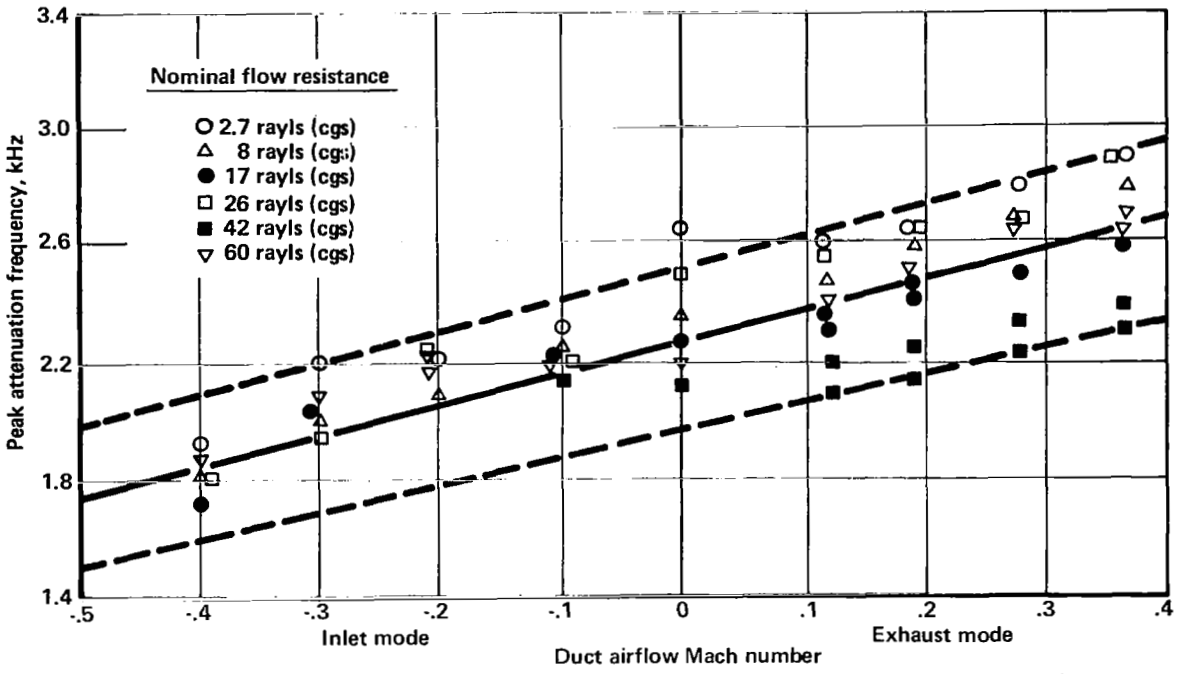

FIGURE 26.—VARIATION OF PEAK FREQUENCY WITH AIRFLOW MACH NUMBER FOR A RANGE OF HIGH-REACTANCE LININGS 0.5 IN. DEEP IN A 6-IN. DUCT

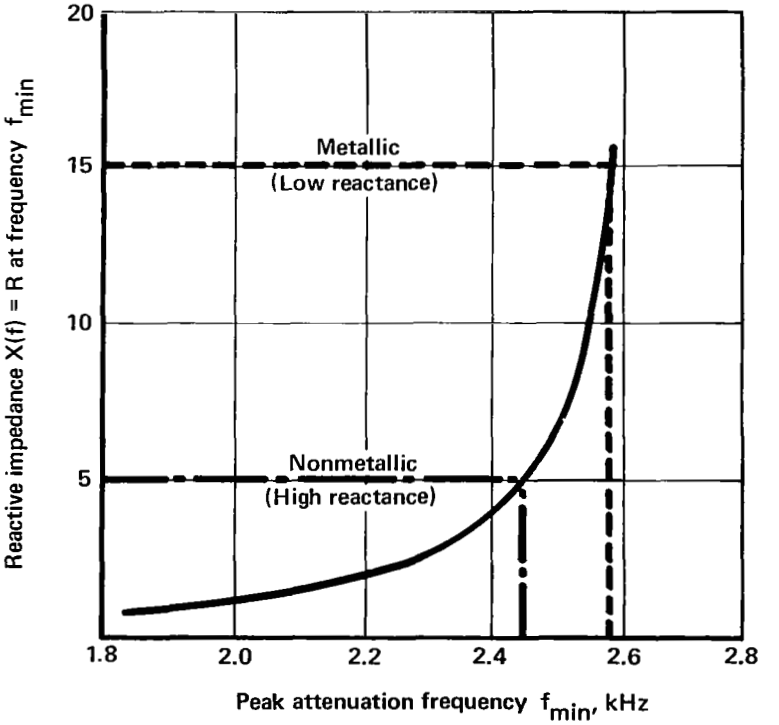

FIGURE 27.—VARIATION OF PEAK FREQUENCY WITH LINING REACTANCE FOR A 30-RAYL (CGS) EFFECTIVE FLOW-RESISTANCE MATERIAL IN A 6-IN. DUCT AT M = 0

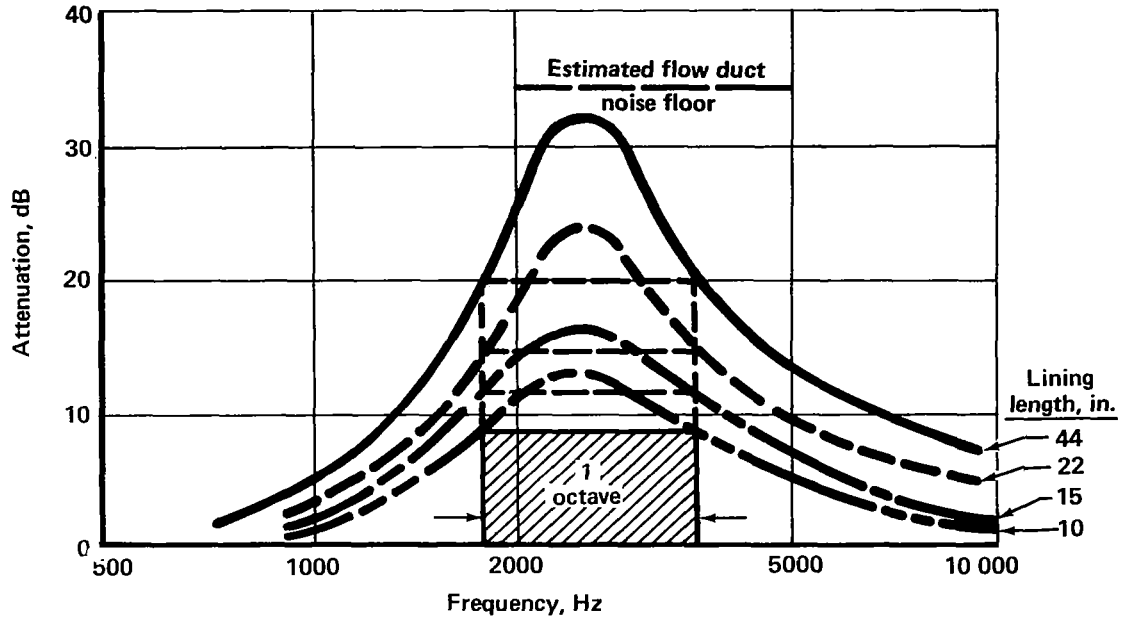

FIGURE 28.—TYPICAL ATTENUATION SPECTRA FOR VARIOUS LINING LENGTHS OF A 30-RAYL (CGS) HIGH-REACTANCE LINING 0.5 IN. DEEP IN A 6-IN. DUCT AT M = 0.28

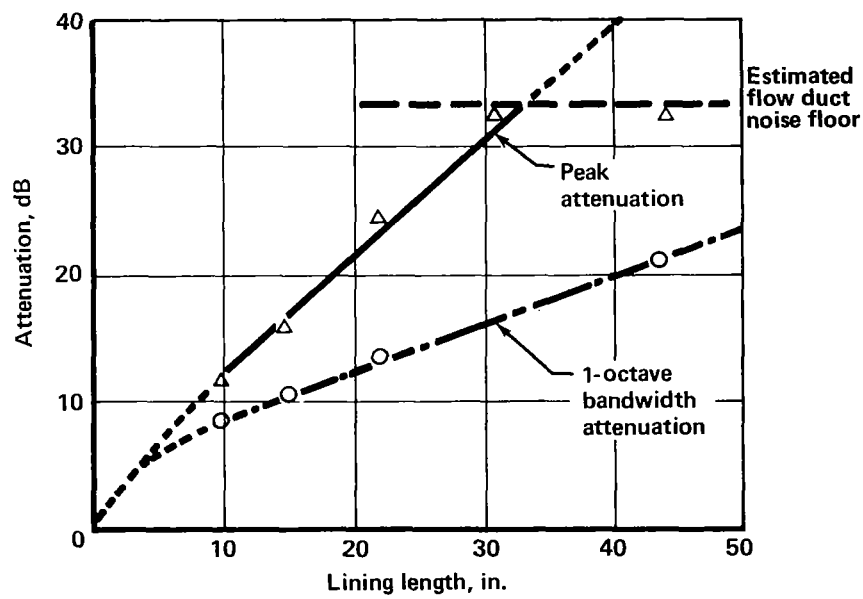

FIGURE 29.—VARIATION OF ATTENUATION WITH LINING LENGTH FOR A 30-RAYL (CGS) HIGH-REACTANCE LINING 0.5 IN. DEEP IN A 6-IN. DUCT AT M = 0.28

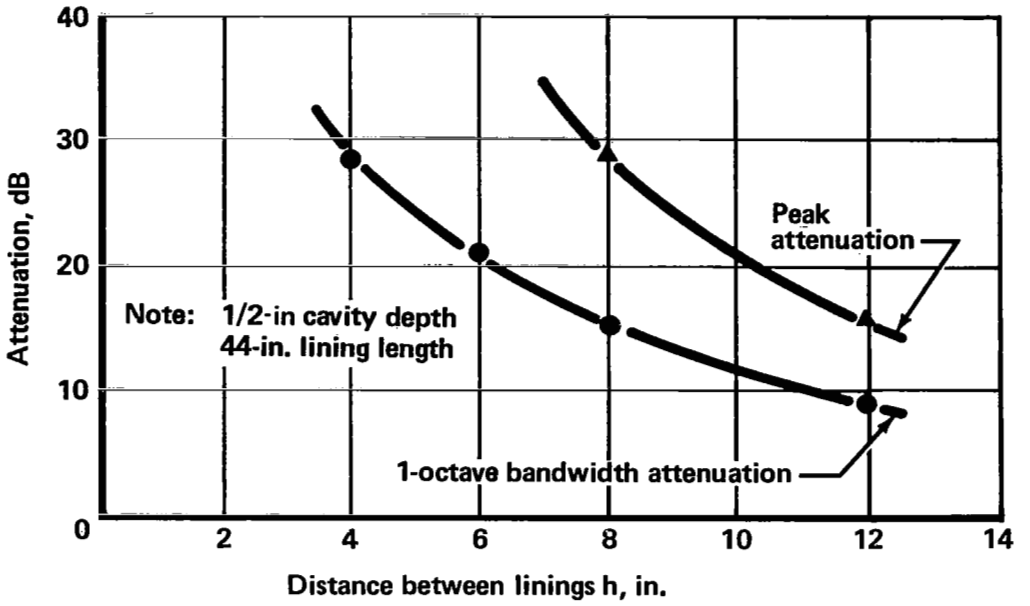

FIGURE 30.– INFLUENCE OF LINING SEPARATION ON ATTENUATION

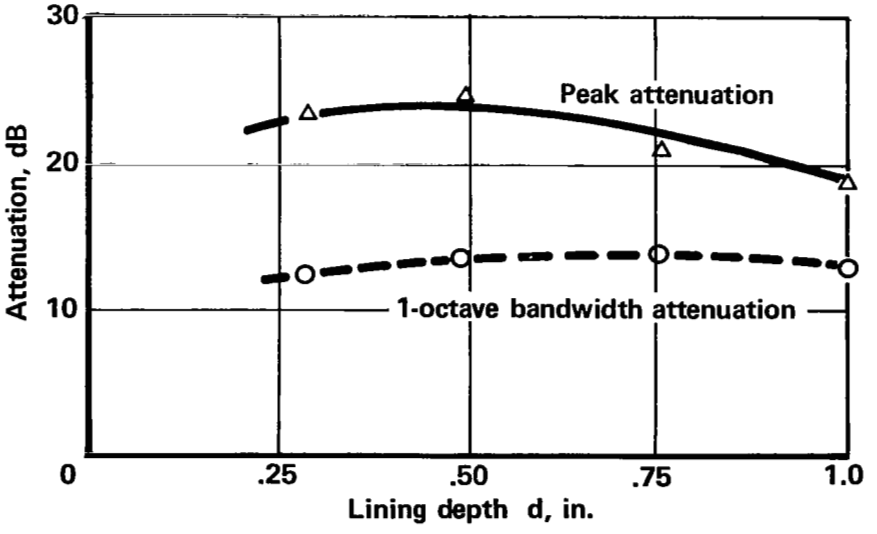

FIGURE 31.–INFLUENCE OF LINING DEPTH ON ATTENUATION

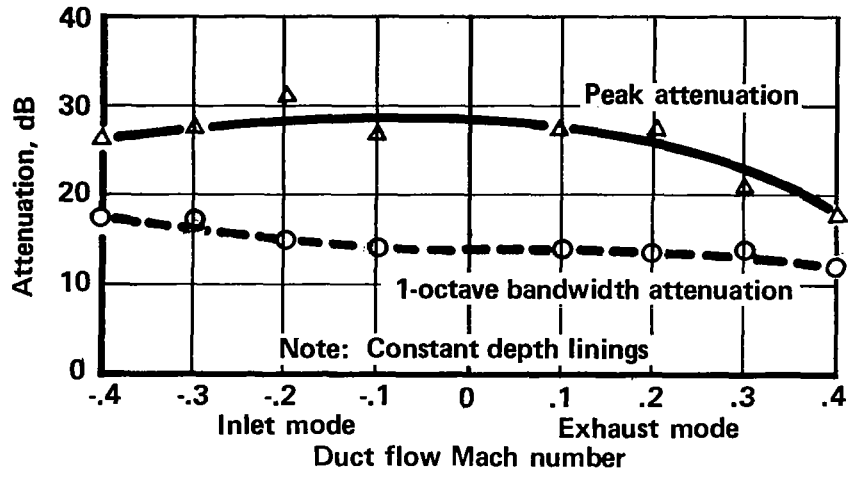

FIGURE 32.—INFLUENCE OF AIRFLOW VELOCITY ON ATTENUATION

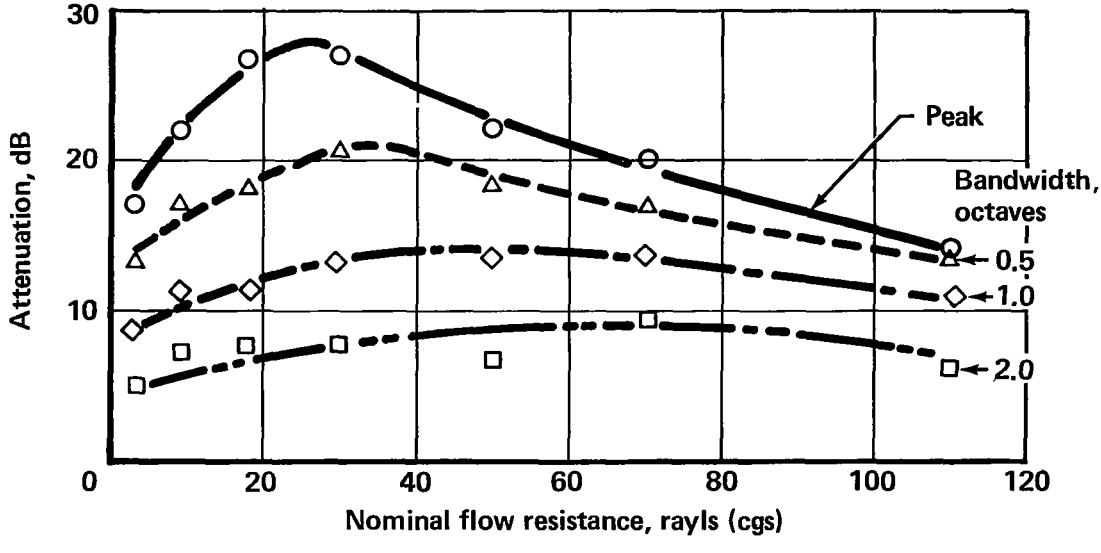

FIGURE 33.—VARIATION OF ATTENUATION WITH LAMINATE FLOW RESISTANCE FOR A HIGH-REACTANCE LINING 0.5 IN. DEEP IN A 6-IN. DUCT AT M = 0.12

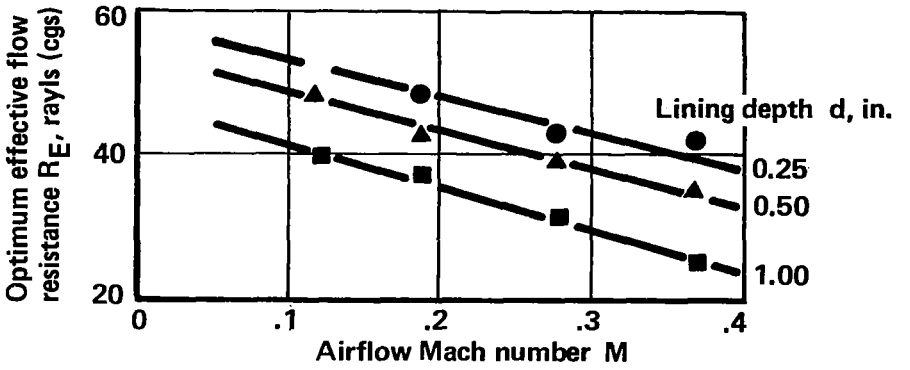

FIGURE 34.—VARIATION OF OPTIMUM EFFECTIVE FLOW RESISTANCE WITH MACH NUMBER AND LINING DEPTH

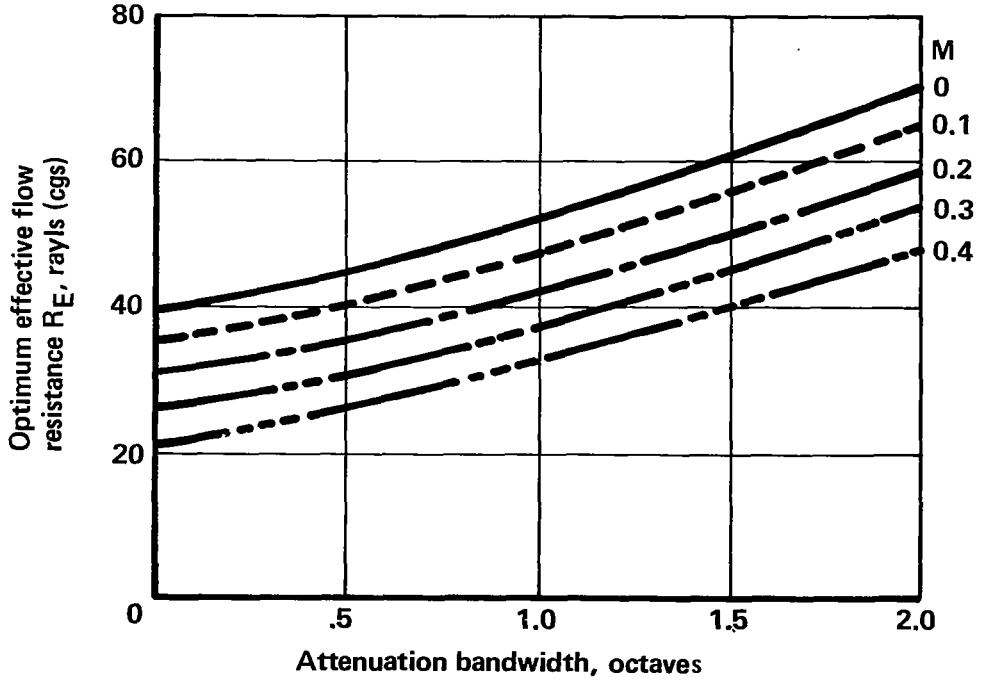

FIGURE 35.—VARIATION OF OPTIMUM EFFECTIVE FLOW RESISTANCE WITH ATTENUATION BANDWIDTH AND MACH NUMBER FOR 0.5-IN-DEEP LININGS IN A 6-IN. DUCT

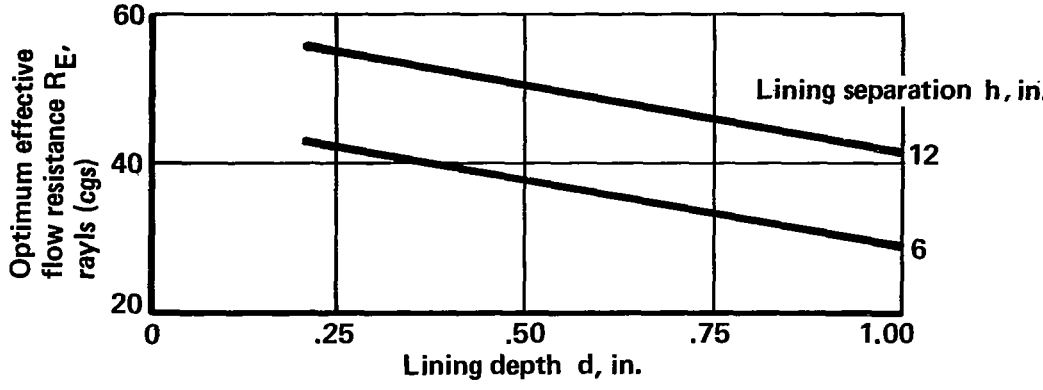

FIGURE 36.—VARIATION OF OPTIMUM EFFECTIVE FLOW RESISTANCE WITH LINING DEPTH AND LINING SEPARATION

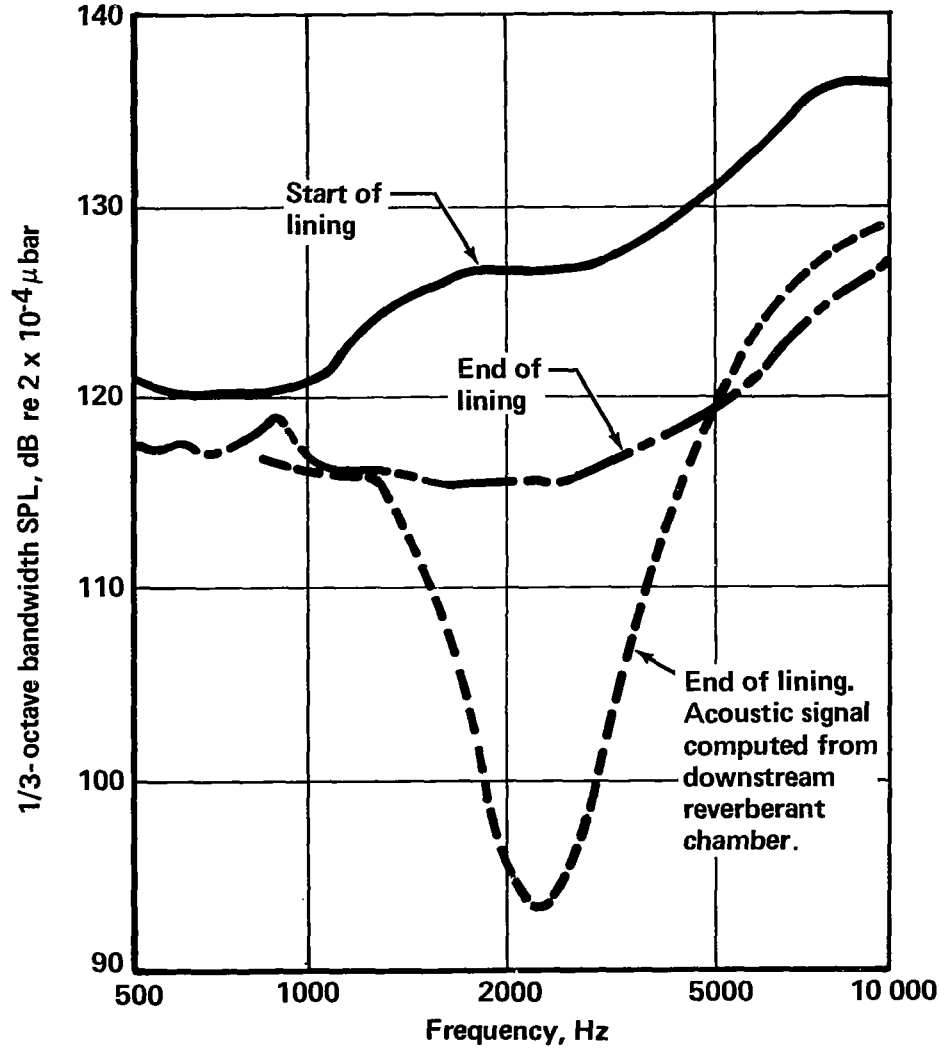

FIGURE 37.—DUCT WALL PRESSURE SPECTRA AS MEASURED BY FLUSH-MOUNTED MICROPHONES IN A 6-IN. DUCT AT M = 0.28

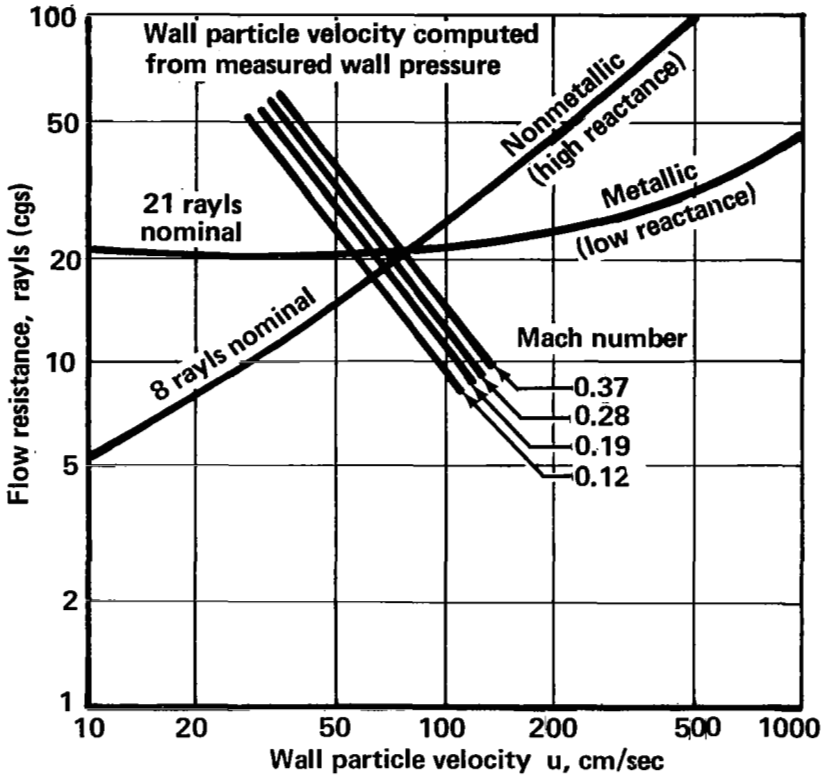

FIGURE 38.—VARIATION OF FLOW RESISTANCE WITH WALL PARTICLE VELOCITY FOR METALLIC AND NONMETALLIC LININGS

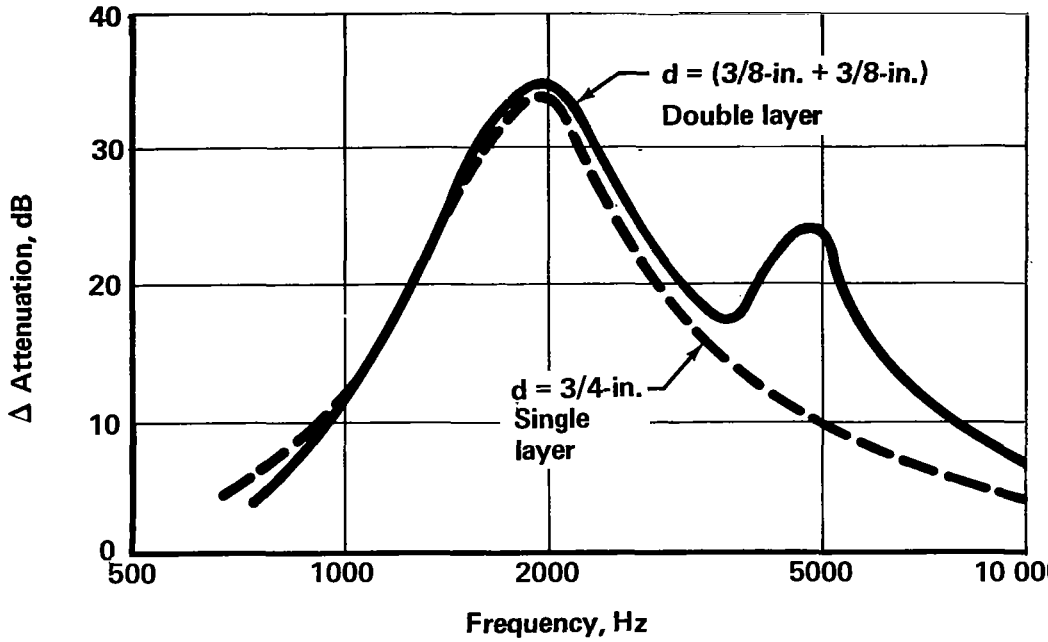

FIGURE 39.—COMPARISON OF ATTENUATION OF SINGLE- AND DOUBLE-LAYER LININGS (CONSTANT LENGTH)

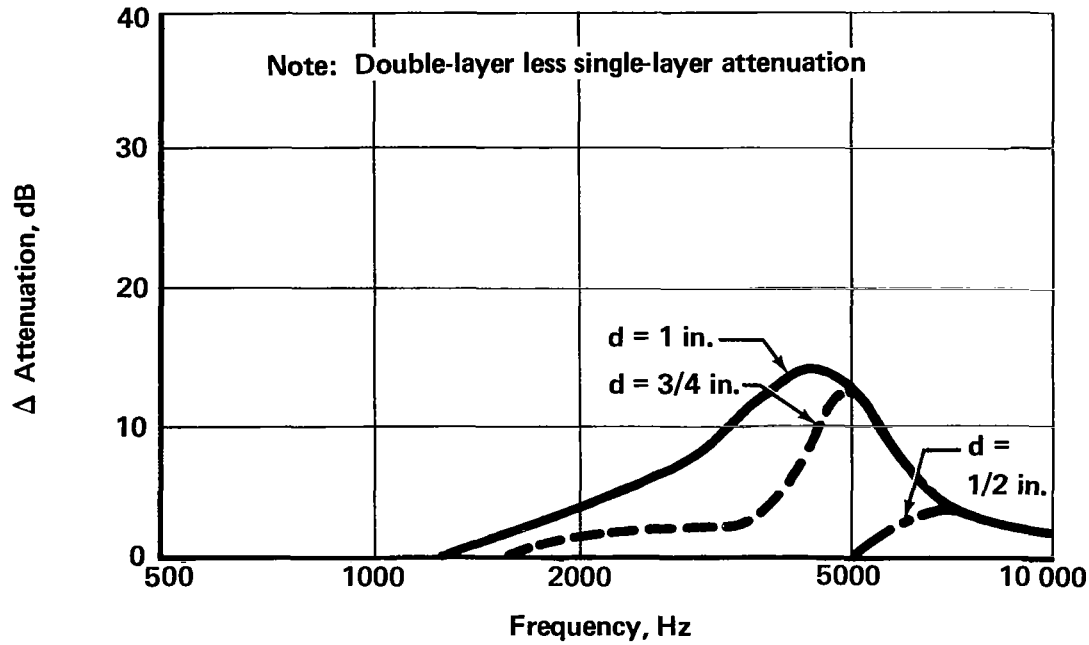

FIGURE 40.—IMPROVEMENT IN ATTENUATION OF DOUBLE- VERSUS SINGLE-LAYER LININGS (CONSTANT LENGTH)

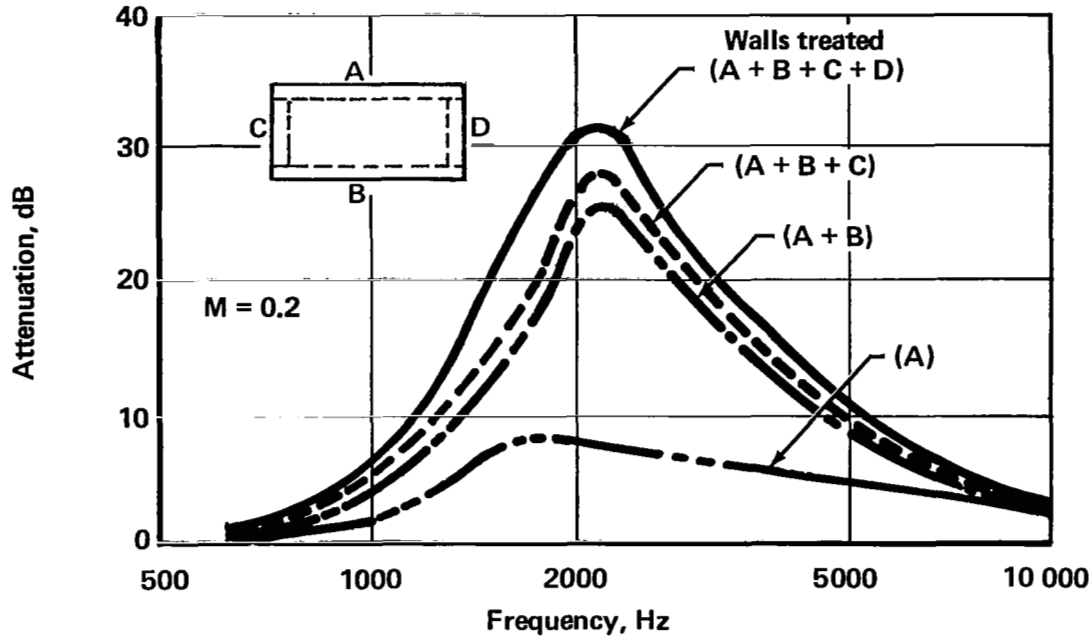

FIGURE 41.—INFLUENCE OF NUMBER OF WALLS TREATED (LINING AREA) ON THE ATTENTUATION

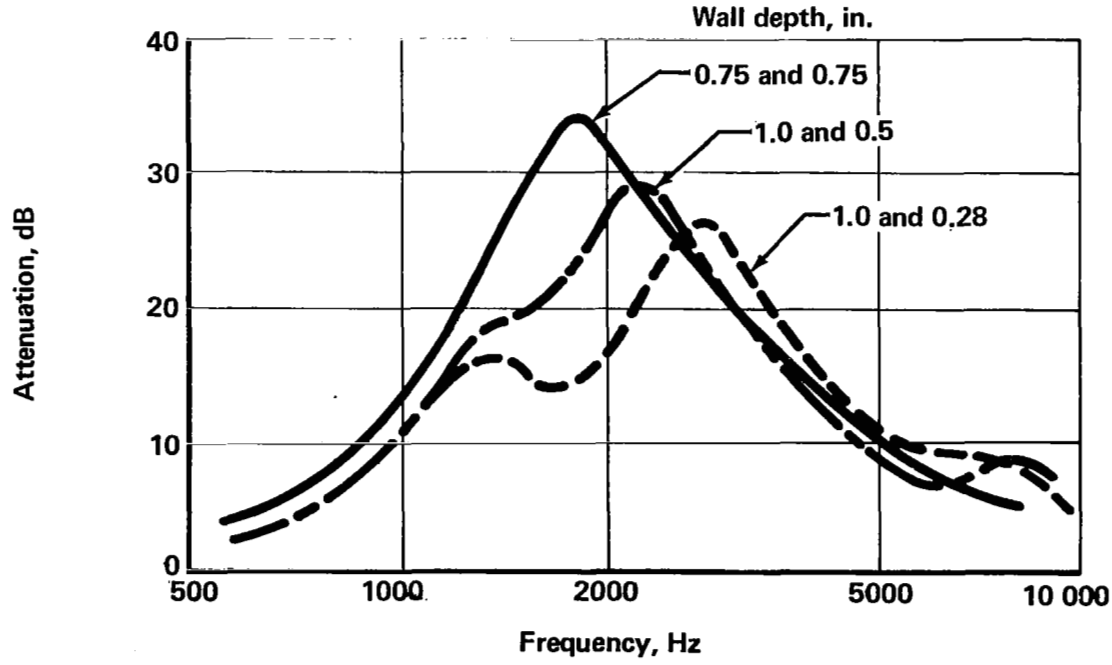

FIGURE 42.—INFLUENCE OF DOUBLE-WALL LINING DEPTH VARIATION ON ATTENUATION

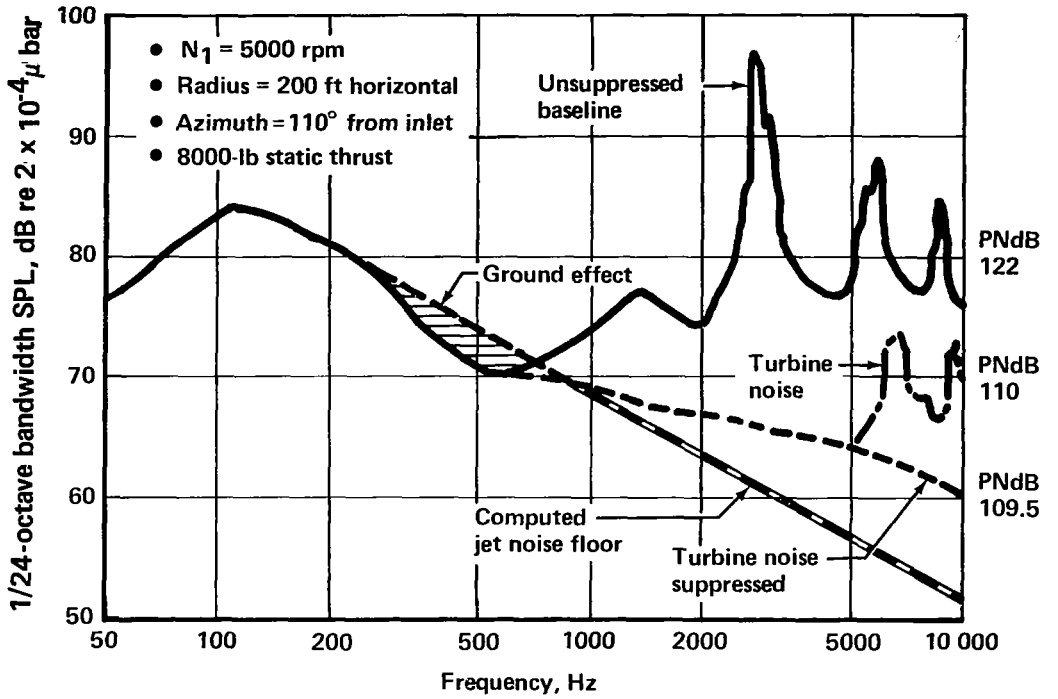

FIGURE 43.—1/24-OCTAVE BANDWIDTH ANALYSIS, CONFIGURATION NUMBER 7 AT 5000 RPM

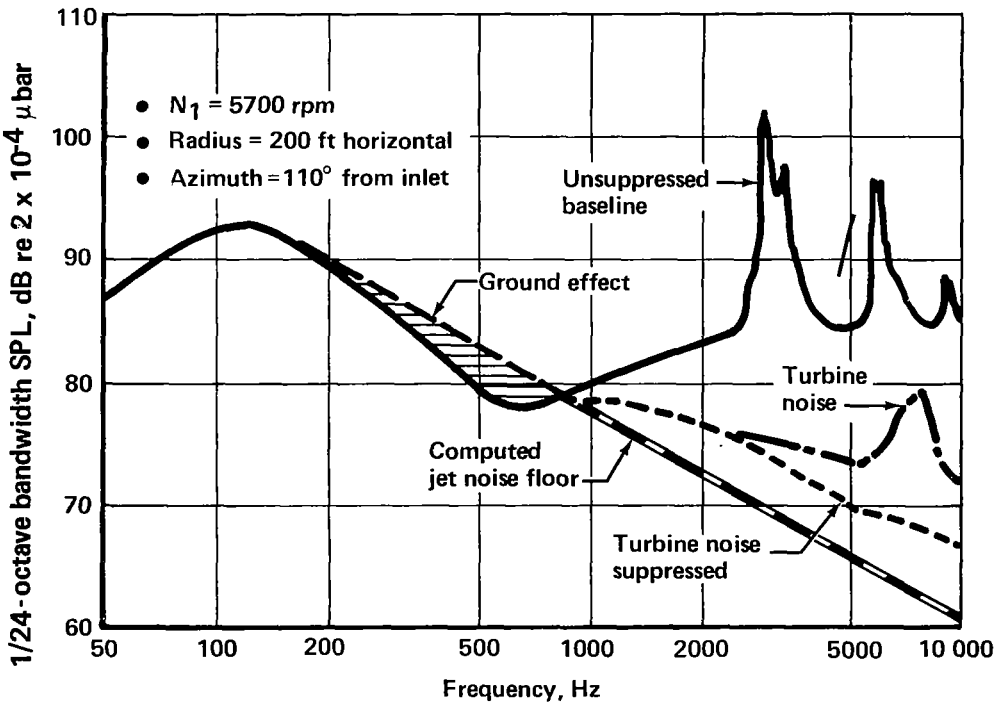

FIGURE 44.—1/24-OCTAVE BANDWIDTH ANALYSIS, CONFIGURATION NUMBER 7 AT 5700 RPM

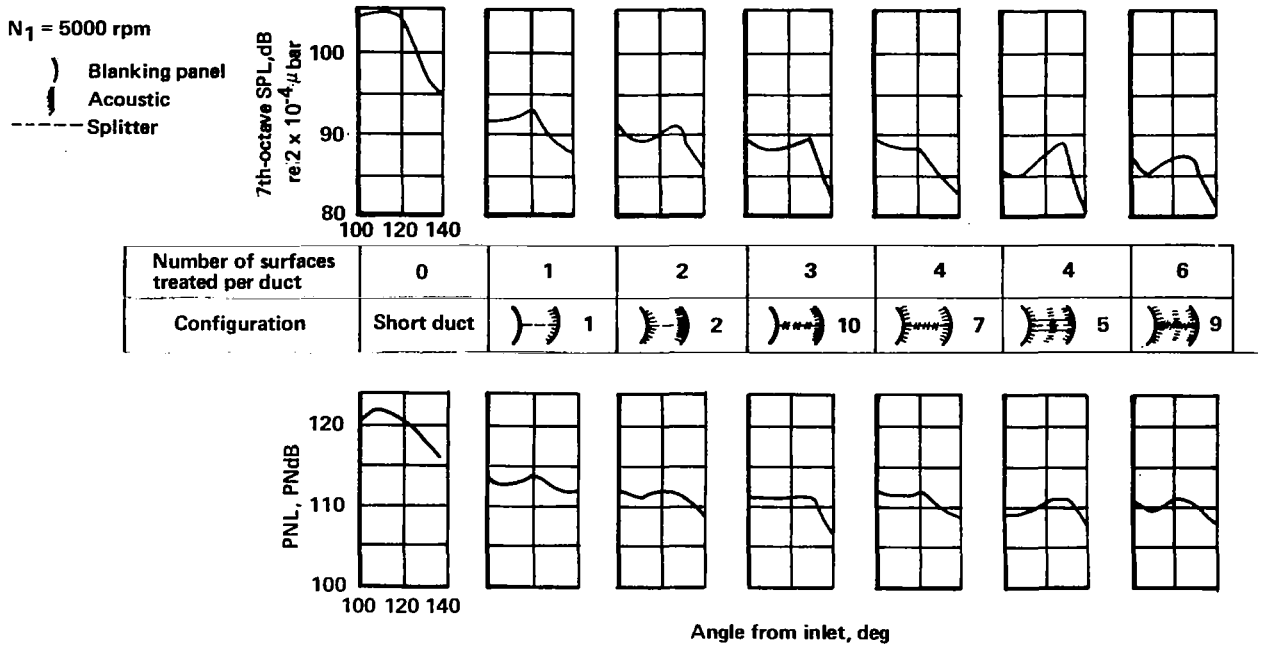

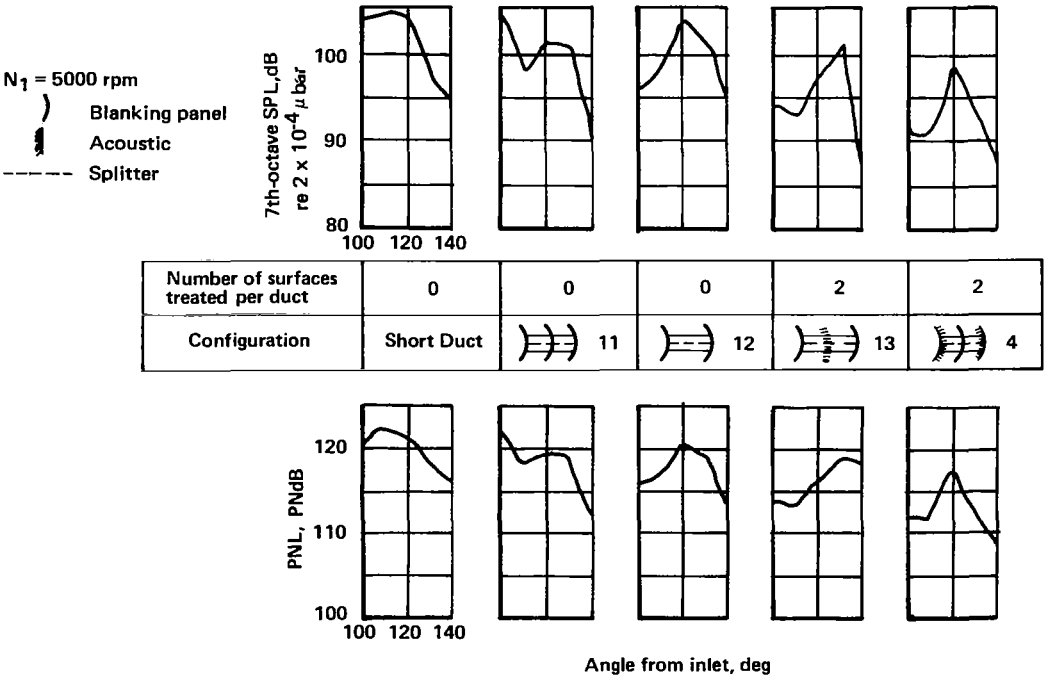

FIGURE 45. –7TH-OCTAVE BANDWIDTH AND PERCEIVED NOISE VERSUS ANGLE

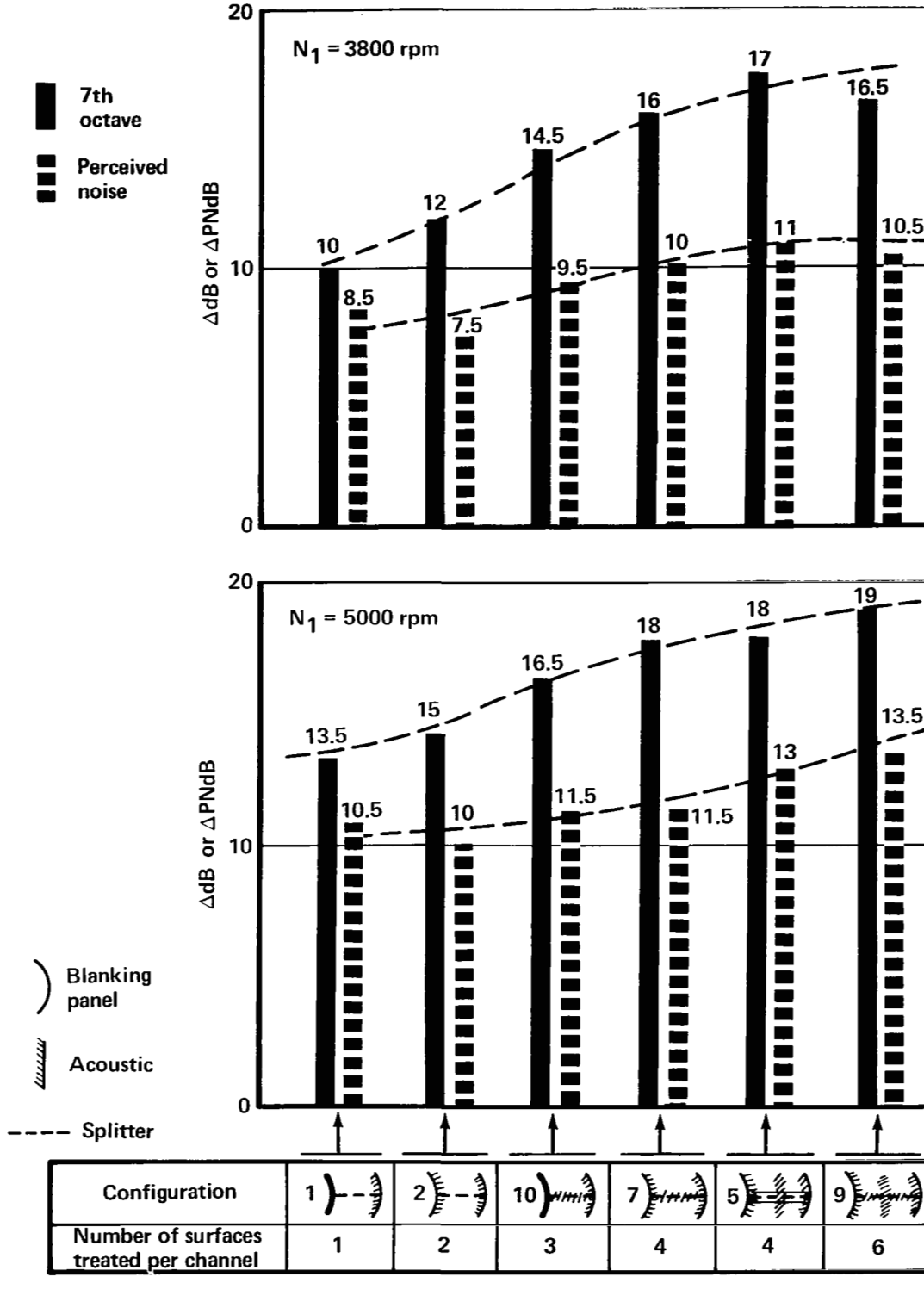

FIGURE 46.—REDUCTIONS OF PEAK LEVELS OF OCTAVE BANDWIDTH AND PERCEIVED NOISE

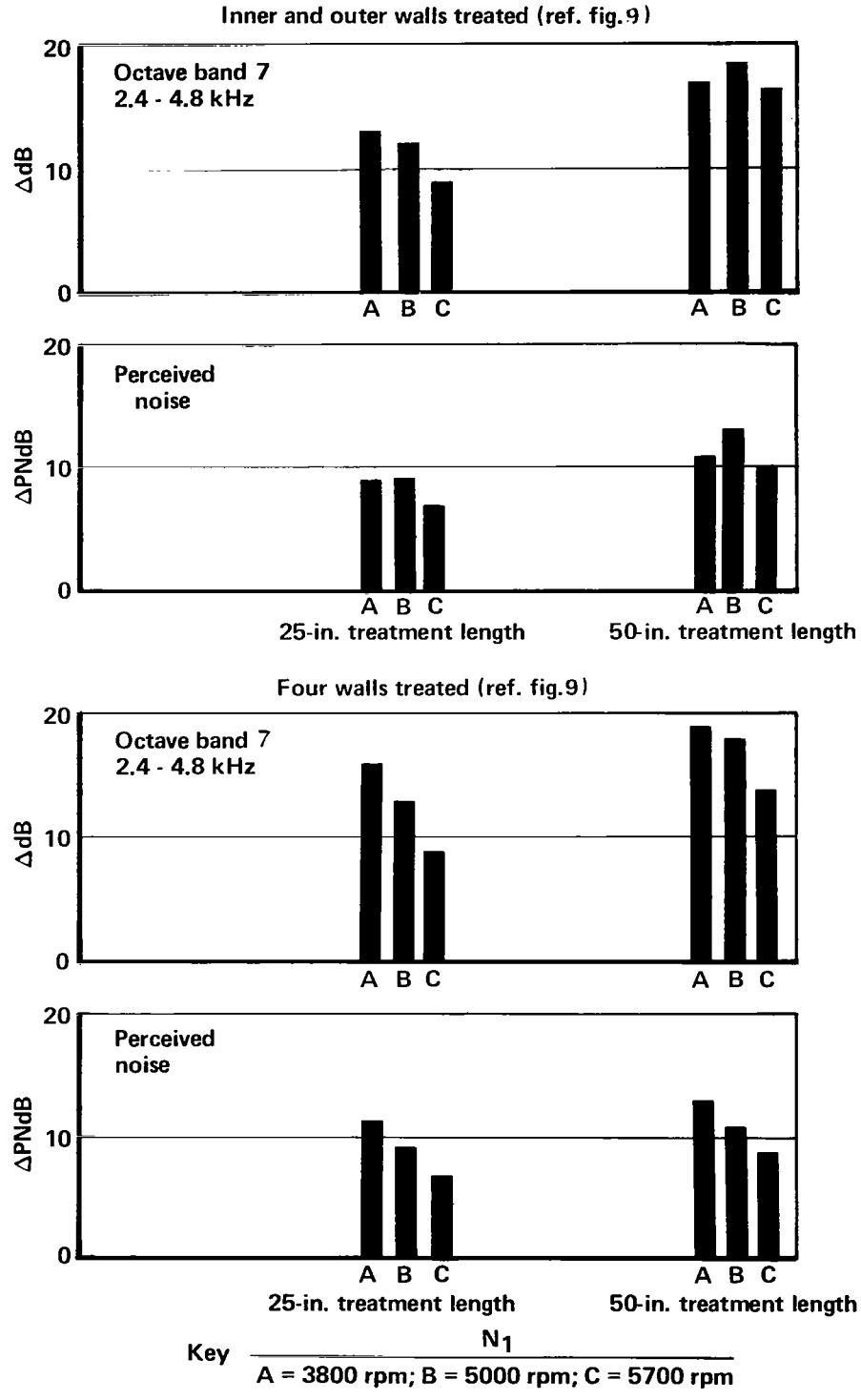

FIGURE 47.—FAN NOISE ATTENUATION FROM 25- AND 50-IN. FAN DUCT TREATMENT LENGTHS ON THE JT3D-3B ENGINE

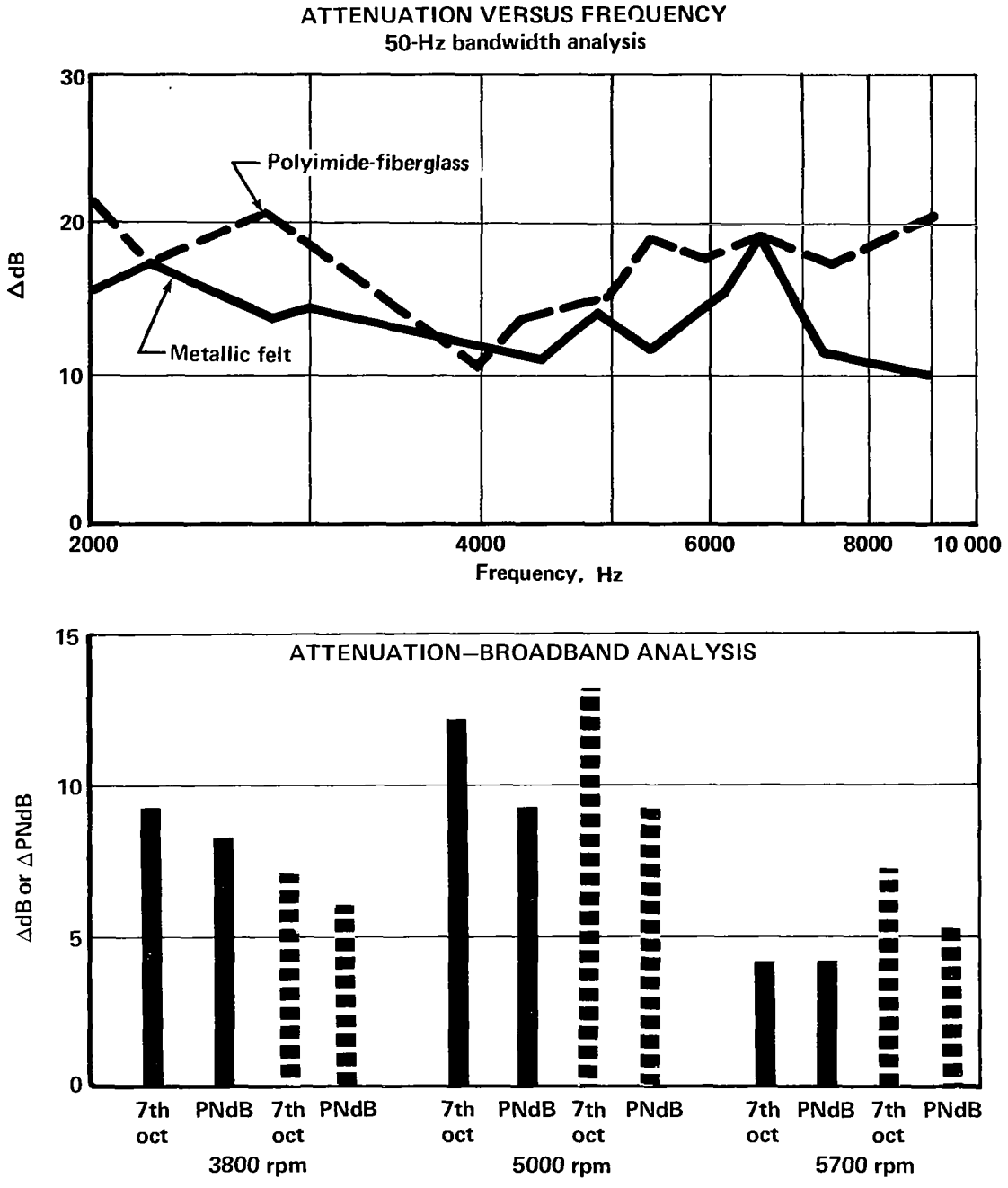

Note: Outer wall only, double-layer treatment in both cases

FIGURE 48.—COMPARISON BETWEEN METALLIC AND NONMETALLIC TREATMENT, FULL-SCALE FAN DUCT

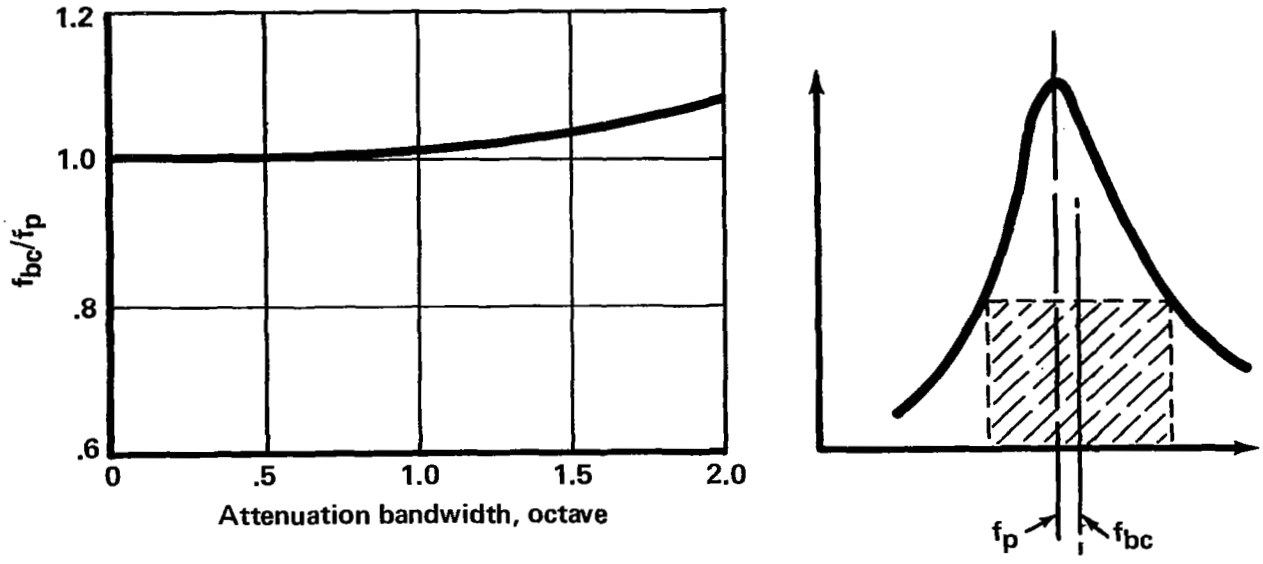

FIGURE 49.—VARIATION OF ATTENUATION BAND CENTER FREQUENCY

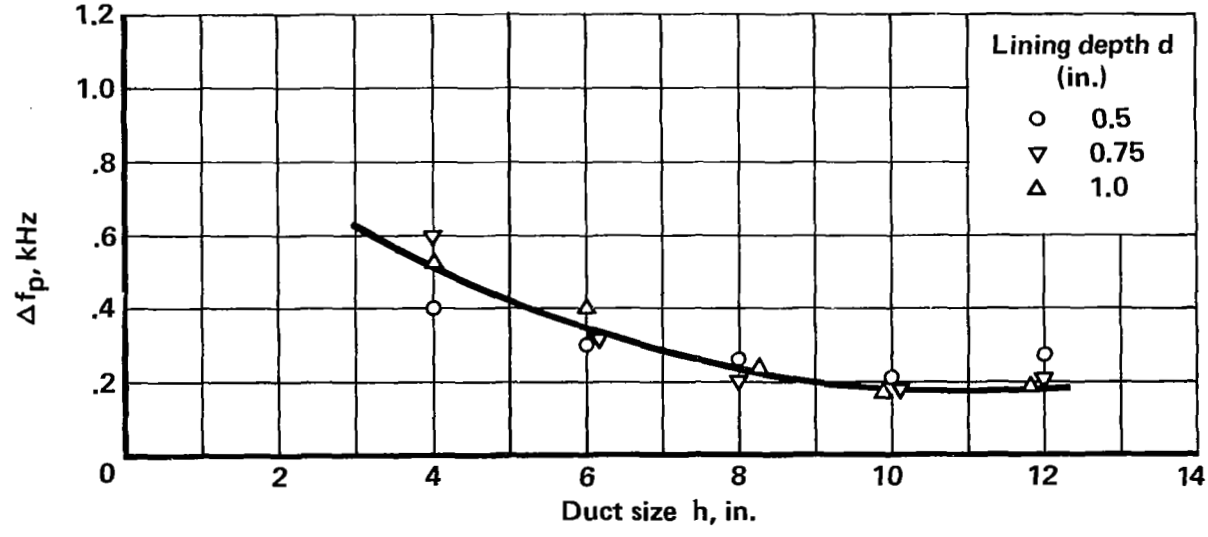

FIGURE 50.—INCREASE IN PEAK FREQUENCY FOR LOW-REACTANCE LININGS AS COMPARED TO HIGH-REACTANCE LININGS

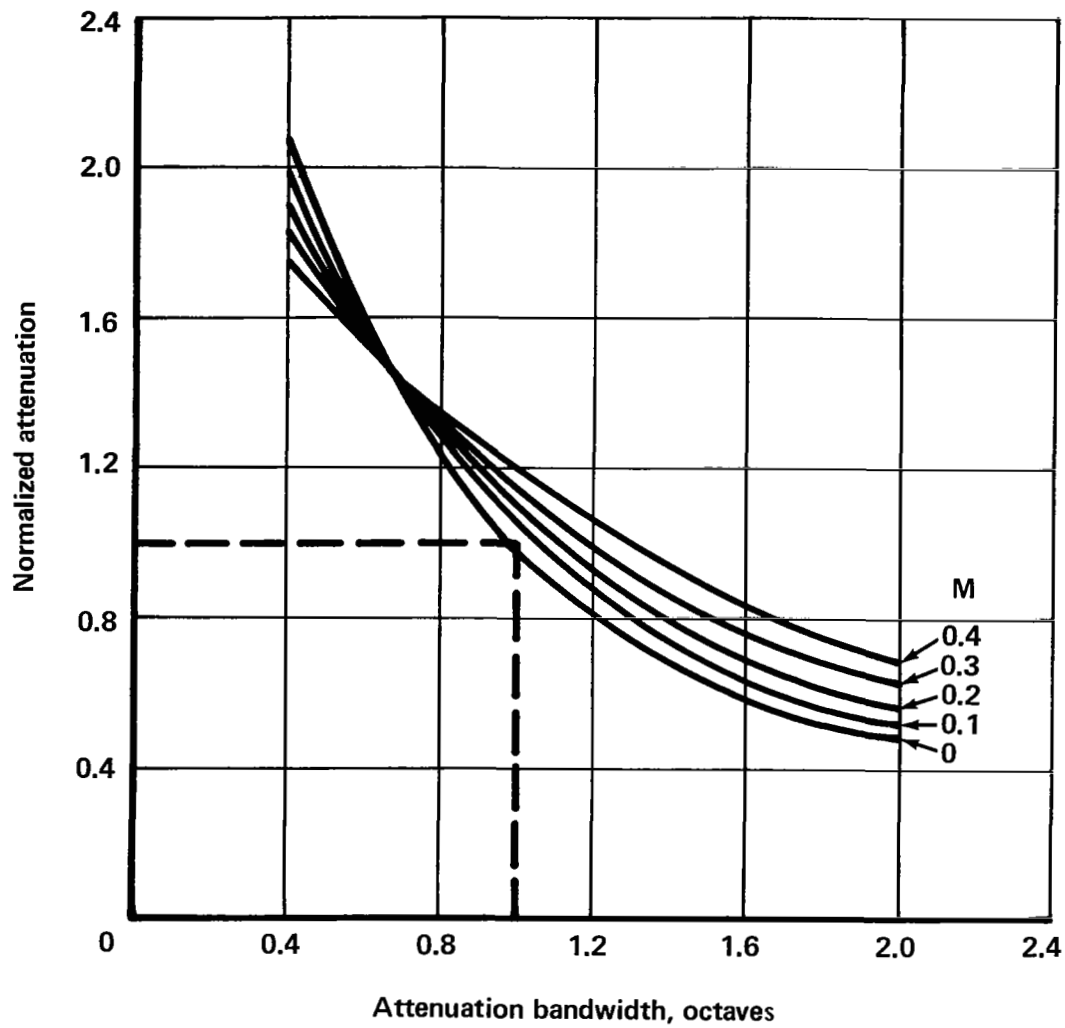

FIGURE 51.—VARIATION OF ATTENUATION WITH BANDWIDTH AND AIRFLOW MACH NUMBER IN THE INLET MODE

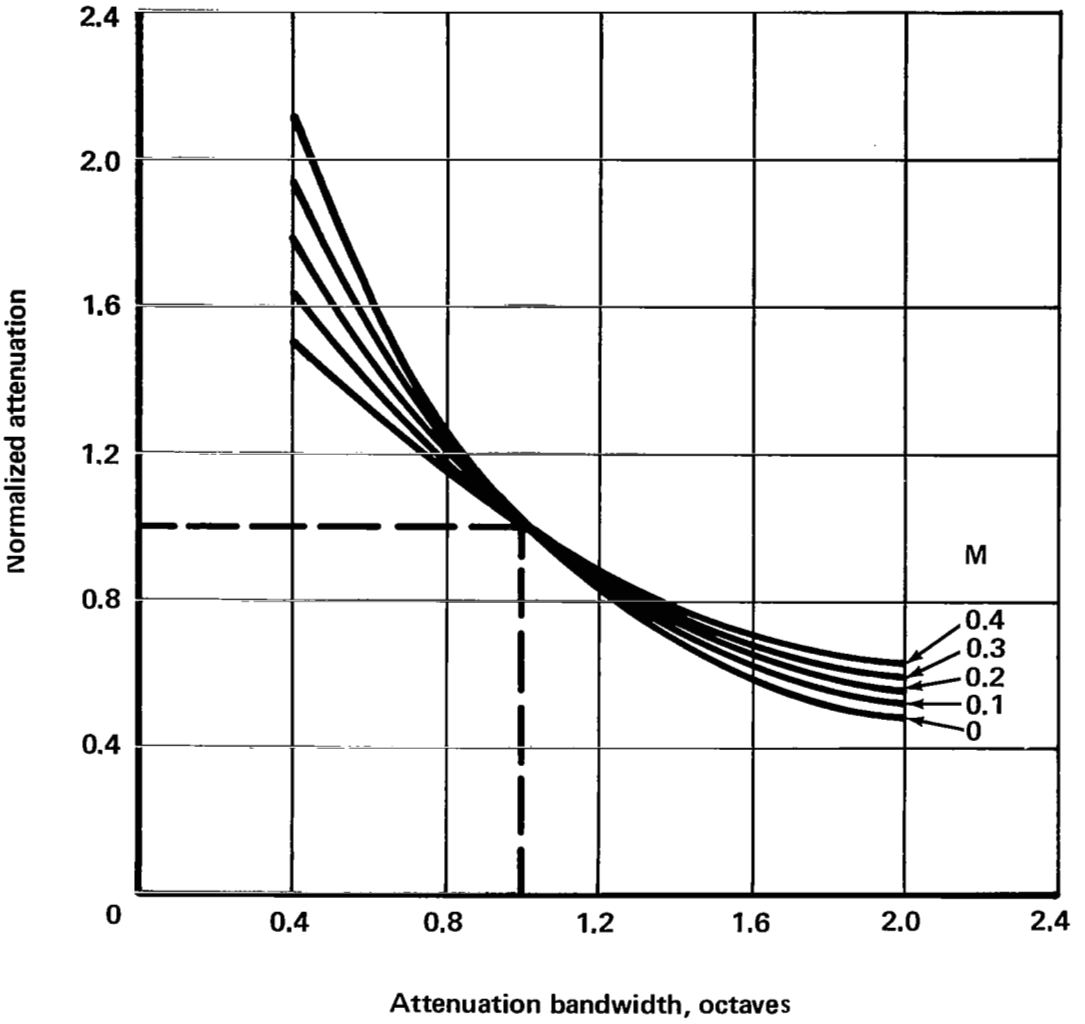

FIGURE 52.–VARIATION OF ATTENUATION WITH BANDWIDTH AND AIRFLOW MACH NUMBER IN THE EXHAUST MODE

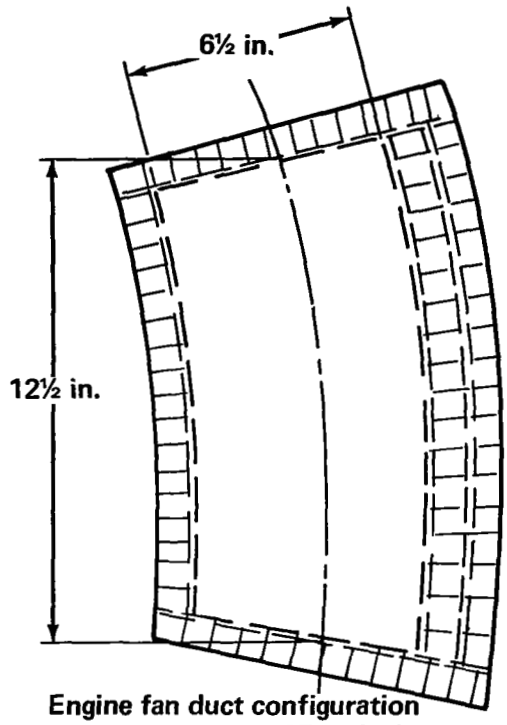

Engine fan duct configuration
treatment lengths, 25 and 50 in.

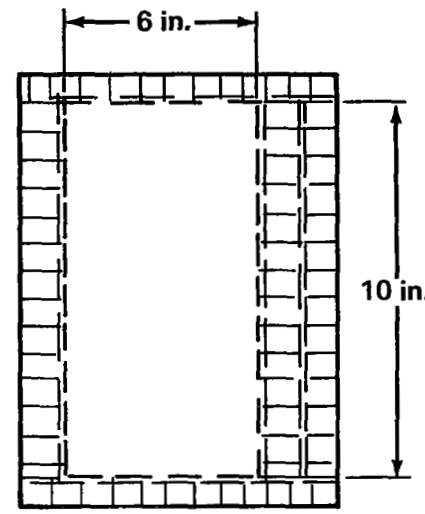

Flow duct facility configuration
treatment lengths, 11, 22, and 44 in.

Note: All lining dimensions and acoustic characteristics are identical in both ducts.

FIGURE 53.–DUCT LINING DETAILS FOR FLOW DUCT AND ENGINE DUCT COMPARISON

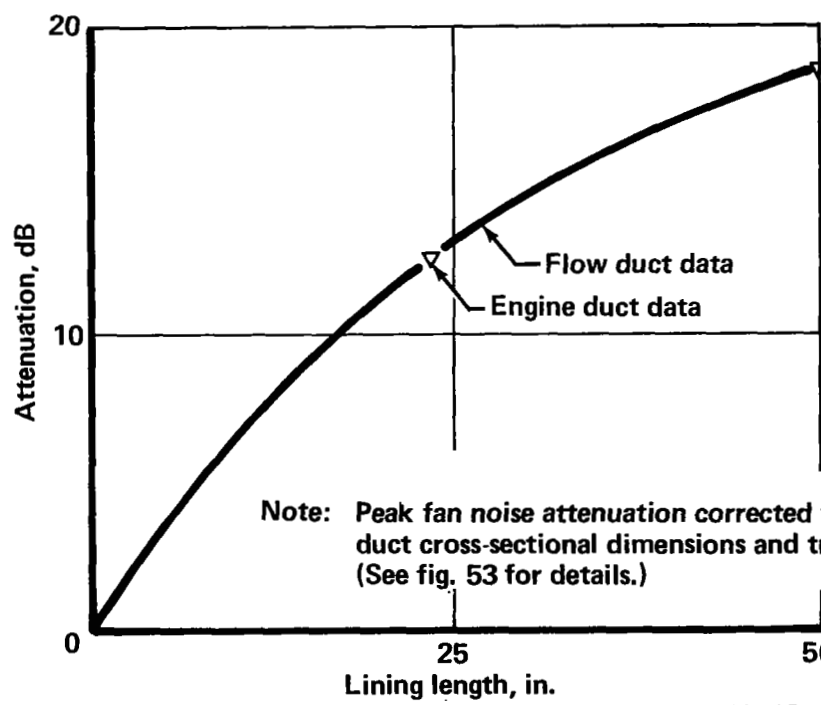

Note: Peak fan noise attenuation corrected for wall pressure level, duct cross-sectional dimensions and treatment length. (See fig. 53 for details.)

FIGURE 54.–COMPARISON OF ACOUSTICAL DUCT LINING ATTENUATION IN JT3D FAN EXHAUST DUCTS AND IN MODEL FLOW DUCT

	Lining thickness, in.
[a] Treated surfaces 4 in. apart 13 radial splitters or circum splitter plus inner and outer walls treated	0.9
[b] Treated surfaces 5 in. apart 10 radial splitters or circum splitter plus inner and outer walls treated	0.8

[c]

Treatment of radial splitters only	No. splitters per duct	Normal Cells
c1	8	0.75
c2	7	0.70
c3	6	0.65
c4	5	0.60
c5	4	0.50

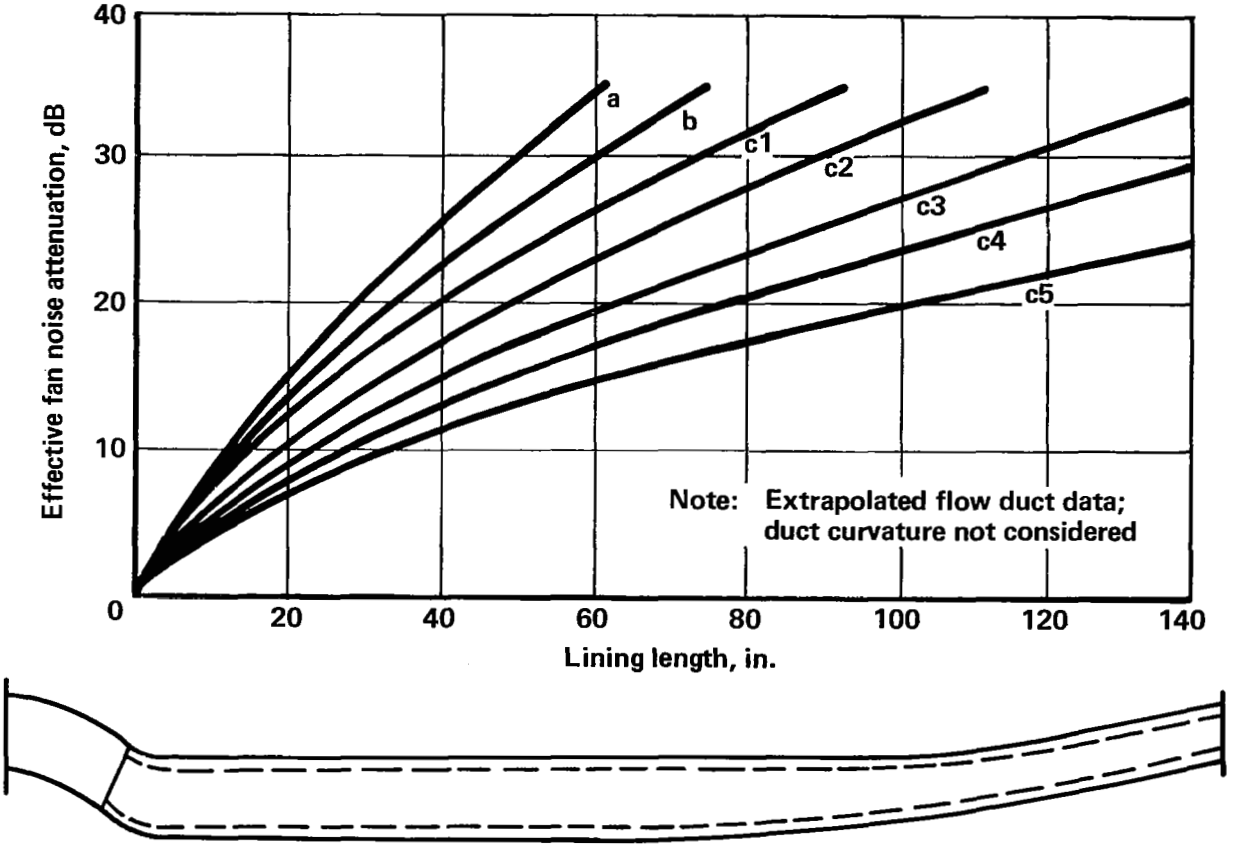

FIGURE 55.—COMPARISONS OF ATTENUATION VERSUS LENGTH FOR VARIOUS SPLITTER CONFIGURATIONS

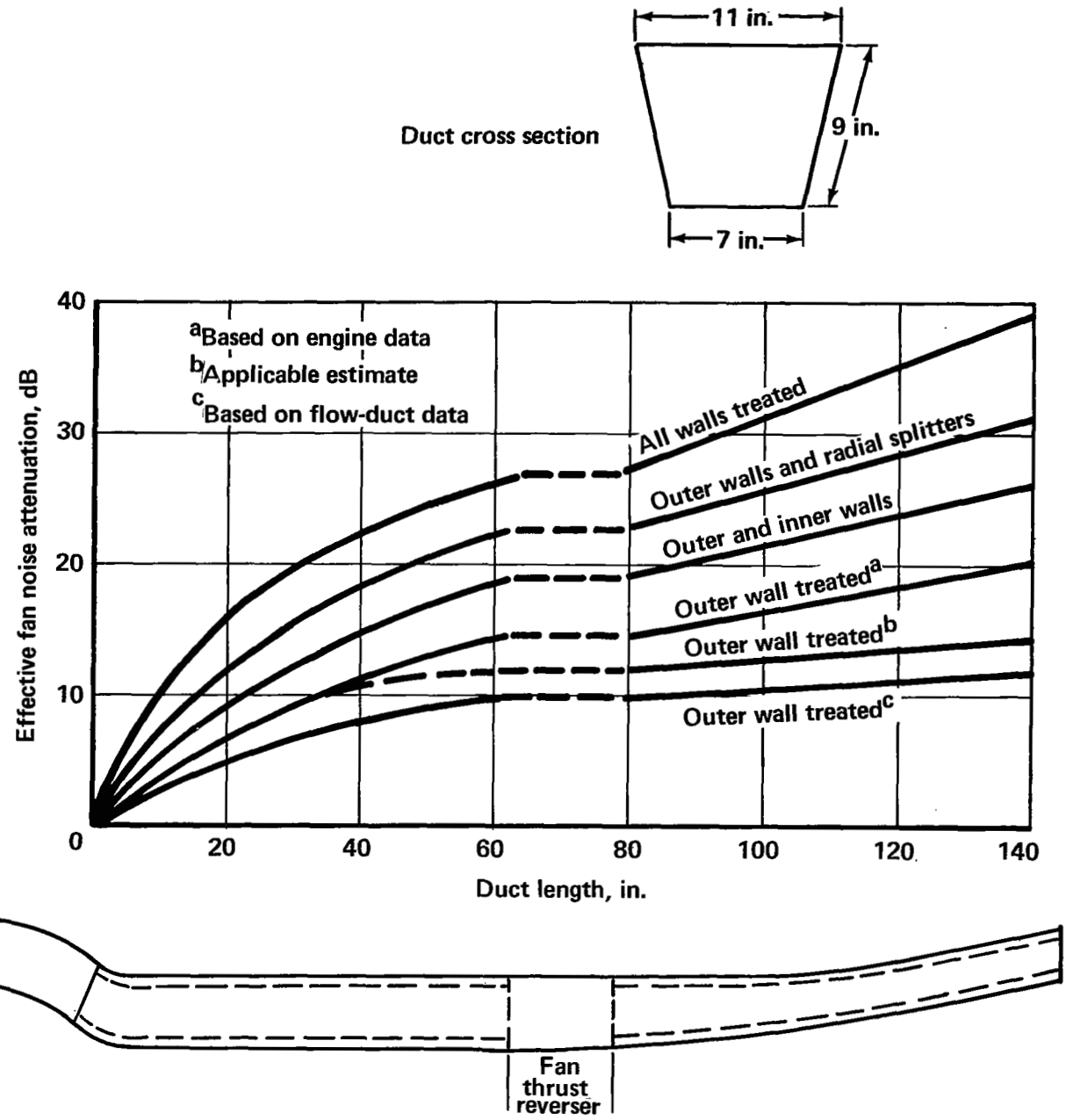

FIGURE 56.—EFFECTIVE FAN NOISE ATTENUATION VERSUS LENGTH FOR VARIOUS TREATMENT APPLICATION GEOMETRIES

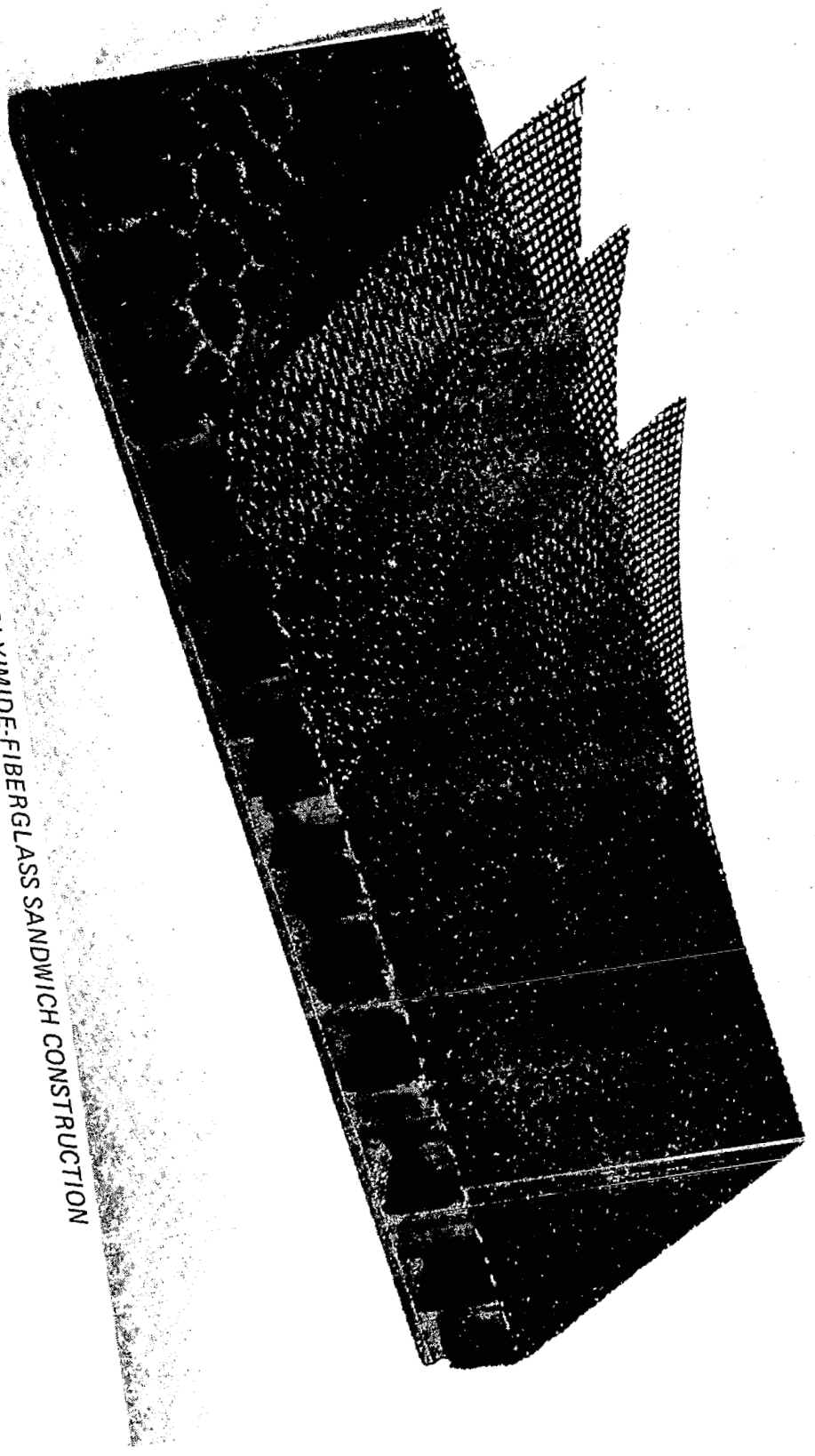

FIGURE 57.—TYPICAL POLYIMIDE-FIBERGLASS SANDWICH CONSTRUCTION

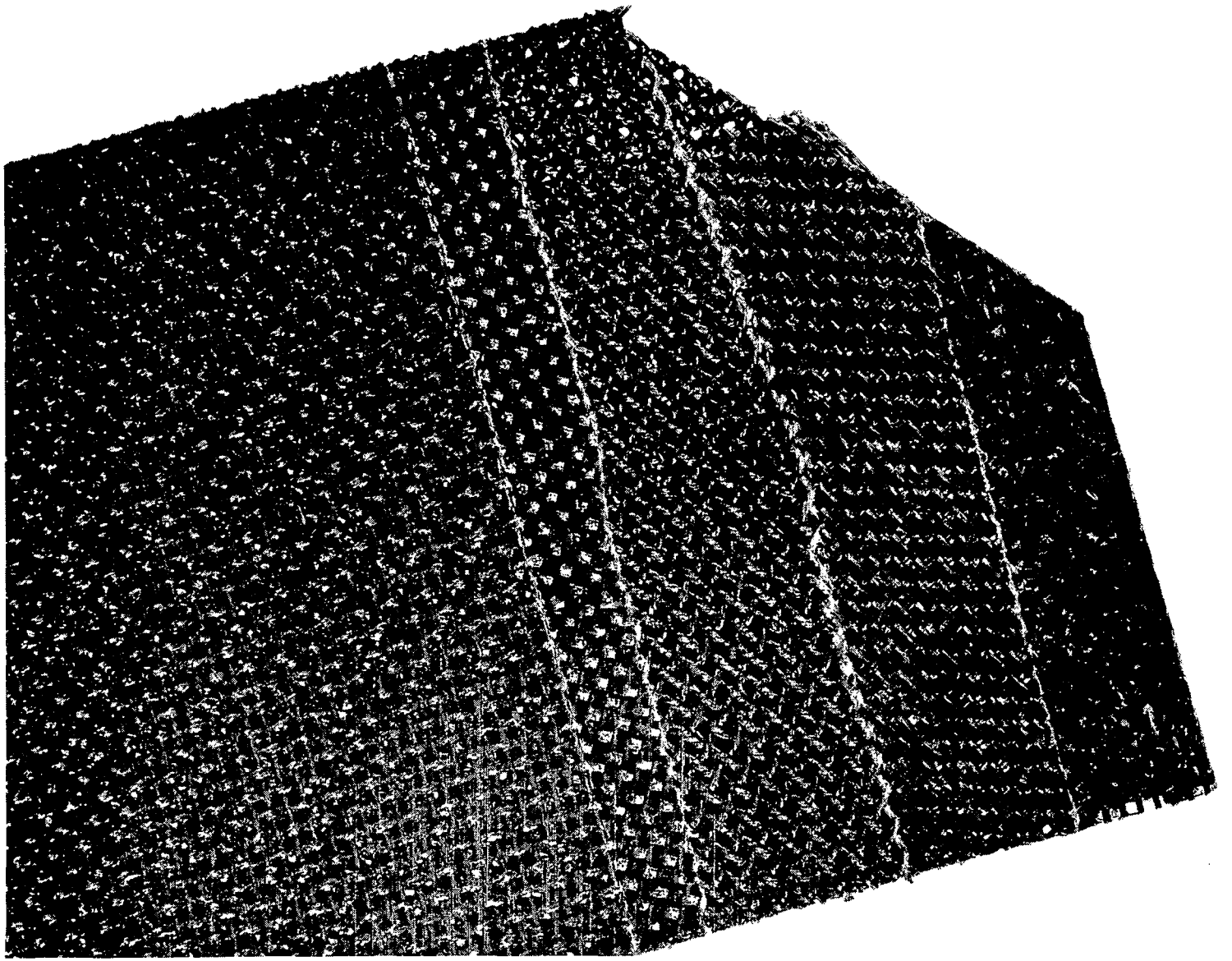

FIGURE 58.—TYPICAL POLYIMIDE-FIBERGLASS POROUS LAMINATE CONSTRUCTION

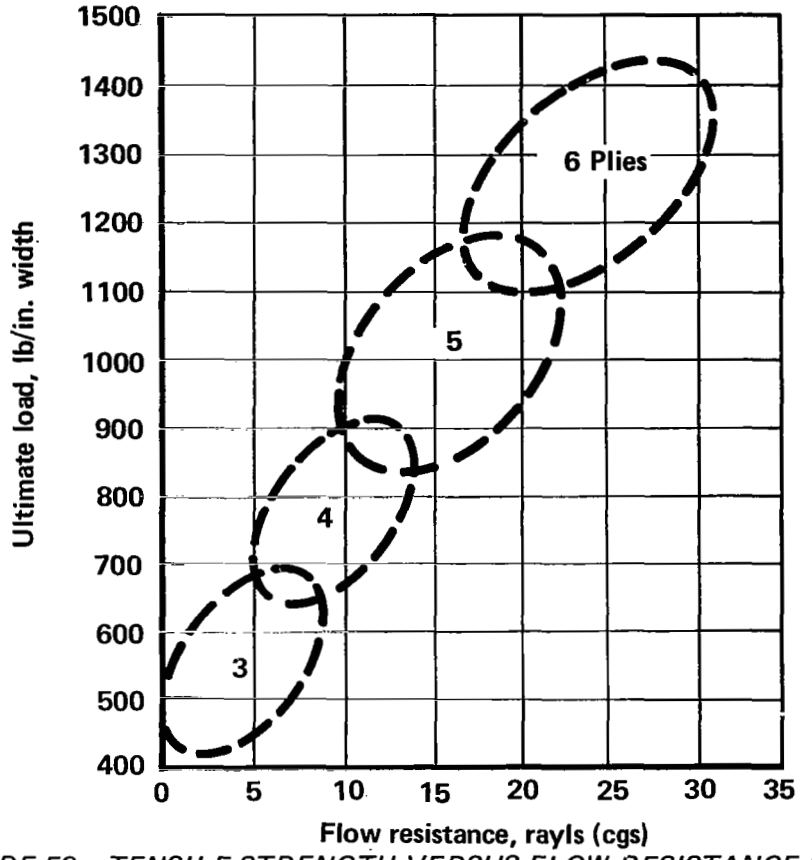

FIGURE 59.—TENSILE STRENGTH VERSUS FLOW RESISTANCE FOR POLYIMIDE-FIBERGLASS POROUS LAMINATE

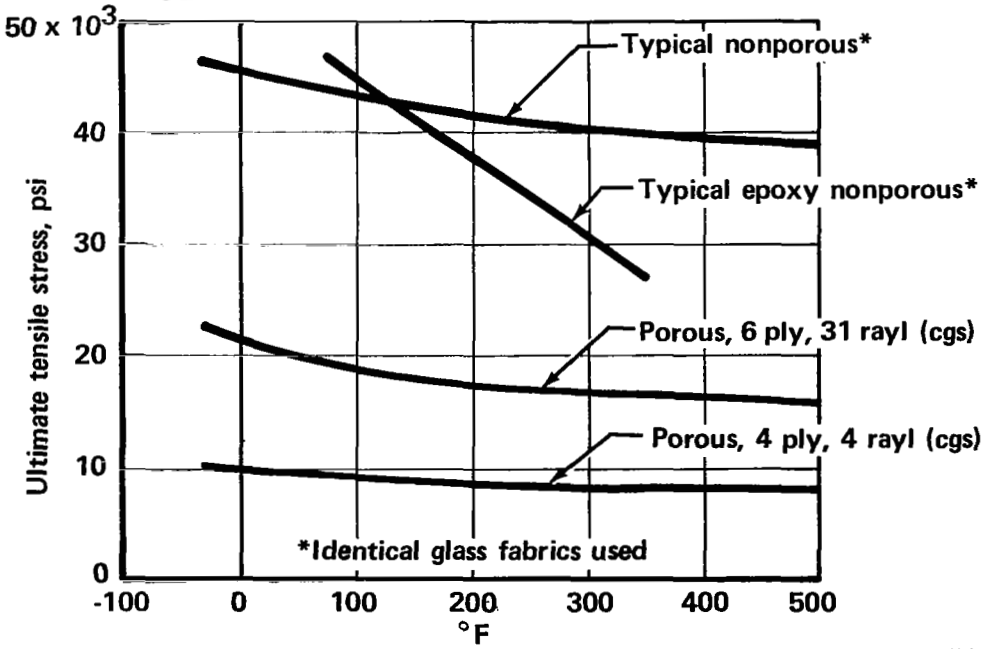

FIGURE 60.—EFFECT OF TEMPERATURE ON LAMINATE TENSILE STRENGTH OF POLYIMIDE-FIBERGLASS MATERIAL

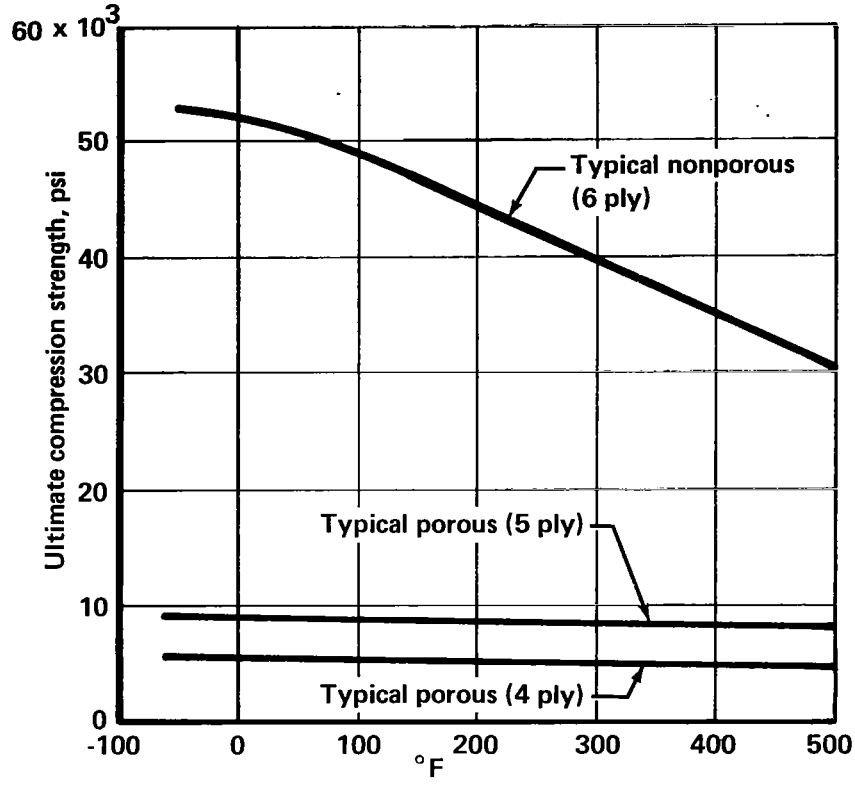

FIGURE 61.—EFFECT OF TEMPERATURE ON LAMINATE COMPRESSION STRENGTH OF POLYIMIDE-FIBERGLASS MATERIAL

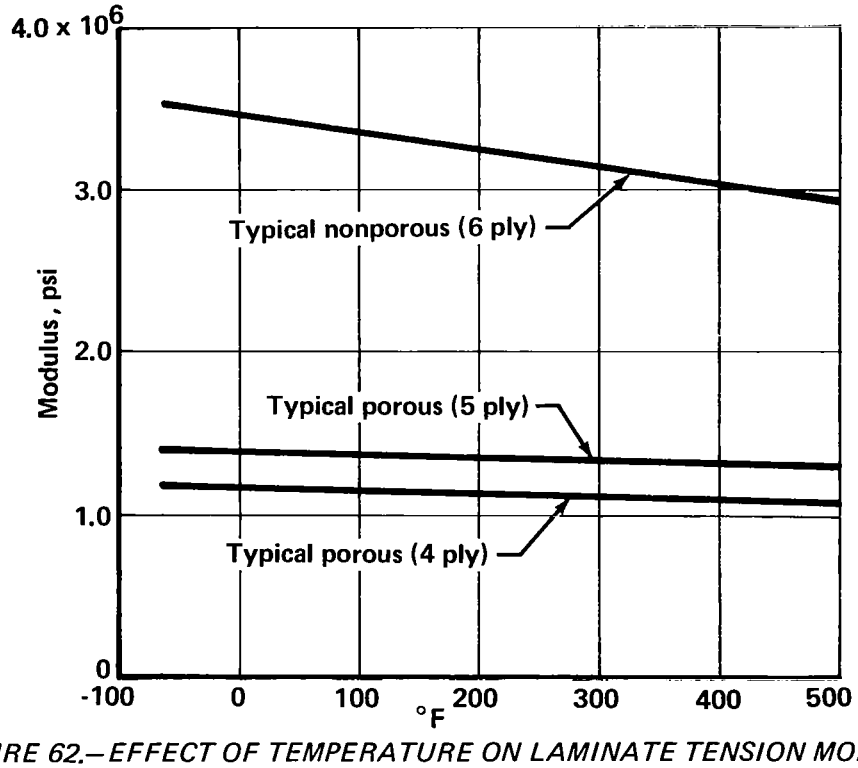

FIGURE 62.—EFFECT OF TEMPERATURE ON LAMINATE TENSION MODULUS OF POLYIMIDE-FIBERGLASS MATERIAL

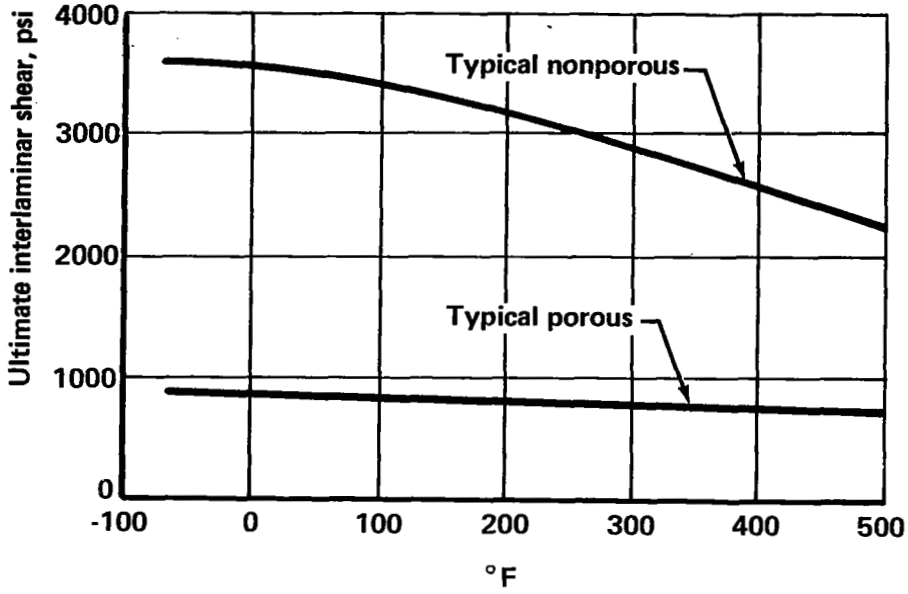

FIGURE 63.– EFFECT OF TEMPERATURE ON LAMINATE INTERLAMINAR SHEAR OF POLYIMIDE-FIBERGLASS MATERIAL

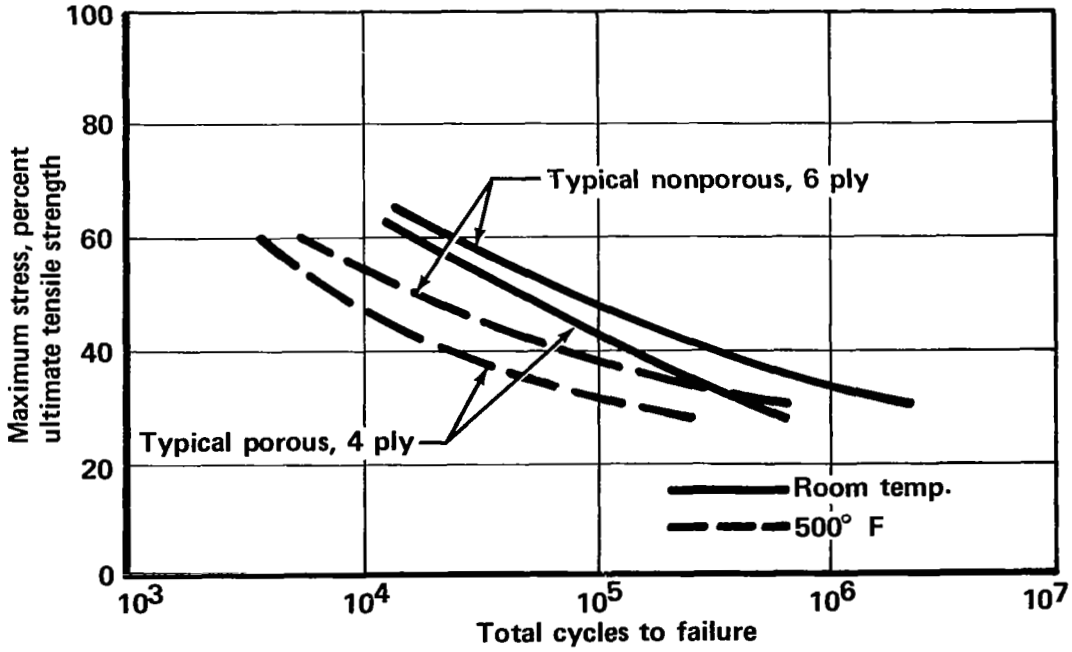

FIGURE 64.– FATIGUE CHARACTERISTICS OF POLYIMIDE LAMINATE SKINS

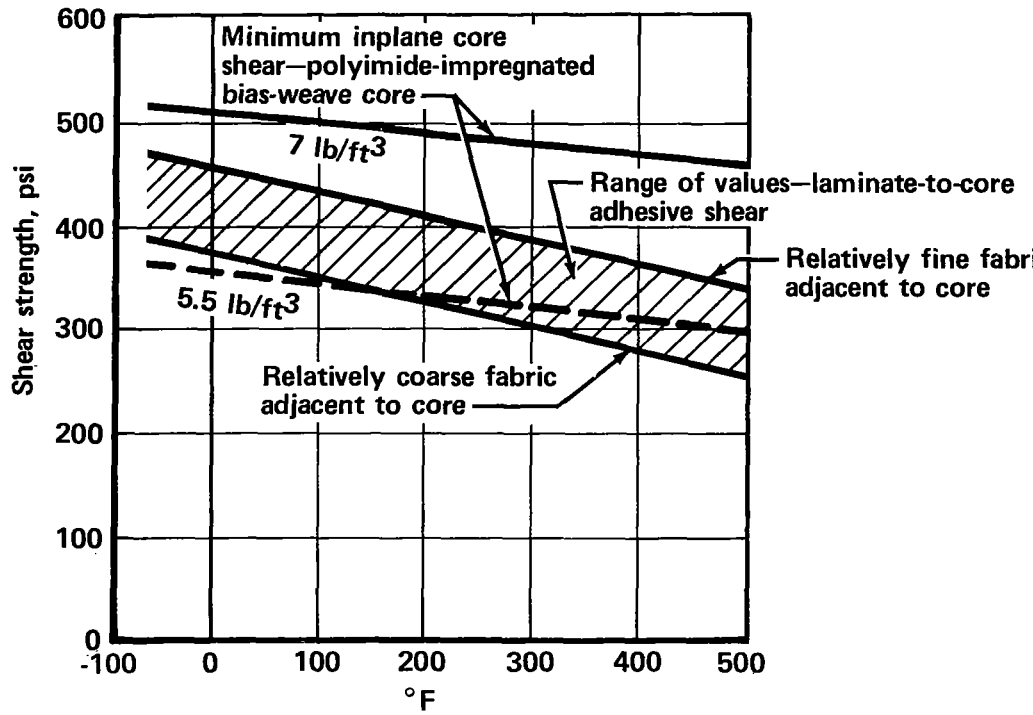

FIGURE 65.— EFFECT OF TEMPERATURE ON SHEAR STRENGTH OF POLYIMIDE-FIBERGLASS MATEPIAL

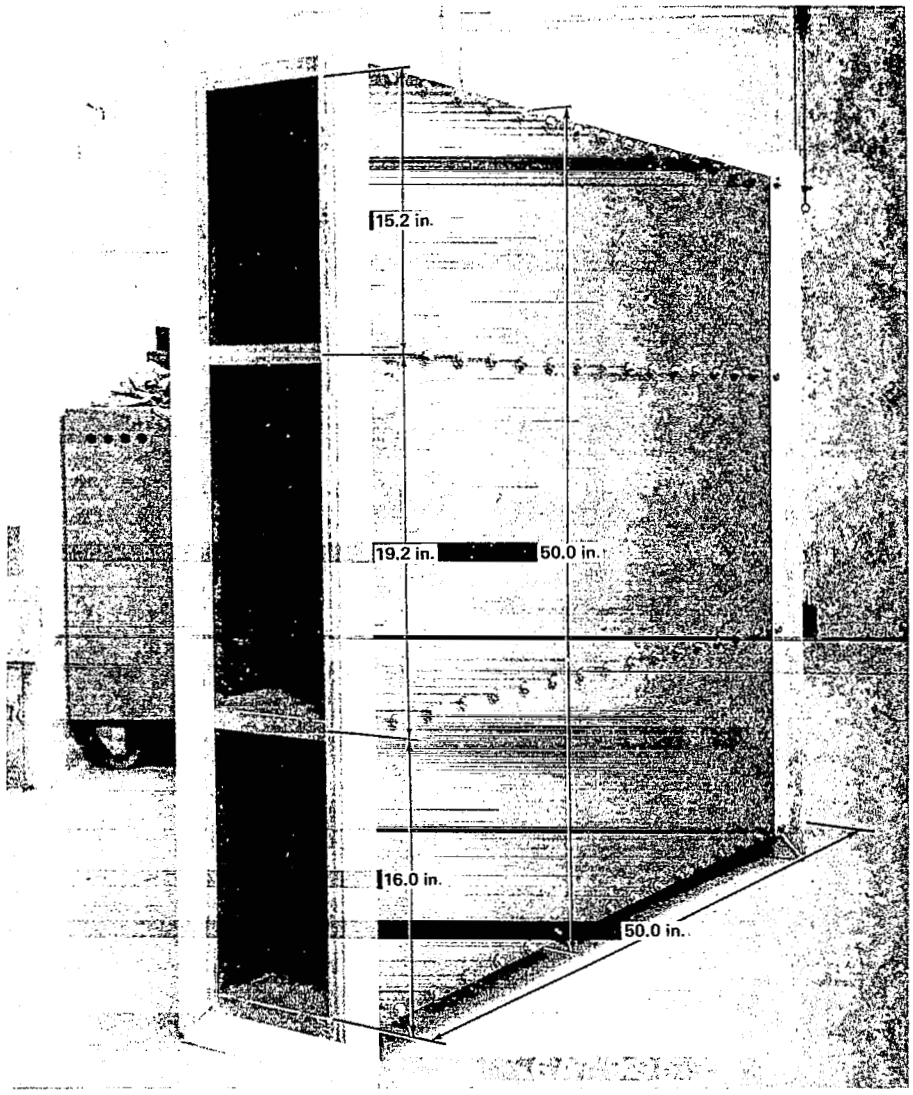

FIGURE 66.– POLYIMIDE-FIBERGLASS SONIC FATIGUE TEST SPECIMEN

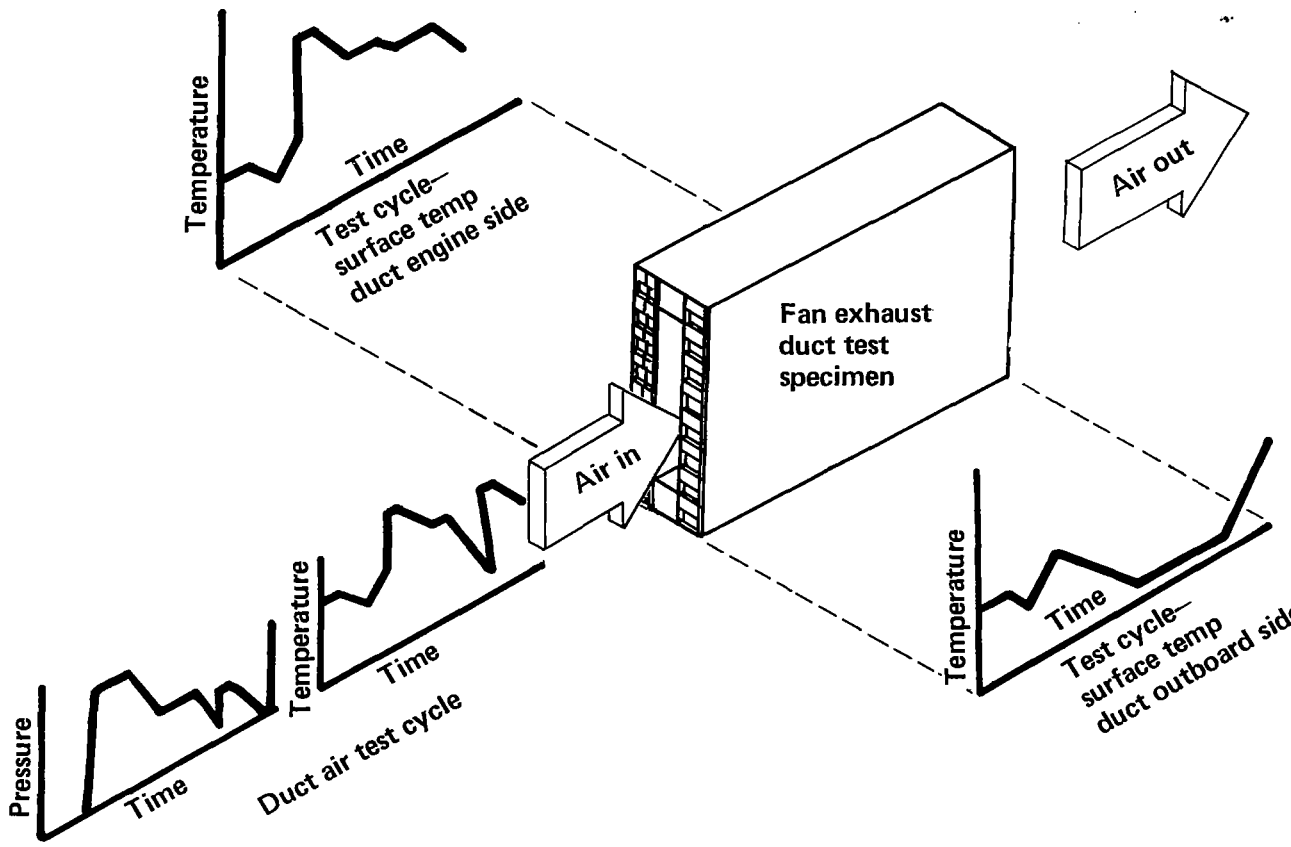

FIGURE 67.–FAN EXHAUST DUCT ENVIRONMENT TEST SETUP

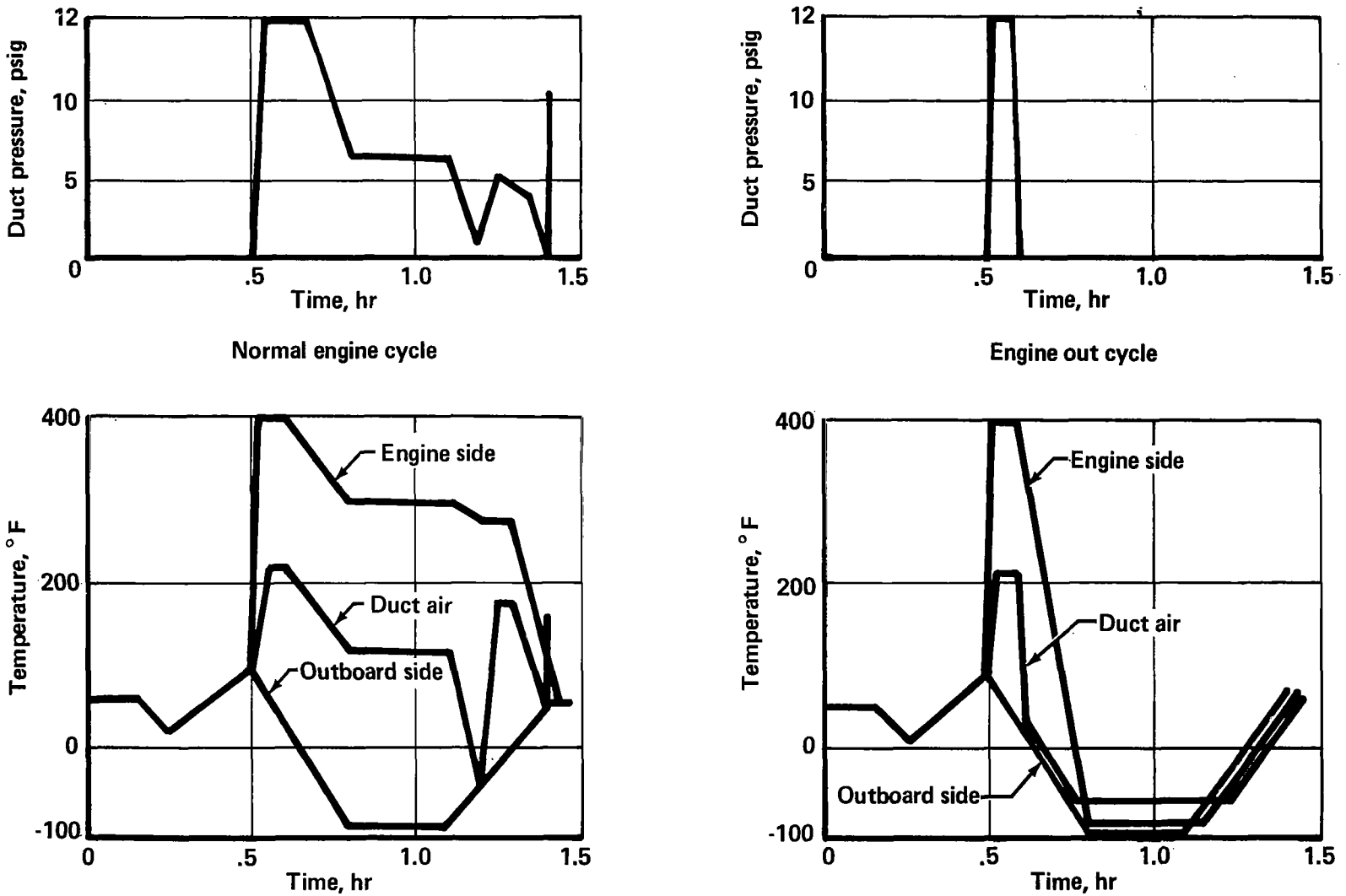

FIGURE 68.–SIMULATED FAN DUCT ENVIRONMENT CYCLE TEST OBJECTIVE

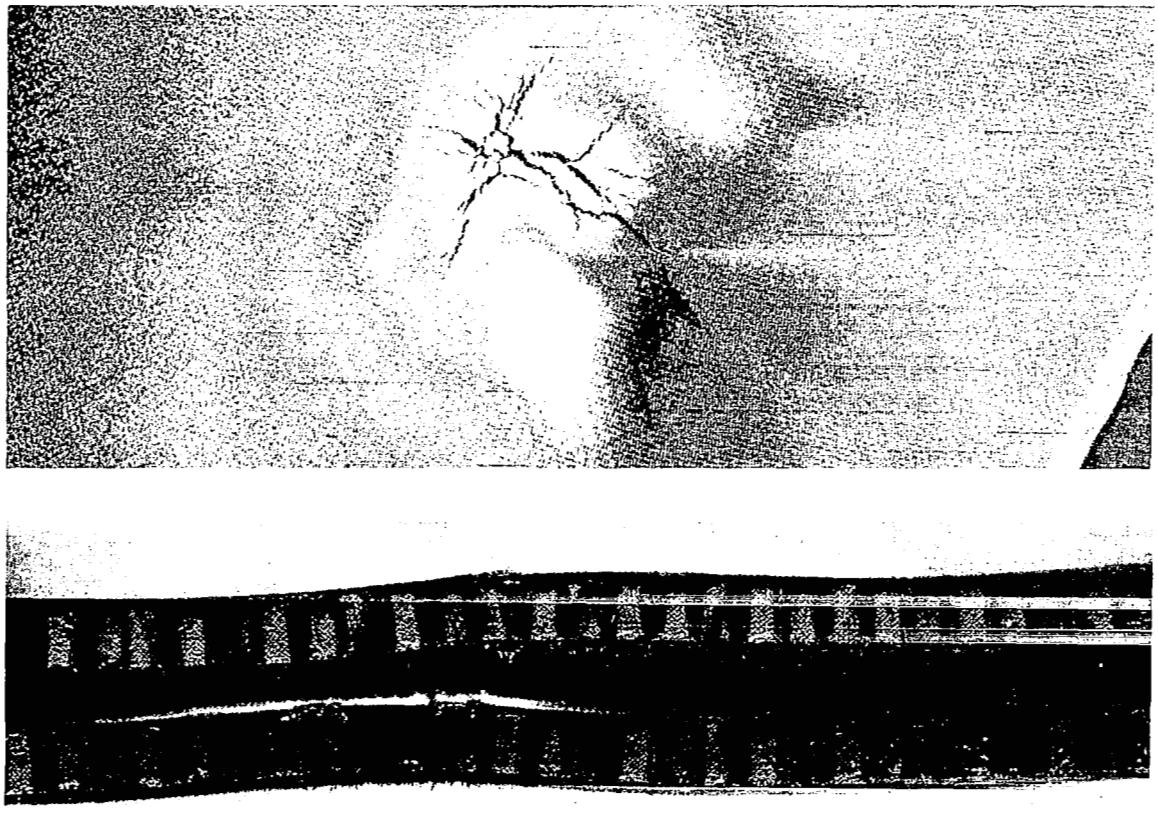

FIGURE 69.—FIRE-RESISTANCE TEST SPECIMEN, POLYIMIDE-FIBERGLASS SANDWICH

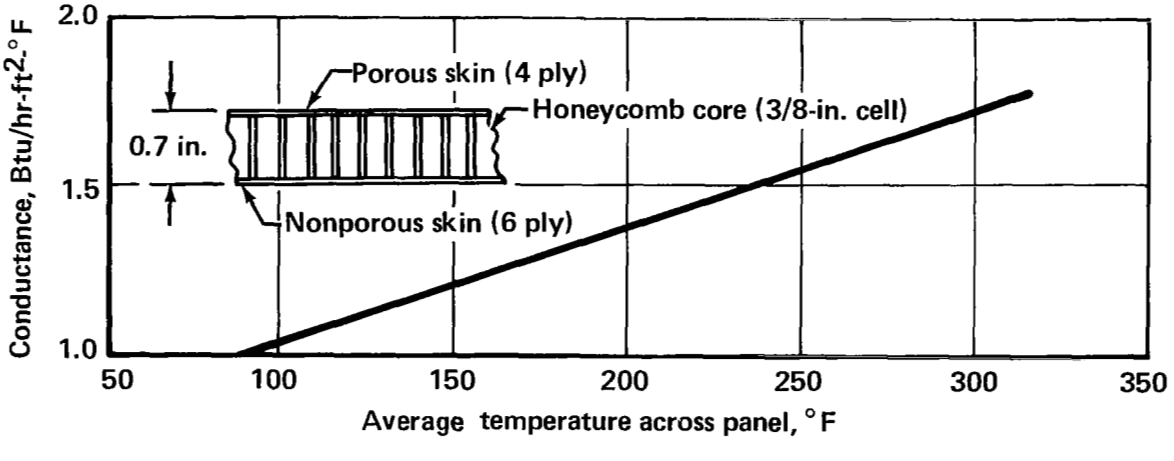

FIGURE 70.—EFFECT OF TEMPERATURE ON POLYIMIDE-FIBERGLASS SANDWICH PANEL THERMAL CONDUCTANCE

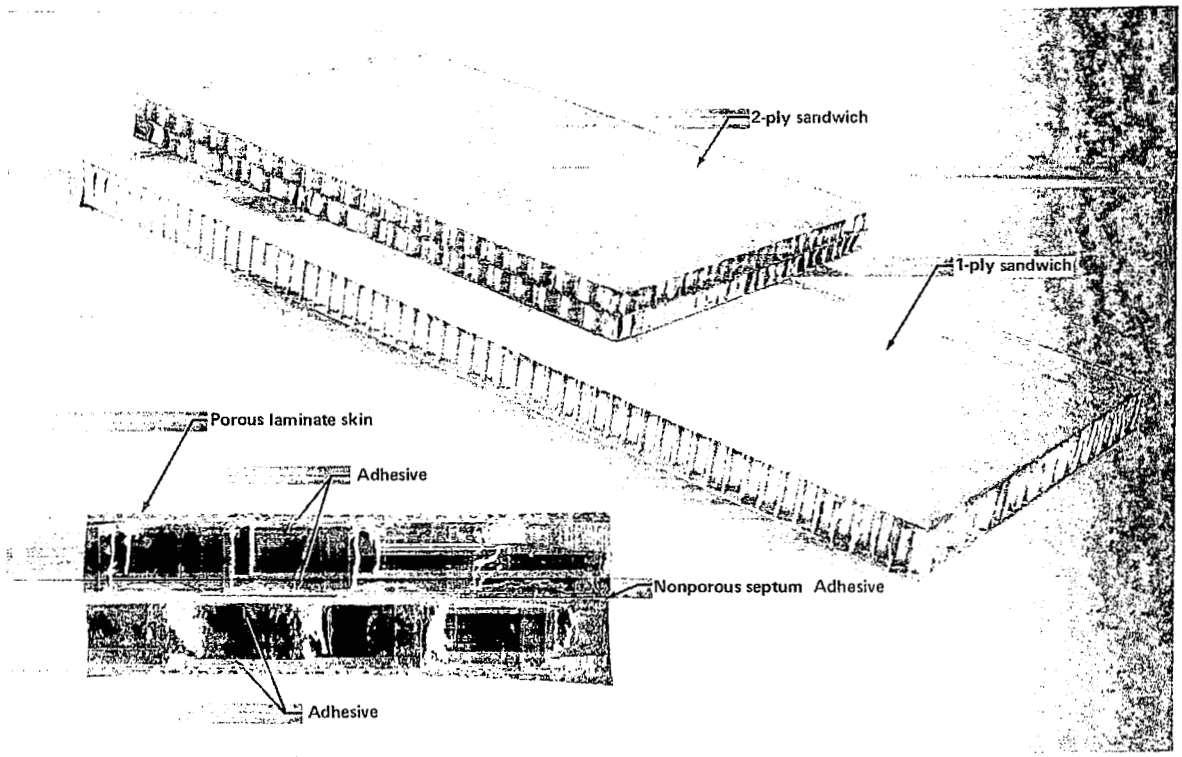

FIGURE 71.—TYPICAL POLYIMIDE-FIBERGLASS PANELS

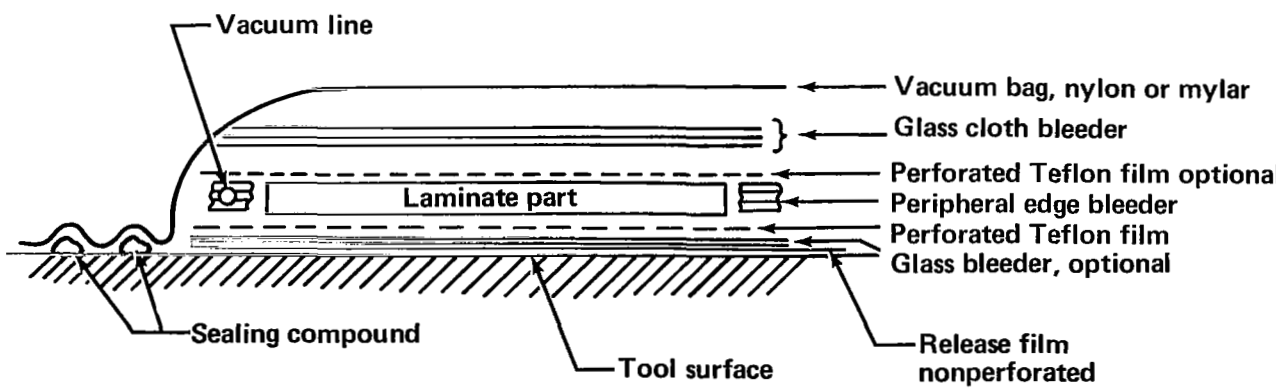

FIGURE 72.—TYPICAL POLYIMIDE-FIBERGLASS LAYUP READY FOR CURE

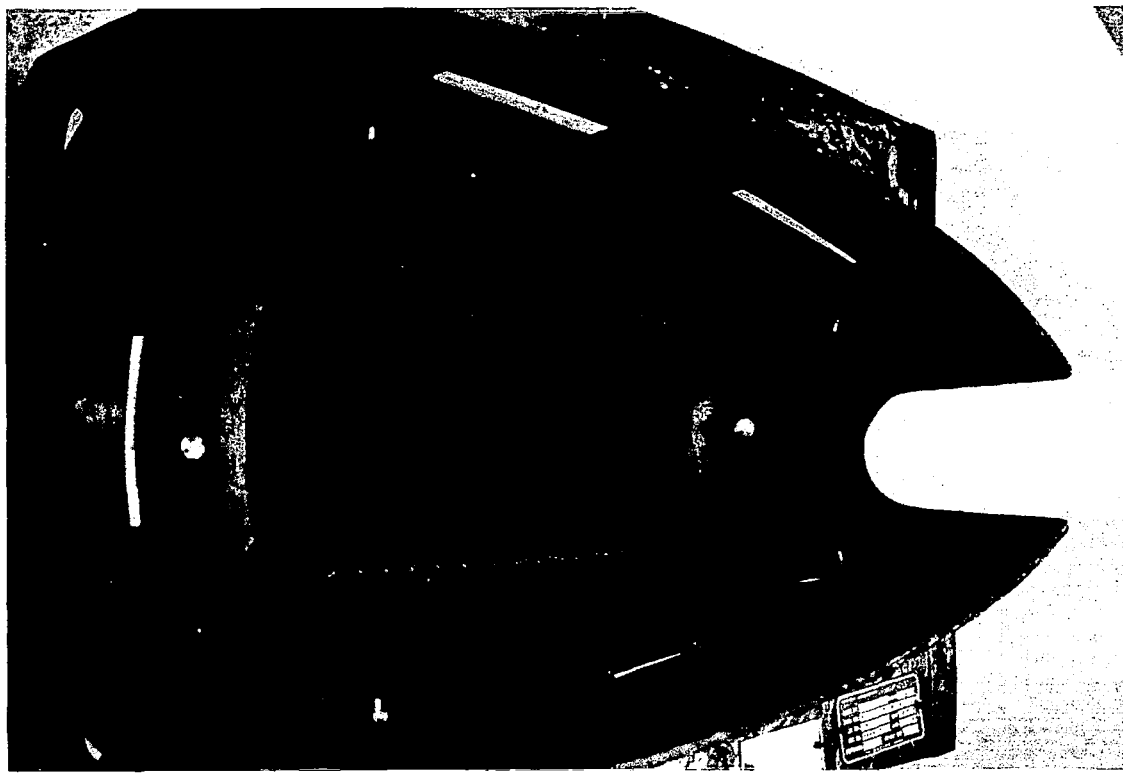

FIGURE 73.– FLIGHTWORTHY NACELLE, CORE SPLICE AND EDGE BOND, CENTERBODY CORE ASSEMBLY

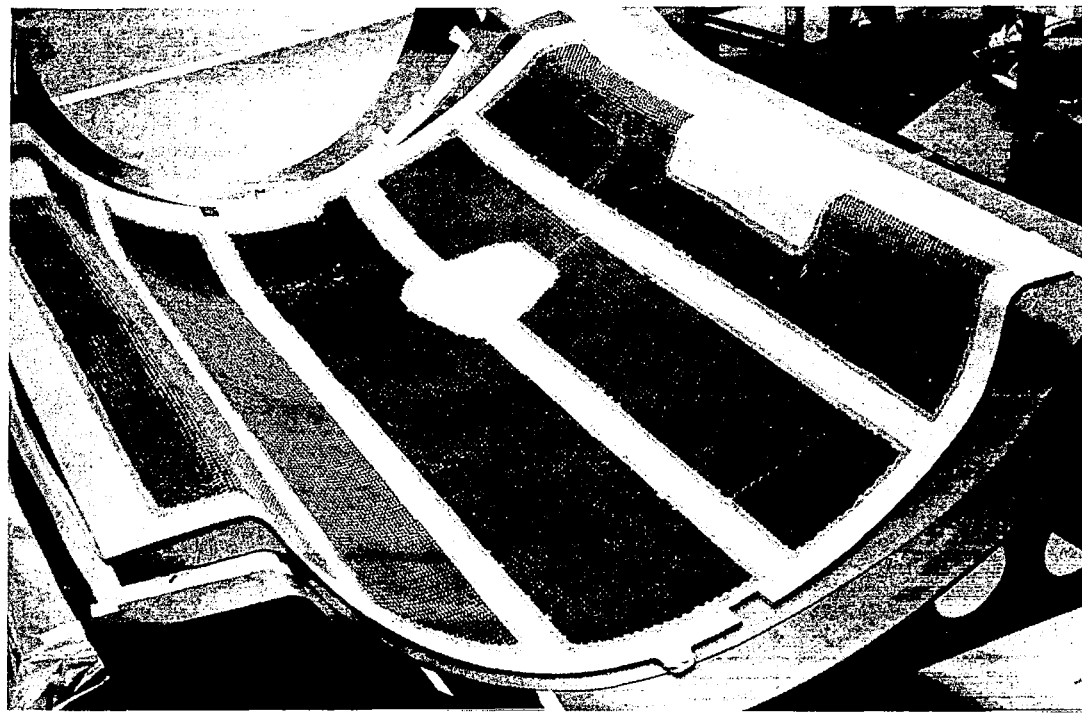

FIGURE 74.–INNER-WALL WRAP COWL

Duct size	6 x 10 in.
Walls lined	One/10 in.
Lining length	44 in.
Lining material	Polyimide

Flow resistance	30 rayls (cgs)
Core depth	0.28 in.
Core type	3/8-in. Hexcel

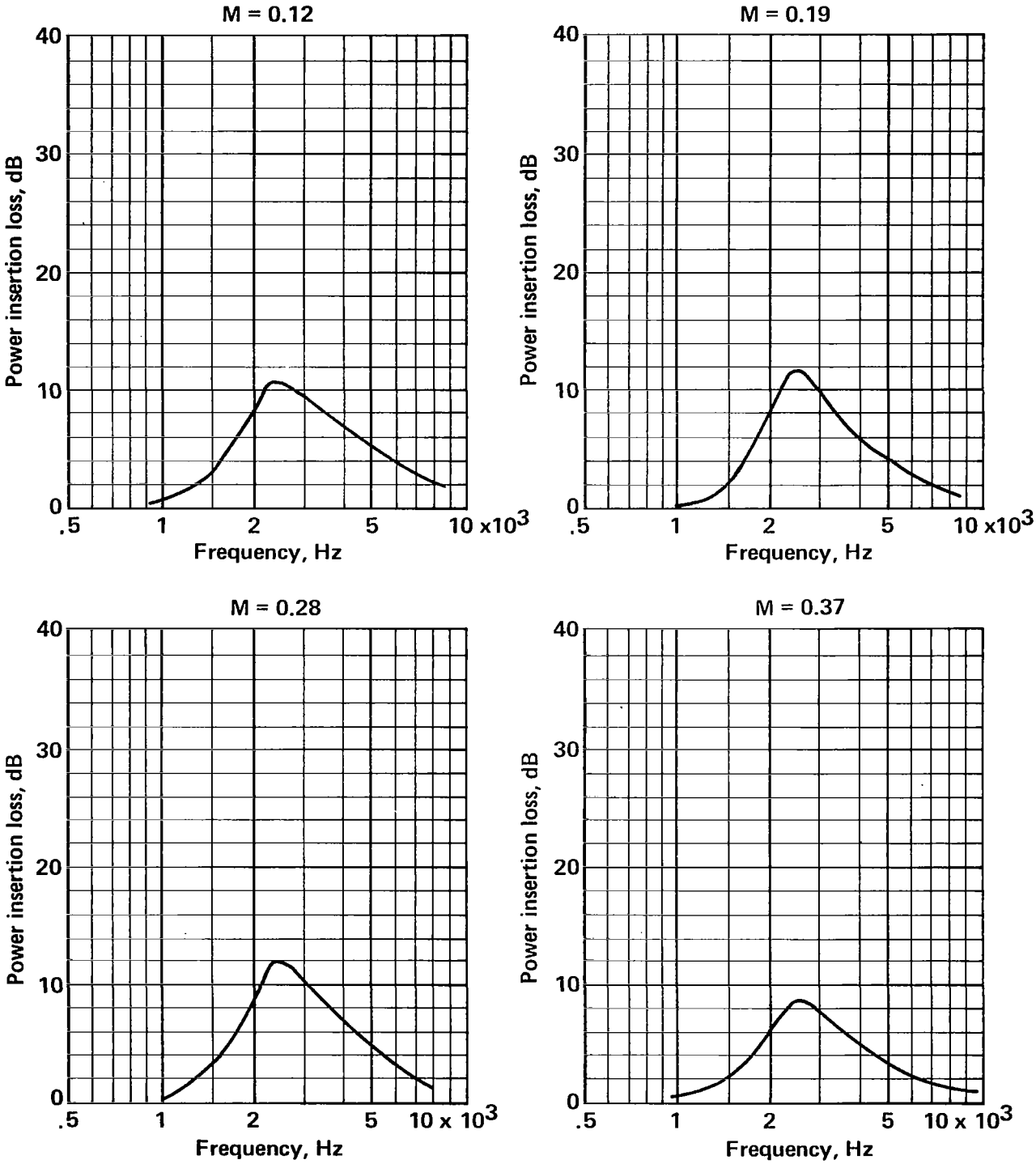

FIGURE A-1.—POWER INSERTION LOSS FOR 30-RAYL (CGS), 1/4-IN.-DEEP LINING ON ONE WALL OF 6-IN. DUCT

Duct size	6 x 10 in.
Walls lined	Two/10 in.
Lining length	22 in.
Lining material	Polyimide

Flow resistance	3 rayls (cgs)
Core depth	0.24 in.
Core type	3/8-in. Hexcel

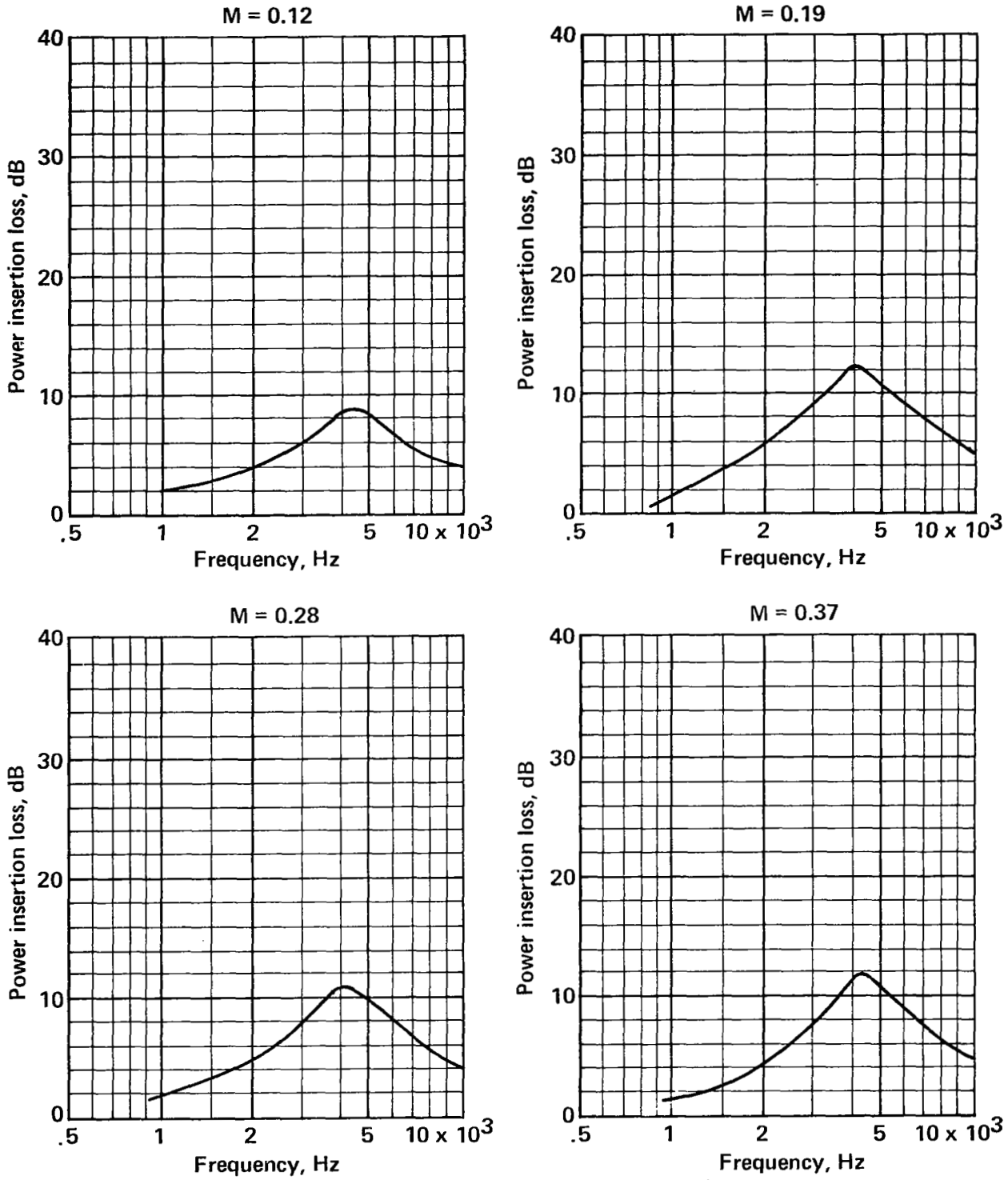

FIGURE A-2.—POWER INSERTION LOSS FOR 3-RAYL (CGS), 1/4-IN.-DEEP LINING ON TWO WALLS OF 6-IN. DUCT

Duct size	6 x 10 in.
Walls lined	Two/10 in.
Lining length	22 in.
Lining material	Polyimide

Flow resistance	9 rayls (cgs)
Core depth	0.16 in.
Core type	3/8-in. Hexcel

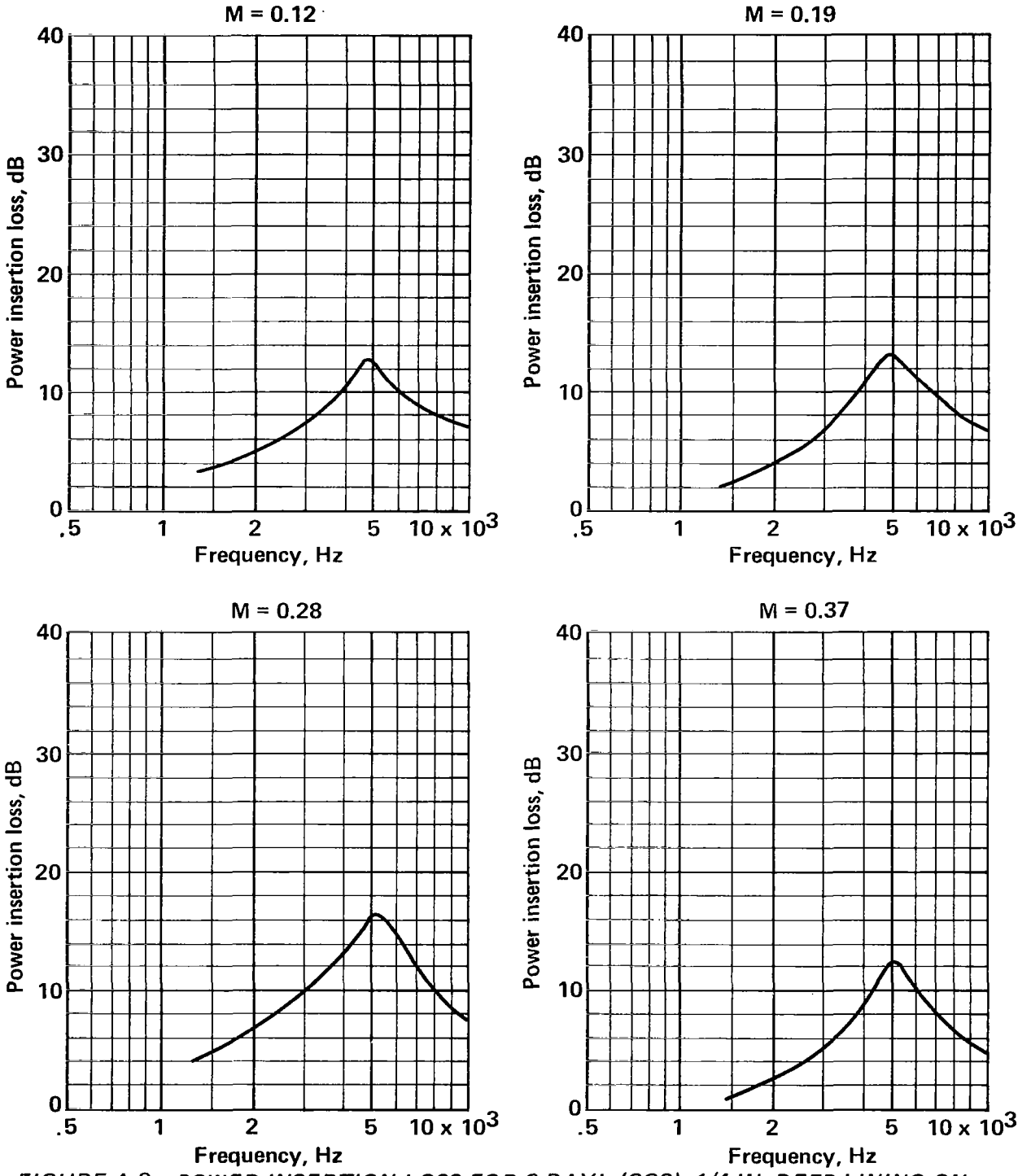

FIGURE A-3.—POWER INSERTION LOSS FOR 9-RAYL (CGS), 1/4-IN.-DEEP LINING ON TWO WALLS OF 6-IN. DUCT

Duct size	6 x 10 in.
Walls lined	Two/10 in.
Lining length	22 in.
Lining material	Polyimide

Flow resistance	18 rayls (cgs)
Core depth	0.18 in.
Core type	3/8-in. Hexcel

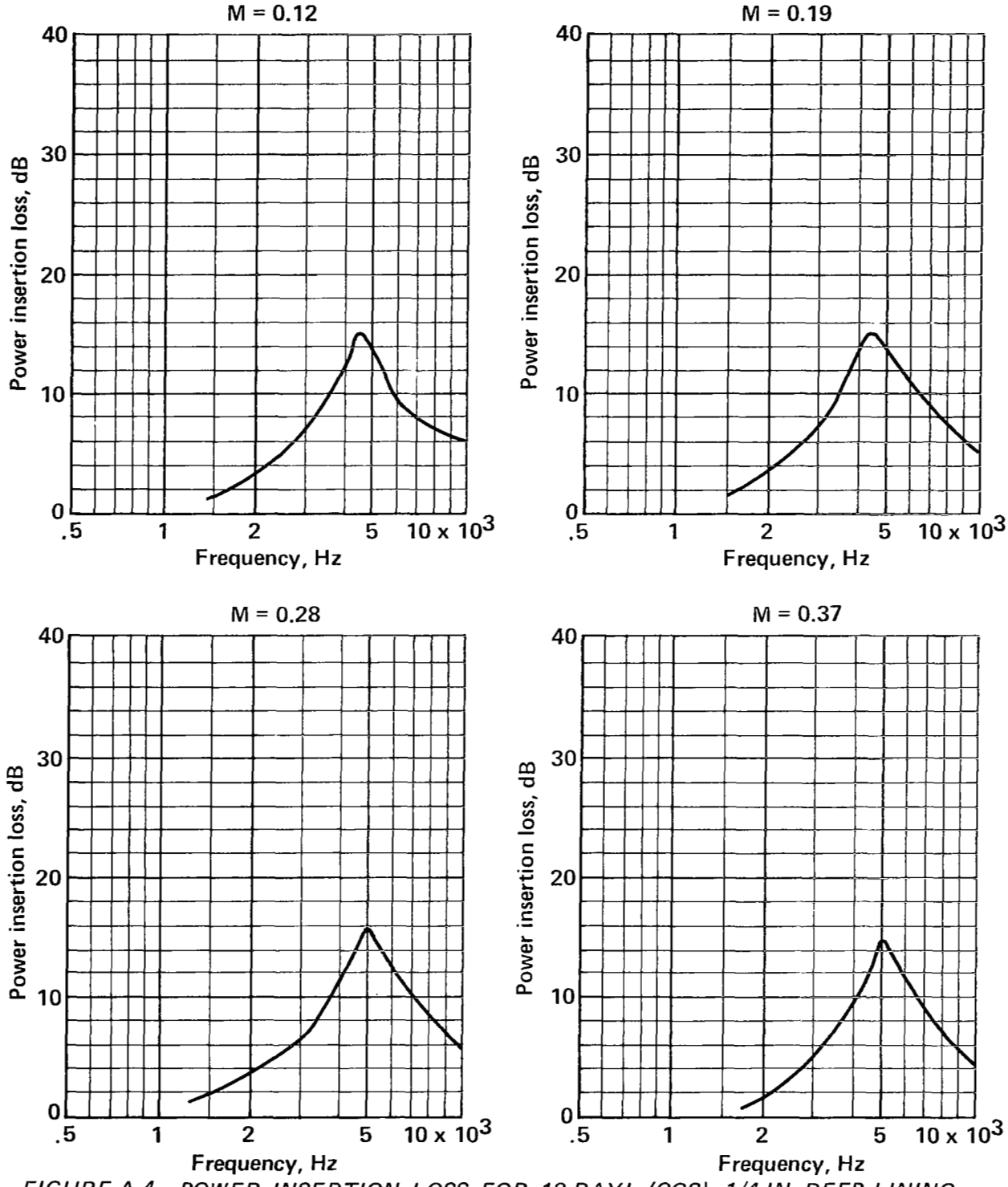

FIGURE A-4.—POWER INSERTION LOSS FOR 18-RAYL (CGS), 1/4-IN.-DEEP LINING ON TWO WALLS OF 6-IN. DUCT

Duct size	6 x 10 in.
Walls lined	Two/10 in.
Lining length	22 in.
Lining material	Polyimide

Flow resistance	30 rayls (cgs)
Core depth	0.28 in.
Core type	3/8-in. Hexcel

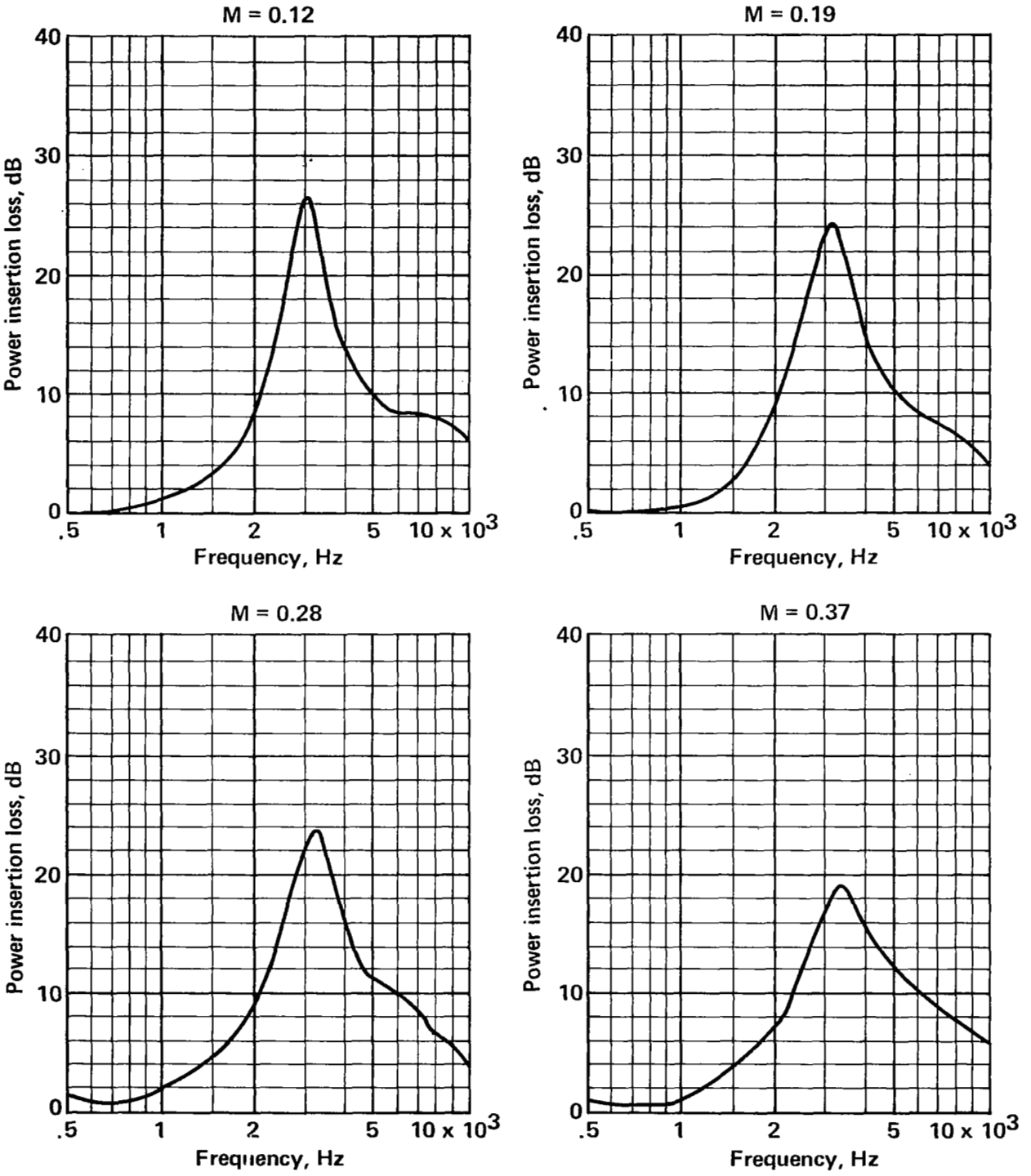

FIGURE A-5.—POWER INSERTION LOSS FOR 30-RAYL (CGS), 1/4-IN.-DEEP LINING ON TWO WALLS OF 6-IN. DUCT

Duct size	6 x 10 in.
Walls lined	Two/10 in.
Lining length	22 in.
Lining material	Polyimide

Flow resistance	50 rayls (cgs)
Core depth	0.25 in.
Core type	3/8-in. Hexcel

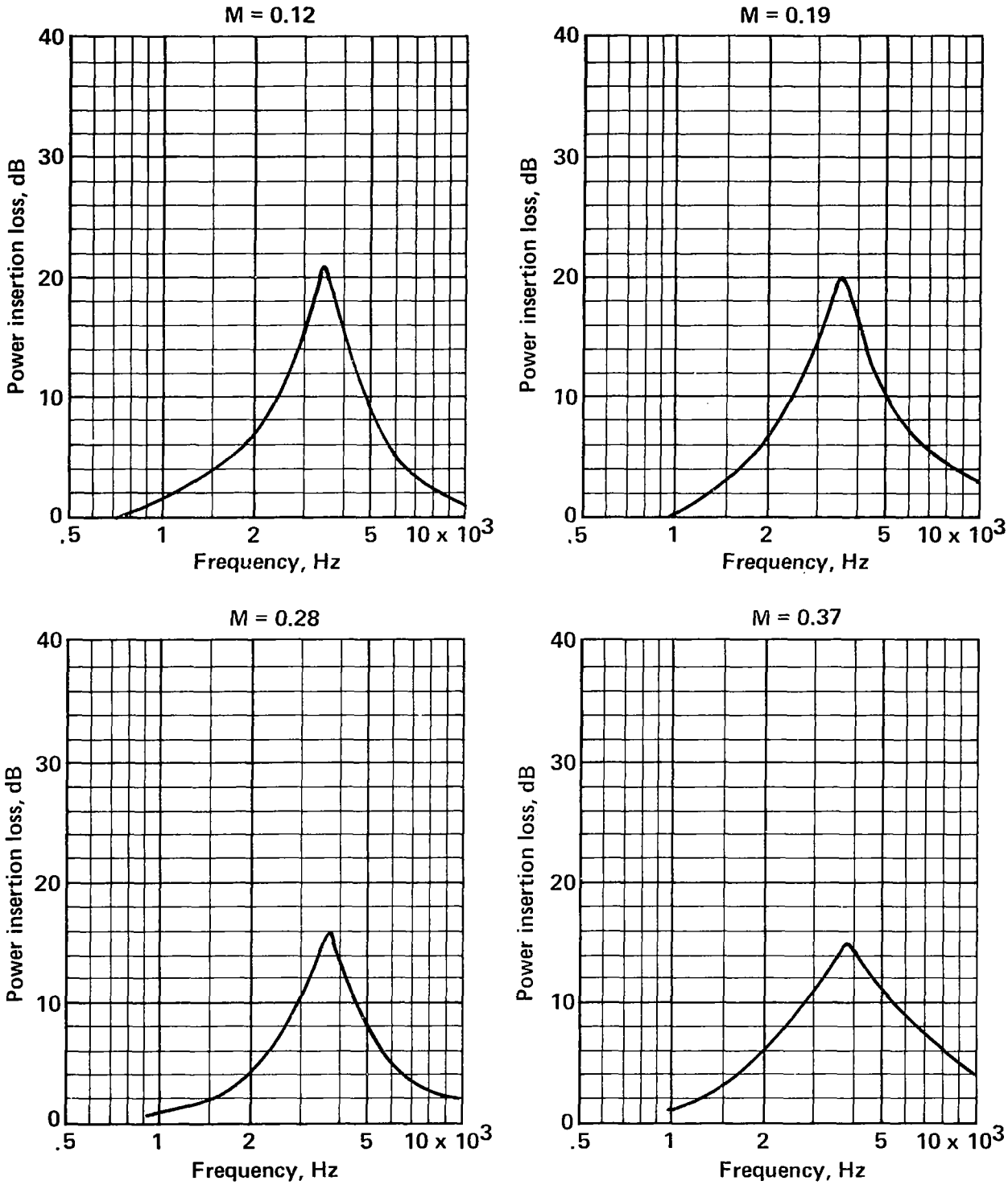

FIGURE A-6.—POWER INSERTION LOSS FOR 50-RAYL (CGS), 1/4-IN.-DEEP LINING ON TWO WALLS OF 6-IN. DUCT

Duct size	6 x 10 in.
Walls lined	Two/10 in.
Lining length	22 in.
Lining material	Polyimide

Flow resistance	70 rayls (cgs)
Core depth	0.25 in.
Core type	3/8-in. Hexcel

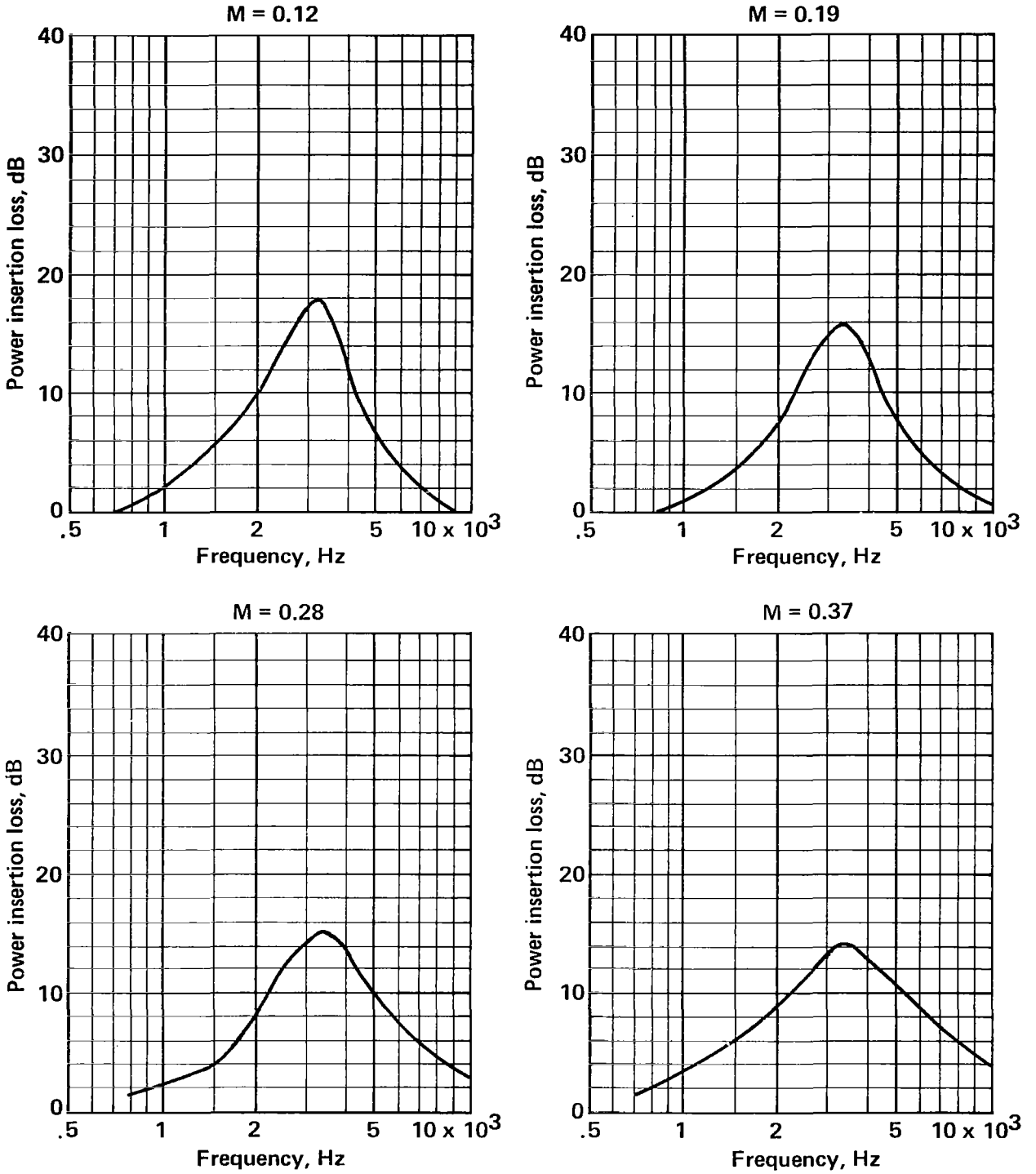

FIGURE A-7.—POWER INSERTION LOSS FOR 70-RAYL (CGS), 1/4-IN.-DEEP LINING ON TWO WALLS OF 6-IN. DUCT

Duct size	6 x 10 in.
Walls lined	One/10 in.
Lining length	44 in.
Lining material	Polyimide

Flow resistance	3 rayls (cgs)
Core depth	0.5 in.
Core type	3/8-in. Hexcel

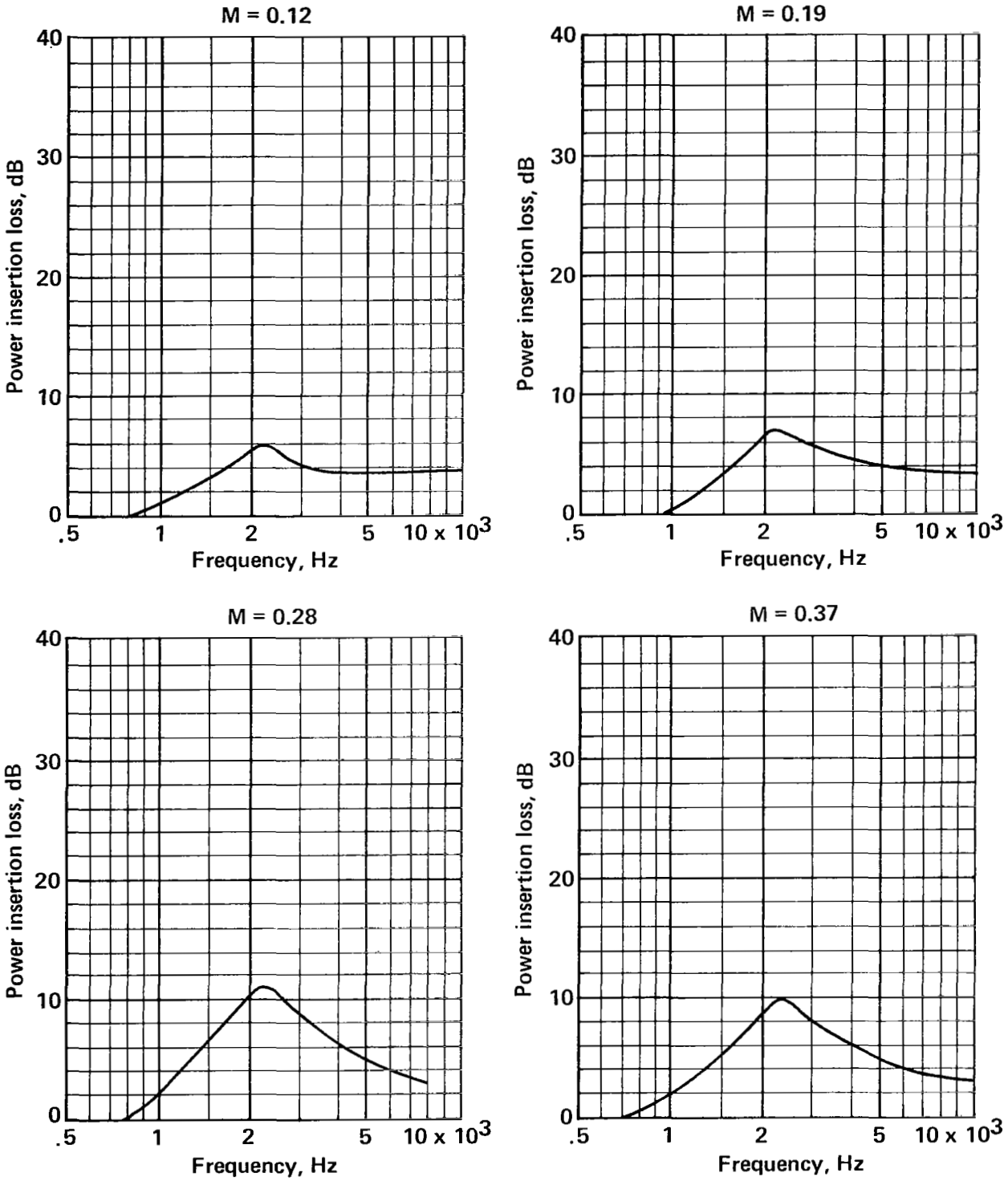

FIGURE A-8.—POWER INSERTION LOSS FOR 3-RAYL (CGS), 1/2-IN.-DEEP LINING ON ONE WALL OF 6-IN. DUCT

Duct size	6 x 10 in.
Walls lined	One/10 in.
Lining length	44 in.
Lining material	Polyimide

Flow resistance	9 rayls (cgs)
Core depth	0.5 in.
Core type	3/8-in. Hexcel

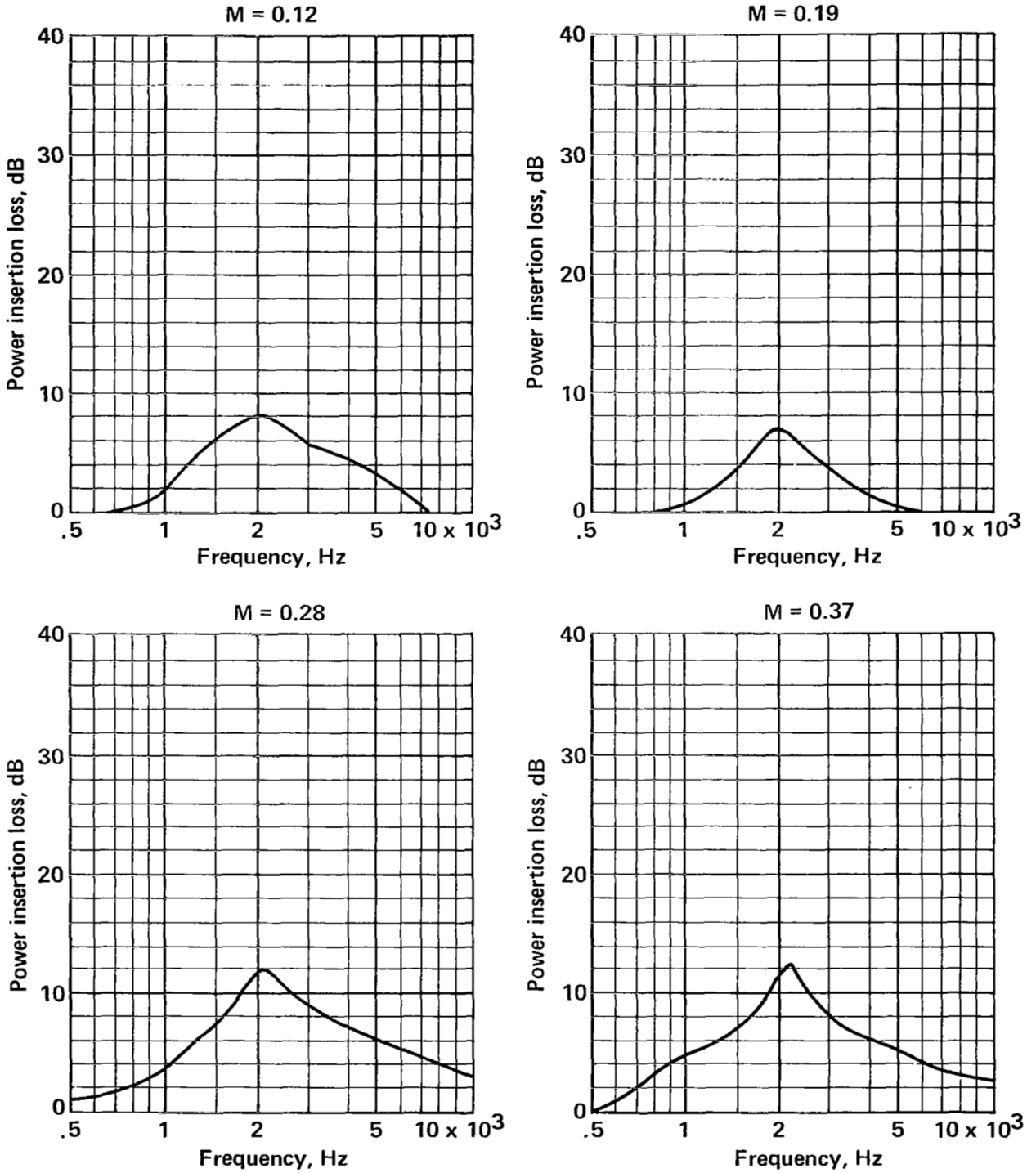

FIGURE A-9.—POWER INSERTION LOSS FOR 9-RAYL (CGS), 1/2-IN.-DEEP LINING ON ONE WALL OF 6-IN. DUCT

Duct size	6 x 10 in.
Walls lined	One/10 in.
Lining length	44 in.
Lining material	Polyimide

Flow resistance	18 rayls (cgs)
Core depth	0.5 in.
Core type	3/8-in. Hexcel

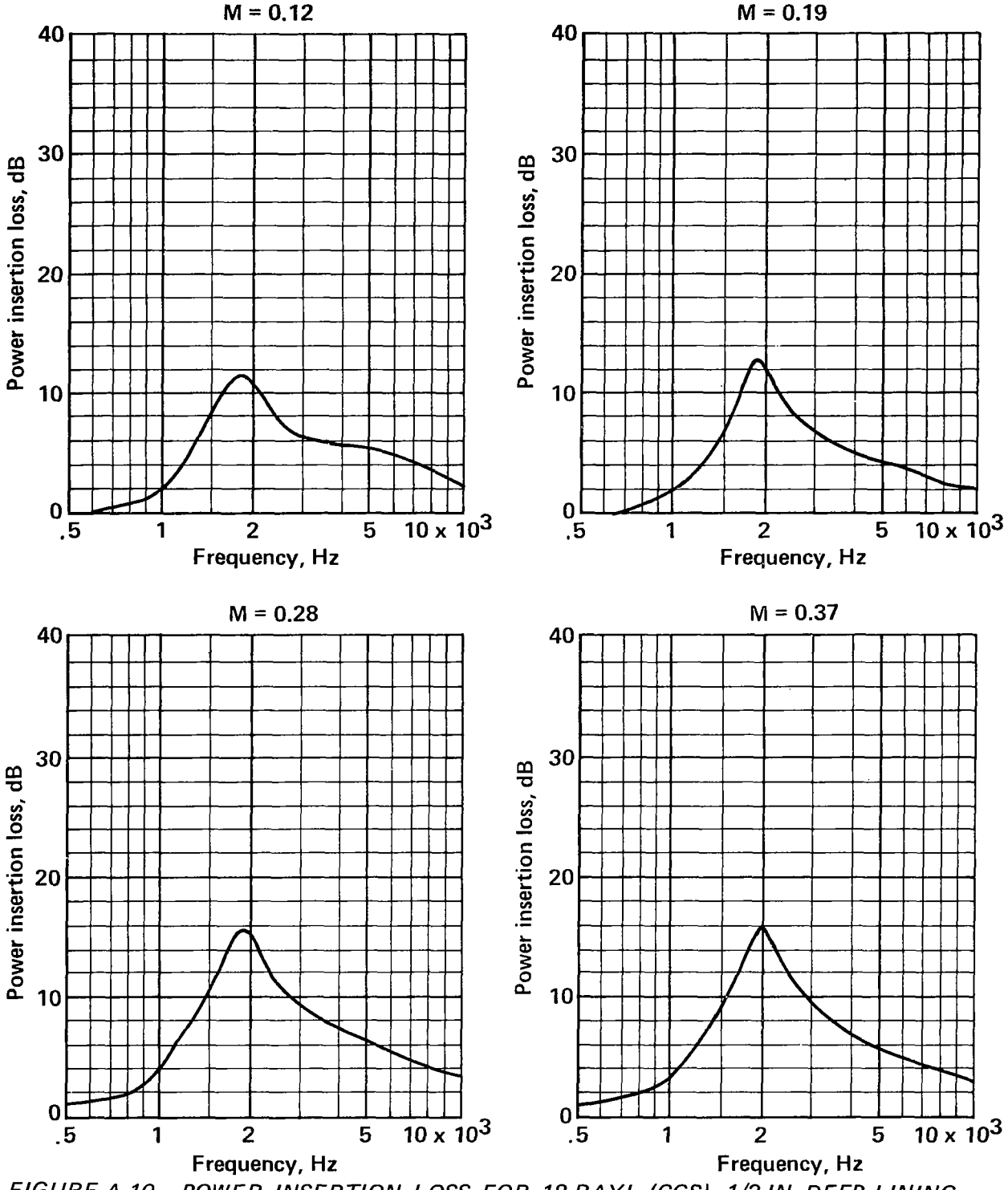

FIGURE A-10.—POWER INSERTION LOSS FOR 18-RAYL (CGS), 1/2-IN.-DEEP LINING ON ONE WALL OF 6-IN. DUCT

Duct size	6 x 10 in.
Walls lined	One/10 in.
Lining length	44 in.
Lining material	Polyimide

Flow resistance	30 rayls (cgs)
Core depth	0.5 in.
Core type	3/8-in. Hexcel

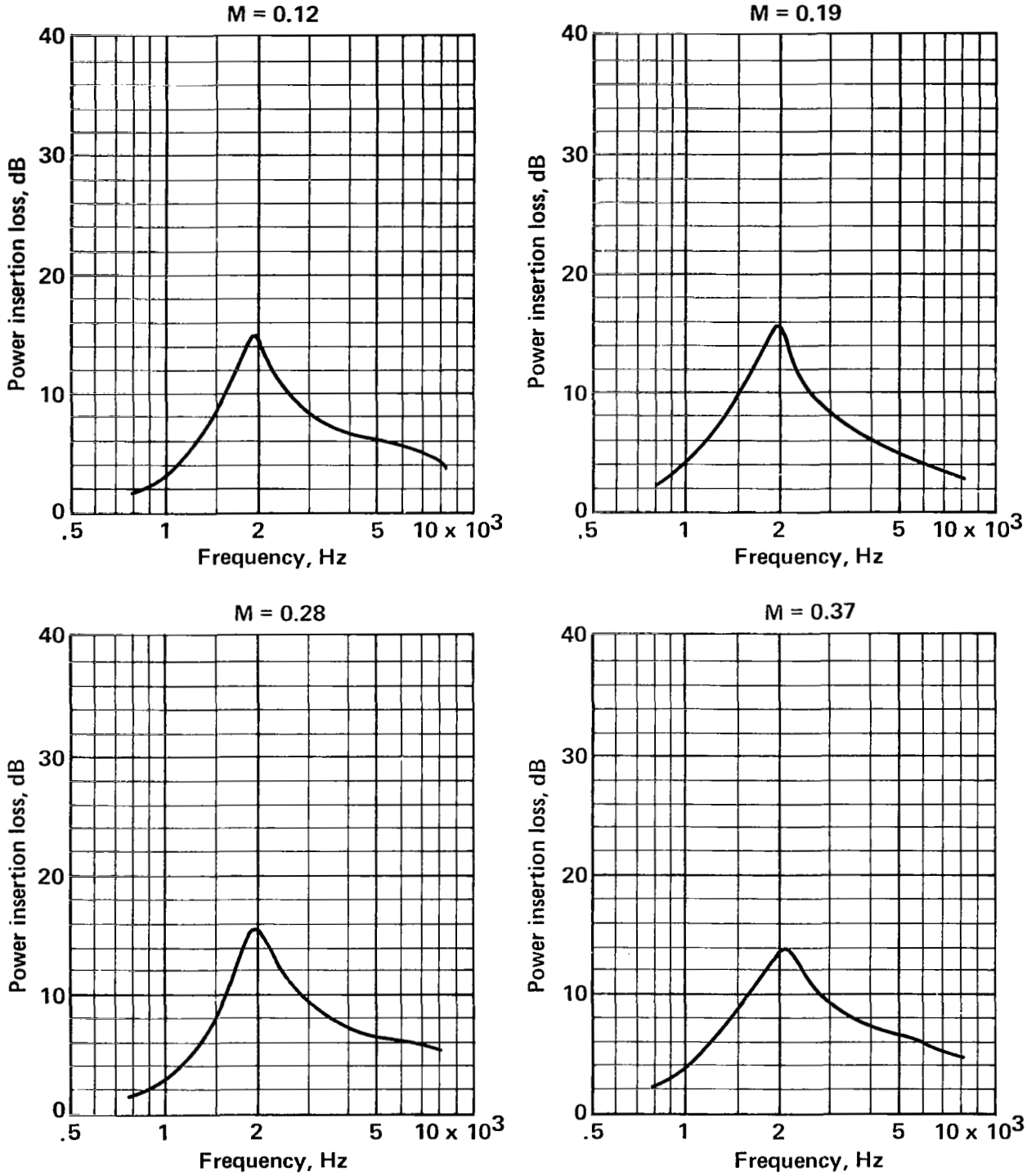

FIGURE A-11.—POWER INSERTION LOSS FOR 30-RAYL (CGS), 1/2-IN.-DEEP LINING ON ONE WALL OF 6-IN. DUCT

Duct size	6 x 10 in.
Walls lined	One/10 in.
Lining length	44 in.
Lining material	Polyimide

Flow resistance	50 rayls (cgs)
Core depth	0.5 in.
Core type	3/8-in. Hexcel

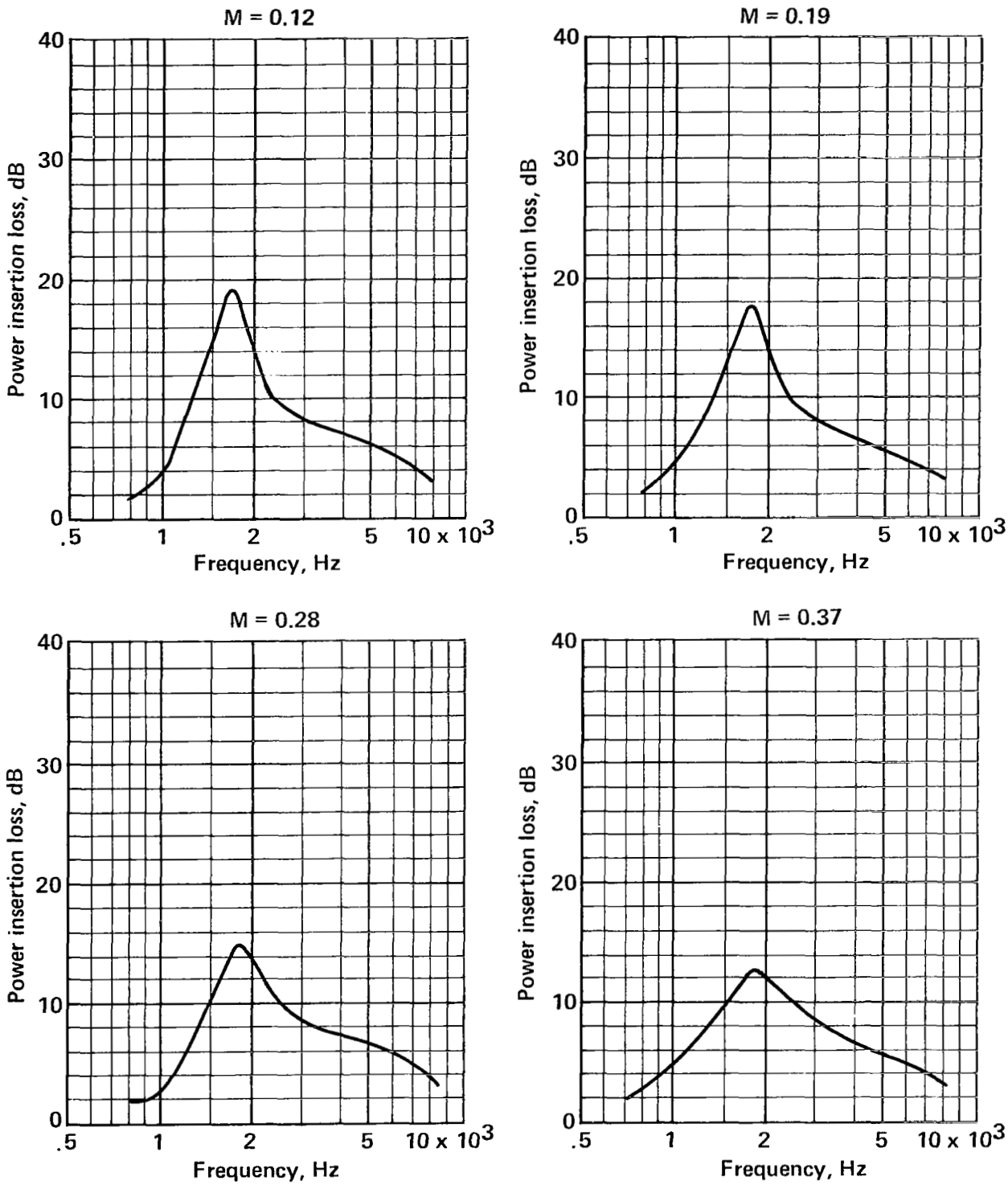

FIGURE A-12.—POWER INSERTION LOSS FOR 50-RAYL (CGS), 1/2-IN.-DEEP LINING ON ONE WALL OF 6-IN. DUCT

Duct size	6 x 10 in.
Walls lined	One/10 in.
Lining length	44 in.
Lining material	Polyimide

Flow resistance	70 rayls (cgs)
Core depth	0.5 in.
Core type	3/8-in. Hexcel

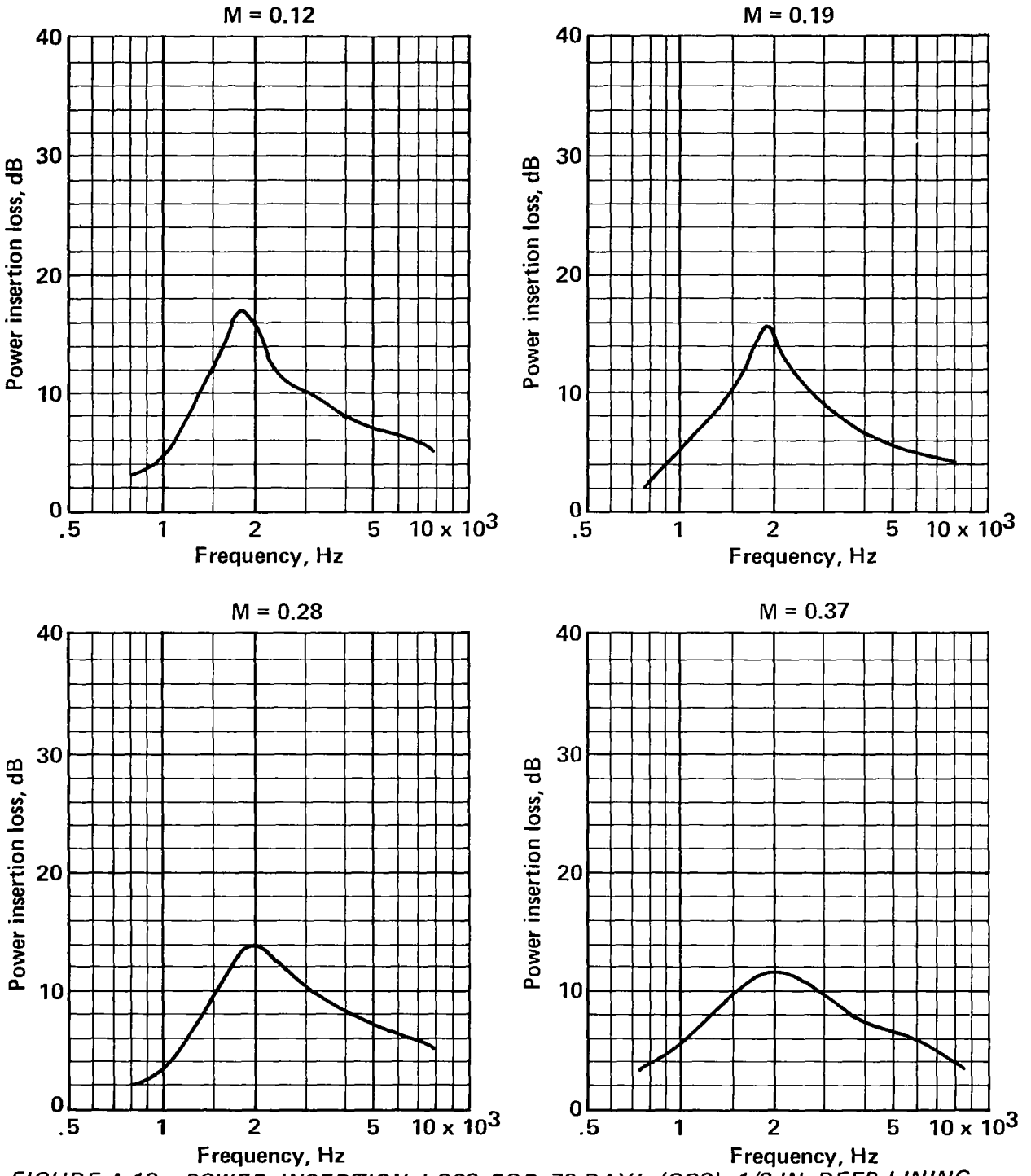

FIGURE A-13.—POWER INSERTION LOSS FOR 70-RAYL (CGS), 1/2-IN.-DEEP LINING ON ONE WALL OF 6-IN. DUCT

Duct size	6 x 10 in.
Walls lined	One/10 in.
Lining length	44 in.
Lining material	Polyimide

Flow resistance	110 rayls (cgs)
Core depth	0.5 in.
Core type	3/8-in. Hexcel

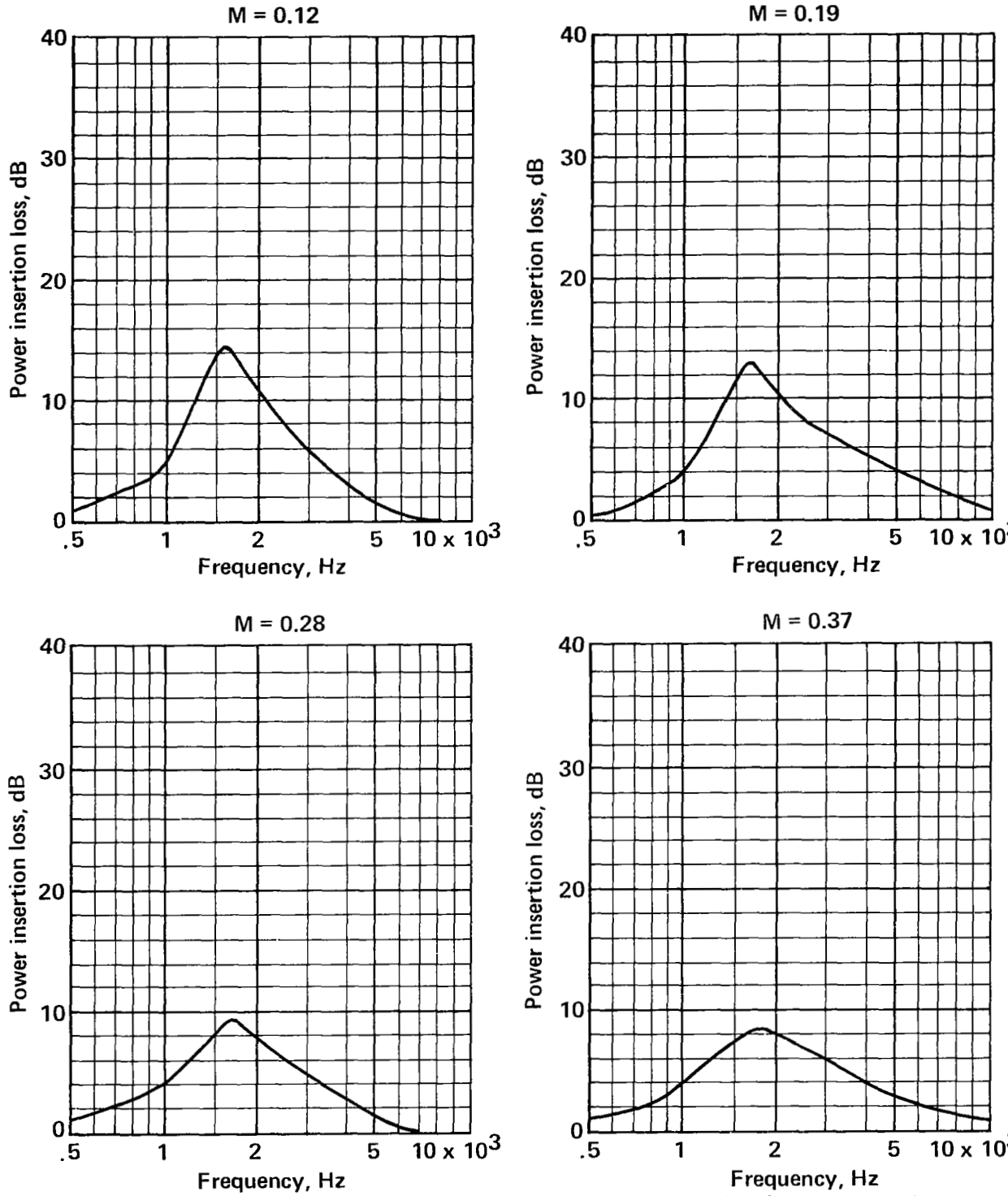

FIGURE A-14.–POWER INSERTION LOSS FOR 110-RAYL (CGS), 1/2-IN.-DEEP LINING ON ONE WALL OF 6-IN. DUCT

Duct size	6 x 10 in.
Walls lined	Two/10 in.
Lining length	22 in.
Lining material	Polyimide

Flow resistance	3 rayls (cgs)
Core depth	0.5 in.
Core type	3/8-in. Hexcel

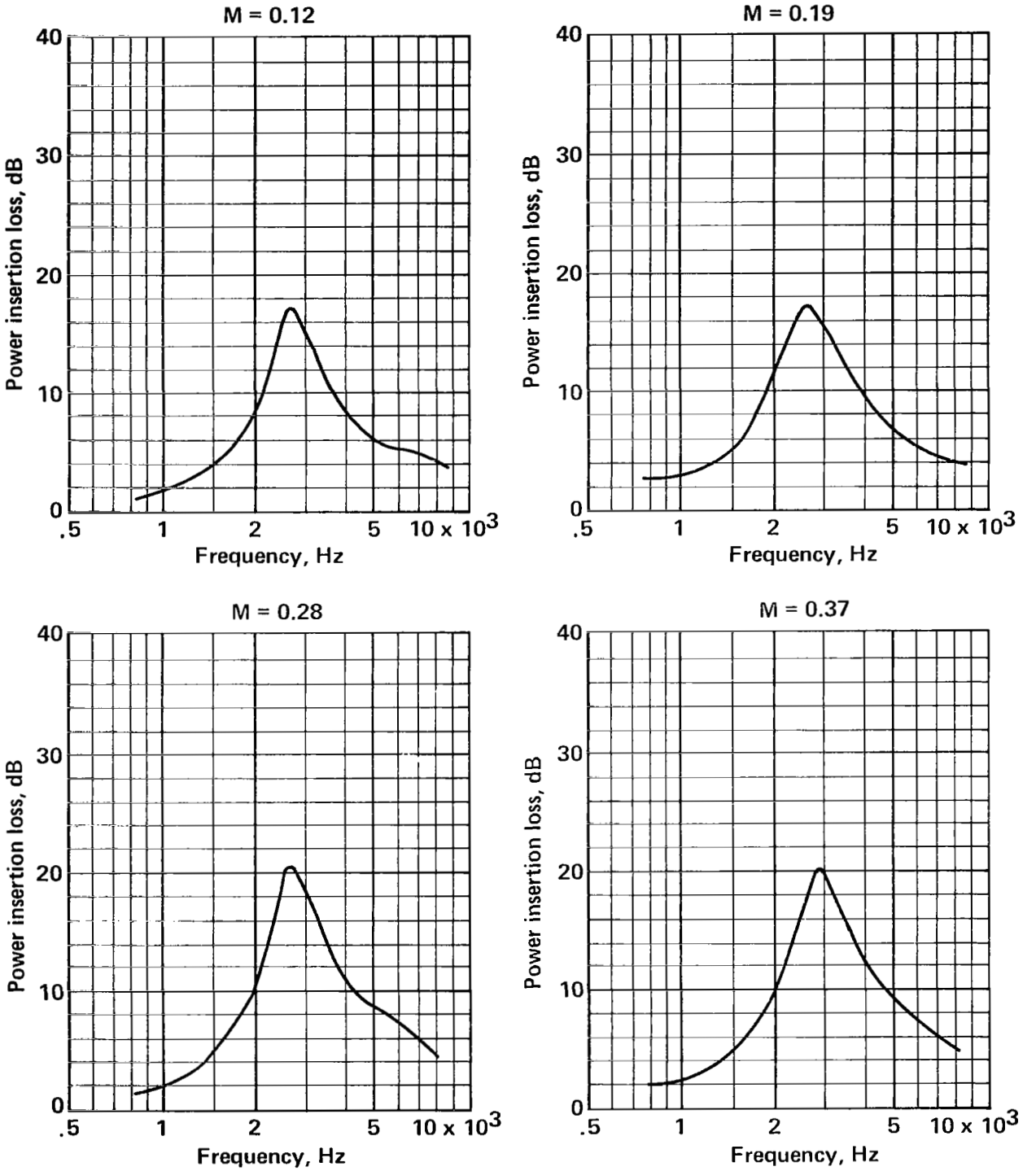

FIGURE A-15.—POWER INSERTION LOSS FOR 3-RAYL (CGS), 1/2-IN.-DEEP LINING ON TWO WALLS OF 6-IN. DUCT

Duct size	6 x 10 in.
Walls lined	Two/10 in.
Lining length	22 in.
Lining material	Polyimide

Flow resistance	9 rayls (cgs)
Core depth	0.5 in.
Core type	3/8-in. Hexcel

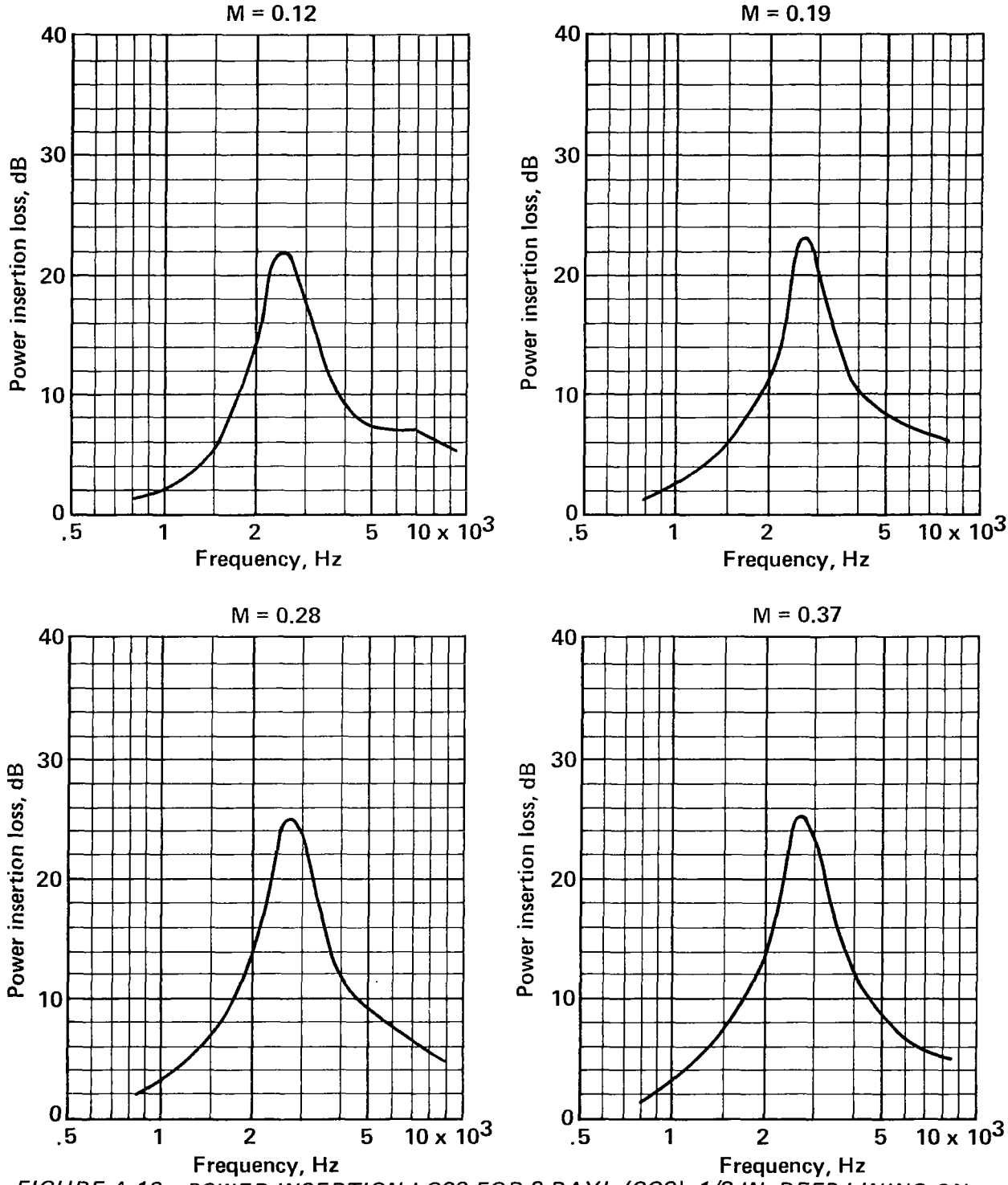

FIGURE A-16.—POWER INSERTION LOSS FOR 9-RAYL (CGS), 1/2-IN.-DEEP LINING ON TWO WALLS OF 6-IN. DUCT

Duct size	6 x 10 in.
Walls lined	Two/10 in.
Lining length	22 in.
Lining material	Polyimide

Flow resistance	18 rayls (cgs)
Core depth	0.5 in.
Core type	3/8-in. Hexcel

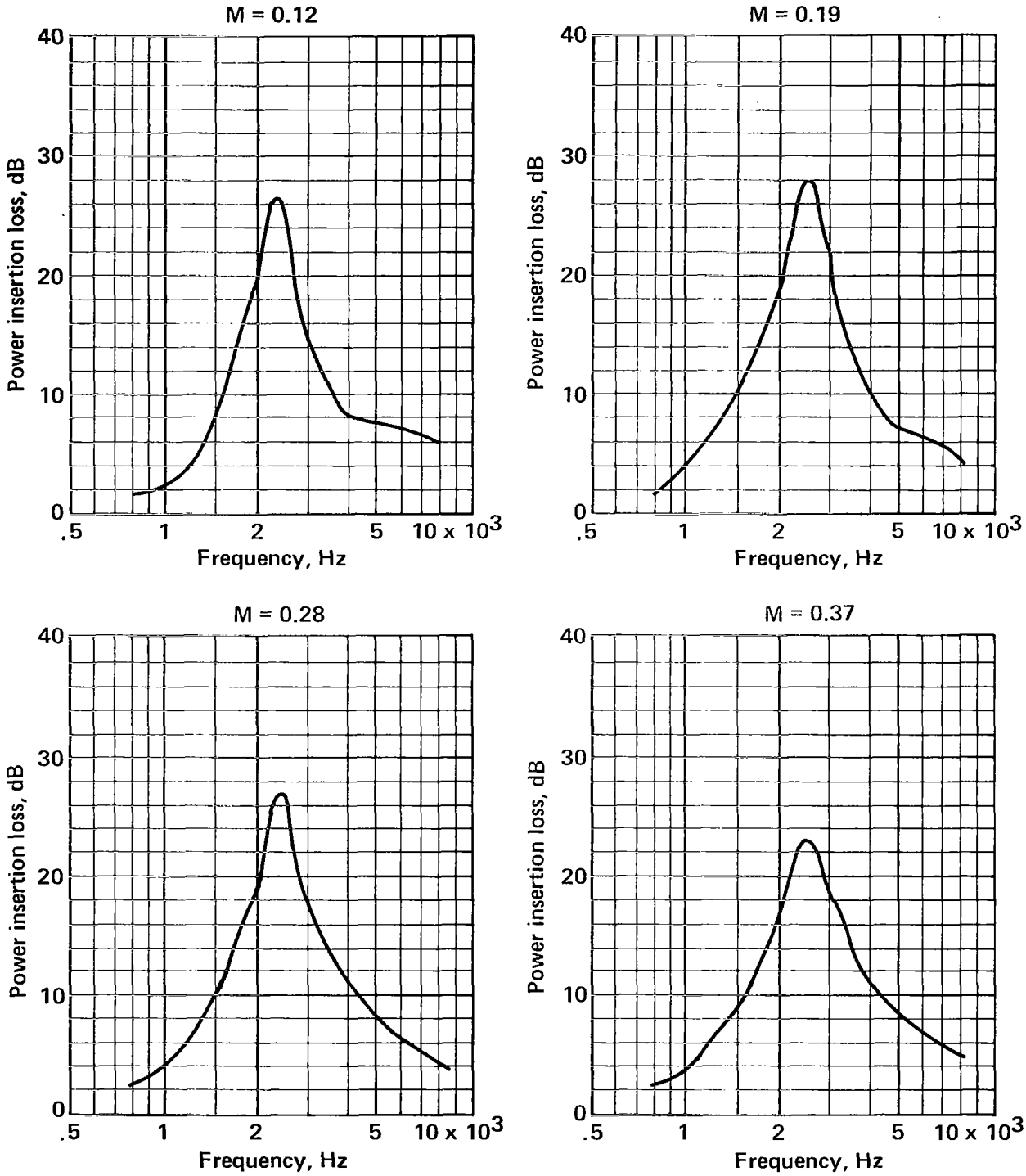

FIGURE A-17.—POWER INSERTION LOSS FOR 18-RAYL (CGS), 1/2-IN.-DEEP LINING ON TWO WALLS OF 6-IN. DUCT

Duct size	6 x 10 in.
Walls lined	Two/10 in.
Lining length	22 in.
Lining material	Polyimide

Flow resistance	30 rayls (cgs)
Core depth	0.5 in.
Core type	3/8-in. Hexcel

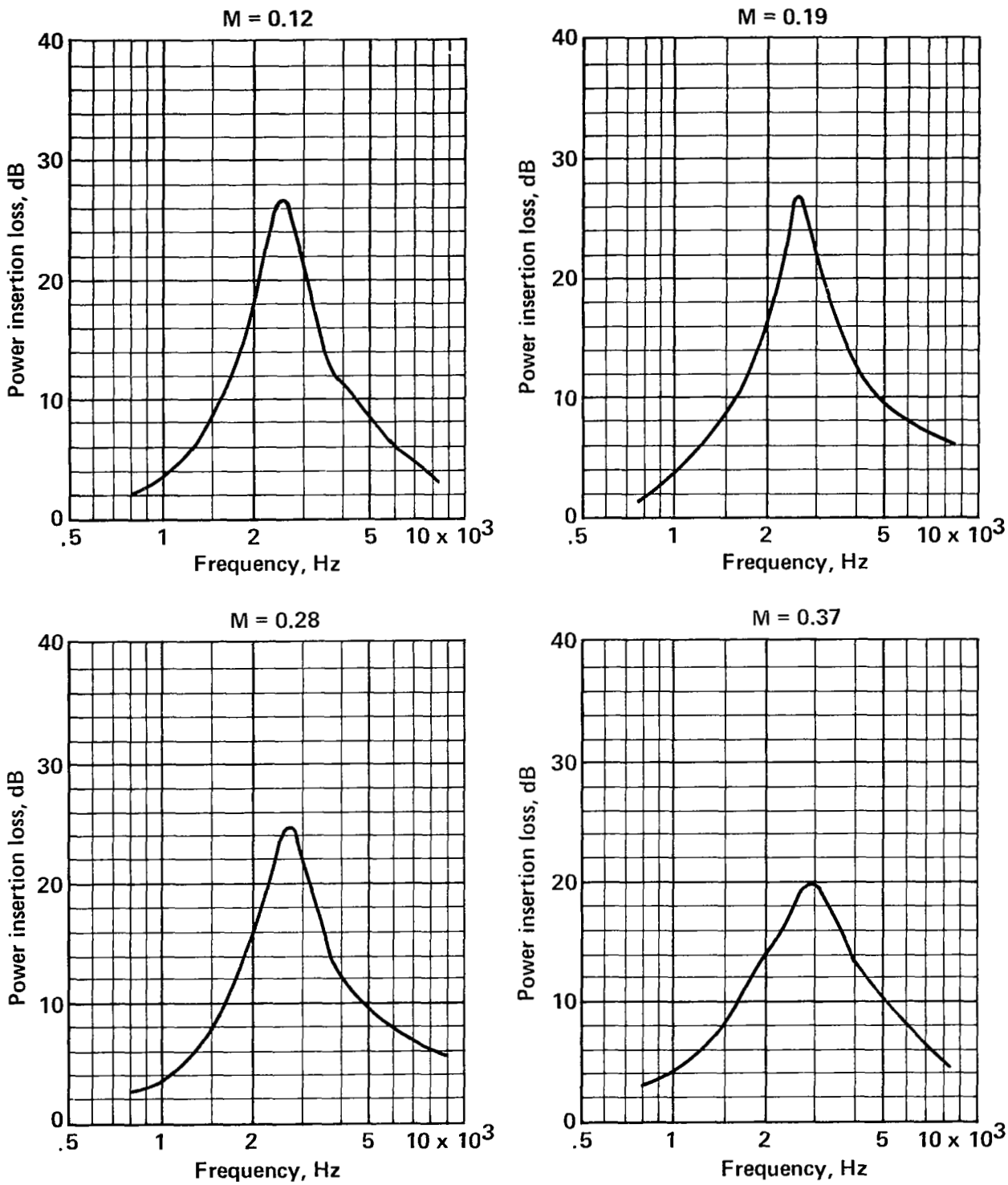

FIGURE A-18.—POWER INSERTION LOSS FOR 30-RAYL (CGS), 1/2-IN.-DEEP LINING ON TWO WALLS OF 6-IN. DUCT

Duct size	6 x 10 in.
Walls lined	Two/10 in.
Lining length	22 in.
Lining material	Polyimide

Flow resistance	50 rayls (cgs)
Core depth	0.5 in.
Core type	3/8-in. Hexcel

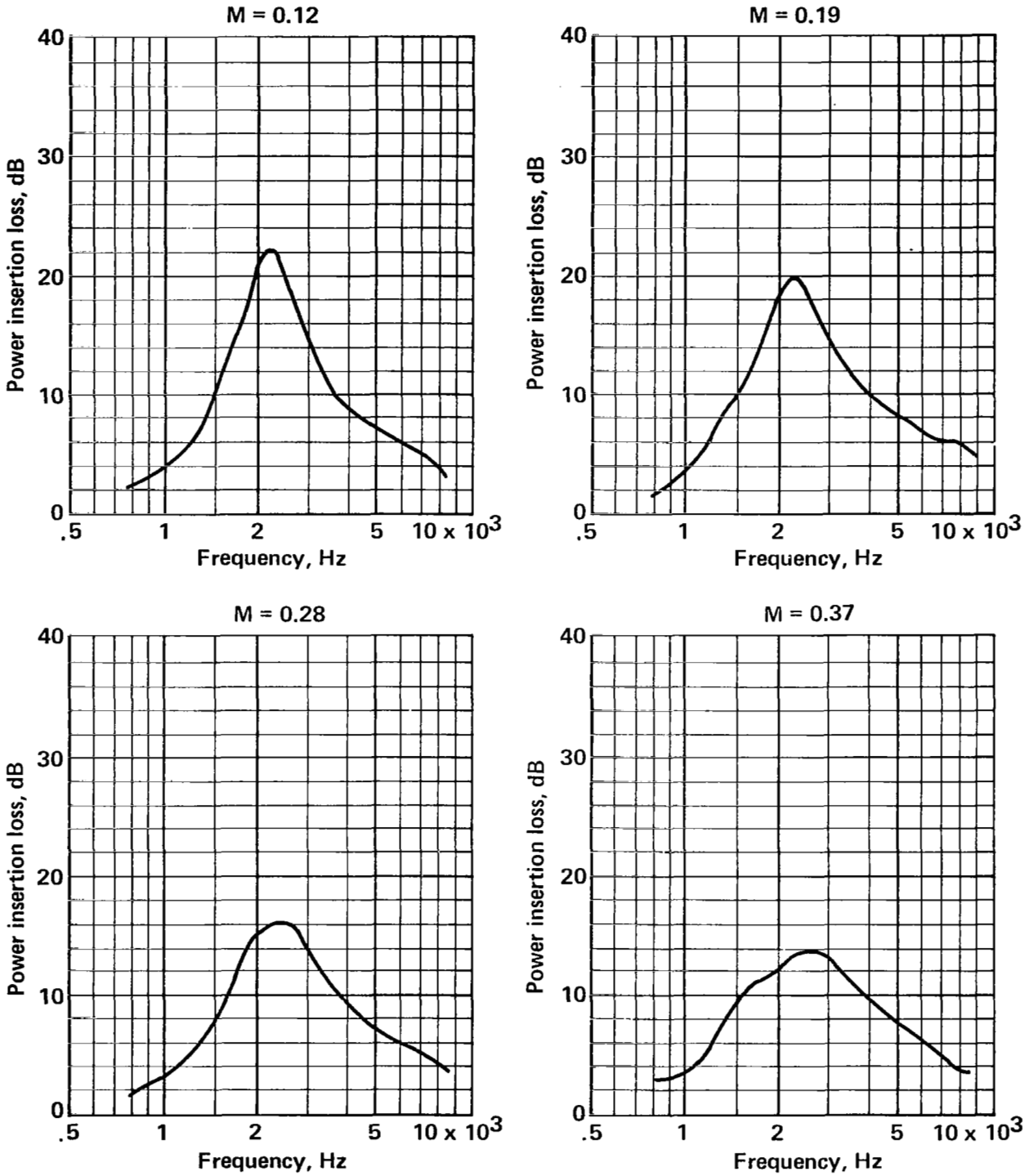

FIGURE A-19.—POWER INSERTION LOSS FOR 50-RAYL (CGS), 1/2-IN.-DEEP LINING ON TWO WALLS OF 6-IN. DUCT

Duct size	6 x 10 in.
Walls lined	Two/10 in.
Lining length	22 in.
Lining material	Polyimide

Flow resistance	70 rayls (cgs)
Core depth	0.5 in.
Core type	3/8-in. Hexcel

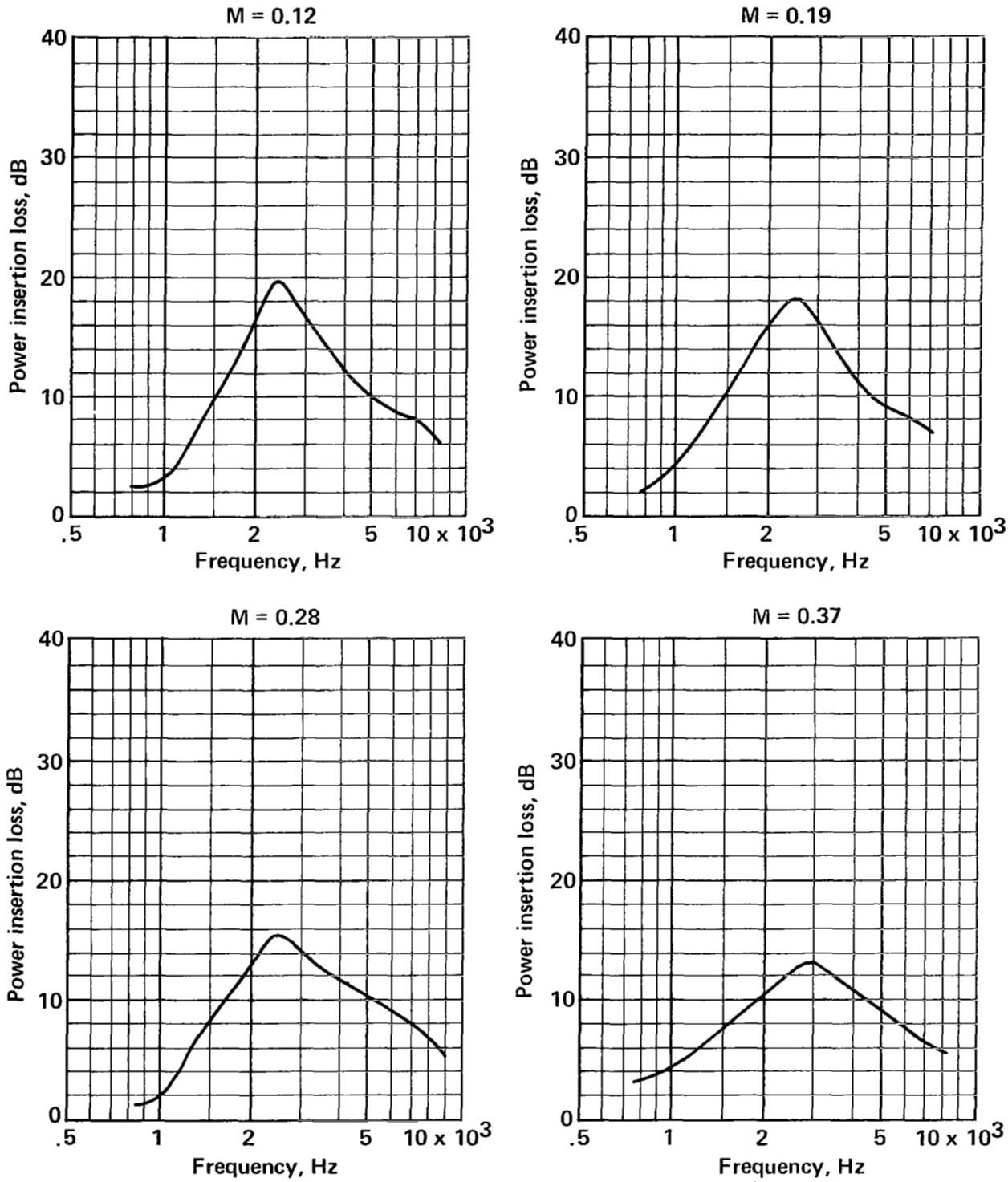

FIGURE A-20.—POWER INSERTION LOSS FOR 70-RAYL (CGS), 1/2-IN.-DEEP LINING ON TWO WALLS OF 6-IN. DUCT

Duct size	6 x 10 in.
Walls lined	Two/10 in.
Lining length	22 in.
Lining material	Polyimide

Flow resistance	110 rayls (cgs)
Core depth	0.5 in.
Core type	3/8-in. Hexcel

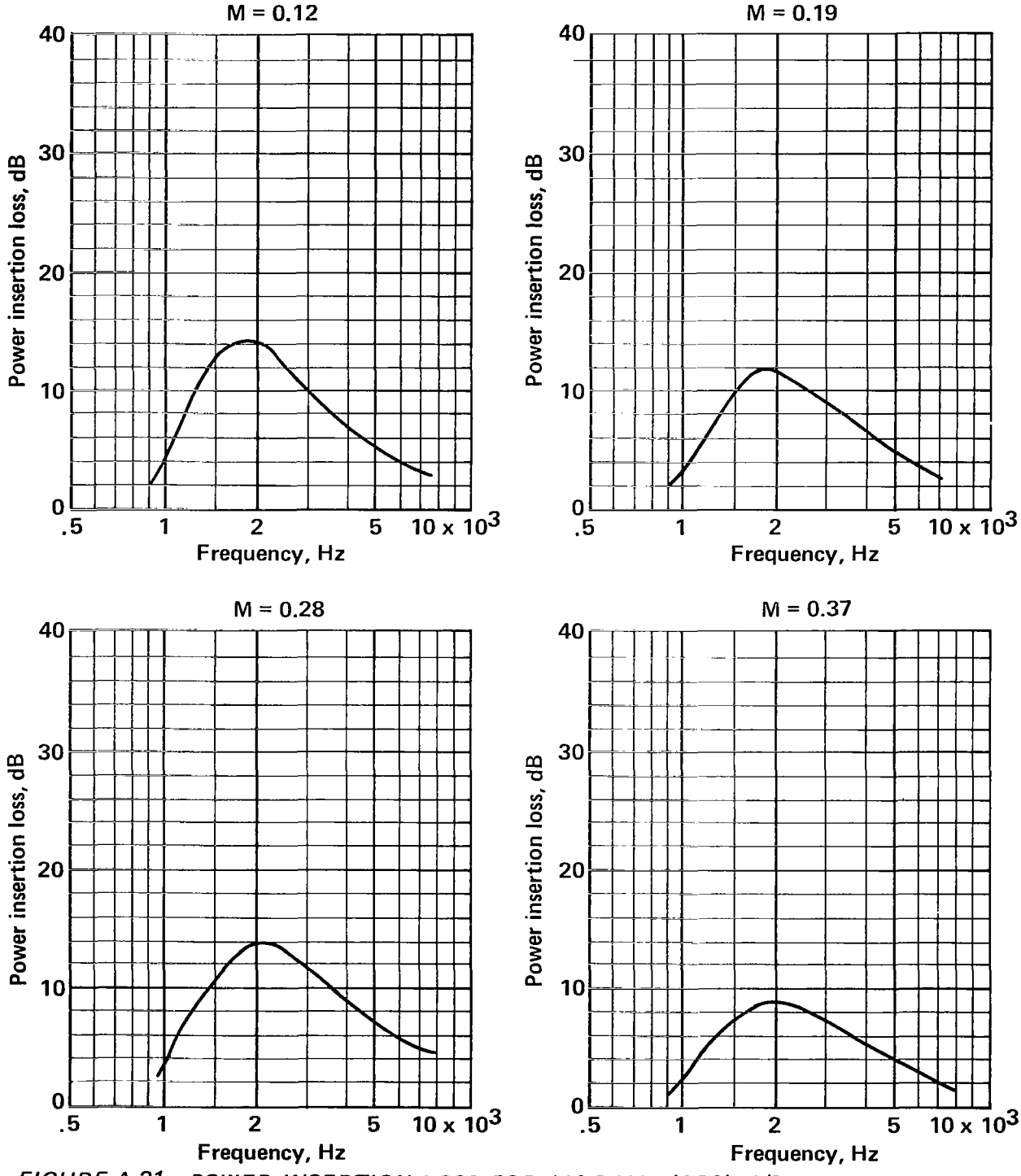

FIGURE A-21.—POWER INSERTION LOSS FOR 110-RAYL (CGS), 1/2-IN.-DEEP LINING ON TWO WALLS OF 6-IN. DUCT

Duct size	6 x 10 in.
Walls lined	One/6 in.
Lining length	22 in.
Lining material	Polyimide

Flow resistance	30 rayls (cgs)
Core depth	0.5 in.
Core type	3/8-in. Hexcel

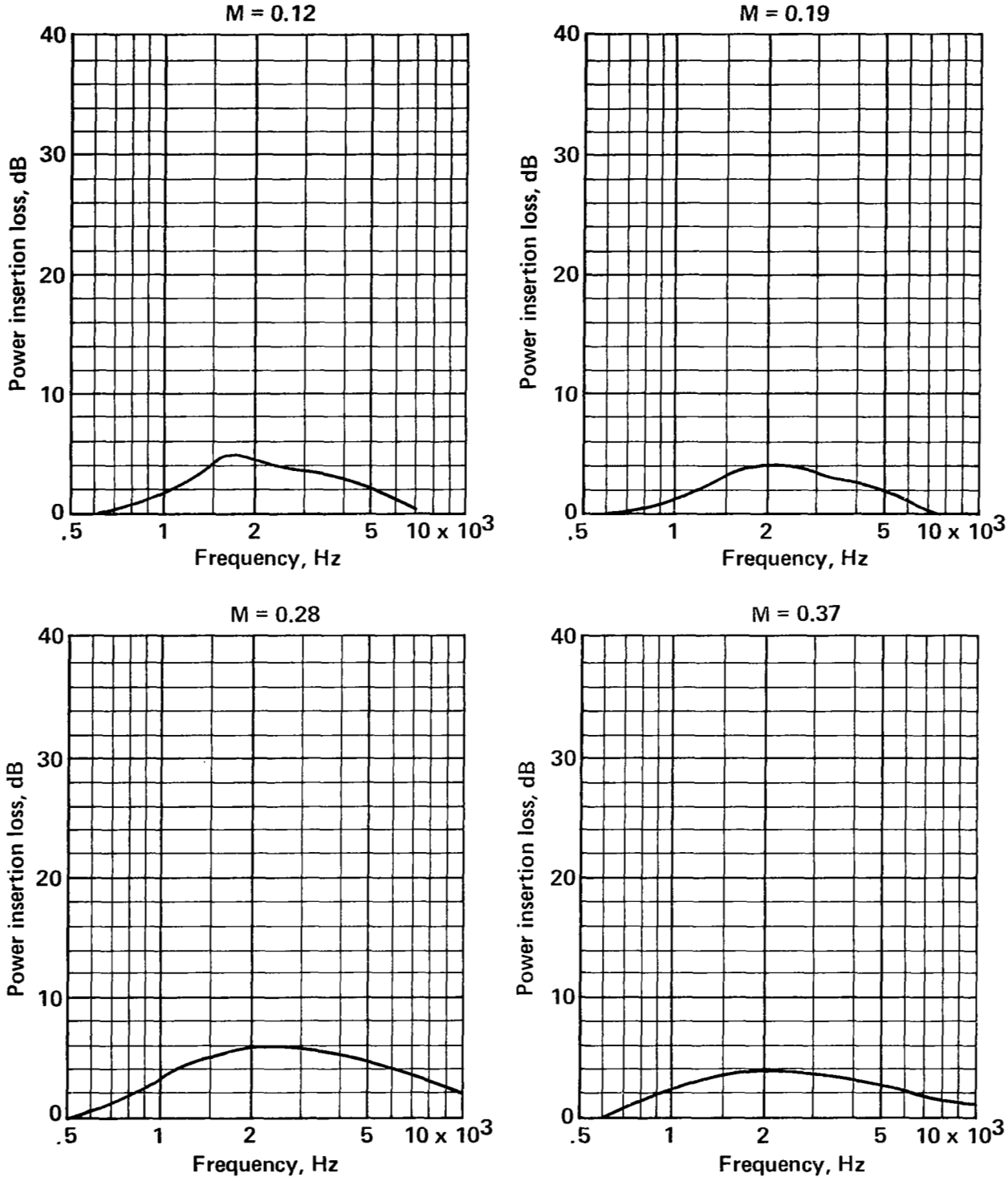

FIGURE A-22.–POWER INSERTION LOSS DUE TO LINING ON ONE 6-IN. WALL

Duct size	6 x 10 in.
Walls lined	One/10 in.
Lining length	22 in.
Lining material	Polyimide

Flow resistance	30 rayls (cgs)
Core depth	0.5 in.
Core type	3/8-in. Hexcel

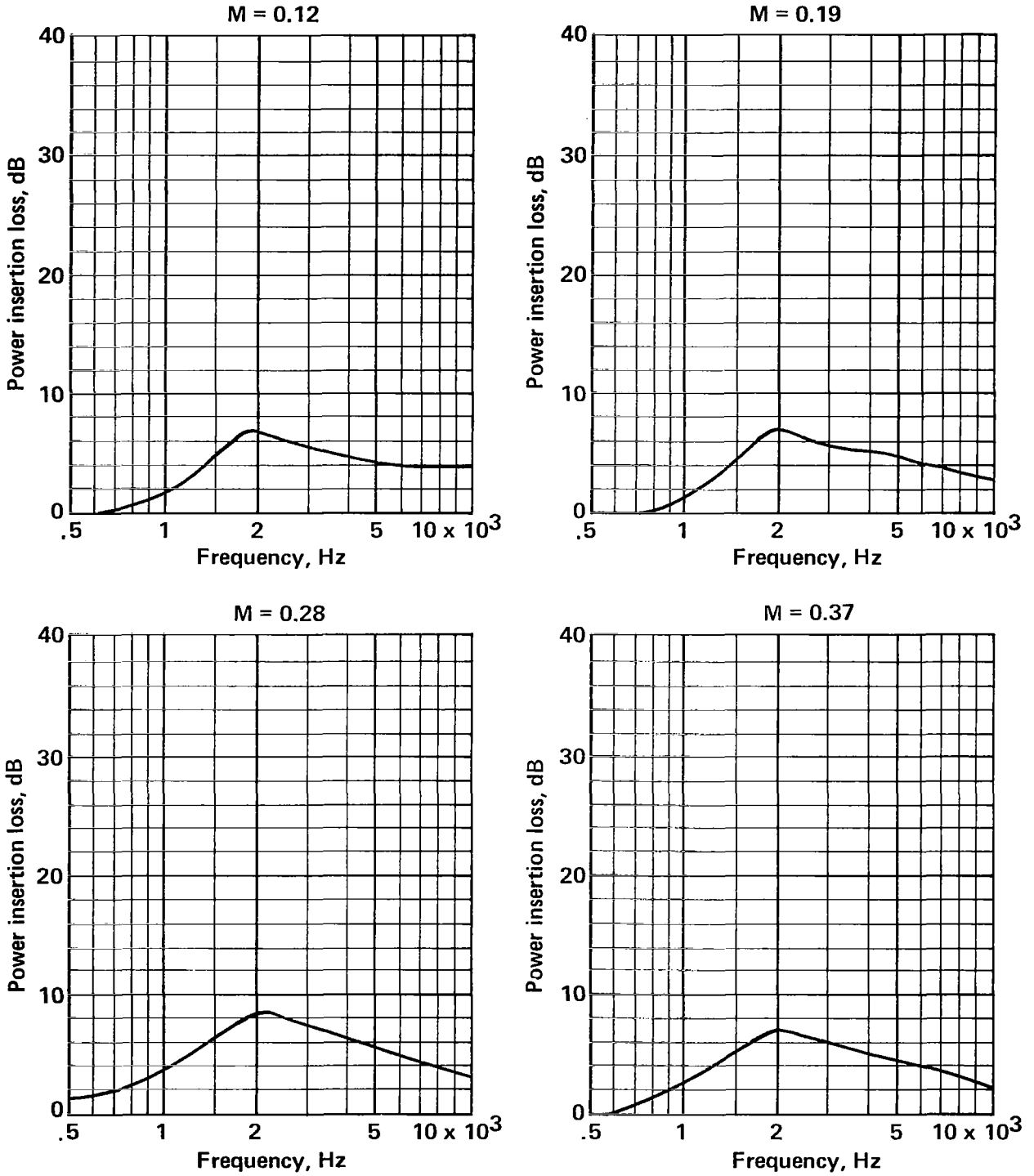

FIGURE A-23.—POWER INSERTION LOSS DUE TO LINING ON ONE 10-IN. WALL

Duct size	6 x 10 in.
Walls lined	Two/6 in.
Lining length	22 in.
Lining material	Polyimide

Flow resistance	30 rayls (cgs)
Core depth	0.5 in.
Core type	3/8-in. Hexcel

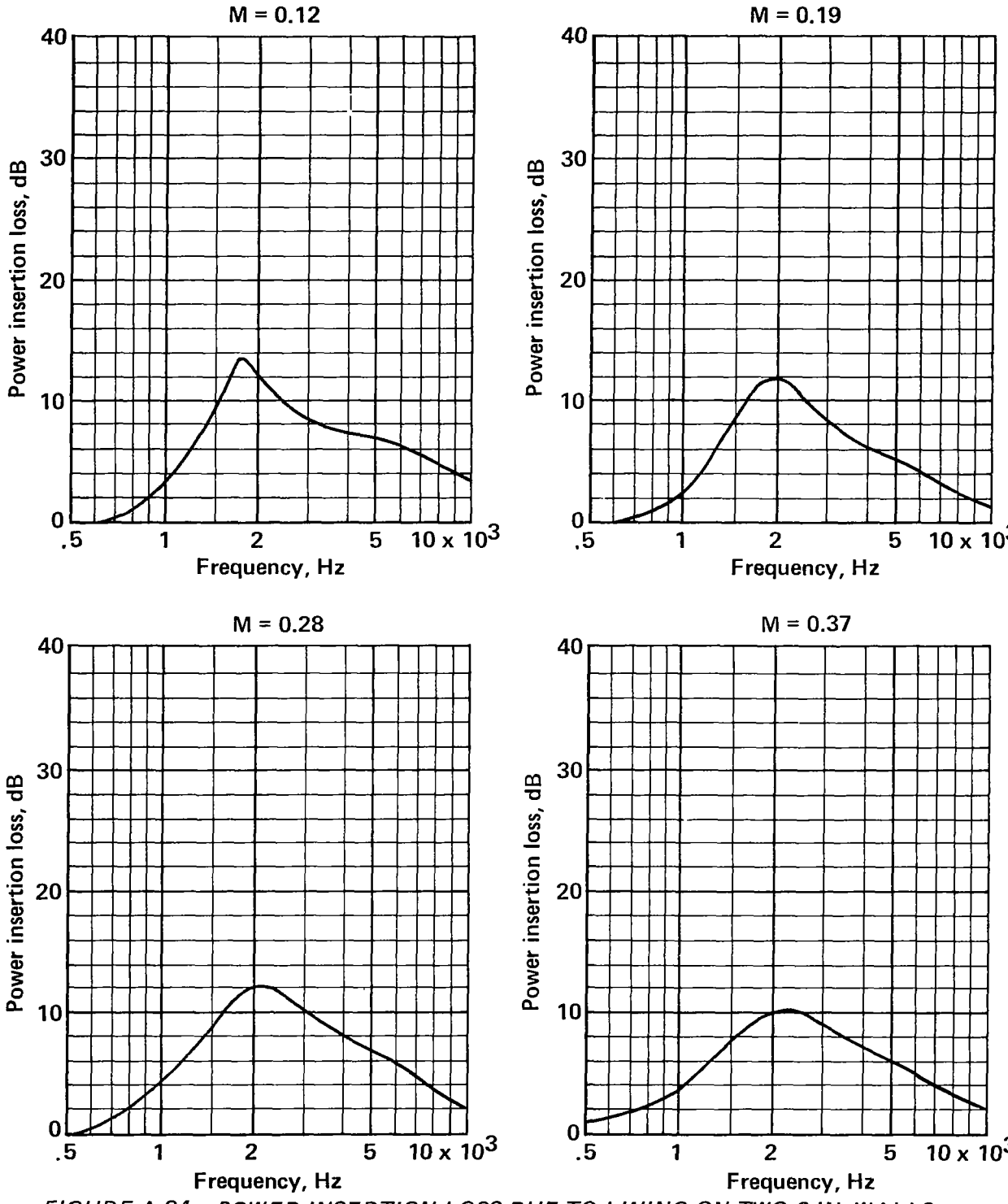

FIGURE A-24.—POWER INSERTION LOSS DUE TO LINING ON TWO 6-IN. WALLS

Duct size	6 x 10 in.
Walls lined	All
Lining length	22 in.
Lining material	Polyimide

Flow resistance	30 rayls (cgs)
Core depth	0.5 in.
Core type	3/8-in. Hexcel

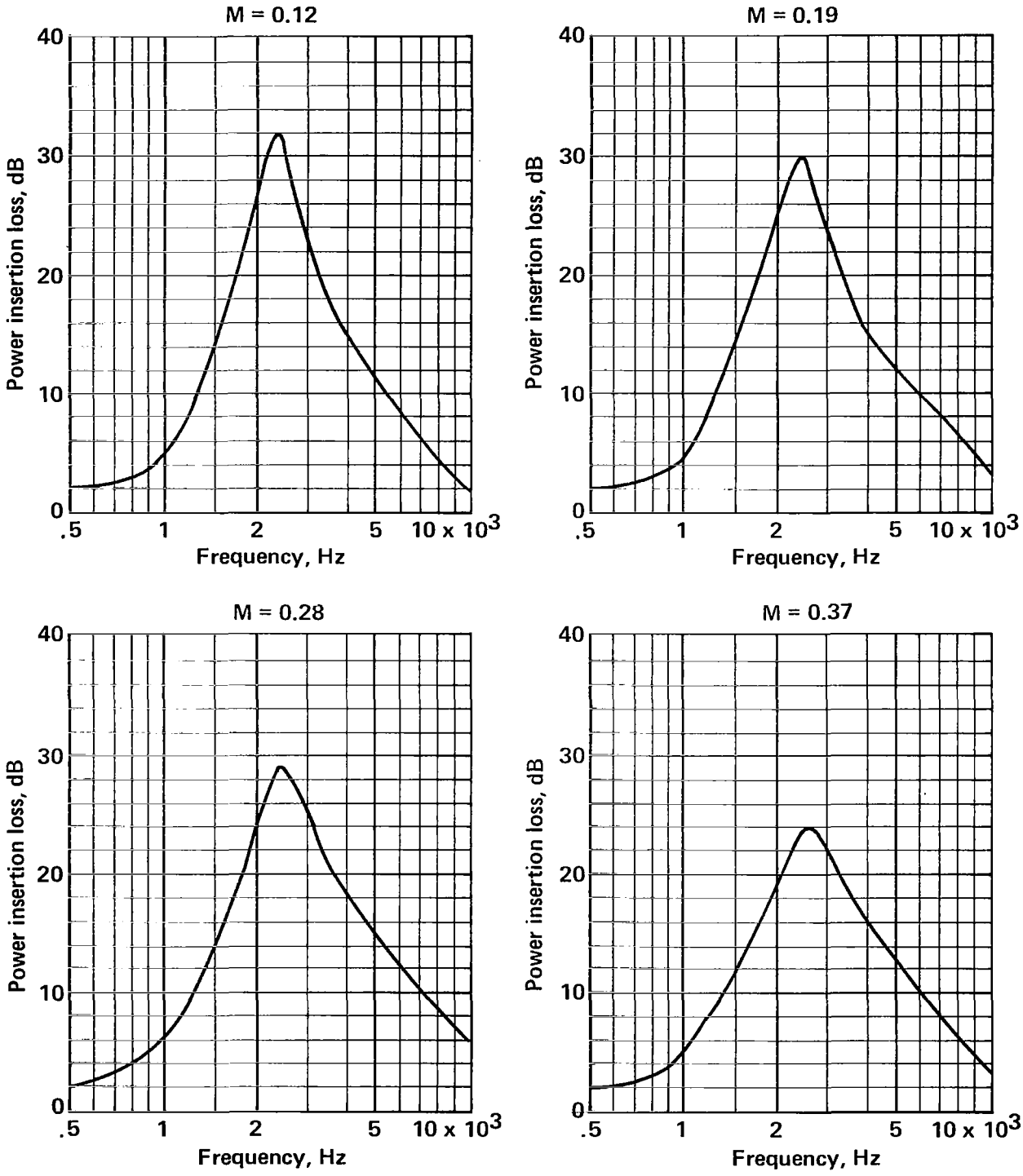

FIGURE A-25.— POWER INSERTION LOSS DUE TO LINING ON ALL FOUR WALLS

Duct size	6 x 10 in.
Walls lined	Two/10 in.
Lining length	10 in.
Lining material	Polyimide

Flow resistance	30 rayls (cgs)
Core depth	0.5 in.
Core type	3/8-in. Hexcel

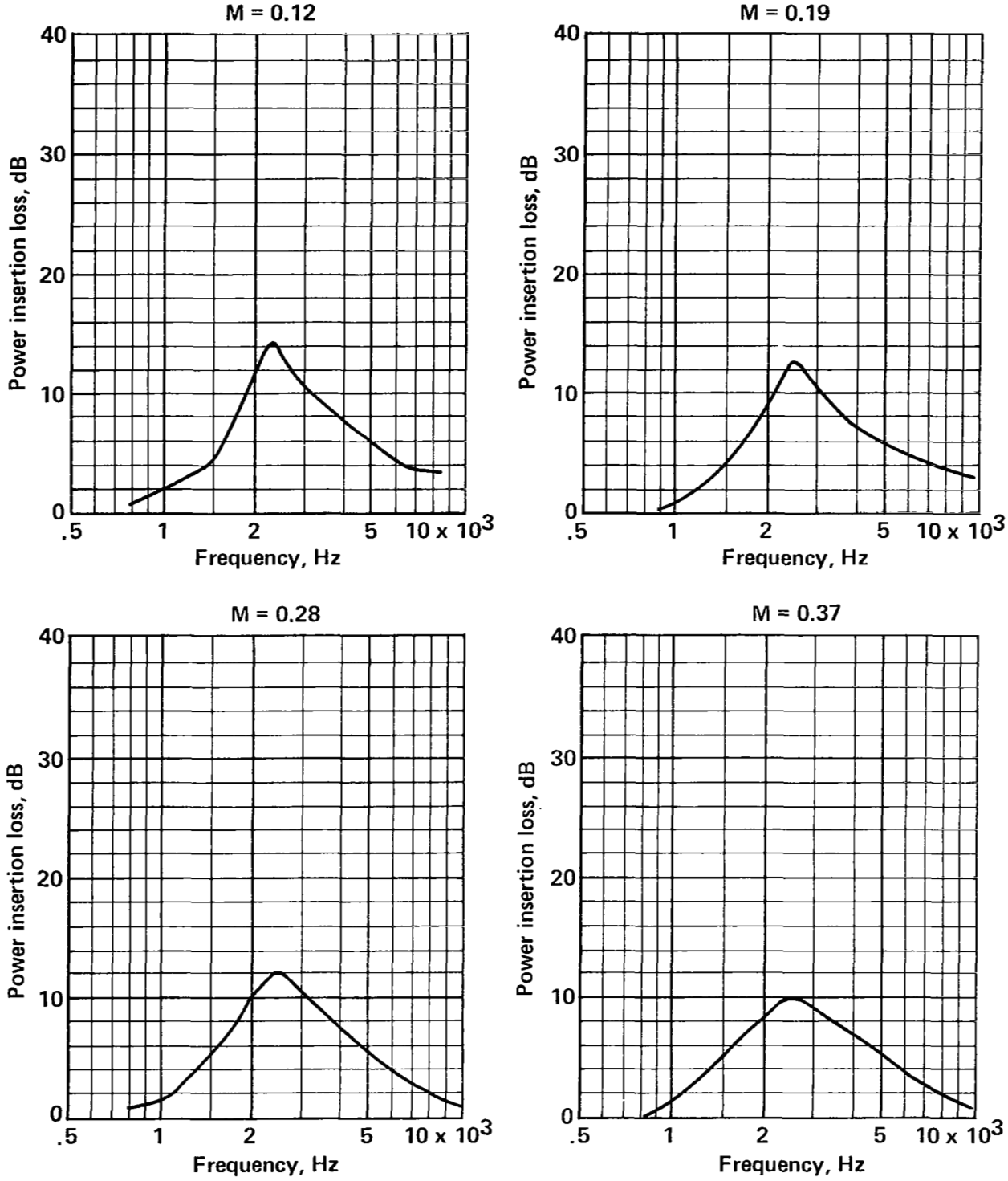

FIGURE A-26.— POWER INSERTION LOSS FOR 10-IN.-LONG LINING

Duct size	6 x 10 in.
Walls lined	Two/10 in.
Lining length	15 in.
Lining material	Polyimide

Flow resistance	30 rayls (cgs)
Core depth	0.5 in.
Core type	3/8-in. Hexcel

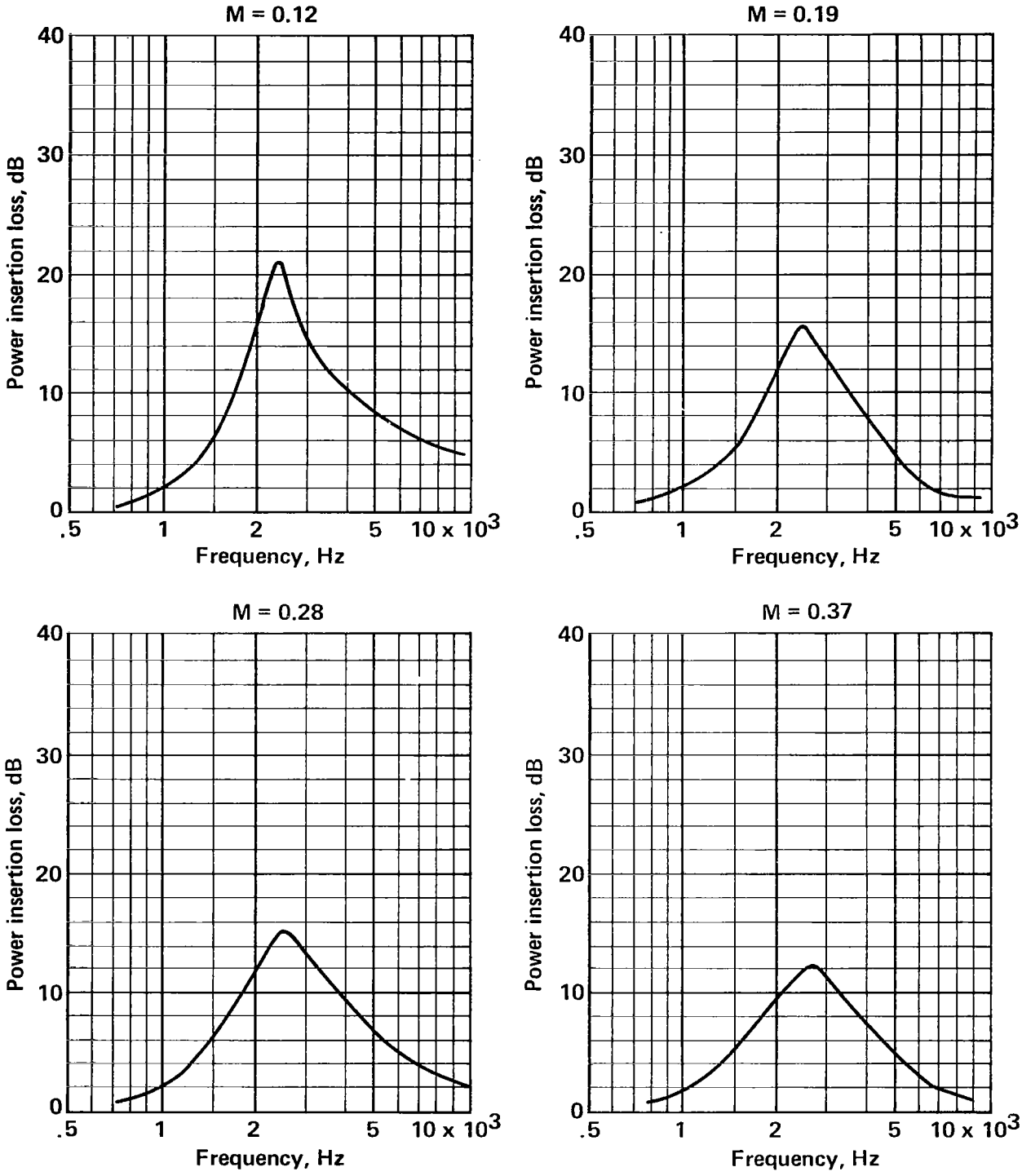

FIGURE A-27.—POWER INSERTION LOSS FOR 15-IN.-LONG LINING

Duct size	6 x 10 in.
Walls lined	Two/10 in.
Lining length	22 in.
Lining material	Polyimide

Flow resistance	30 rayls (cgs)
Core depth	0.75 in.
Core type	3/8-in. Hexcel

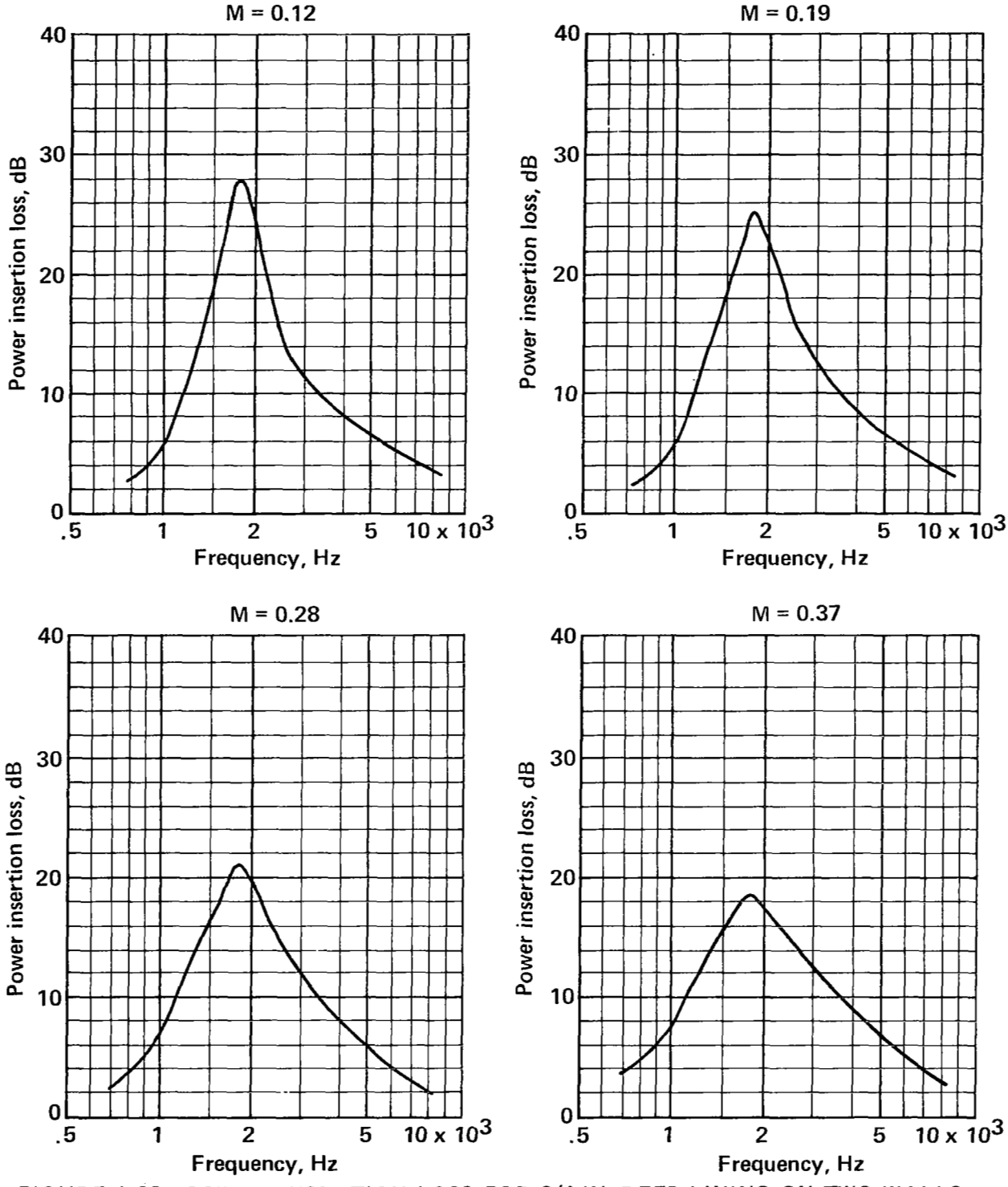

FIGURE A-28.—POWER INSERTION LOSS FOR 3/4-IN.-DEEP LINING ON TWO WALLS OF 6-IN. DUCT

Duct size	6 x 10 in.
Walls lined	One/10 in.
Lining length	44 in.
Lining material	Polyimide

Flow resistance	30 rayls (cgs)
Core depth	1.0 in.
Core type	3/8-in. Hexcel

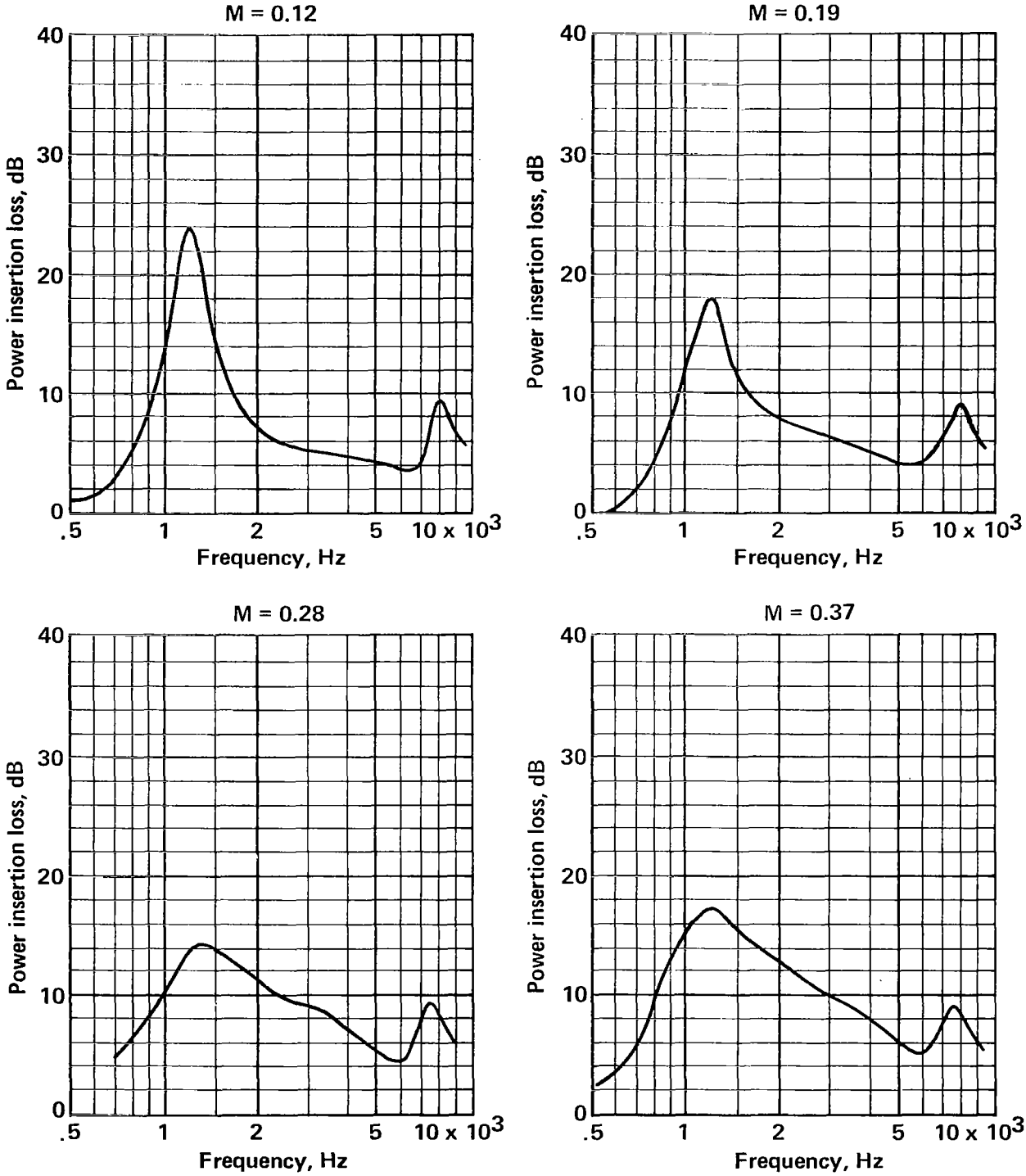

FIGURE A-29.—POWER INSERTION LOSS FOR 1-IN.-DEEP LINING ON ONE WALL OF 6-IN. DUCT

Duct size	6 x 10 in.
Walls lined	Two/10 in.
Lining length	22 in.
Lining material	Polyimide

Flow resistance	3 rayls (cgs)
Core depth	1.0 in.
Core type	3/8-in. Hexcel

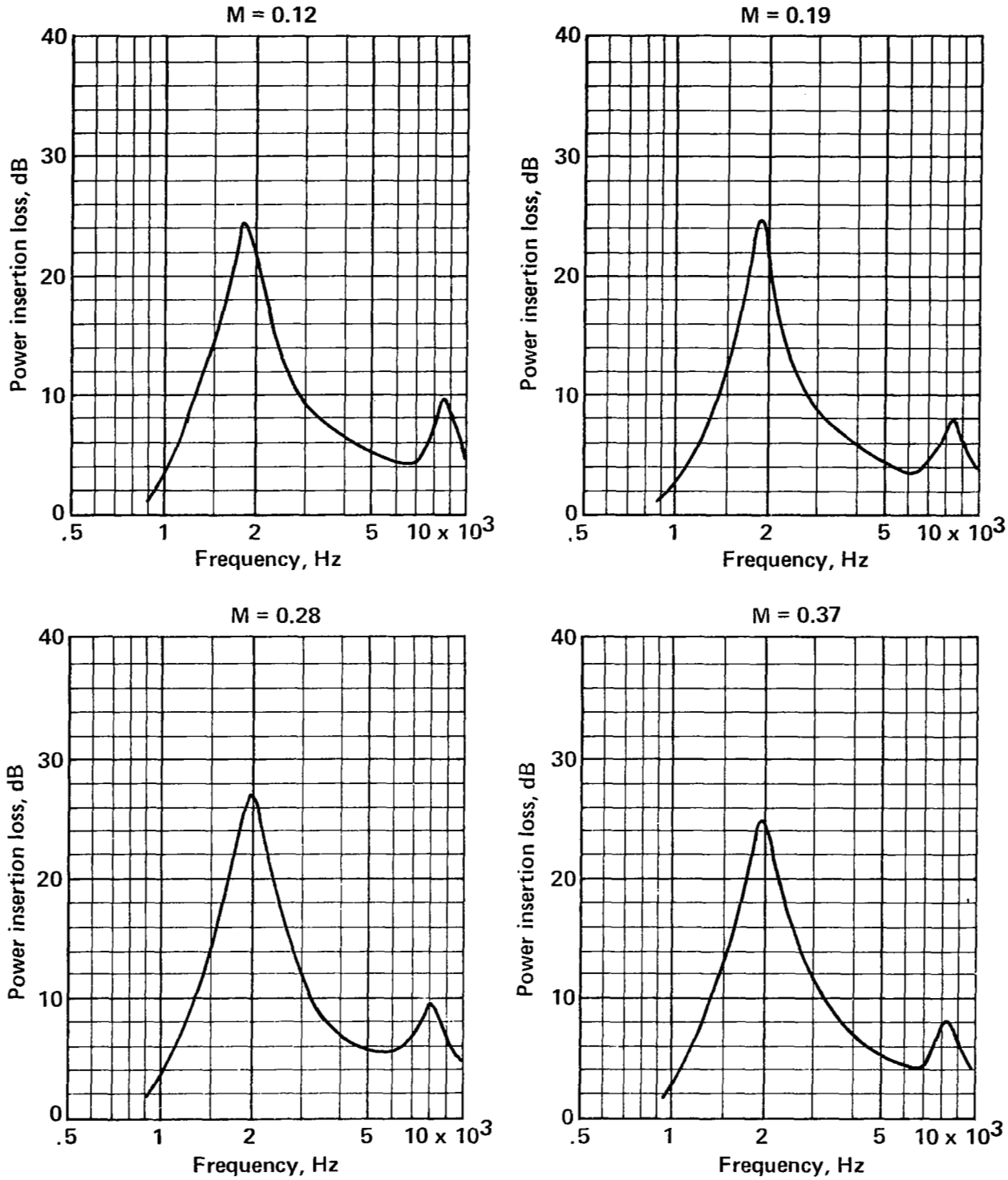

FIGURE A-30.—POWER INSERTION LOSS FOR 3-RAYL (CGS), 1-IN.-DEEP LINING ON TWO WALLS OF 6-IN. DUCT

Duct size	6 x 10 in.
Walls lined	Two/10 in.
Lining length	22 in.
Lining material	Polyimide

Flow resistance	9 rayls (cgs)
Core depth	0.9 in.
Core type	3/8-in. Hexcel

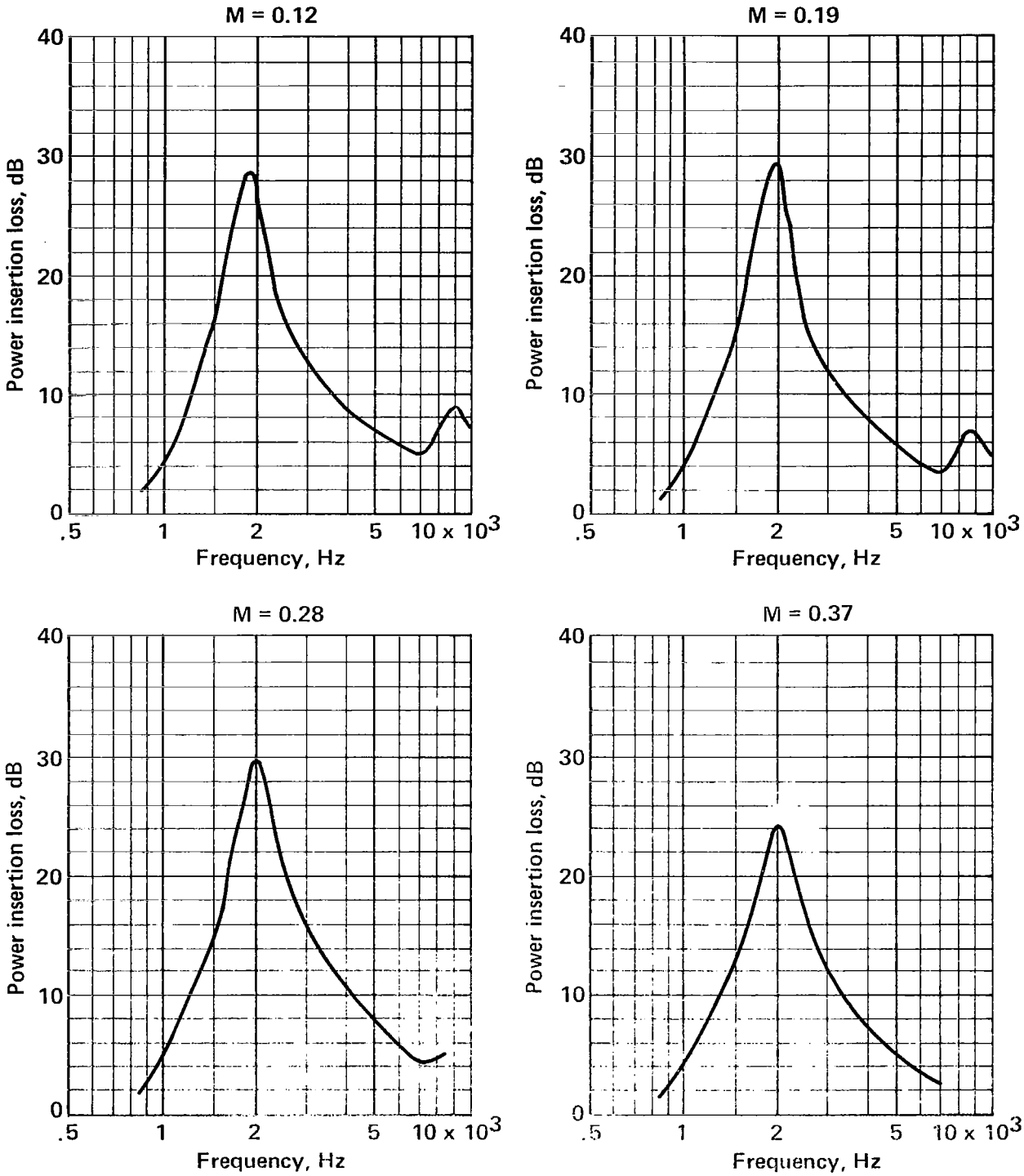

FIGURE A-31.—POWER INSERTION LOSS FOR 9-RAYL (CGS), 1-IN.-DEEP LINING ON TWO WALLS OF 6-IN. DUCT

Duct size	6 x 10 in.
Walls lined	Two/10 in.
Lining length	22 in.
Lining material	Polyimide

Flow resistance	18 rayls (cgs)
Core depth	0.98 in.
Core type	3/8-in. Hexcel

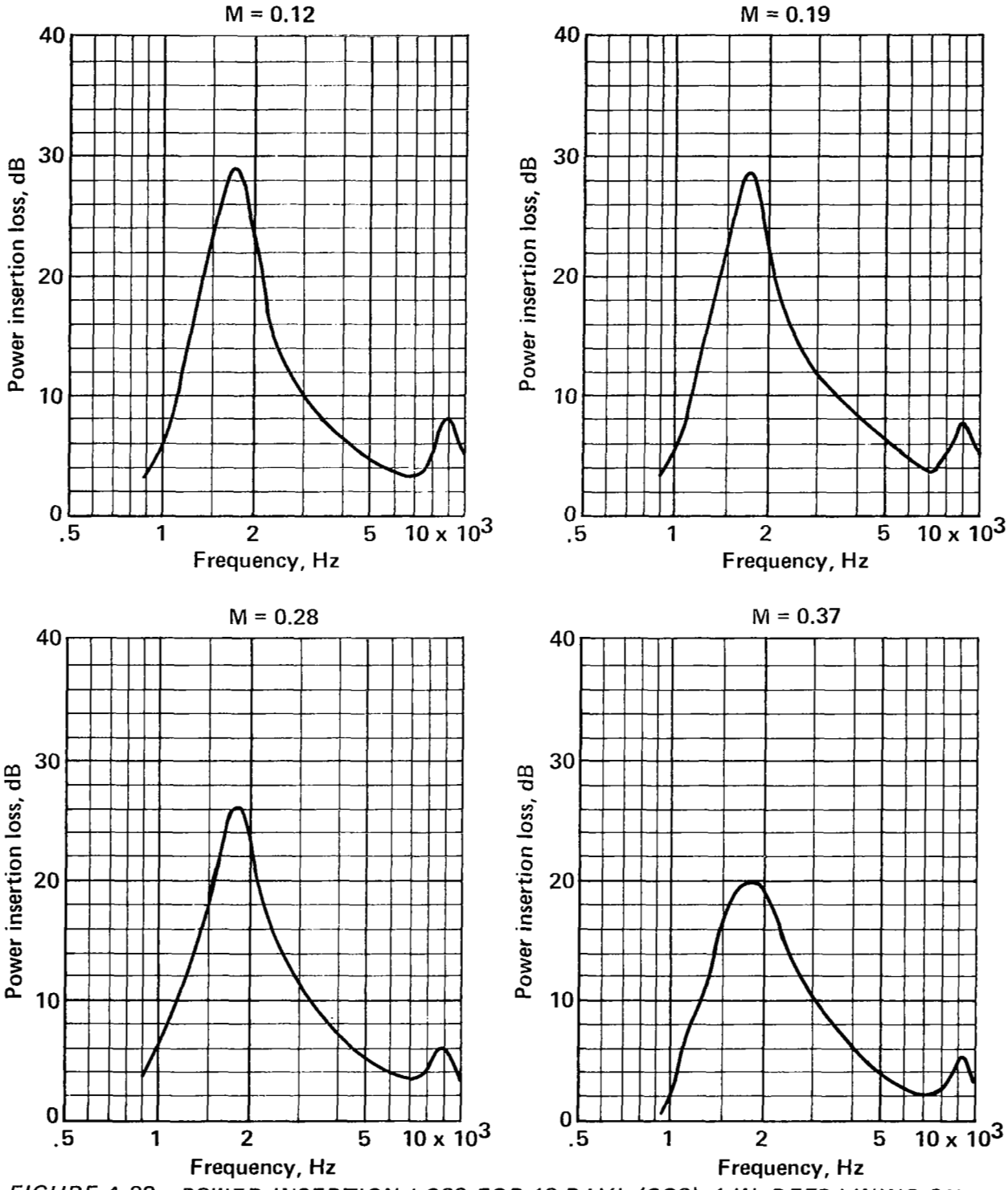

FIGURE A-32.—POWER INSERTION LOSS FOR 18-RAYL (CGS), 1-IN.-DEEP LINING ON TWO WALLS OF 6-IN. DUCT

Duct size	6 x 10 in.
Walls lined	Two/10 in.
Lining length	22 in.
Lining material	Polyimide

Flow resistance	30 rayls (cgs)
Core depth	1.0 in.
Core type	3/8-in. Hexcel

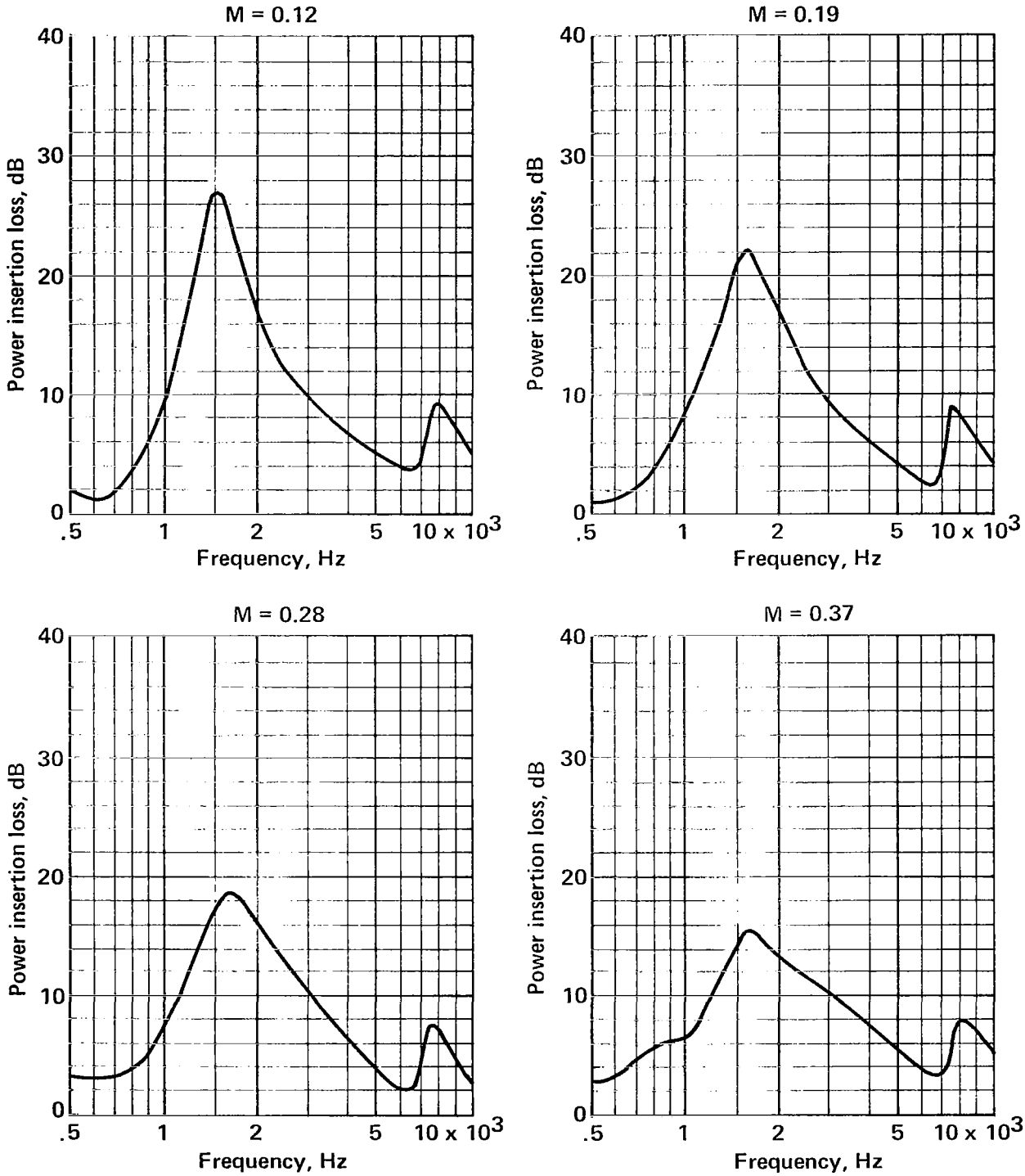

FIGURE A-33.—POWER INSERTION LOSS FOR 30-RAYL (CGS), 1-IN.-DEEP LINING ON TWO WALLS OF 6-IN. DUCT

Duct size	6 x 10 in.
Walls lined	Two/10 in.
Lining length	22 in.
Lining material	Polyimide

Flow resistance	50 rayls (cgs)
Core depth	1.0 in.
Core type	3/8-in. Hexcel

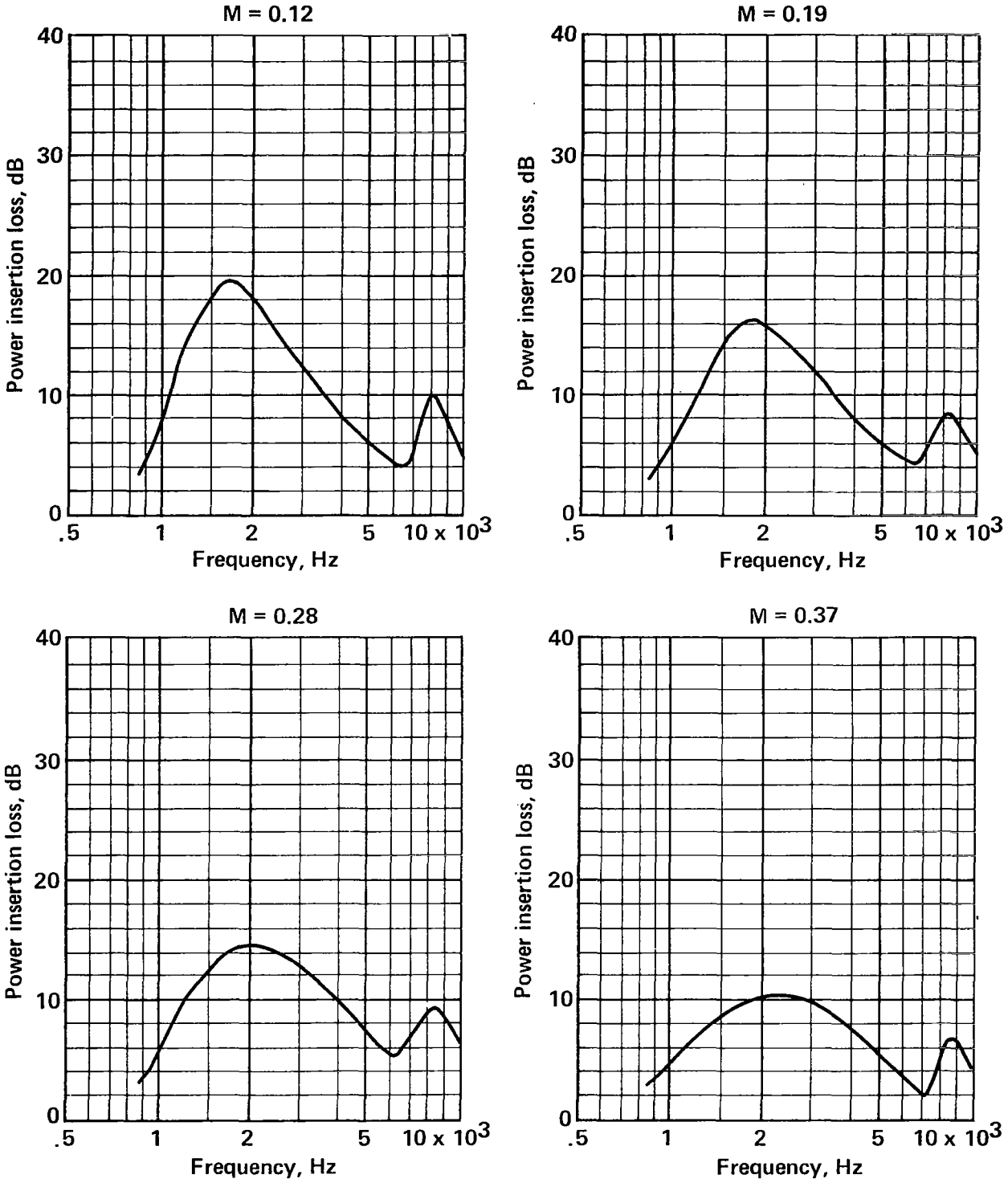

FIGURE A-34.—POWER INSERTION LOSS FOR 50-RAYL (CGS), 1-IN.-DEEP LINING ON TWO WALLS OF 6-IN. DUCT

Duct size	6 x 10 in.
Walls lined	Two/10 in.
Lining length	22 in.
Lining material	Polyimide

Flow resistance	70 rayls (cgs)
Core depth	1.0 in.
Core type	3/8-in. Hexcel

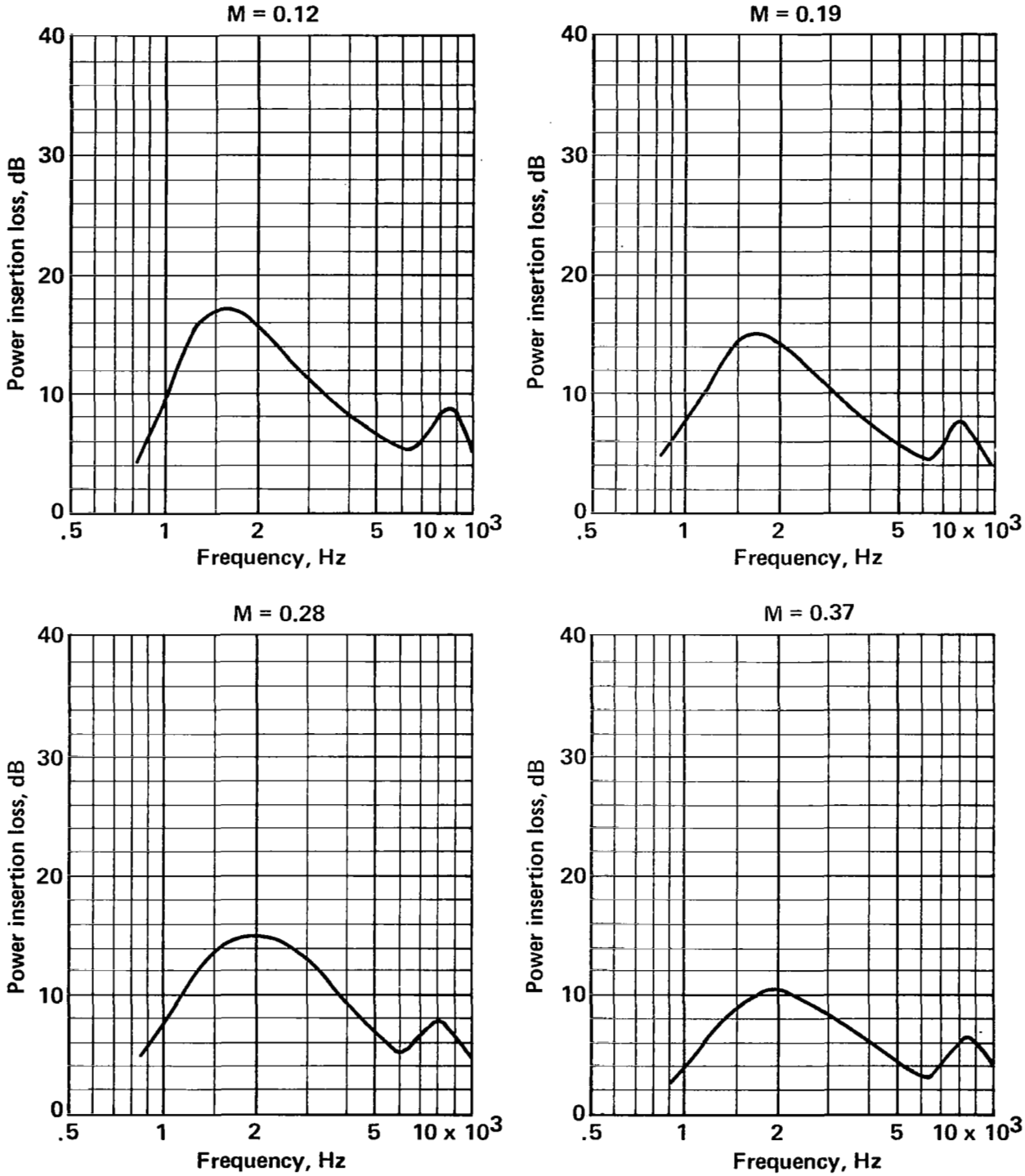

FIGURE A-35.—POWER INSERTION LOSS FOR 70-RAYL (CGS), 1-IN.-DEEP LINING ON TWO WALLS OF 6-IN. DUCT

Duct size	6 x 10 in.
Walls lined	Two/10 in.
Lining length	22 in.
Lining material	Woven metallic

Flow resistance	6 rayls (cgs)
Core depth	0.5 in.
Core type	3/8-in. Hexcel

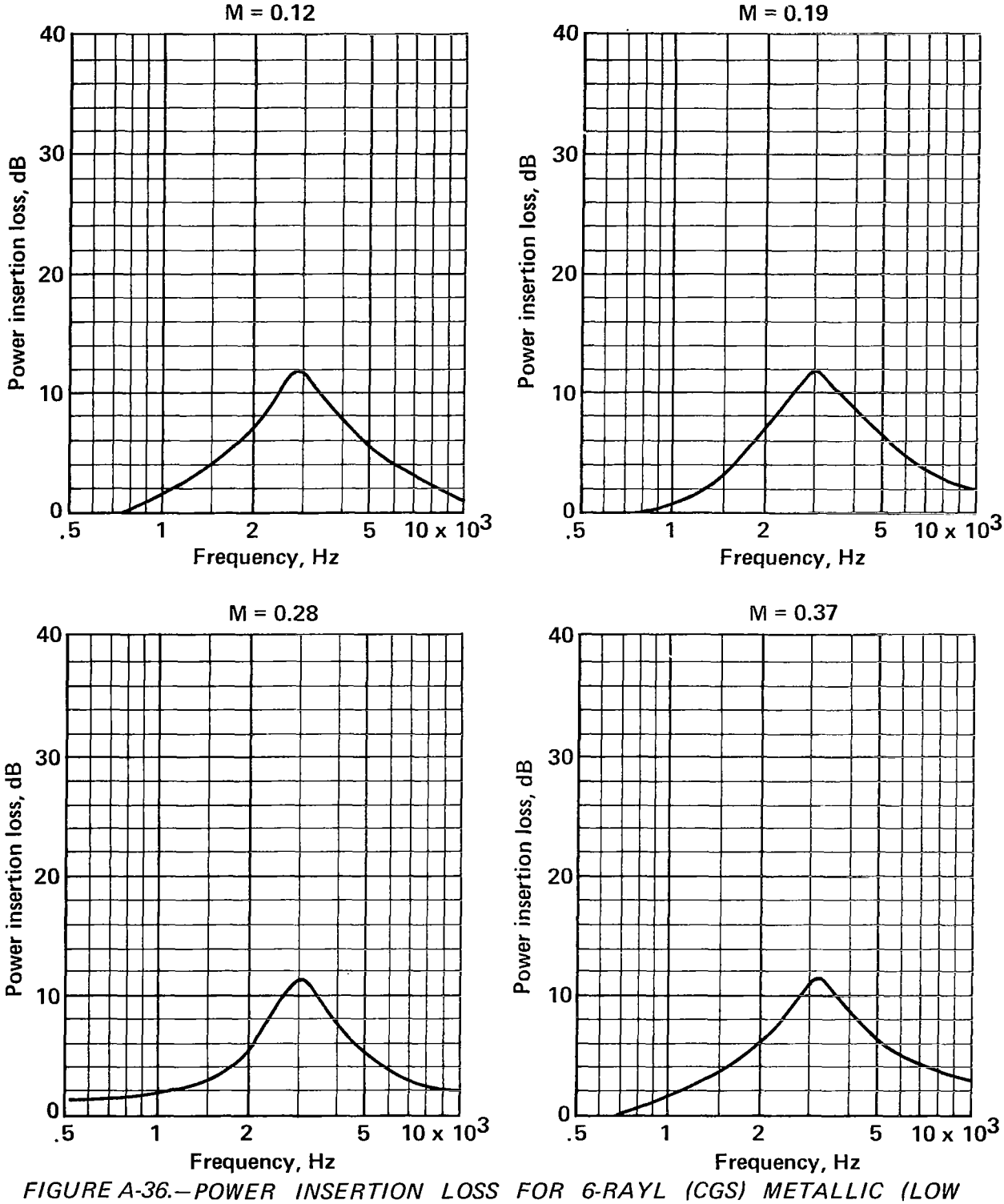

FIGURE A-36.—POWER INSERTION LOSS FOR 6-RAYL (CGS) METALLIC (LOW REACTANCE) LINING IN 6-IN. DUCT

Duct size	6 x 10 in.
Walls lined	Two/10 in.
Lining length	22 in.
Lining material	Woven metallic

Flow resistance	12 rayls (cgs)
Core depth	0.5 in.
Core type	3/8-in. Hexcel

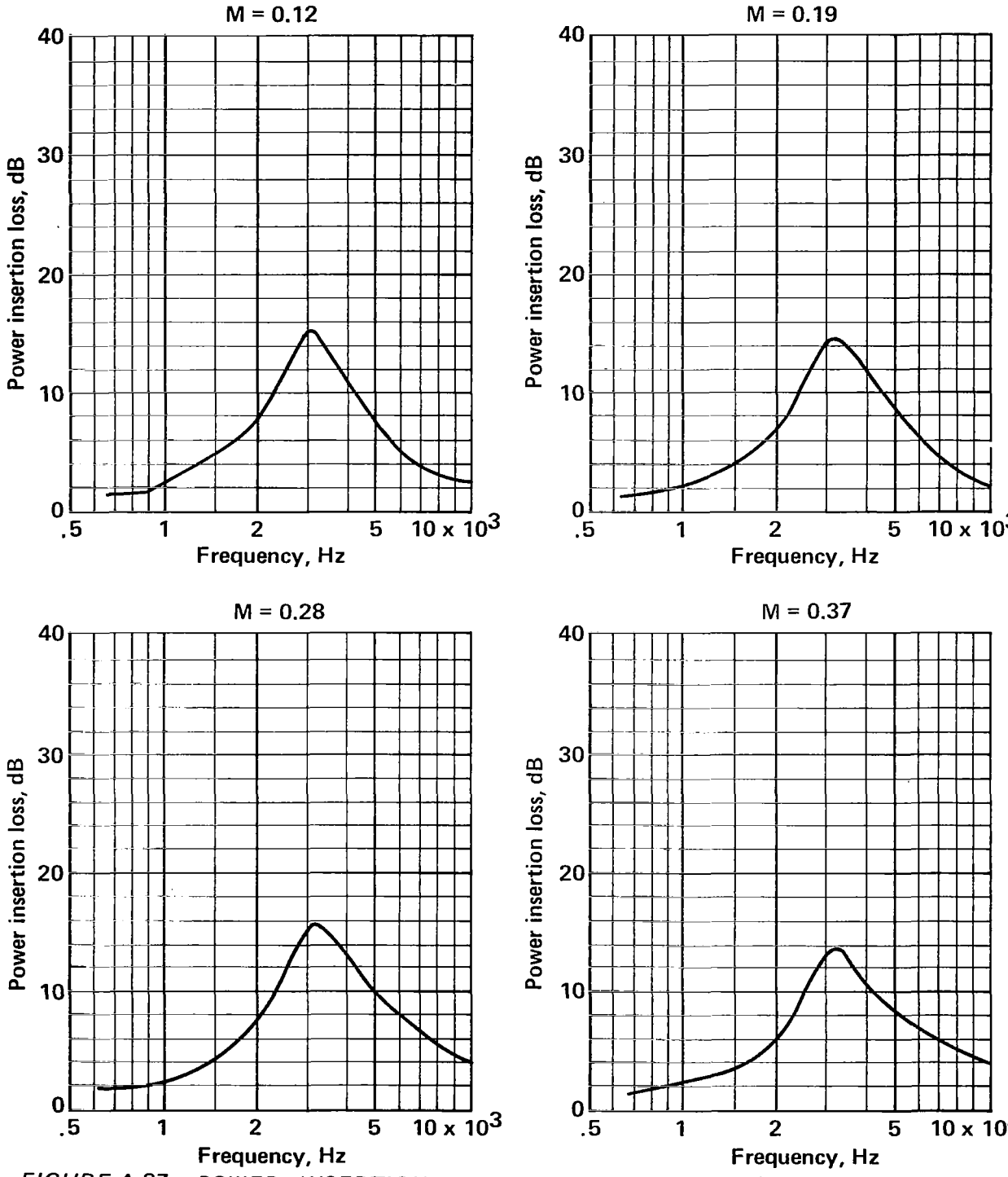

FIGURE A-37.— POWER INSERTION LOSS FOR 12-RAYL (CGS) METALLIC (LOW REACTANCE) LINING IN 6-IN. DUCT

Duct size	6 x 10 in.
Walls lined	Two/10 in.
Lining length	22 in.
Lining material	Woven metallic

Flow resistance	22 rayls (cgs)
Core depth	0.5 in.
Core type	3/8-in. Hexcel

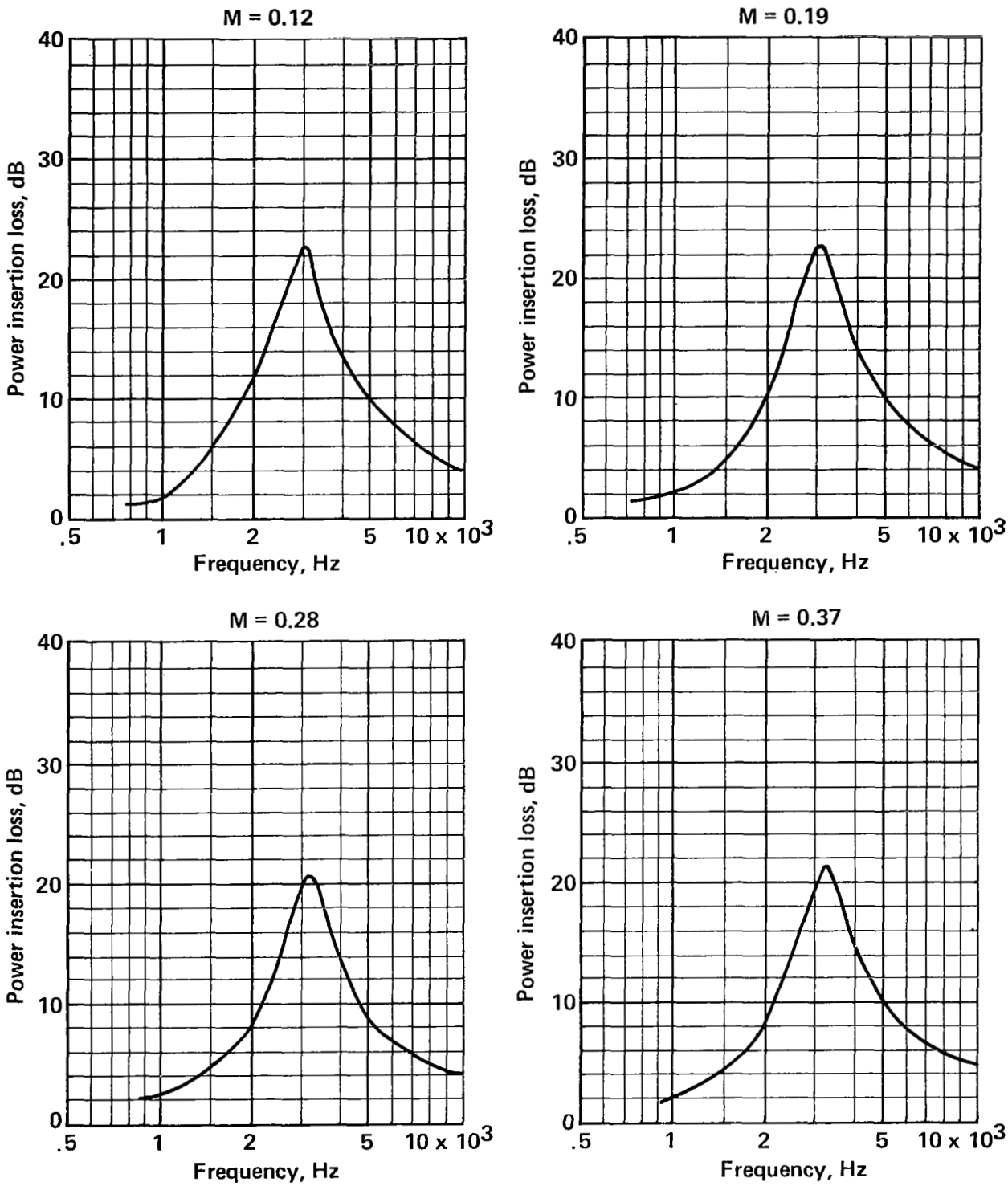

FIGURE A-38.—POWER INSERTION LOSS FOR 22-RAYL (CGS) METALLIC (LOW REACTANCE) LINING IN 6-IN. DUCT

Duct size	6 x 10 in.
Walls lined	Two/10 in.
Lining length	22 in.
Lining material	Woven metallic

Flow resistance	30 rayls (cgs)
Core depth	0.5 in.
Core type	3/8-in. Hexcel

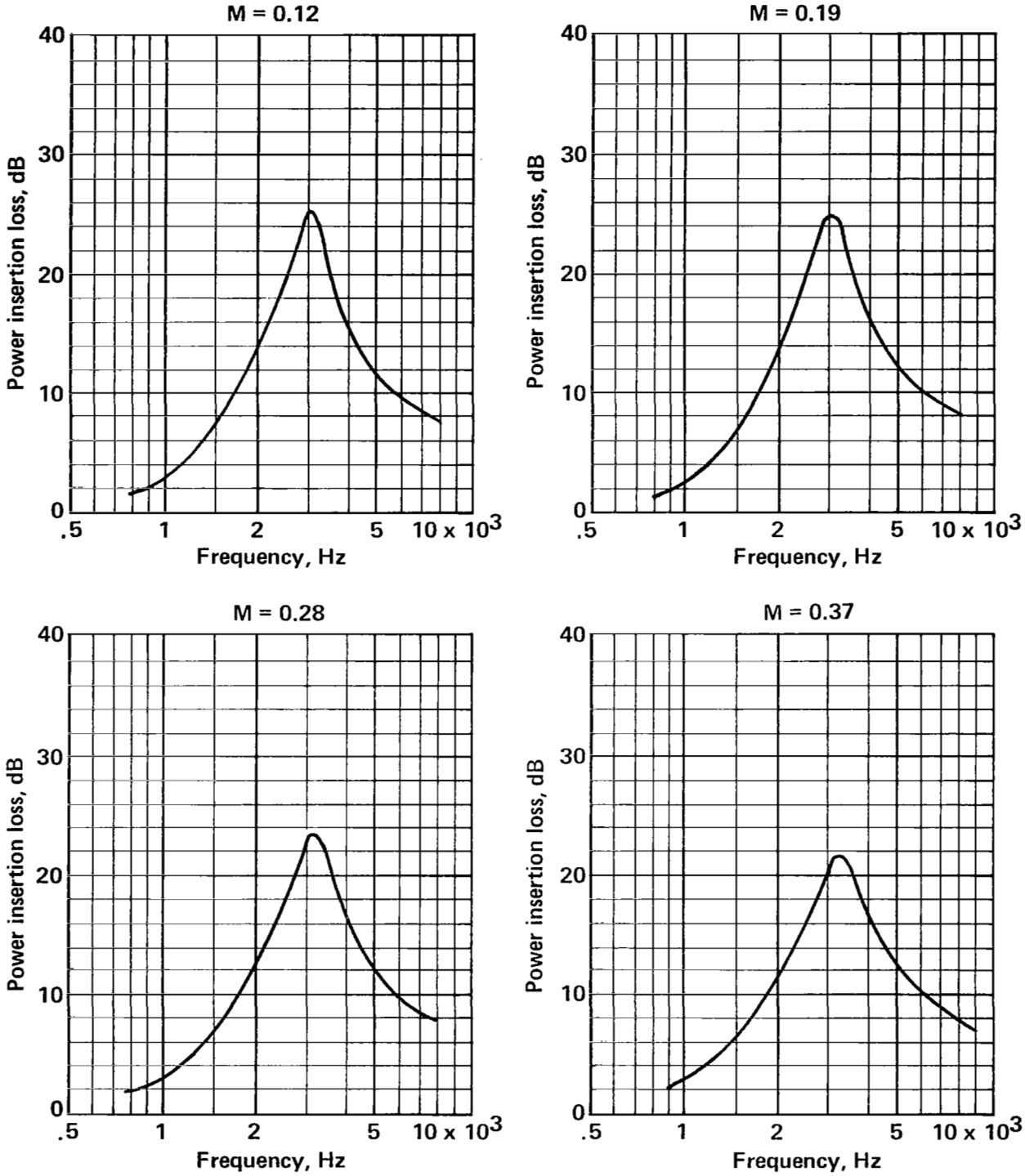

FIGURE A-39.—POWER INSERTION LOSS FOR 30-RAYL (CGS) METALLIC (LOW REACTANCE) LINING IN 6-IN. DUCT

Duct size	6 x 10 in.
Walls lined	Two/10 in.
Lining length	22 in.
Lining material	Woven metallic

Flow resistance	44 rayls (cgs)
Core depth	0.5 in.
Core type	3/8-in. Hexcel

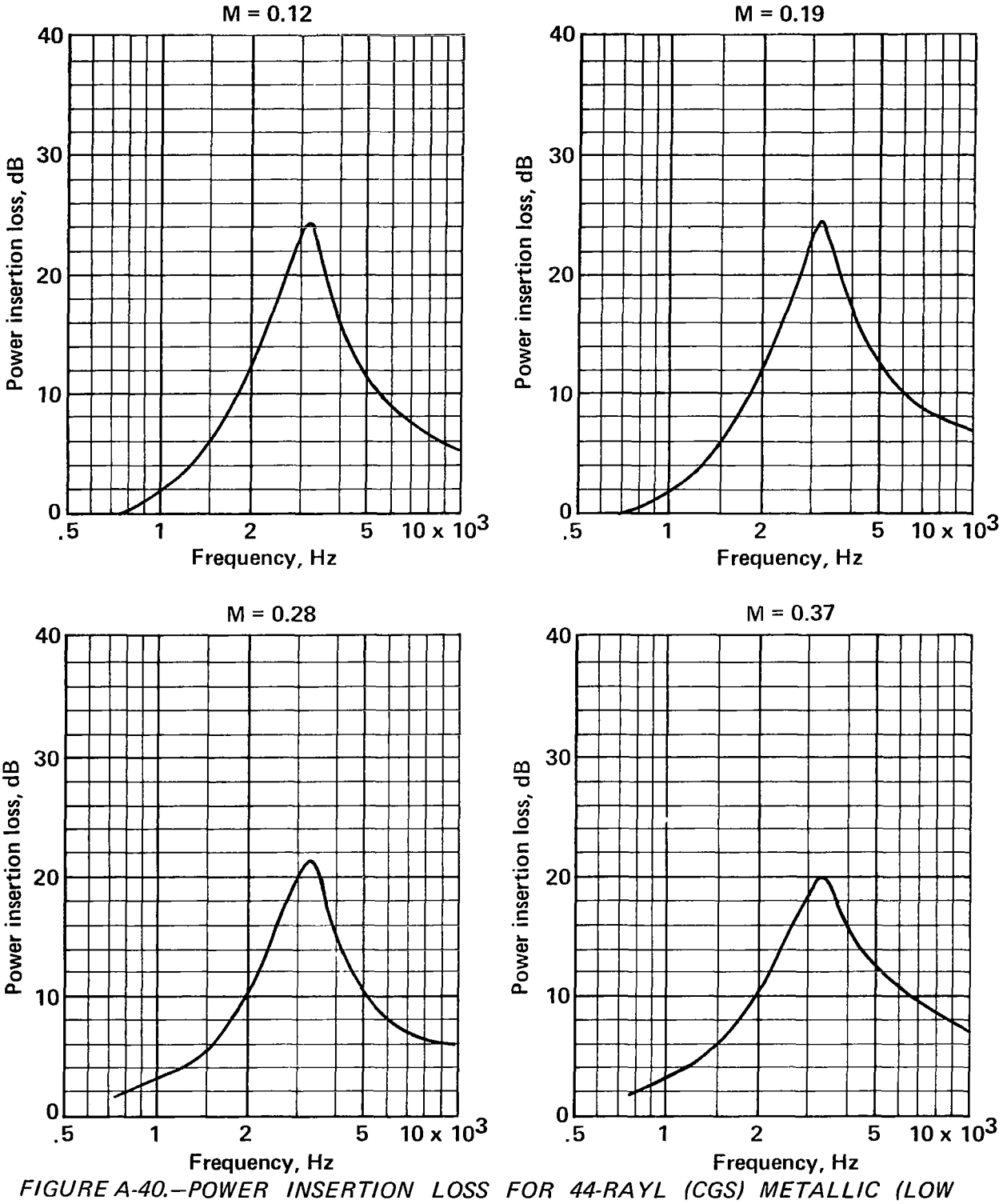

FIGURE A-40.—POWER INSERTION LOSS FOR 44-RAYL (CGS) METALLIC (LOW REACTANCE) LINING IN 6-IN. DUCT

Duct size	6 x 10 in.
Walls lined	Two/10 in.
Lining length	22 in.
Lining material	Woven metallic

Flow resistance	80 rayls (cgs)
Core depth	0.5 in.
Core type	3/8-in. Hexcel

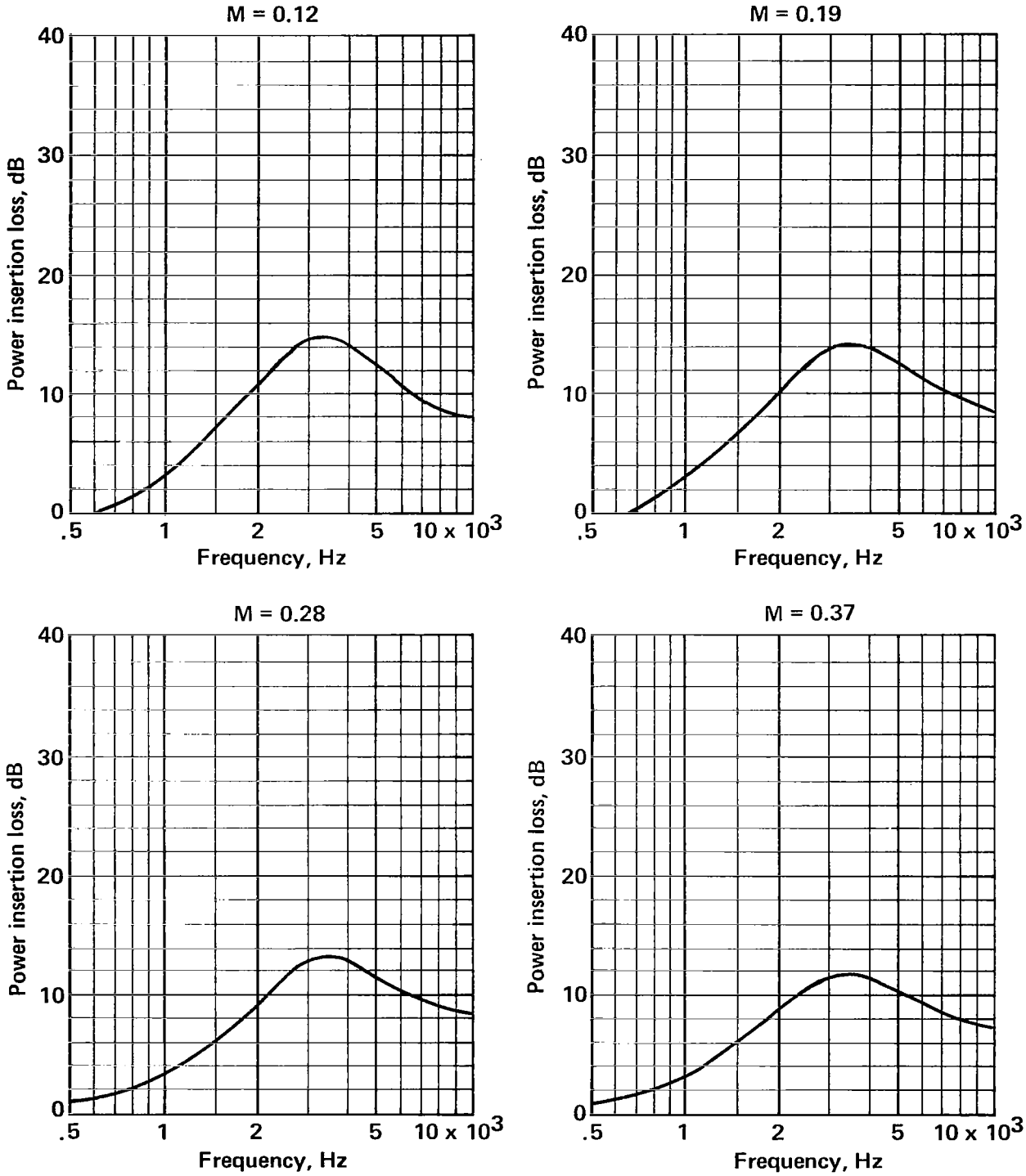

FIGURE A-41.— POWER INSERTION LOSS FOR 80-RAYL (CGS) METALLIC (LOW REACTANCE) LINING IN 6-IN. DUCT

Duct size	6 x 10 in.
Walls lined	Two/10 in.
Lining length	22 in.
Lining material	Polyimide

Flow resistance	30 rayls (cgs)
Core depth	0.5 in.
Core type	1/8-in. Hexcel

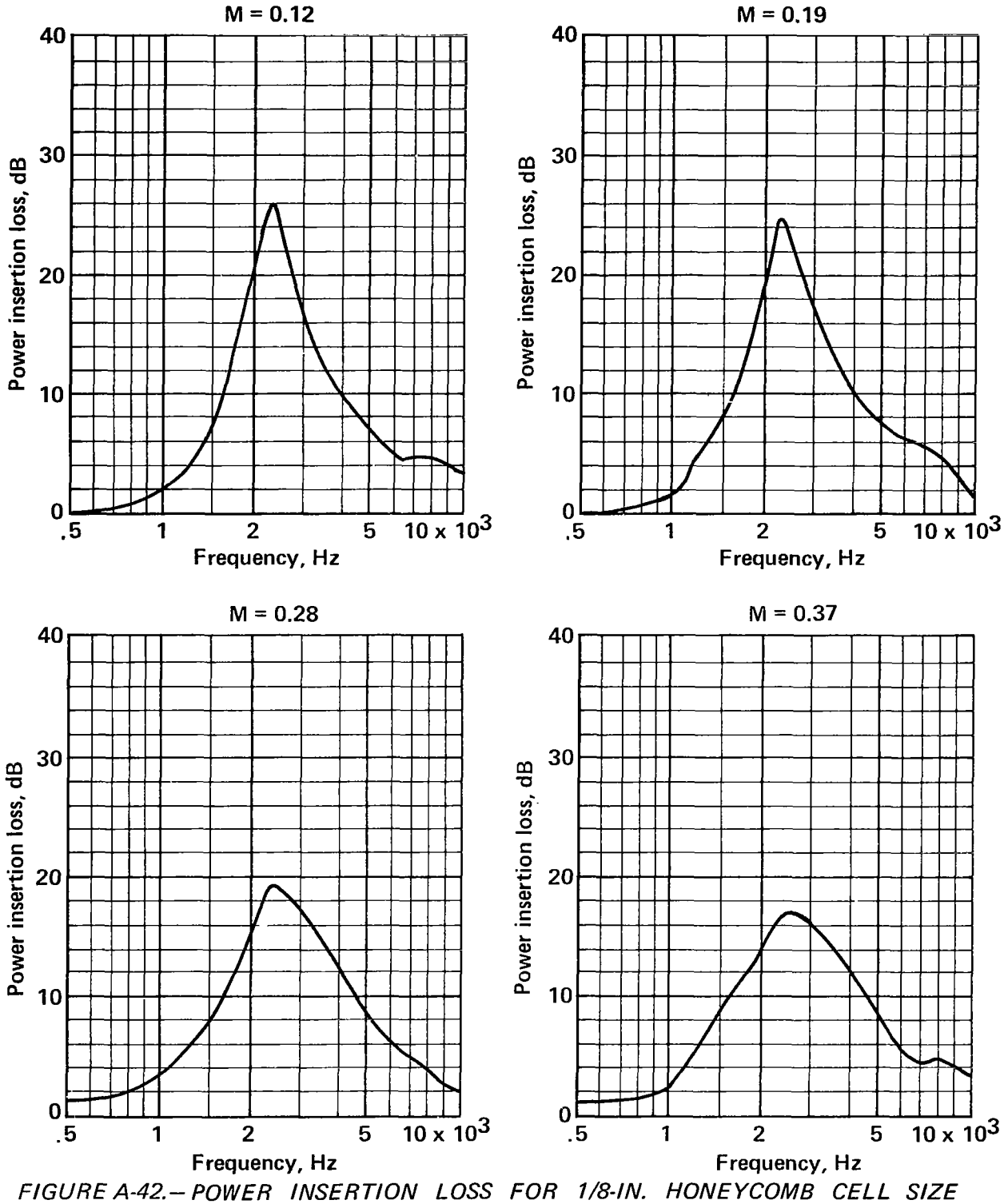

FIGURE A-42.— POWER INSERTION LOSS FOR 1/8-IN. HONEYCOMB CELL SIZE LINING IN 6-IN. DUCT

Duct size	6 x 10 in.
Walls lined	Two/10 in.
Lining length	22 in.
Lining material	Polyimide

Flow resistance	30 rayls (cgs)
Core depth	0.5 in.
Core type	1/2-in. Hexcel

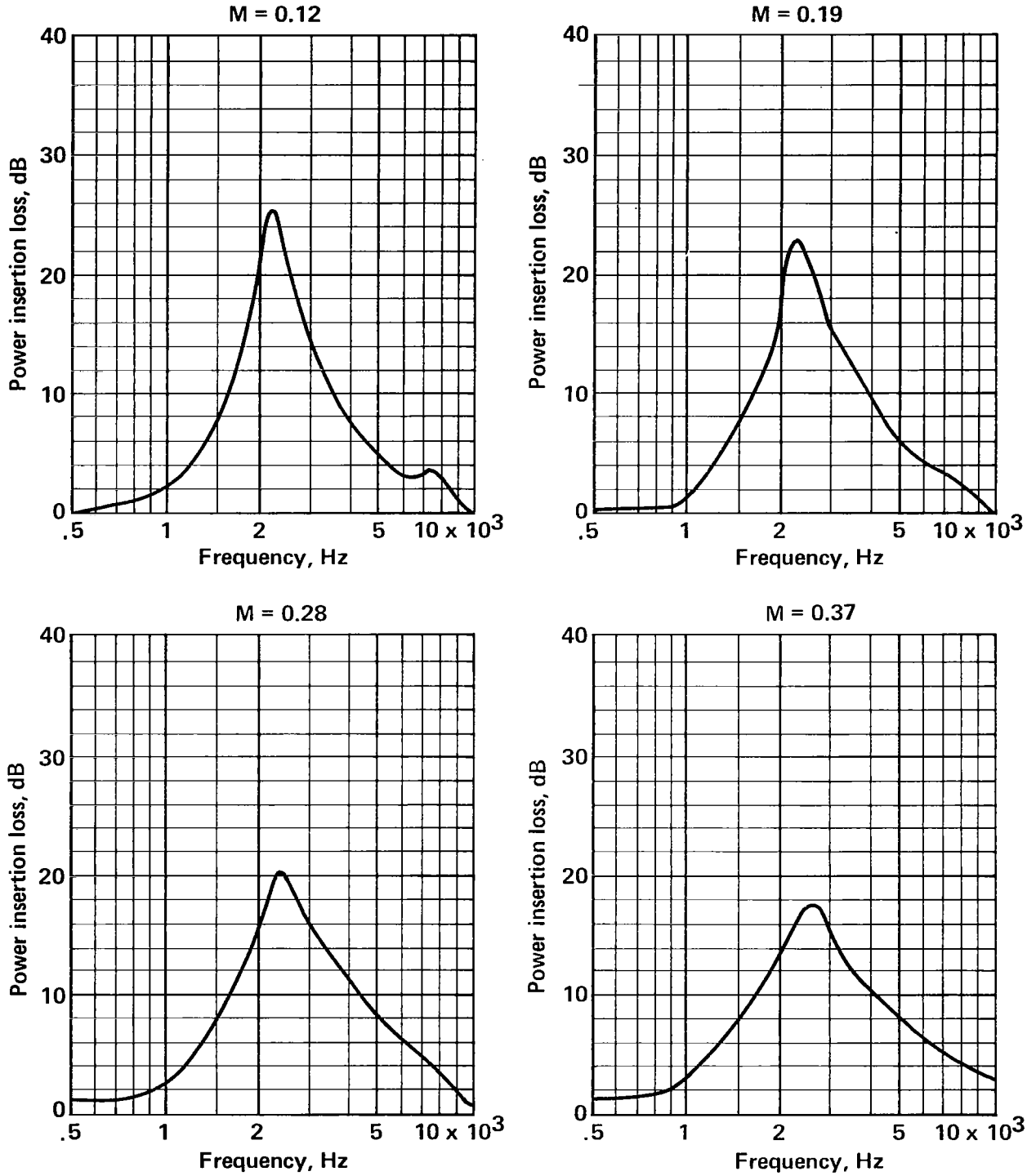

FIGURE A-43.— POWER INSERTION LOSS FOR 1/2-IN. HONEYCOMB CELL SIZE LINING IN 6-IN. DUCT

Duct size	6 x 10 in.
Walls lined	Two/10 in.
Lining length	22 in.
Lining material	Polyimide

Flow resistance	30 rayls (cgs)
Core depth	0.5 in.
Core type	1 x 1 in.

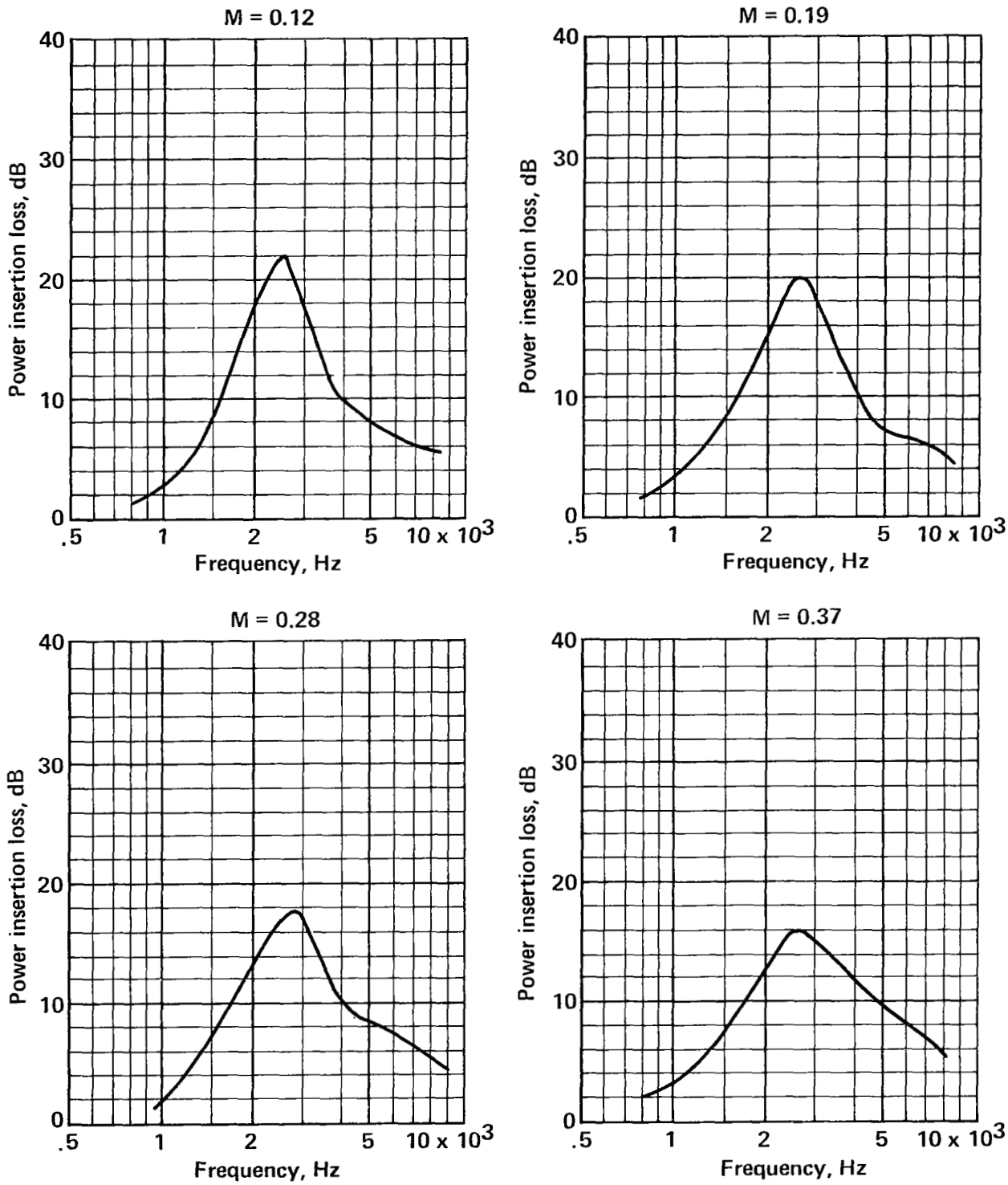

FIGURE A-44.– POWER INSERTION LOSS FOR 1-IN. EGGCRATE CELL SIZE LINING IN 6-IN. DUCT

Duct size	6 x 10 in.
Walls lined	Two/10 in.
Lining length	22 in.
Lining material	Polyimide

Flow resistance	10 + 40 rayls (cgs)
Core depth	0.25 + 0.25 in.
Core type	3/8-in. Hexcel

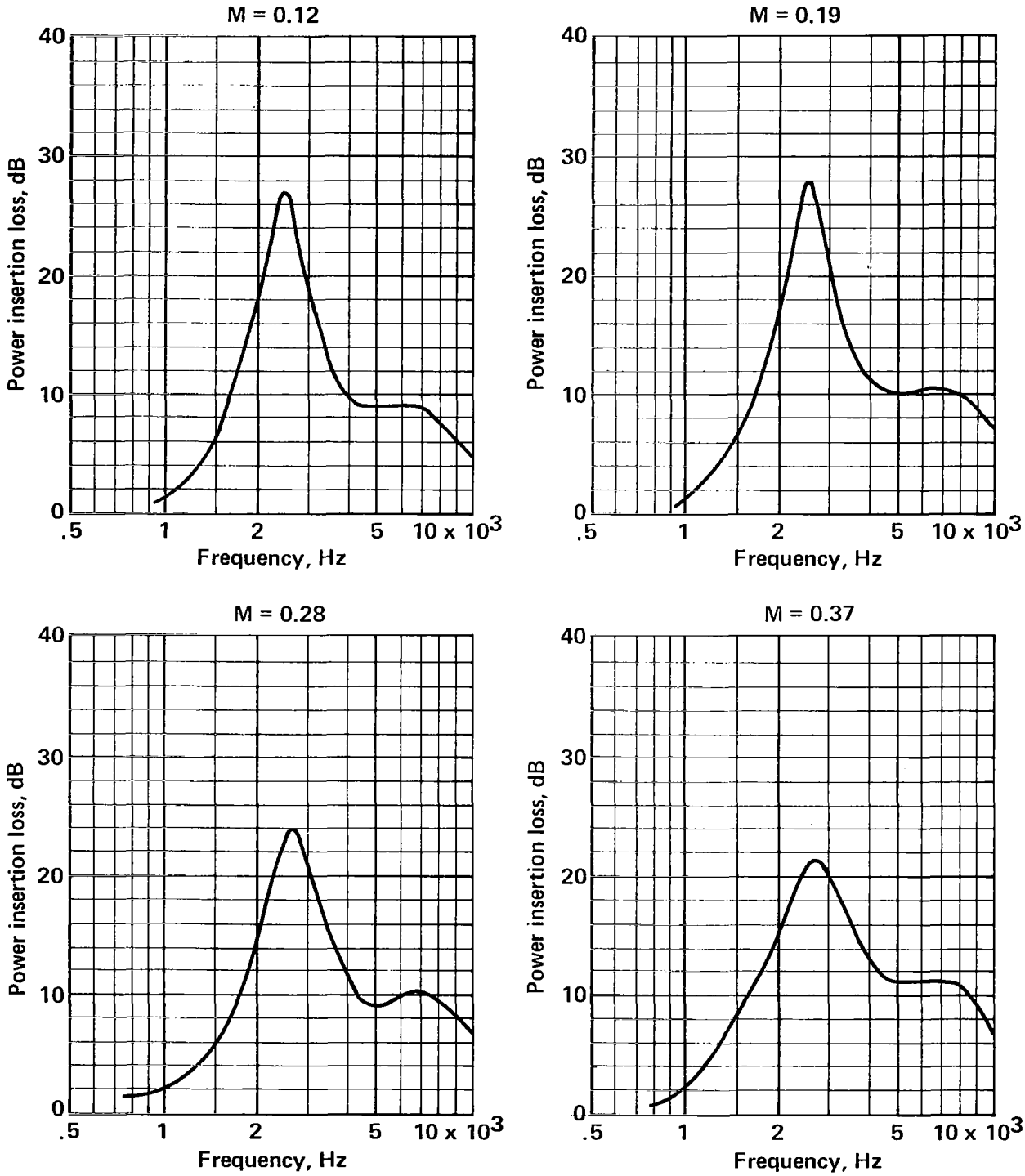

FIGURE A-45.– POWER INSERTION LOSS FOR (1/4 + 1/4)-IN.-DEEP DOUBLE-LAYER LINING IN 6-IN. DUCT

Duct size	6 x 10 in.
Walls lined	Two/10 in.
Lining length	22 in.
Lining material	Polyimide

Flow resistance	10 + 40 rayls (cgs)
Core depth	3/8 + 3/8 in.
Core type	3/8-in. Hexcel

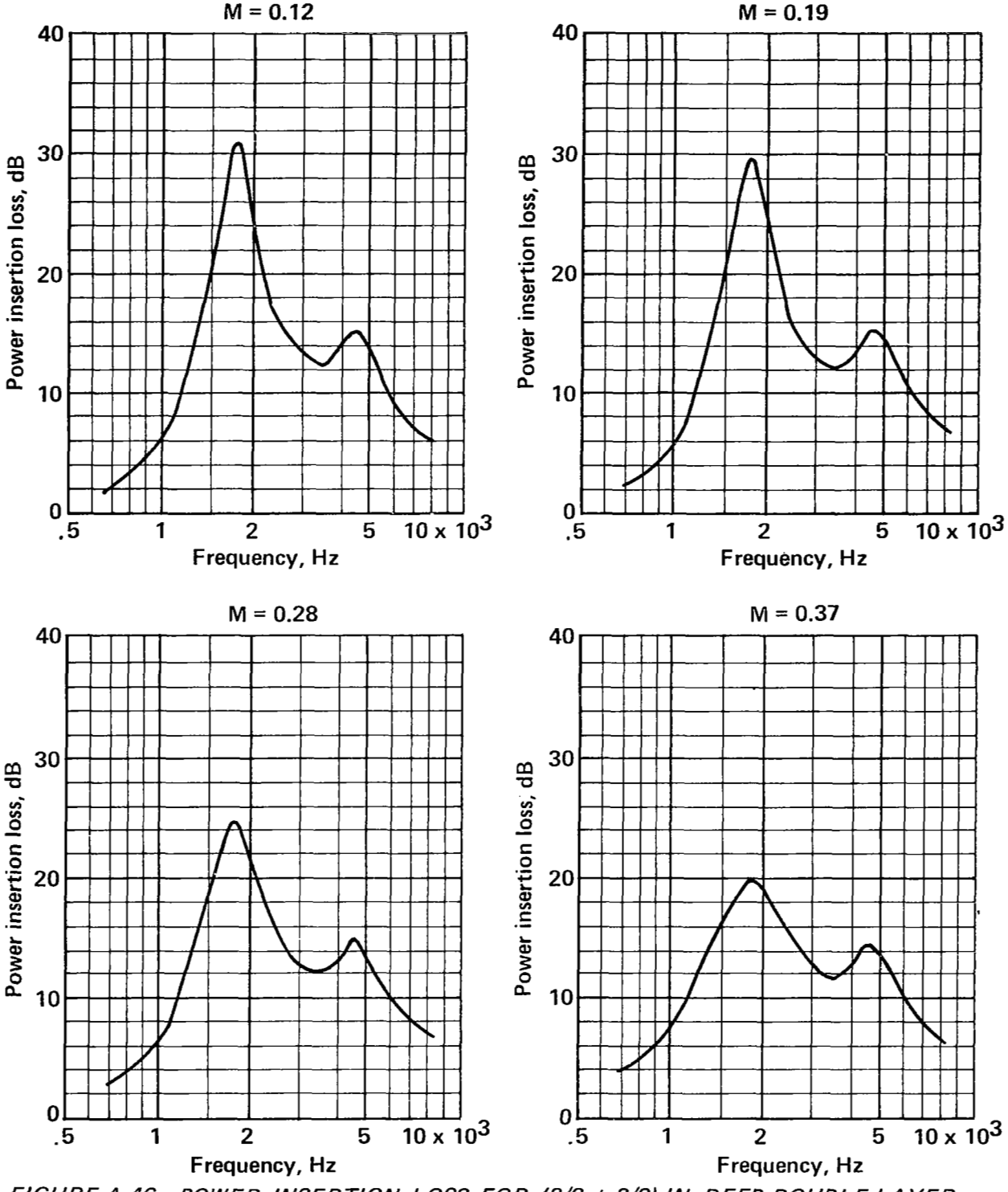

FIGURE A-46.—POWER INSERTION LOSS FOR (3/8 + 3/8)-IN.-DEEP DOUBLE-LAYER LINING IN 6-IN. DUCT

Duct size	6 x 10 in.
Walls lined	Two/10 in.
Lining length	22 in.
Lining material	Polyimide

Flow resistance	10 + 40 rayls (cgs)
Core depth	0.5 + 0.5 in.
Core type	3/8-in. Hexcel

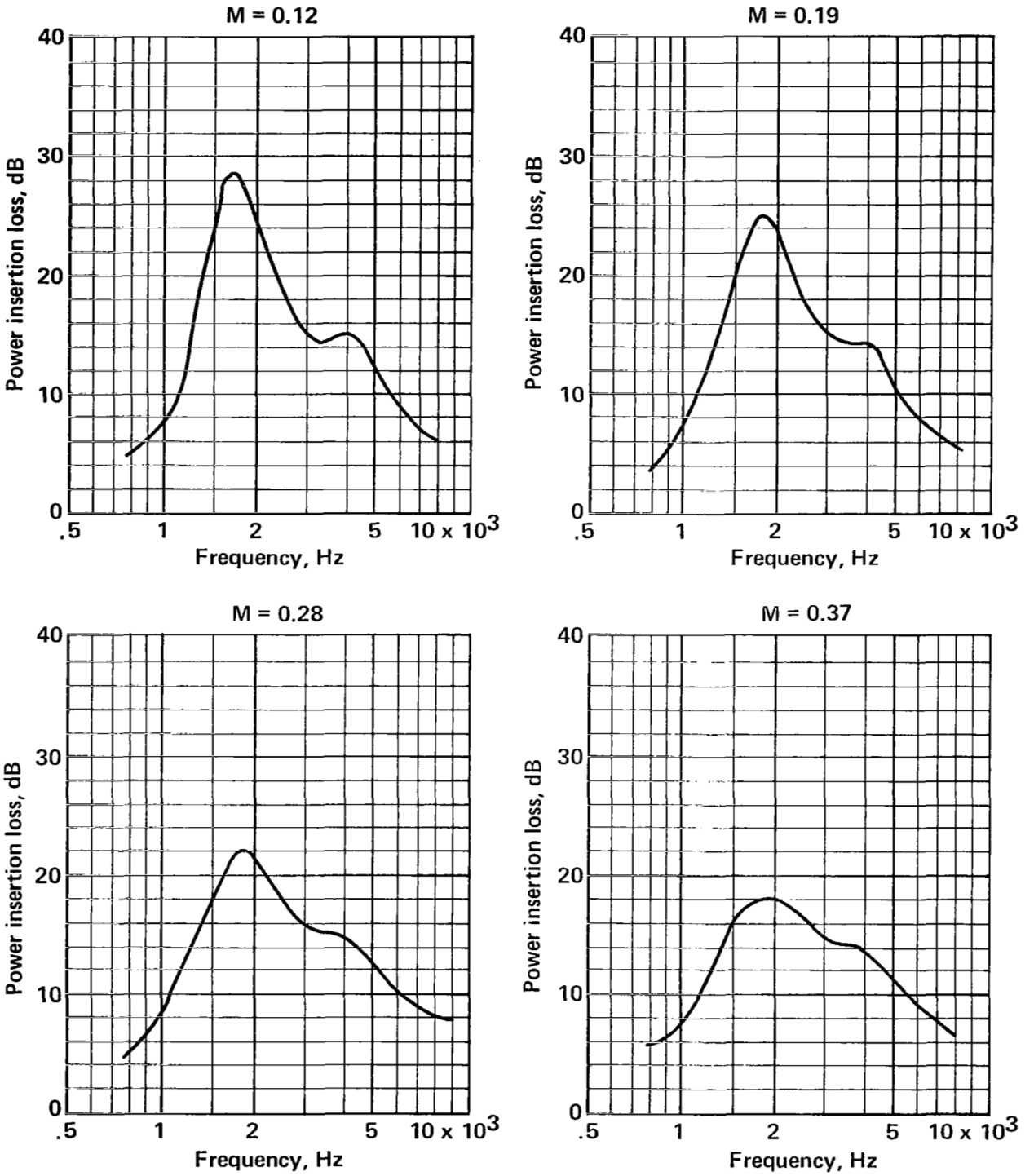

FIGURE A-47.—POWER INSERTION LOSS FOR (1/2 + 1/2)-IN.-DEEP DOUBLE-LAYER LINING IN 6-IN. DUCT

Duct size	6 x 10 in.
Walls lined	Two/10 in.
Lining length	22 in.
Lining material	Polyimide

Flow resistance	10 + 40 rayls (cgs)
Core depth	1.0 + 1.0 in.
Core type	3/8-in. Hexcel

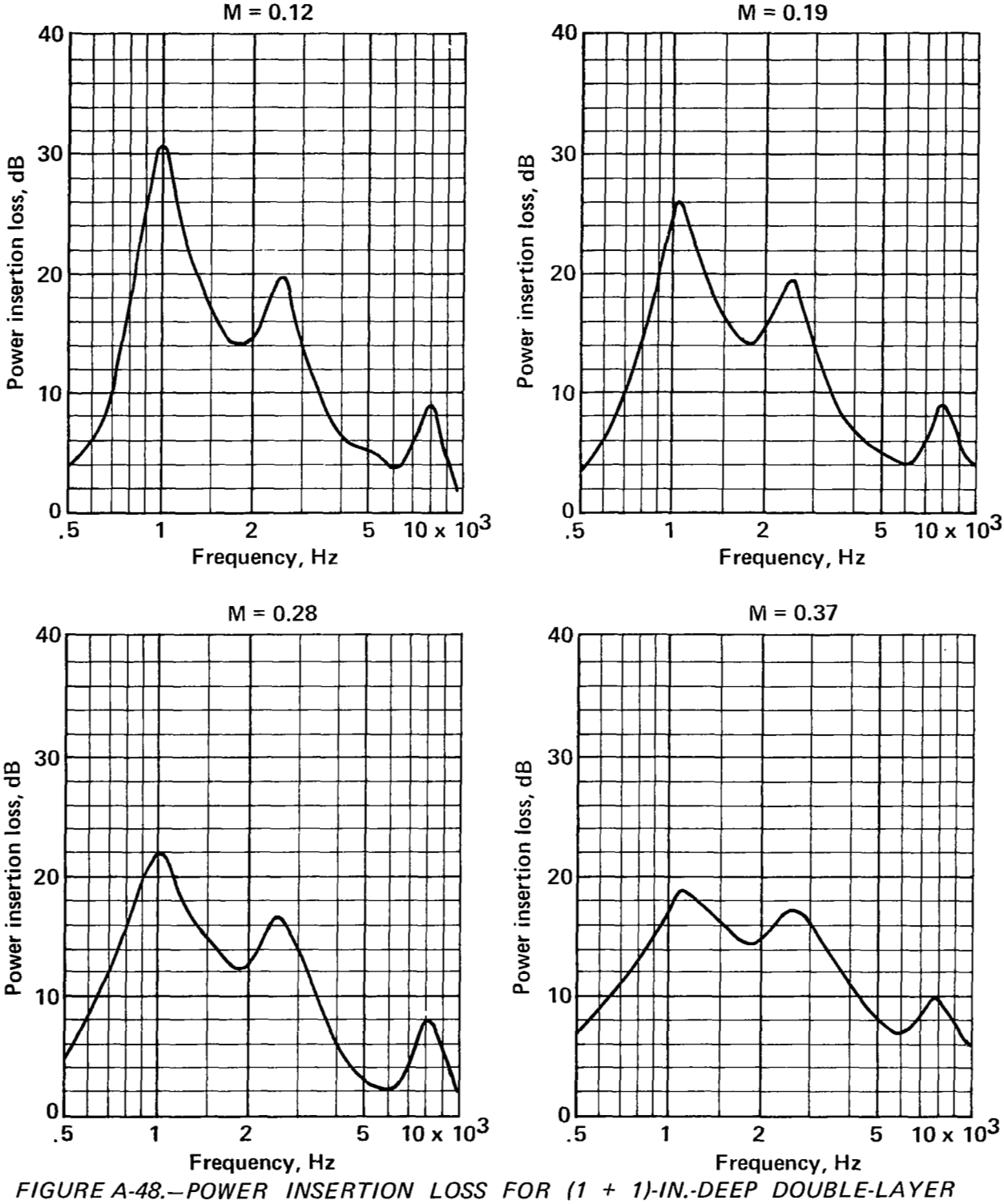

FIGURE A-48.—POWER INSERTION LOSS FOR (1 + 1)-IN.-DEEP DOUBLE-LAYER LINING IN 6-IN. DUCT

Duct size	4 x 10 in.
Walls lined	Two/10 in.
Lining length	22 in.
Lining material	Polyimide

Flow resistance	3 rayls (cgs)
Core depth	0.5 in.
Core type	3/8-in. Hexcel

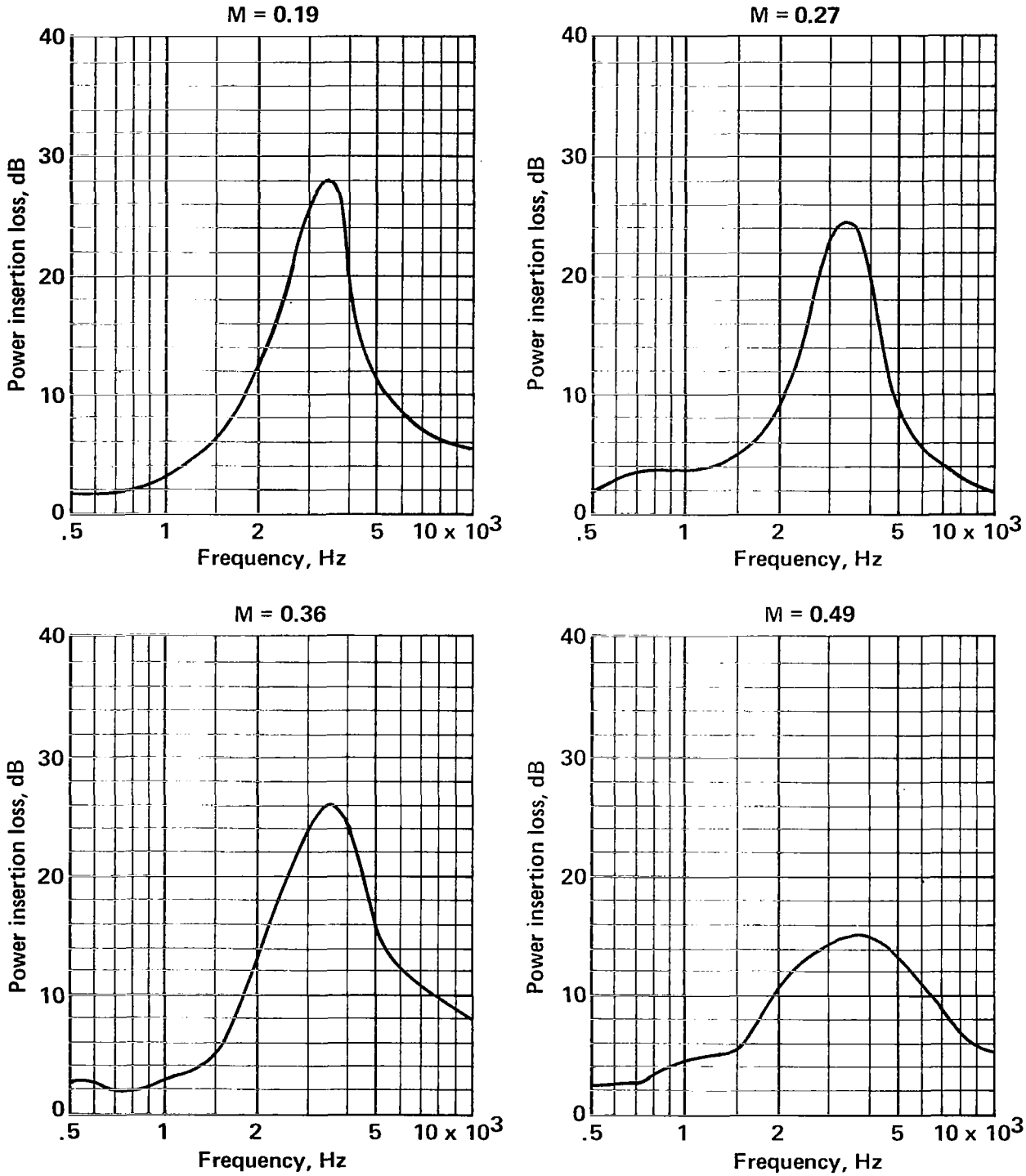

FIGURE A-49.— POWER INSERTION LOSS FOR 3-RAYL (CGS), 1/2-IN.-DEEP LINING ON TWO WALLS OF 4-IN. DUCT

Duct size	4 x 10 in.
Walls lined	Two/10 in.
Lining length	22 in.
Lining material	Polyimide

Flow resistance	9 rayls (cgs)
Core depth	0.5 in.
Core type	3/8-in. Hexcel

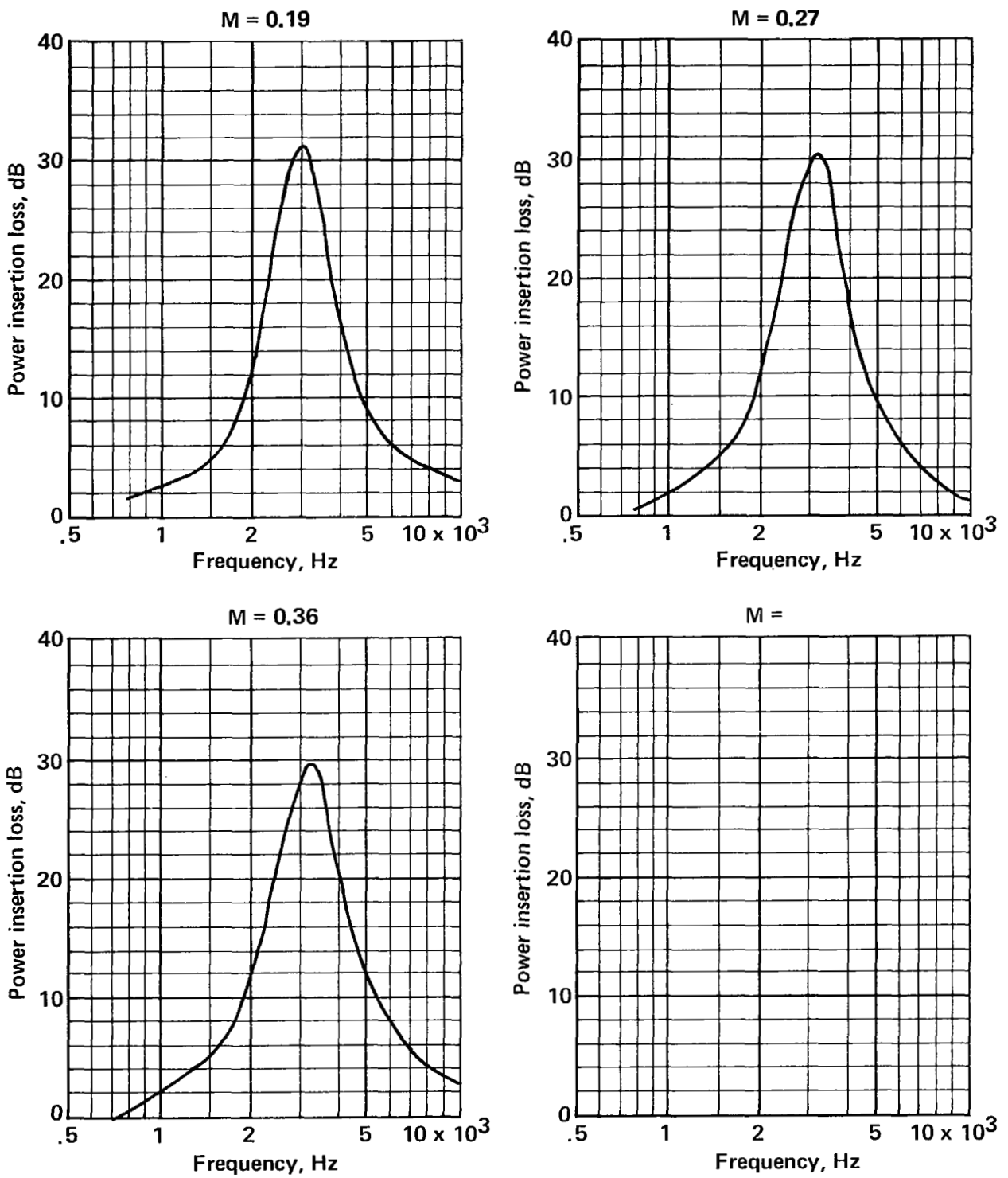

FIGURE A-50.—POWER INSERTION LOSS FOR 9-RAYL (CGS), 1/2-IN.-DEEP LINING ON TWO WALLS OF 4-IN. DUCT

Duct size	4 x 10 in.
Walls lined	Two/10 in.
Lining length	22 in.
Lining material	Polyimide

Flow resistance	18 rayls (cgs)
Core depth	0.5 in.
Core type	3/8-in. Hexcel

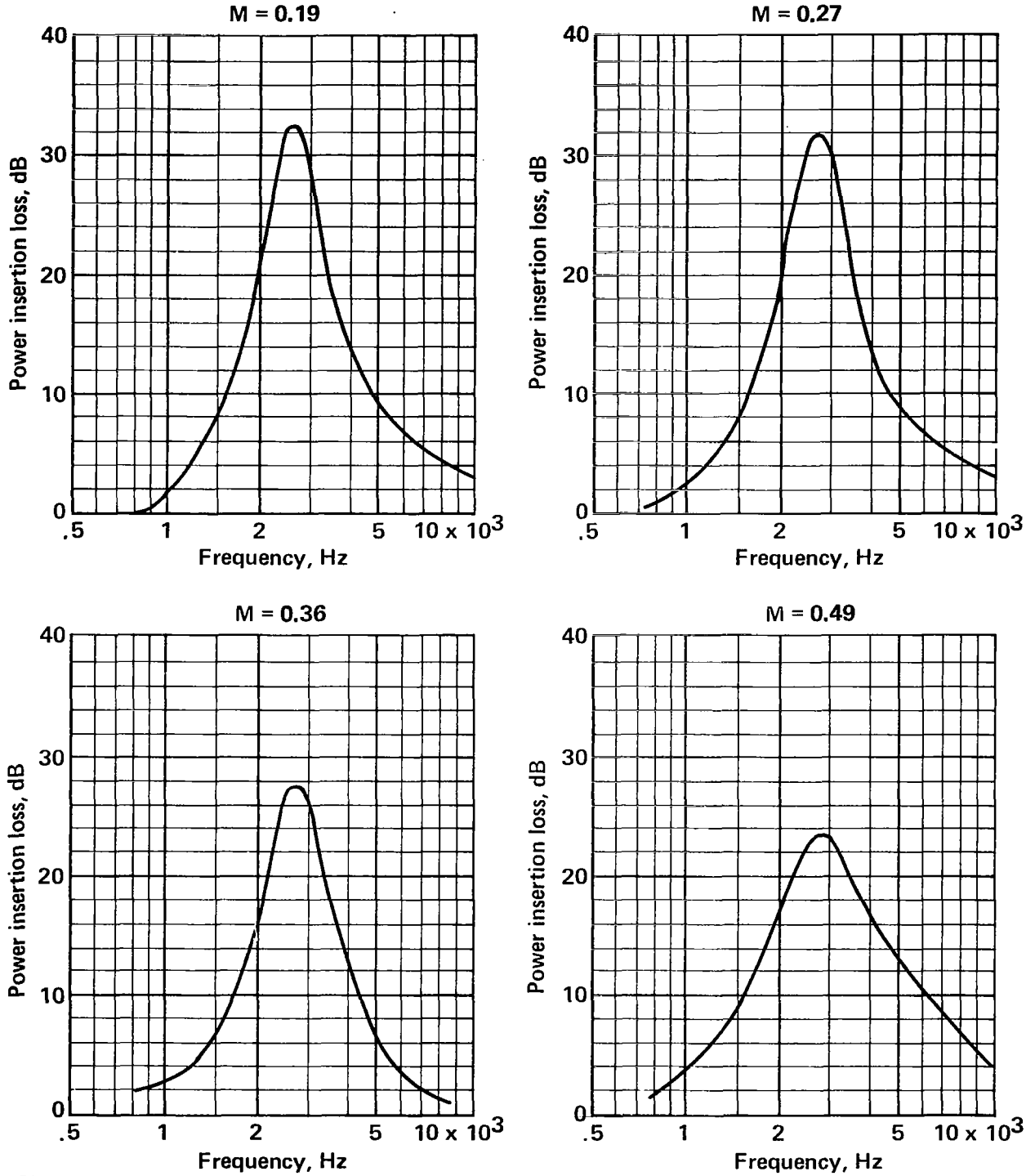

FIGURE A-51.—POWER INSERTION LOSS FOR 18-RAYL (CGS), 1/2-IN.-DEEP LINING ON TWO WALLS OF 4-IN. DUCT

Duct size	4 x 10 in.
Walls lined	Two/10 in.
Lining length	22 in.
Lining material	Polyimide

Flow resistance	30 rayls (cgs)
Core depth	0.5 in.
Core type	3/8-in. Hexcel

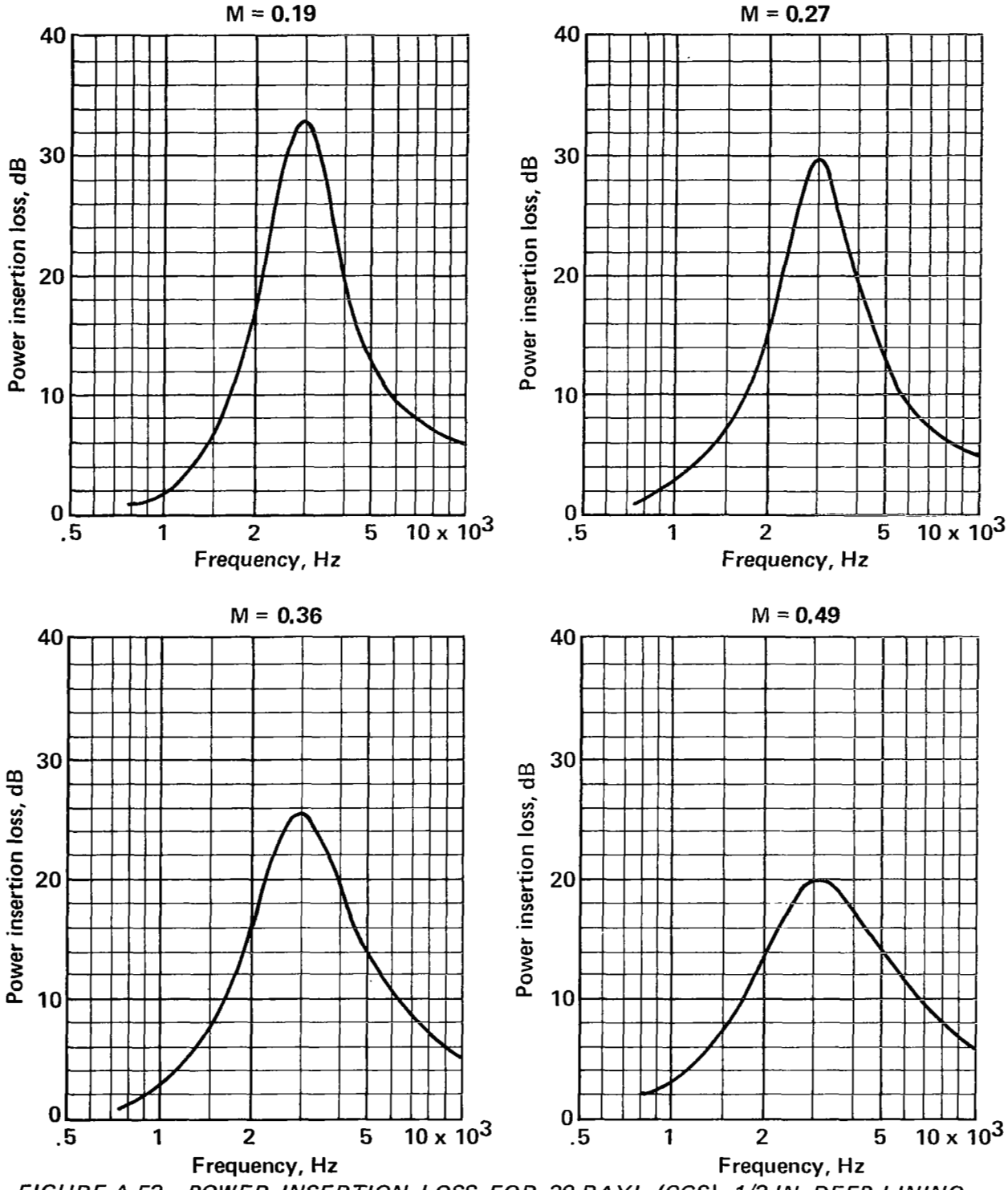

FIGURE A-52.—POWER INSERTION LOSS FOR 30-RAYL (CGS), 1/2-IN.-DEEP LINING ON TWO WALLS OF 4-IN. DUCT

Duct size	4 x 10 in.
Walls lined	Two/10 in.
Lining length	22 in.
Lining material	Polyimide

Flow resistance	50 rayls (cgs)
Core depth	0.5 in.
Core type	3/8-in. Hexcel

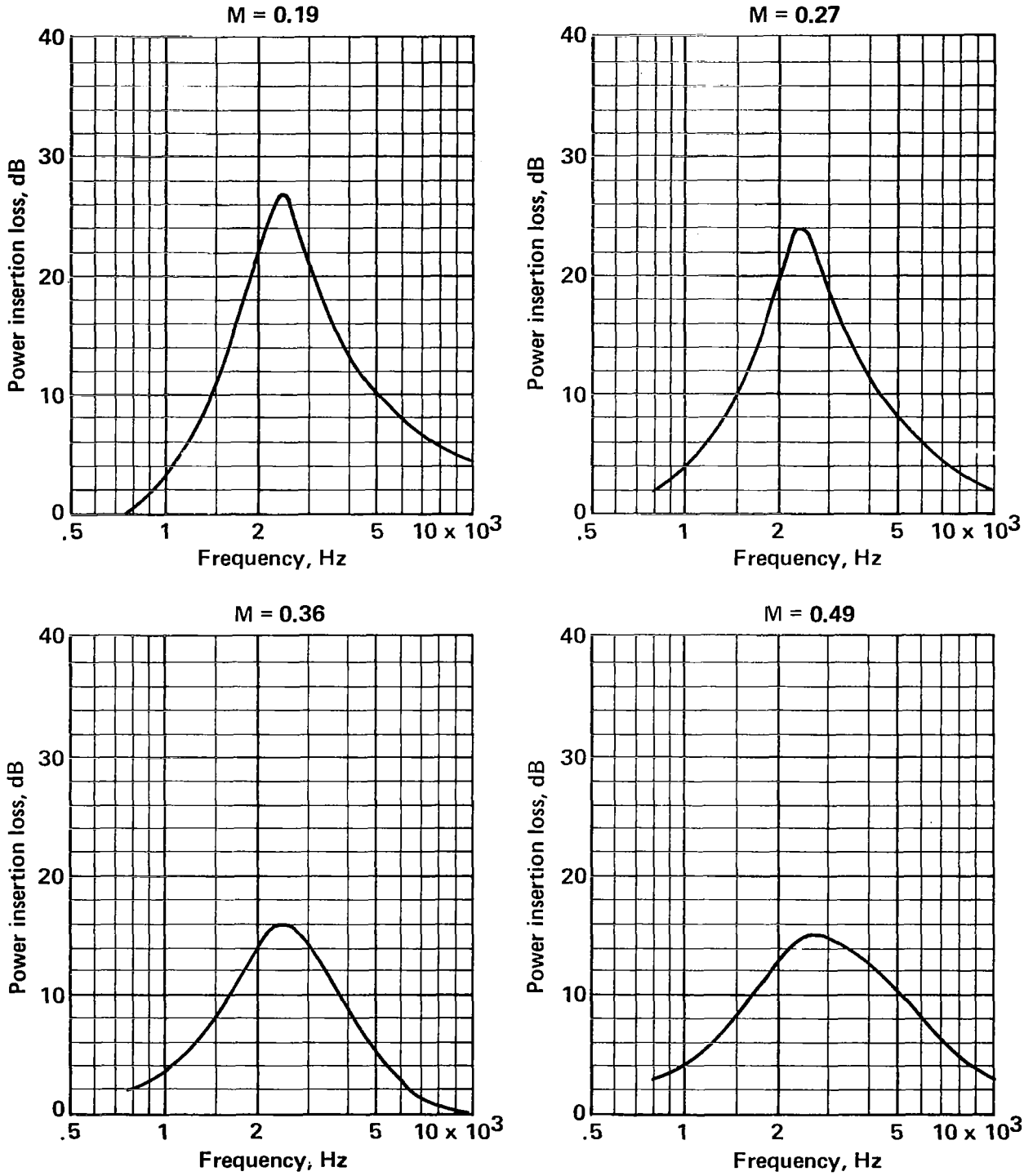

FIGURE A-53.—POWER INSERTION LOSS FOR 50-RAYL (CGS), 1/2-IN.-DEEP LINING ON TWO WALLS OF 4-IN. DUCT

Duct size	4 x 10 in.
Walls lined	Two/10 in.
Lining length	22 in.
Lining material	Polyimide

Flow resistance	70 rayls (cgs)
Core depth	0.5 in.
Core type	3/8-in. Hexcel

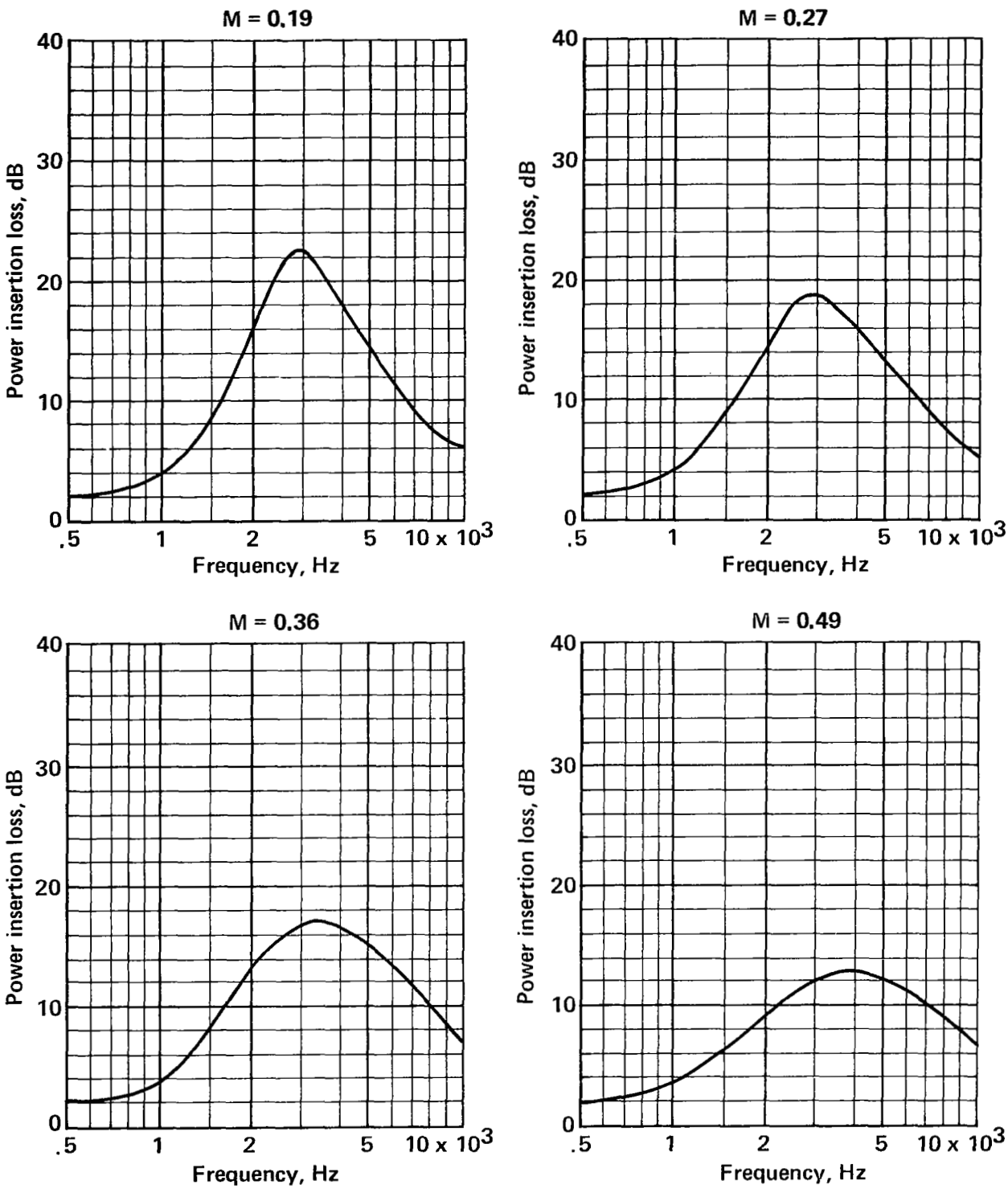

FIGURE A-54.—POWER INSERTION LOSS FOR 70-RAYL (CGS), 1/2-IN.-DEEP LINING ON TWO WALLS OF 4-IN. DUCT

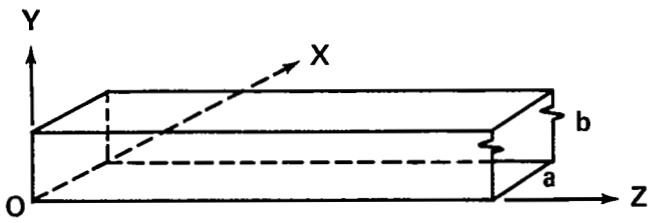

FIGURE B-1.—DUCT COORDINATE SYSTEM

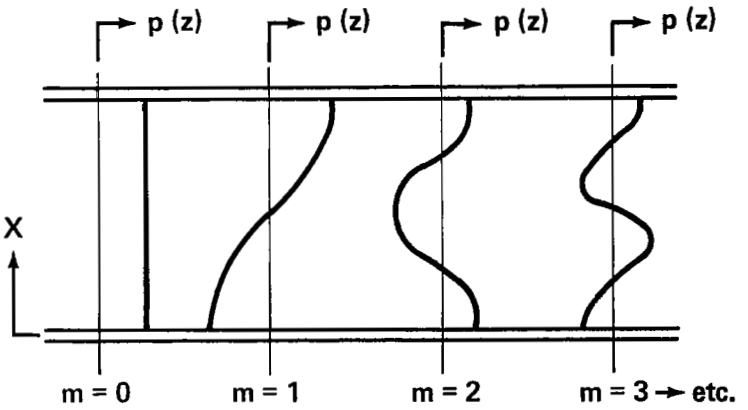

FIGURE B-2.—PROPAGATING MODES IN A DUCT

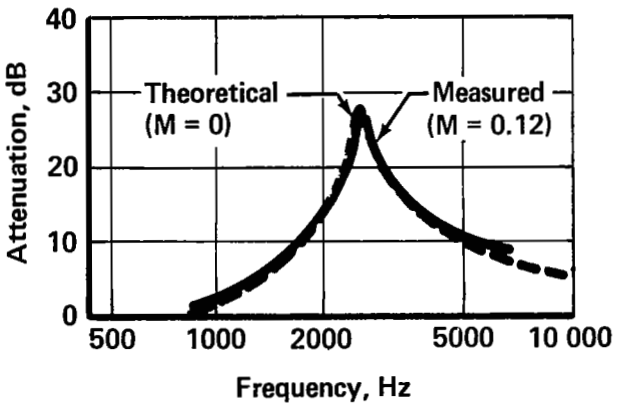

FIGURE B-3.—COMPARISON OF THEORETICAL AND MEASURED ATTENUATION (MACH 0.12)

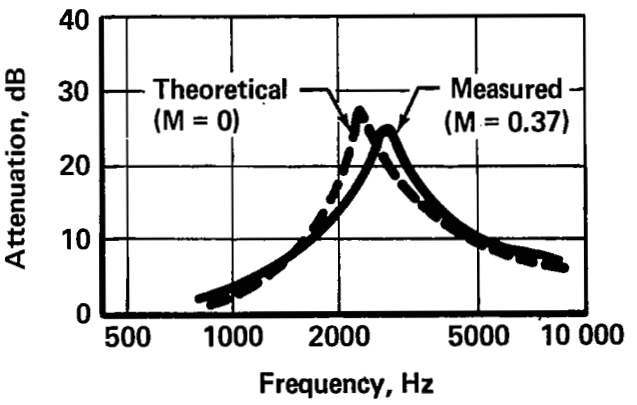

FIGURE B-4.—COMPARISON OF THEORETICAL AND MEASURED ATTENUATION (MACH 0.37)

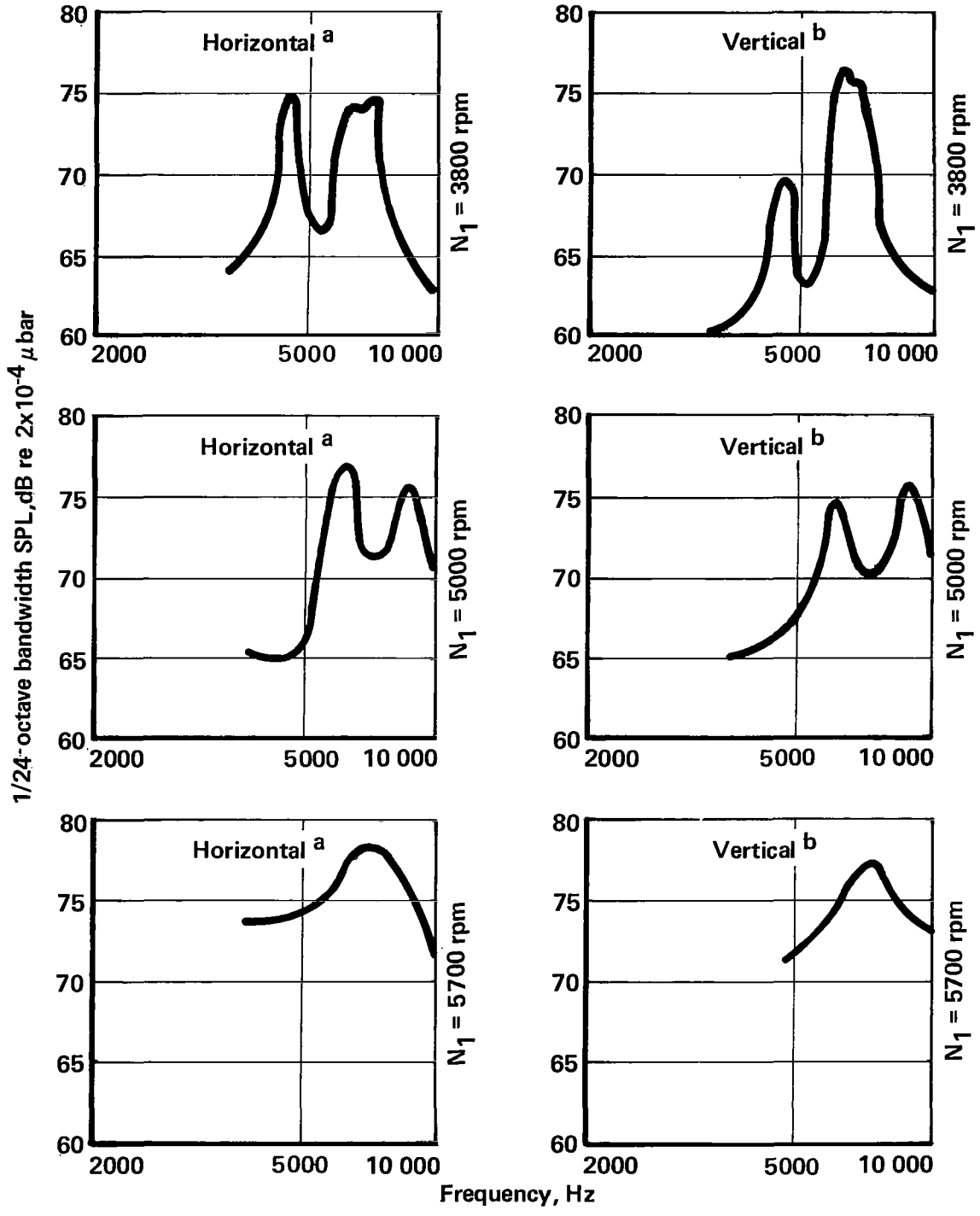

a 200-ft distance from engine
b 75-ft distance from engine

FIGURE C-1.– TURBINE NOISE SPECTRA AT ANGLES OF PEAK LEVELS

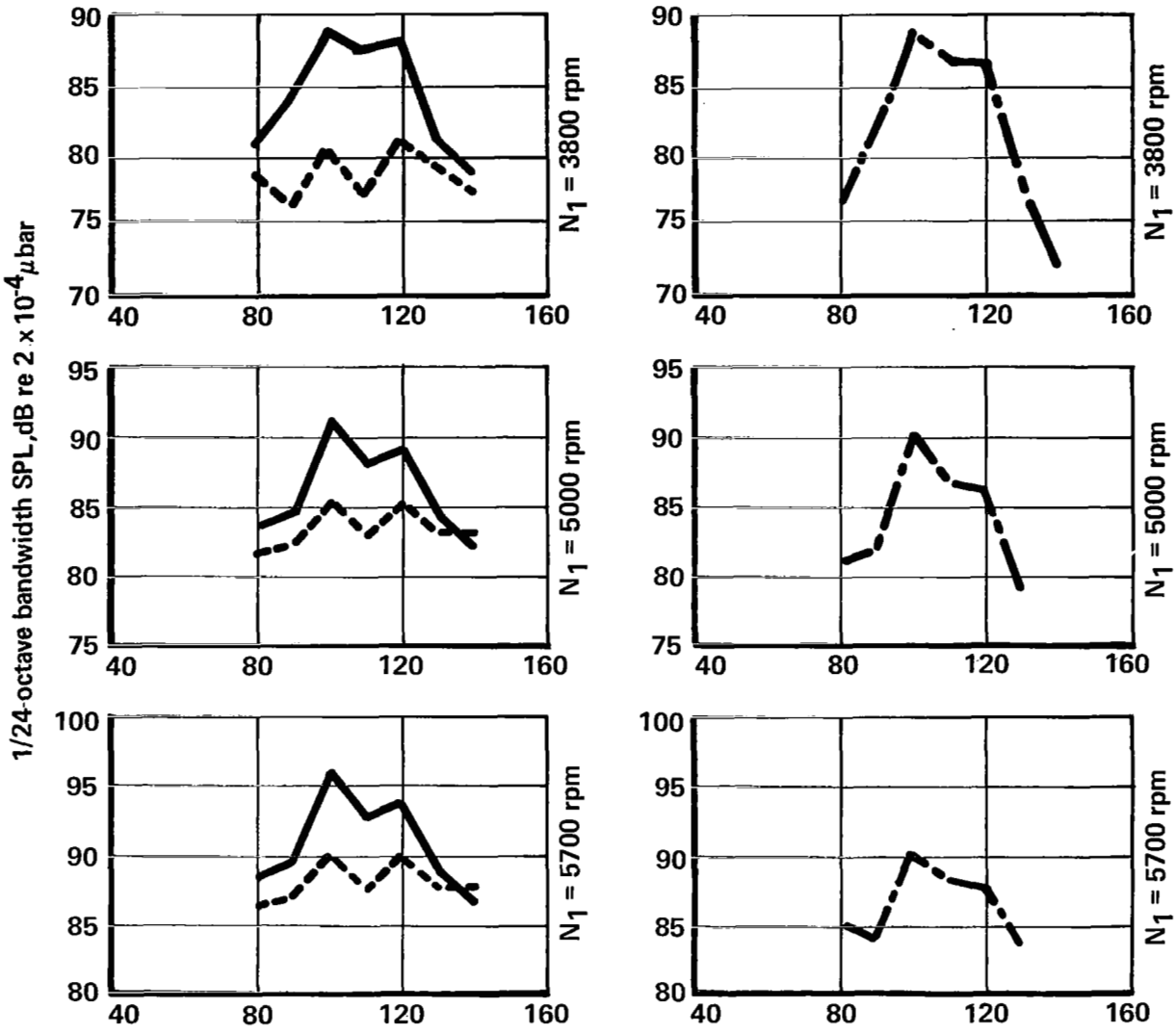

FIGURE C-2.—OCTAVE BAND TURBINE NOISE LEVELS CORRECTED FOR BACKGROUND NOISE LEVELS ON JT3D-3B ENGINE

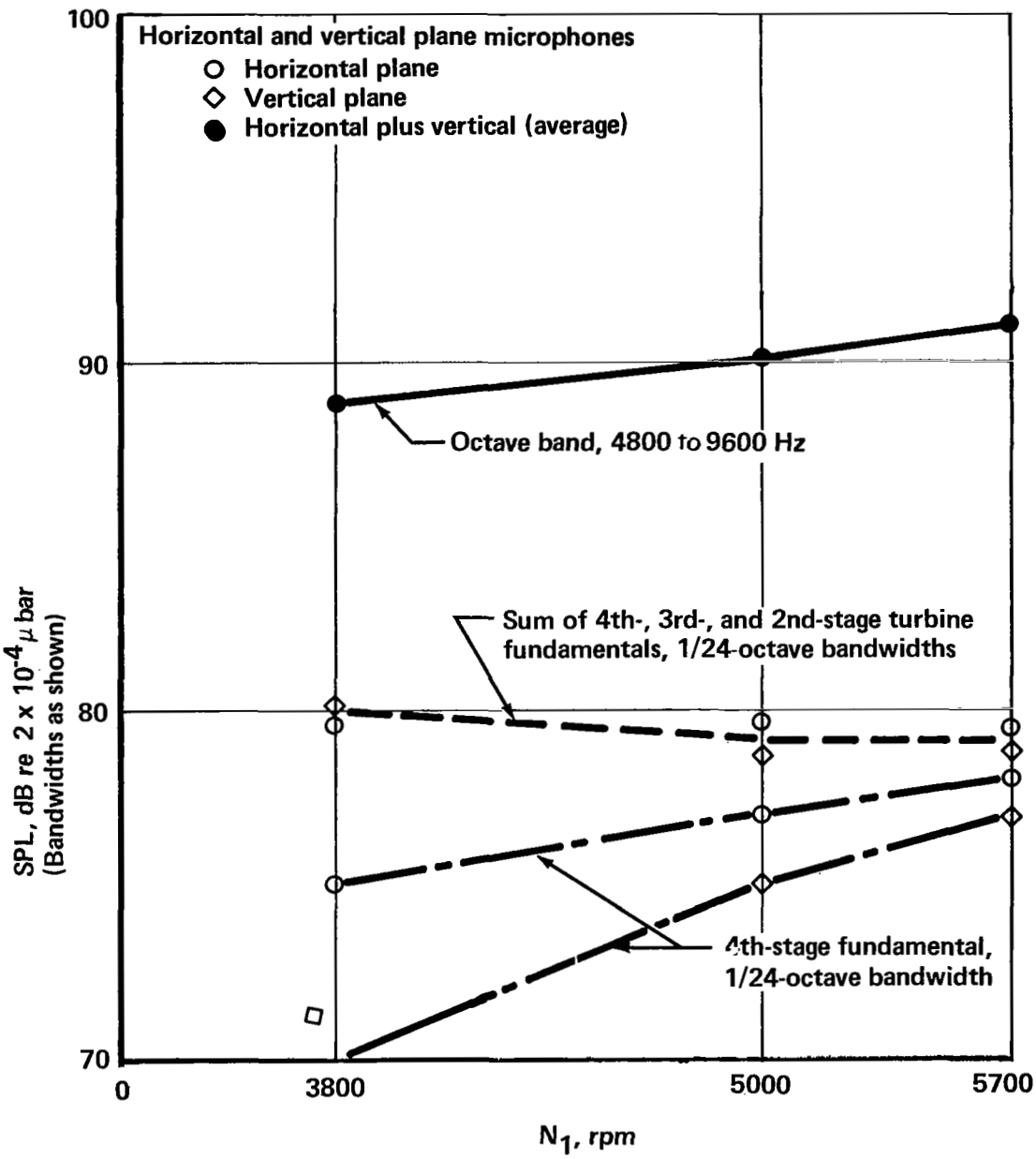

FIGURE C-3.—PEAK TURBINE NOISE VERSUS ROTOR SPEED N_1

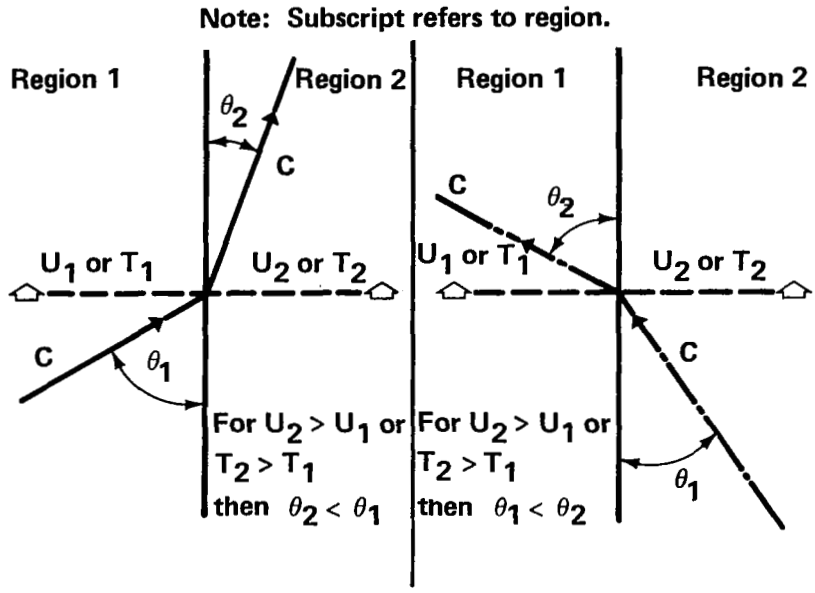

FIGURE C-4.—REFRACTION AT THE INTERFACE BETWEEN TWO REGIONS OF A MEDIUM IN RELATIVE MOTION OR RELATIVE TEMPERATURE

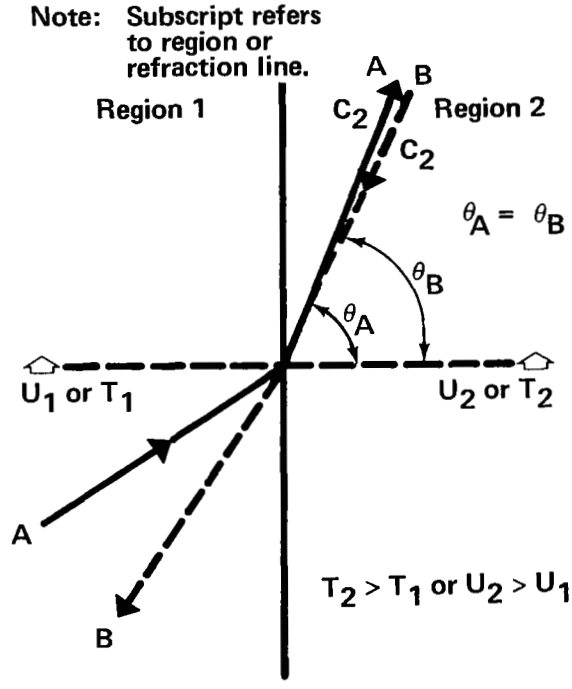

FIGURE C-5.—NONRECIPROCITY OF REFRACTION BETWEEN TWO REGIONS OF A MEDIUM IN RELATIVE MOTION OR RELATIVE TEMPERATURE

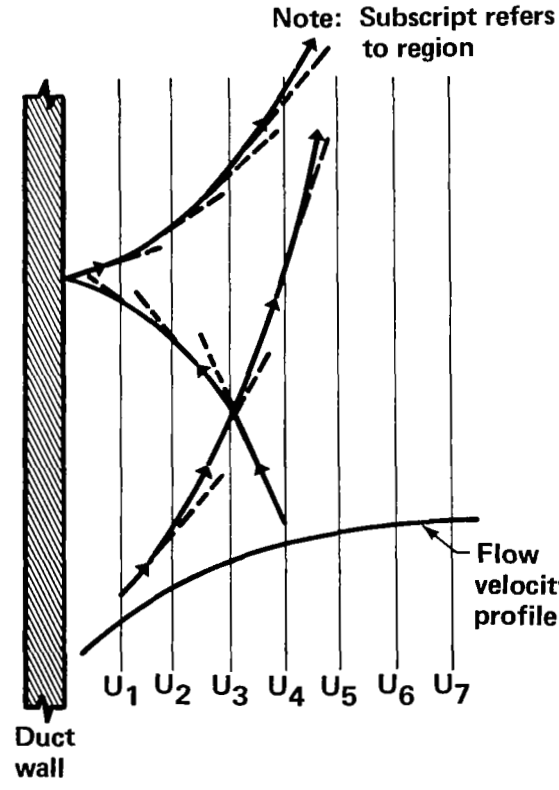

FIGURE C-6.—REFRACTED PATH OF ACOUSTIC RAY THROUGH MEDIUM WITH FLOW VELOCITY PROFILE

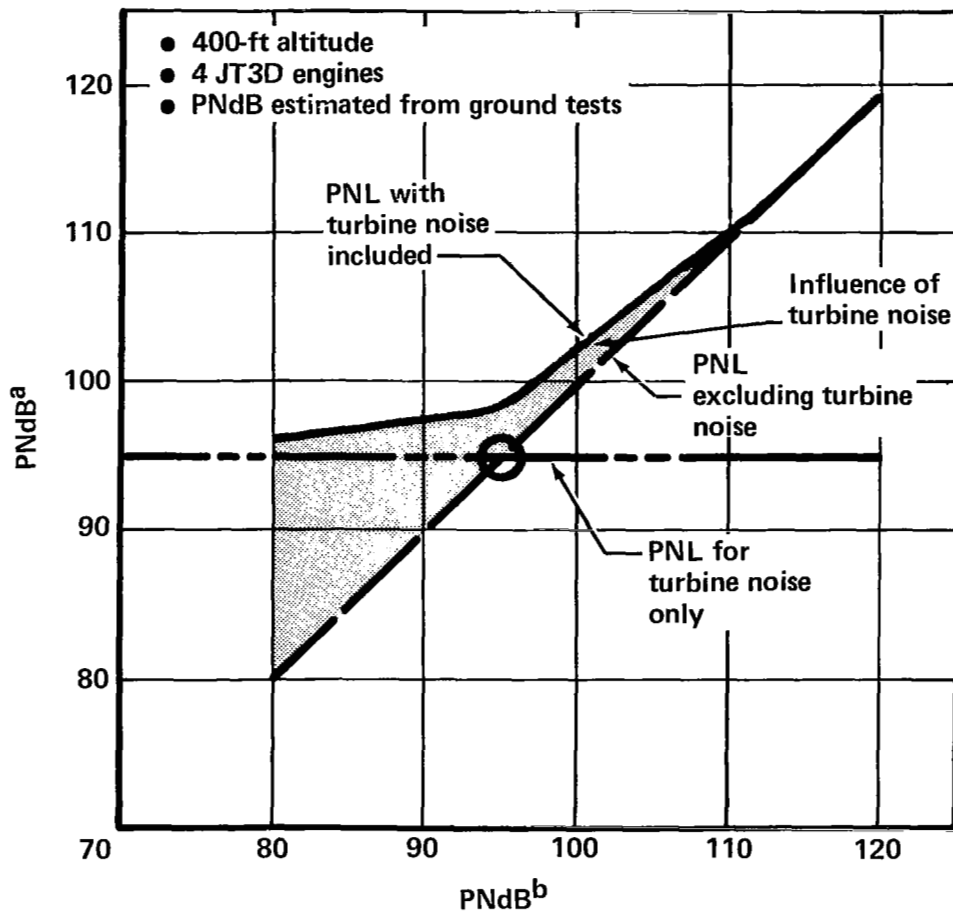

[a] Composite and component PNL's

[b] PNL excluding turbine noise—varies with engine condition or noise suppression

FIGURE C-7.—EFFECT OF TURBINE NOISE ON COMPOSITE PERCEIVED NOISE LEVELS

NASA-Langley, 1971 — 2